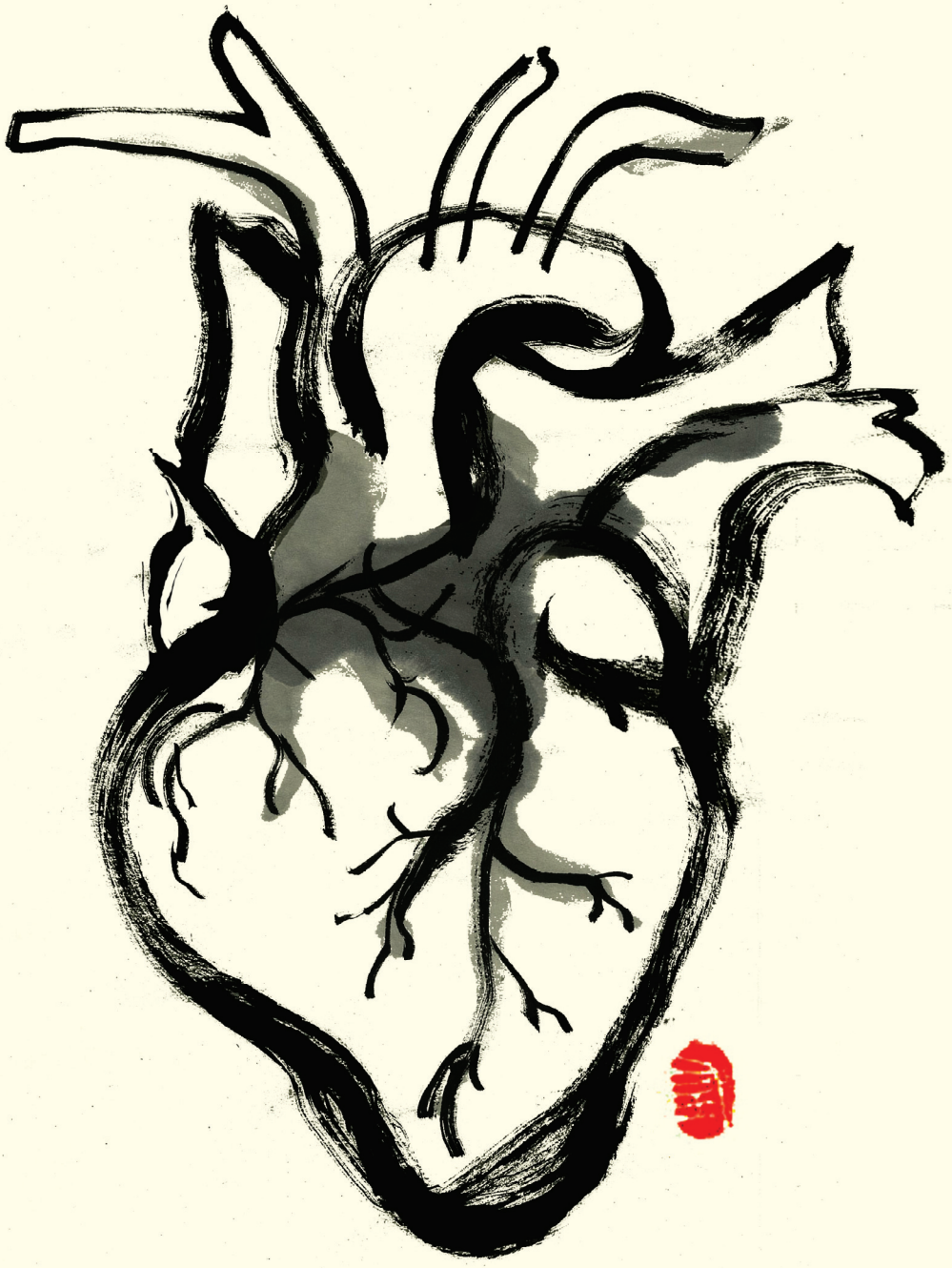

Advanced Three-Dimensional Echocardiography

Ben Ren

Advanced Three-Dimensional Echocardiography

Ben Ren

ISBN: 978-94-6169-572-7
Advanced Three-Dimensional Echocardiography
Ben Ren

Cover design: Lu Tang 唐璐
Layout and printing: Optima Grafische Communicatie, Rotterdam, The Netherlands

© Ben Ren 2014.
All rights reserved. For all articles published or accepted, the copyright has been transferred to the respective publisher. No part of this publication may be reproduced or distributed in any form or by any means, or stored in a database or retrieval system, without the prior written permission of the author, or where appropriate, of the publisher of the publications.

Advanced Three-Dimensional Echocardiography

Geavanceerde driedimensionale echocardiografie

Proefschrift

ter verkrijging van de graad van doctor aan de
Erasmus Universiteit Rotterdam
op gezag van de rector magnificus

Prof.dr. H.A.P. Pols

en volgens besluit van het College voor Promoties.

De openbare verdediging zal plaatsvinden op
dinsdag 28/10/2014 om 15.30 uur

door

Ben Ren
geboren te Chengdu, China

ERASMUS UNIVERSITEIT ROTTERDAM

PROMOTIECOMMISSIE

Promotor:	Prof.dr. F. Zijlstra
Overige leden:	Prof.dr.ir. H. Boersma Prof.dr.ir. A.F.W van der Steen Dr. O. Kamp Prof.dr. J.W. Roos-Hesselink Dr. R.B.A. van den Brink
Co-promotoren:	Dr. M.L. Geleijnse Dr.ir. J.G. Bosch

Financial support for the publication of this thesis was generously provided by:

Erasmus Universteit Rotterdam
Cardialysis
TomTec
St. Jude Medical Nederland B.V.
Abbott Vascular

The researches included in this thesis were supported by China Scholarship Council.

Financial support by the Dutch Heart Foundation for the publication of this thesis is gratefully acknowledged.

Every beginning is only a sequel, after all.
And the book of events
is always open halfway through.

Wislawa Szymborska

To my mother

CONTENTS

Part I	**Introduction**	
Chapter 1.1	General introduction	13
Part II	**3D echocardiography in mitral valve regurgitation**	
Chapter 2.1	Geometric Errors of the Pulsed Wave Doppler Flow Method in Quantifying Degenerative Mitral Valve Regurgitation: A Three-Dimensional Echocardiography Study	41
Chapter 2.2	Left Atrial Compliance in Asymptomatic versus Symptomatic Patients with Mitral Valve Regurgitation	59
Chapter 2.3	Left Atrial Function in Patients with Mitral Valve Regurgitation	75
Part III	**3D echocardiography in assessing left ventricular function**	
Chapter 3.1	Single-Beat Real-Time Three-Dimensional Echocardiographic Automated Contour Detection for Quantification of Left Ventricular Volumes and Systolic Function	95
Chapter 3.2	Application of Siemens Automated Three-Dimensional Echocardiographic Algorithm for Assessing Left Ventricular Systolic Function in the Real World	111
Chapter 3.3	Accuracy of Fully Automated Left Ventricular Function Quantification by Three-Dimensional Echocardiography	117
Part IV	**3D echocardiography in reconstructing left atrium**	
Chapter 4.1	A Transoesophageal Echocardiographic Image Acquisition Protocol for Wide-View Fusion of Three-Dimensional Datasets to Support the Atrial Fibrillation Catheter Ablation	135
Chapter 4.2	Fusion of Three-Dimensional Transesophageal Echocardiographic Images of Left Atrium for Supporting Catheter Ablation Procedures: Comparison with Computed Tomography	147
Chapter 4.3	Segmentation of Multiple Cavities of the Heart in Fused Wide-View 3D Transesophageal Echocardiograms	163

Part V **Discussion**

Chapter 5.1 Summary 185

Chapter 5.2 General discussion 191

Part VI **Appendix**

Chapter 6.1 Nederlandse samenvatting 213

Chapter 6.2 Curriculum vitae 219

Chapter 6.3 PhD portfolio 223

Chapter 6.4 List of publications 227

Chapter 6.5 Acknowledgements 233

Part I

Introduction

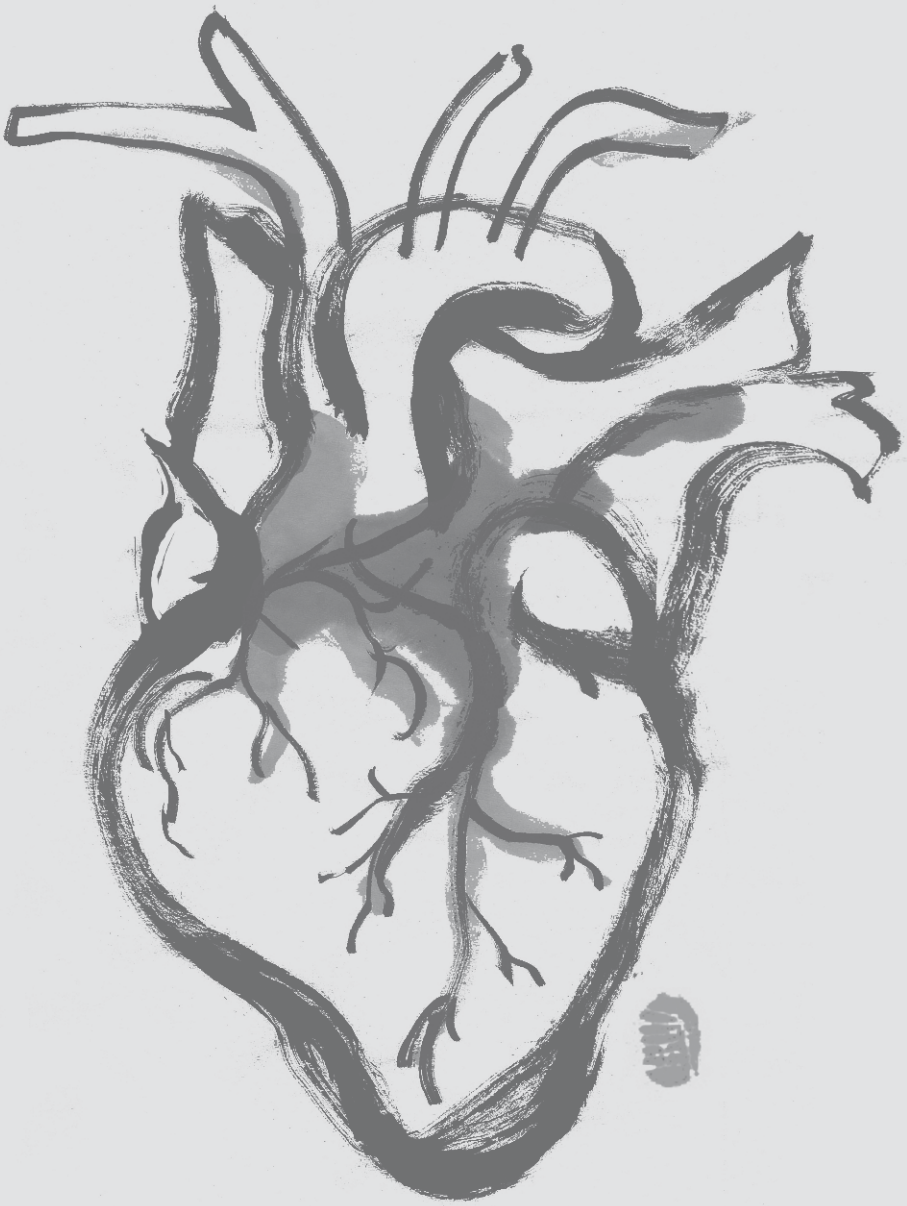

Chapter 1.1

General introduction

INTRODUCTION

3D echocardiography

During the development of echocardiography, 3D echocardiography imaging represents a major innovation in cardiovascular ultrasound (Figure 1). Advancements in computer and transducer technologies permit real-time 3D acquisition and presentation of cardiac structures from any view. An important milestone in the history of real-time 3D echocardiography was reached shortly after the year 2000, with the development of fully sampled matrix-array transducers (Figure 2). These transducers provide excellent real-time imaging of the beating heart in three dimensions and require significant

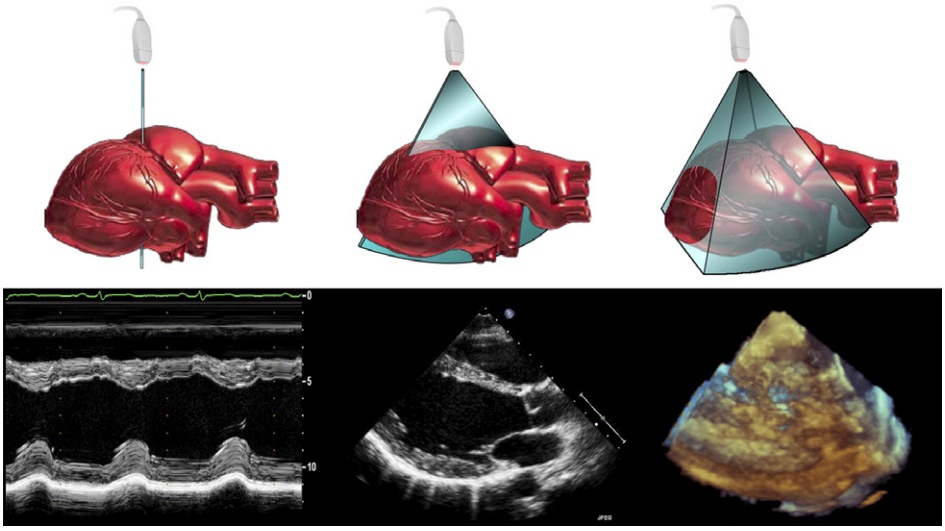

Figure 1 Development of the echocardiography: from M-mode to 2D B-mode to 3D echocardiography. Courtesy of René Frowijn.

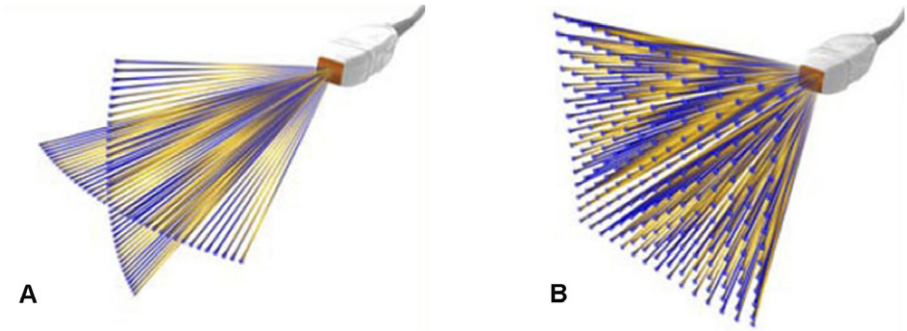

Figure 2 The 3D matrix-array transducers. A, Live xPlane imaging creates two full-resolution views simultaneously; B, Live volume imaging allows the acquisition and rendering of full volume data in real time.

technological developments in both hardware and software. Currently, 3D matrix-array transducers are composed of nearly 3,000 piezoelectric elements with operating frequencies ranging from 2 to 4 MHz for transthoracic echocardiographic imaging and from 2 to 7 MHz for transoesophageal echocardiographic (TOE) imaging. Basically, there are two different methods for data acquisition: real-time or live 3D imaging and electrocardiographically triggered multiple-beat 3D imaging. Real-time or live 3D echocardiography refers to the acquisition of multiple pyramidal data sets per second in a single heartbeat, including Live 3D, 3D Zoom and Live 3D colour modes. Limited by the temporal resolution and field of view, the live acquisition modes are mainly used in visualising individual cardiac structure, e.g. mitral valve, atrial septum and left atrial appendage. In contrast, the electrocardiographically triggered multiple-beat 3D echocardiography provides datasets of wider view and/or higher temporal and spatial

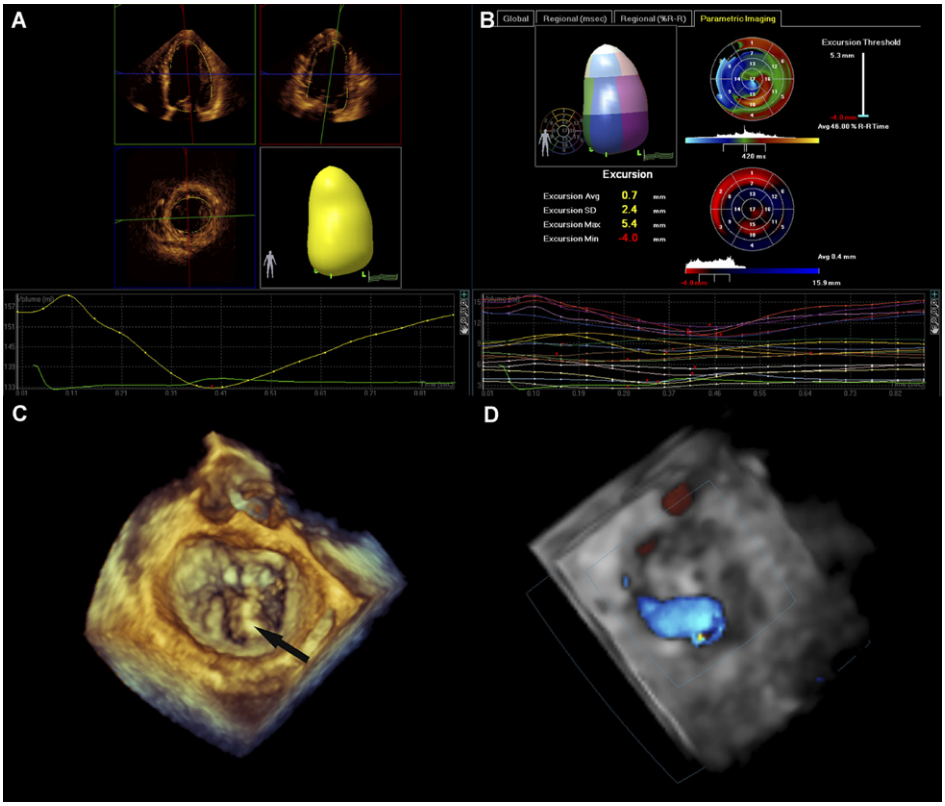

Figure 3 Clinical uses of 3D echocardiography. A, 3D echocardiographic calculation of left ventricular global volumes and ejection fraction; B, 3D echocardiographic calculation of left ventricular segmental function and dyssynchrony; C, the "en-face" view (also the surgical view) of mitral valve showing the P2 prolapse, acquired with the 3D zoom mode of transoesophageal echocardiography (the black arrow points to the prolapsed area); D, an elliptical flow convergent zone of functional mitral regurgitation acquired with the 3D colour Doppler imaging of transthoracic echocardiography.

resolutions. This is achieved through multiple acquisitions of narrow subvolumes of data over several heartbeats (ranging from two to seven cardiac cycles) that are subsequently stitched together to create a single volumetric (full volume) dataset. Because of better temporal and spatial resolutions, 3D (colour) full volume acquisition modes are often used in clinical researches for quantitative analysis of valve morphology and chamber function. However, the gated imaging of the heart may produce imaging artefacts created by the patient (body or respiratory motion) or irregular cardiac rhythms.

The usefulness of 3D echocardiography has been demonstrated in 1) the evaluation of cardiac chamber volumes and mass without geometric assumptions (Figure 3A), 2) the assessment of regional left ventricular (LV) wall motion and quantification of systolic dyssynchrony (Figure 3B), 3) presentation of realistic (en-face) views of heart valves (Figure 3C), 4) volumetric evaluation of regurgitant lesions and shunts with 3D colour Doppler imaging (Figure 3D), and 5) 3D stress imaging[1].

Quantification of mitral valve regurgitation

Degenerative mitral regurgitation (MR) is the second most common valvular heart disease in Europe[2], and causes symptoms such as dyspnea, fatigue, orthopnea, and palpitations[3,4]. Quantification of MR is essential to determine the severity of MR[5] and clinical outcomes[6]. The two most used quantitative parameters are the regurgitant volume and effective regurgitant orifice area (EROA), which may be calculated by the proximal isovelocity surface area (PISA) and pulsed wave Doppler flow methods.

The *PISA method* is the most frequently used quantitative approach[6]. It is derived from the hydrodynamic principle stating that, as blood approaches a regurgitant orifice, its velocity increases forming concentric, roughly hemispheric shells of increasing velocity and decreasing surface area[7]. Colour flow mapping enables the imaging of one of these hemispheres corresponding to the Nyquist limit of the instrument. If a Nyquist limit can be chosen at which the flow convergence has a hemispheric shape, flow rate through the regurgitant orifice is calculated as the product of the surface area of the hemisphere ($2\pi r^2$) and the aliasing velocity (Va) as: $2\pi r^2 \times Va$ (Figure 4). Assuming that the maximal PISA radius occurs at the time of peak regurgitant flow and peak regurgitant velocity, the maximal EROA is derived as: $EROA = 2\pi r^2 \times Va / PkV_{Regurg}$, where PkV_{Regurg} is the peak velocity of MR. The PISA method is based on the assumption of hemispheric symmetry of the velocity distribution proximal to the regurgitant lesion, which may not hold for eccentric jets, multiple jets, or complex or elliptical regurgitant orifices. The regurgitant volume and EROA are used to grade the severity of MR, as an EROA $\geq$ 40 mm^2 or a regurgitant volume $\geq$ 60 ml indicates severe organic MR. In functional MR, severe MR is defined as an EROA $\geq$ 20 mm^2 or a regurgitant volume $\geq$ 30 ml.

The *pulsed wave Doppler flow method* can be used as an additive or alternative method, especially when the PISA is not accurate or not applicable. Pulsed wave Dop-

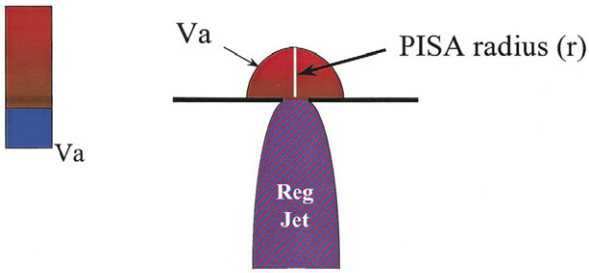

$$\text{Reg Flow} = 2\pi\, r^2 \times \text{Va}$$
$$\text{EROA} = \text{Reg Flow} / \text{PkV}_{\text{Reg}}$$

Figure 4 Schematic depiction of the flow convergence or proximal isovelocity surface area method for quantitating valvular regurgitation[5]. Va is the velocity at which aliasing occurs in the flow convergence towards the regurgitant orifice. PkV_{Reg}, Peak velocity of the regurgitant jet, determined by continuous wave Doppler. Reg flow, regurgitant flow; EROA, effective regurgitant orifice area; Reg jet, regurgitation jet. Permission obtained from Elsevier (License no. 3387000893041).

pler recordings of flow velocity can be combined with 2D measurements to derive flow rates and stroke volume (SV)[8]. Briefly, SV at any valve annulus is derived as the product of cross-sectional area (CSA) and the velocity time integral (VTI) of flow at the annulus. For MR, the mitral annulus (MA) and left ventricular outflow tract (LVOT) are usually chosen for calculating the SVs. The diameter of the MA is usually measured in the transthoracic apical 4-chamber view in early-to-mid diastole (Figure 5A) and that of the LVOT is measured in the parasternal long-axis view in early-to-mid systole (Figure 5B). Thus,

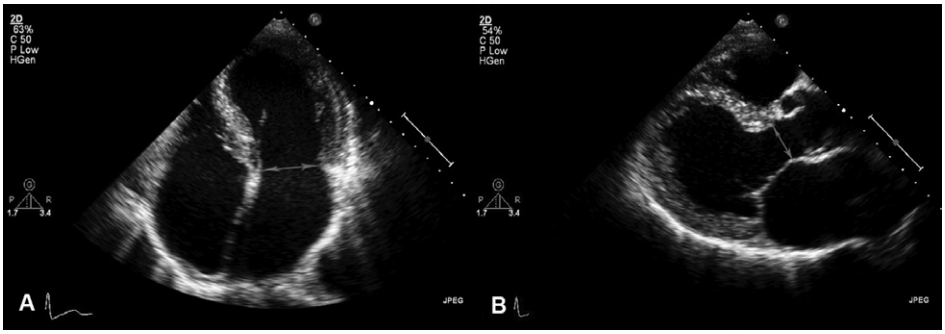

Figure 5 Dimension measurements in the 2D pulsed wave Doppler flow method. A, the diameter of the mitral annulus is measured between the inner edges of the base of the posterior and anterior leaflets in early-to-mid diastole at the maximal opening of the mitral valve in the apical 4-chamber view; B, the diameter of the left ventricular outflow tract is measured just below the aortic valve in early-to-mid systole in the parasternal long-axis view.

$$\text{Regurgitant volume} = SV_{MA} - SV_{LVOT} = \pi r_{MA}^2 \times VTI_{MA} - \pi r_{LVOT}^2 \times VTI_{LVOT}$$

$$\text{EROA} = \text{Regurgitant volume} / VTI_{MR}$$

The Doppler volumetric method is a more time-consuming approach, and therefore not recommended as a first line method to quantify MR severity[9]. The most common error encountered in determining these parameters is failure to measure the valve annulus properly and the potential error is squared in the formula. In fact, the MA is of a saddle shape with two high points at the middle of the anterior leaflet adjacent to the aortic valve and the middle of the posterior leaflet (Figure 6A). Moreover, the cross sections of both MA and LVOT may be oval rather than circular with major-axis and minor-axis diameters (Figure 6B).

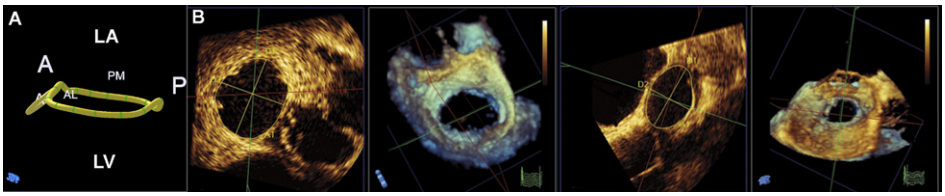

Figure 6 Mitral annulus dimensions. A, a 3D model of the mitral annulus reconstructed with 3D transoesophageal echocardiographic dataset. The mitral annulus is of a saddle shape with two high points at the middle of the anterior leaflet adjacent to the aortic valve and the middle of the posterior leaflet; B, the "en face" views and cross sections of the mitral annulus and left ventricular outflow tract shown with 3D transoesophageal echocardiography. Both the mitral annulus and left ventricular outflow tract are oval. A, anterior; AL, anterolateral; LA, left atrium; LV, left ventricle; P, posterior; PM, posteromedial.

Quantification of left atrial function

The left atrium (LA) fulfills three major physiologic roles that impact on LV filling and performance. The LA acts as a contractile pump that delivers 15% to 30% of the LV filling, as a reservoir that collects pulmonary venous return during ventricular systole, and as a conduit for the passage of stored blood from the LA to the LV during early ventricular diastole[10]. Increased LA size is associated with adverse cardiovascular outcomes, such as atrial fibrillation (AF) and stroke[11-15] and mortality in patients with ischemic[16,17] or dilated cardiomyopathy[18-21]. LA enlargement is a marker of both the severity and chronicity of diastolic dysfunction and magnitude of LA pressure elevation[22-24]. Any comprehensive assessment of LA function should include an accurate assessment of LA pressure, which can be indirectly estimated by echocardiography. Generally, 2D/3D echocardiographic measurements of LA volumes, speckle-tracking imaging analysis of LA mechanics, and Doppler analysis of mitral valve and pulmonary vein (PV) flows can provide a picture of LA function.

Echocardiographic quantification of LA volumes

Conventionally, the LA size is measured at the end-ventricular systole when the LA chamber is at its greatest dimension. The LA size can be reflected with its linear dimension and volume. The M-mode or 2D anteroposterior linear dimension obtained from the parasternal long-axis view is the standard for linear LA measurement and used in many research papers[11,12,15,19] (Figure 7). However, predominant enlargement in the superior-inferior and medial-lateral dimensions will alter LA geometry such that the anteroposterior dimension may not be representative of LA size[25,26]. For these reasons, the measure of LA size should be accompanied by LA volume measurement[27].

When LA size is measured in clinical practice, volume determinations are preferred over linear dimensions because they allow accurate assessment of the asymmetric remodeling of the LA[26]. Using 2D echocardiography, LA volumes are best calculated using either an ellipsoid model or Simpson's rule[14,17,24,26,28-31]. The *ellipsoid model* assumes that the LA can be represented as an ellipse with a volume of $8 \times (A1) \times (A2) / 3\pi(L)$, where A1 and A2 represent the maximal planimetered LA area acquired from the apical 4- and 2-chamber views, and L is length (Figure 8). In the area-length formula the length is measured in both the 4- and 2-chamber views and the shortest of these 2 length measurements is used in the formula.

LA volume may also be measured using the *modified bi-plane Simpson* method, similar to its application for LV measurements, in which the volume of a geometric figure can be calculated from the sum of the volumes of smaller figures of similar shape. The Simpson's algorithm divides the LA into a series of stacked oval disks whose height is h and whose orthogonal minor and major axes are D1 and D2. The volume of the entire LA can be derived from the sum of the volume of the individual disks, thus volume $= \pi / 4 \times (h) \times \sum(D1)(D2)$. The formula is integrated into the ultrasound system and the volume can be calculated with the software online (Figure 9).

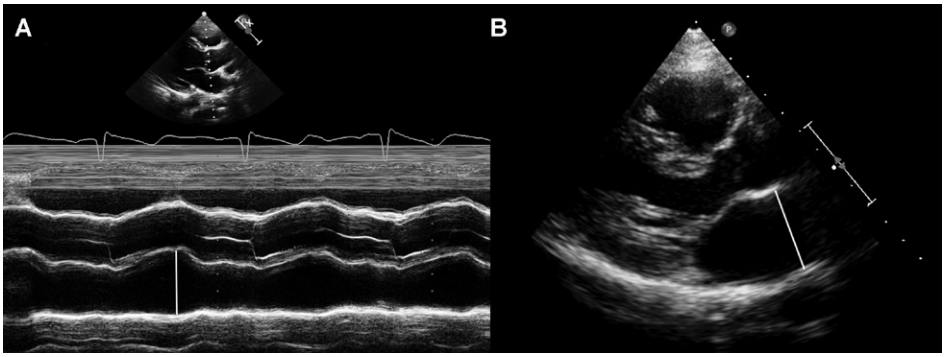

Figure 7 Measurements of left atrial diameter indicated with the white line. A, from M-mode, guided by parasternal long-axis; B, from B-mode in the parasternal long-axis view.

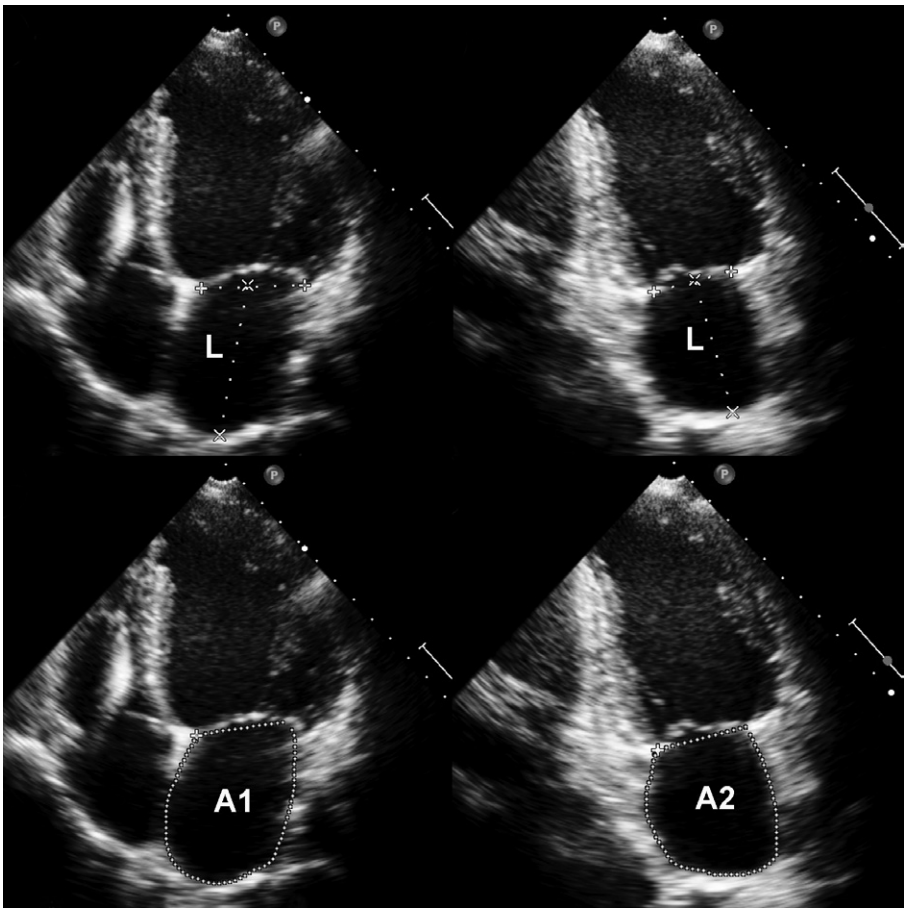

Figure 8 Measurement of left atrial volume using area-length method in the apical 4-chamber (left column) and 2-chamber (right column) views at end systole. The shorter length either from the 4-chamber or 2-chamber view is used in the formula.

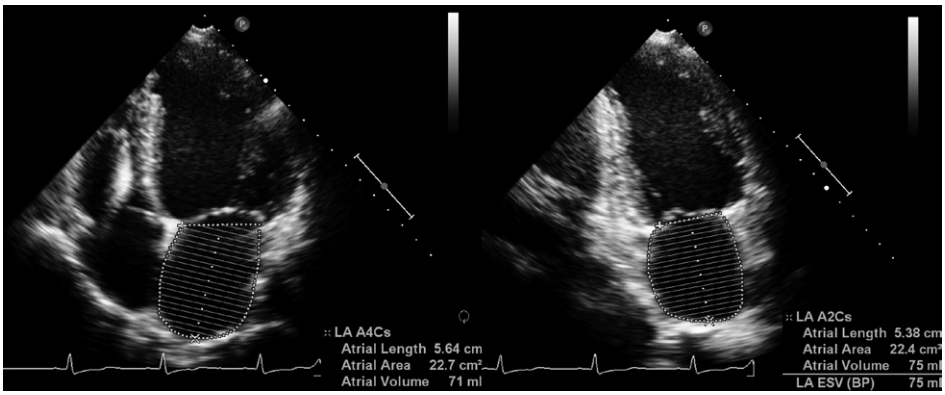

Figure 9 Measurement of left atrial volume using the modified bi-plane Simpson's method in apical 4-chamber and 2-chamber views at end systole.

Because 2D echocardiography is limited by the use of geometric models and by possible errors due to foreshortening, it may underestimate LA volume compared with computed tomography (CT), biplane contrast ventriculography, and magnetic resonance imaging (MRI)[29,30,32]. *3D echocardiography* should provide the most accurate evaluation of LA volume (Figure 10). In recent years, 3D echocardiography has been

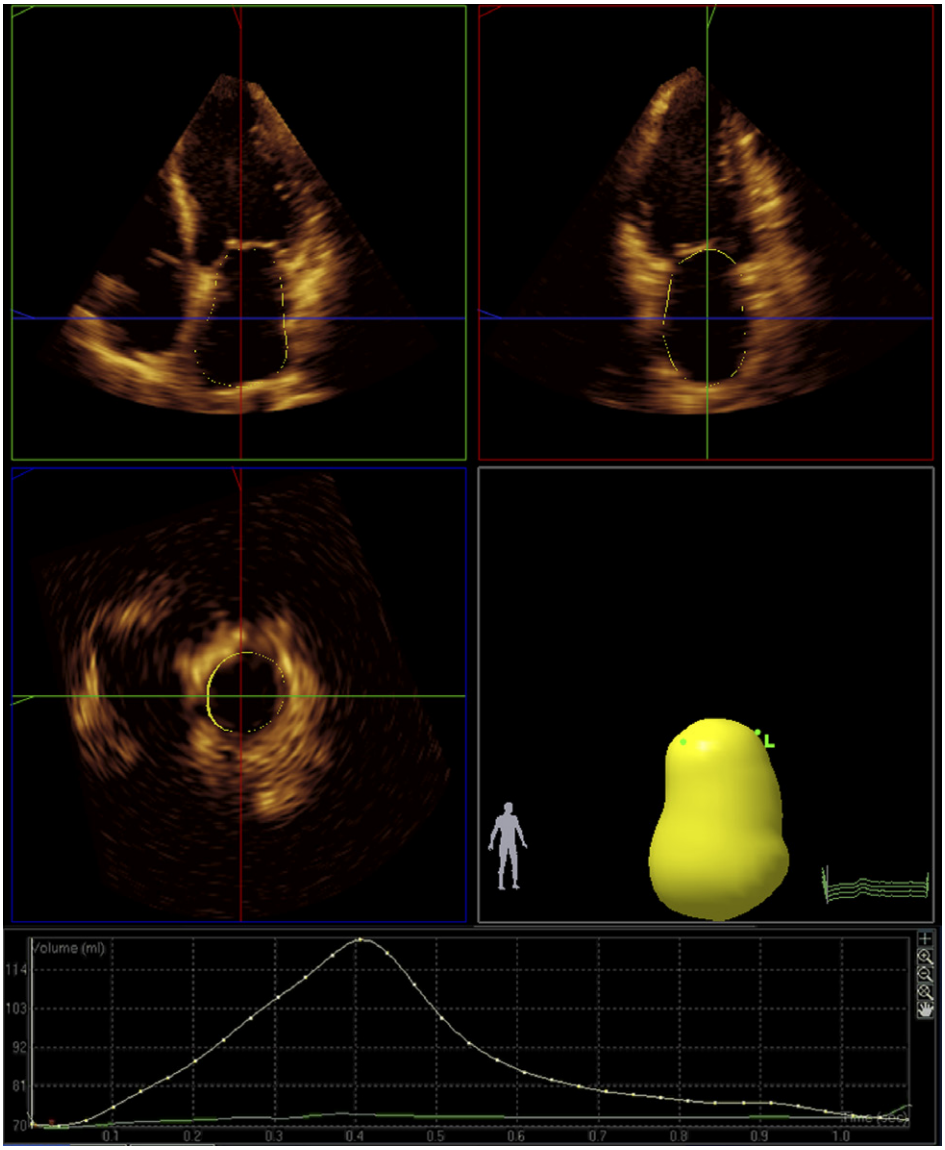

Figure 10 Calculation of left atrial volume using 3D transthoracic echocardiography. The 3D dataset is displayed as three multiplanar reconstruction views. The reconstructed 3D model of the left atria and the volume-time curve are also seen.

assessed in calculating LA volume and function by comparing with other imaging modalities in different patient populations[33-38]. Similarly as LV volume quantification, 3D echocardiography provides improvement in accuracy and observer variability with respect to 2D echocardiography, but tends to provide smaller volume than CT, MRI and angiography do. In 2012, a recommendation of 3D acquisition of LA for volume quantification was made by European Association of Echocardiography/American Society of Echocardiography[1]. However, to date no consensus exists on normal values for LA volume and function 3D echocardiography.

Because of the three functional phases of the LA, extra volumes are necessary for assessing the function besides the LA maximal volume. Furthermore, the LA minimal volume was recently found to correlate better with cardiovascular events[39-43]. The LA function indices can be calculated as the volume changes and corresponding emptying fraction as:

- LA reservoir function
  Total SV = LAV_{max} - LAV_{min}
  Distensibility = (LAV_{max} - LAV_{min})/LAV_{min} × 100%
- LA conduit function
  Passive filling volume = LAV_{max} – $LAV_{pre\text{-}A}$
  Passive emptying fraction = (LAV_{max} – $LAV_{pre\text{-}A}$)/LAV_{max} × 100%
- LA contractile function
  Active SV = $LAV_{pre\text{-}A}$ – LAV_{min}
  Active emptying fraction = ($LAV_{pre\text{-}A}$ – LAV_{min})/$LAV_{pre\text{-}A}$ × 100%

LAV_{max} is the maximum LA volume measured at end systole just before mitral valve opening; LAV_{min} is the minimum LA volume measured at end diastole just before the mitral valve closure; and $LAV_{pre\text{-}A}$ is the volume before atrial contraction measured at the frame just before mitral valve reopening.

Frank–Starling law

The Frank–Starling law of the heart is commonly applied in assessing LV function and states that the stroke volume of the heart increases in response to an increase in the volume of blood filling the heart (end diastolic volume) when all other factors remain constant (Figure 11). The increased volume of blood stretches the cardiac wall, causing cardiac muscle to contract more forcefully. SV may also increase as a result of greater contractility of the cardiac muscle during exercise, independent of the end-diastolic volume. The Frank–Starling mechanism appears to make its greatest contribution to increasing SV at lower work rates, and contractility has its greatest influence at higher work rates. The Frank–Starling behaviour has also been found existing in the LA muscle in an animal study[44] and in a few clinical studies including different patient populations[45-47].

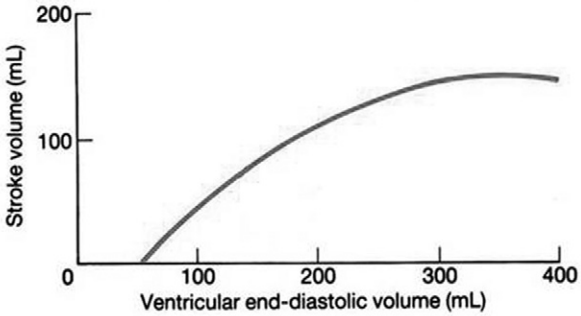

Figure 11 Frank–Starling law of the heart. The stroke volume increases in response to an increase in the end diastolic volume.

2D speckle-tracking echocardiographic quantification of LA mechanics

Echocardiographic imaging is ideally suited for the evaluation of cardiac mechanics because of its intrinsically dynamic nature. Two techniques have mainly been used in research: 1) Doppler based tissue velocity measurements referred as tissue Doppler, and 2) speckle tracking on the basis of displacement measurements. Both types of techniques lead to derivations of multiple parameters of myocardial function. *Speckle-tracking echocardiography* is a relatively new and angle-independent technique used for the evaluation of myocardial function. The speckles seen in grayscale B-mode images are the result of constructive and destructive interference of ultrasound backscattered from structures smaller than the ultrasound wavelength, resulting in small temporally stable and unique myocardial features, referred to as speckles[48,49]. Blocks or kernels of speckles can be tracked from frame to frame (simultaneously in multiple regions within an image plane) using block matching, and provide local displacement information, from which parameters of myocardial function such as velocity, strain, and strain rate can be derived (Figure 12). In addition, instantaneous velocity vectors can be calculated and superimposed on the dynamic images (Figure 13). In contrast to tissue Doppler imaging, analysis of these velocity vectors allows the quantification of strain and strain rate in any direction within the imaging plane. Depending on spatial resolution, selective analysis of epicardial, myocardial, and endocardial functions are also possible[50-52]. 2D speckle-tracking echocardiography allows measurements of myocardial mechanics by tracking groups of intramyocardial speckles (displacement or velocity) or myocardial deformation (strain or strain rate) in the imaging plane. It has been validated for the assessment of the LV myocardial deformation against sonomicrometry[49,53,54] and clinically against tissue Doppler imaging[55] and MRI[56]. Assessment of 2D strain by speckle-tracking echocardiography is a semiautomatic method, which requires manual definition of the myocardium. When automated tracking does not fit with the visual impression of wall motion, regions of interest need to be adjusted manually until optimal tracking is achieved.

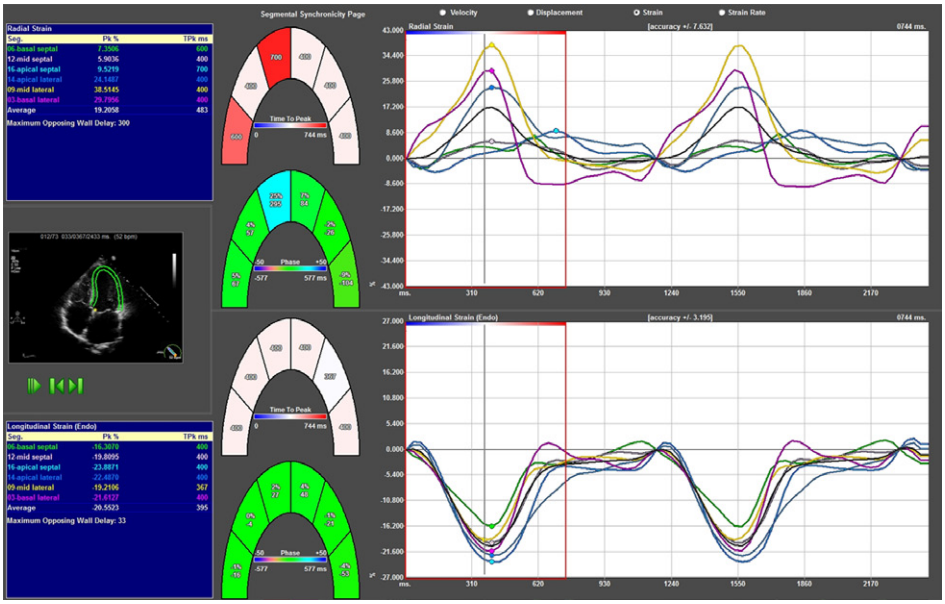

Figure 12 Radial and longitudinal strain curves of left ventricle measured using 2D speckle-tracking echocardiography in apical 4-chamber view. Different colour curves represent different left ventricular segments. Curves of other parameters such as velocity, displacement and strain rate can also be obtained.

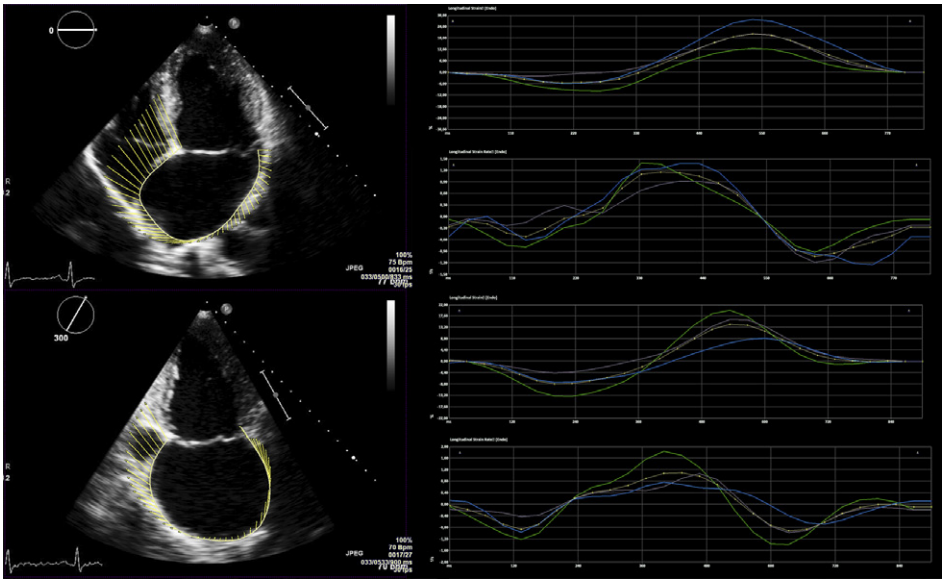

Figure 13 Vectors of the velocities of the left atrial endocardial points and graphic displays of the left atrial regional and global strain and strain rate during one cardiac cycle obtained using 2D speckle-tracking echocardiography in the apical 4-chamber and 2-chamber views. Different colour curves represent different left atrial regions.

Assessment of 2D strain using speckle-tracking echocardiography can be applied to both ventricles and atria. However, because of the thin wall of the atria, signal quality may be suboptimal. For the LA, 2D speckle-tracking echocardiography can provide volume curves during one cardiac cycle, from which various LA mechanical indices can be obtained[57,58]. It also allows a direct assessment of LA endocardial contractility and deformation. Two different approaches have been proposed. The first takes as a reference point the QRS onset and measures the positive peak atrial longitudinal strain (corresponding to atrial reservoir)[57]. The second uses the P-wave as the reference point, enabling the measurement of a first negative peak atrial longitudinal strain (corresponding to atrial systole), a positive peak atrial strain (corresponding to LA conduit function), and their sum[58].

Quantification of left ventricular volumes and ejection fraction

LV volumes and ejection fraction are the most used parameters in assessing LV function and have important prognostic significance[59,60]. With the development of echocardiography, LV function has subsequently been quantified with M-mode, 2D and 3D echocardiographic techniques. Similarly as the LA volume measurements, the linear and 2D approaches incompletely characterize the 3D chamber volume and function, especially in patients with regional LV dysfunction. Although in the past, these inaccuracies have been considered inevitable and of minor clinical importance, in most situations accurate measurements are required, particularly when the LV dimension and function decide the timing of treatment, e.g. surgery or when following the course of a disease with serial examinations. During the last two decades, several 3D echocardiographic techniques became available to measure LV volumes and function[61-68]. These can be conceptually divided into two techniques, which are based on offline reconstruction from a set of multiple 2D cross sections, and online data acquisition using a matrix-array transducer, also known as real-time 3D echocardiography. After acquisition of the raw data, calculation of LV volumes and mass requires identification of endocardial borders using semi-automated and automatic algorithms (Figure 14).

Regardless of which acquisition or analysis method is used, 3D echocardiography does not rely on geometric assumptions for volume calculations and is not subject to plane positioning errors leading to chamber foreshortening. Studies comparing 3D echocardiographic LV volumes with MRI have confirmed 3D echocardiography to be better in accuracy and reproducibility than 2D echocardiography[69-76].

Left atrial anatomy for catheter ablation procedures

AF is increasingly treated by catheter ablation, including PV isolation and complex left atrial ablation for non-PV triggers, thus eliminating the triggers initiating AF[77]. Studies found that AF is most commonly initiated by a premature beat from the ostia of the

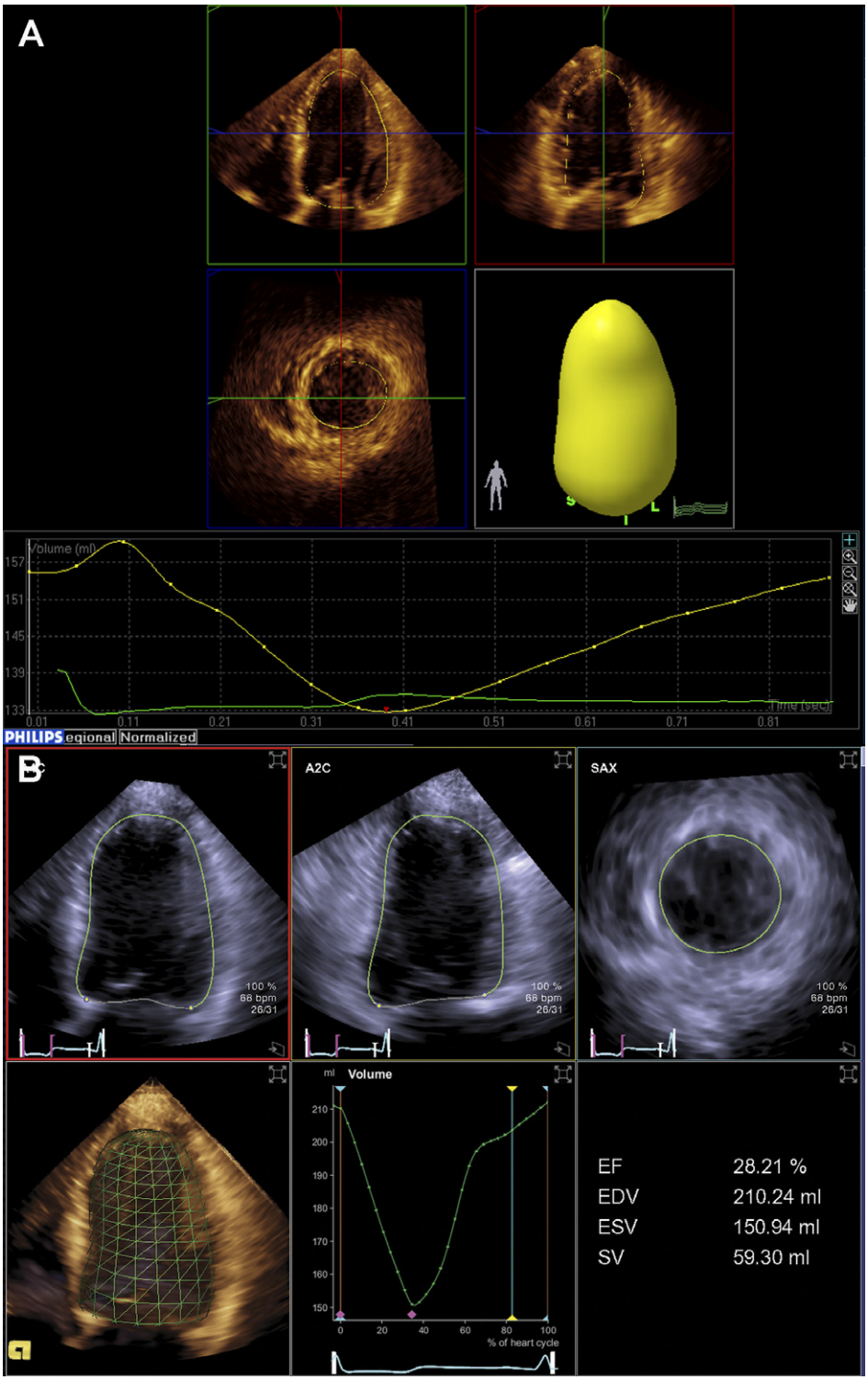
A
Volume (ml)
157
151
145
139
133
0.01
0.11
0.21
0.31
0.41
0.51
0.61
0.71
0.81
Time (sec)
PHILIPS
Normalized
B
A2C
SAX
100 %
68 bpm
26/31
Volume
ml
210
200
190
180
170
160
150
0
20
40
60
80
100
% of heart cycle
EF 28.21 %
EDV 210.24 ml
ESV 150.94 ml
SV 59.30 ml

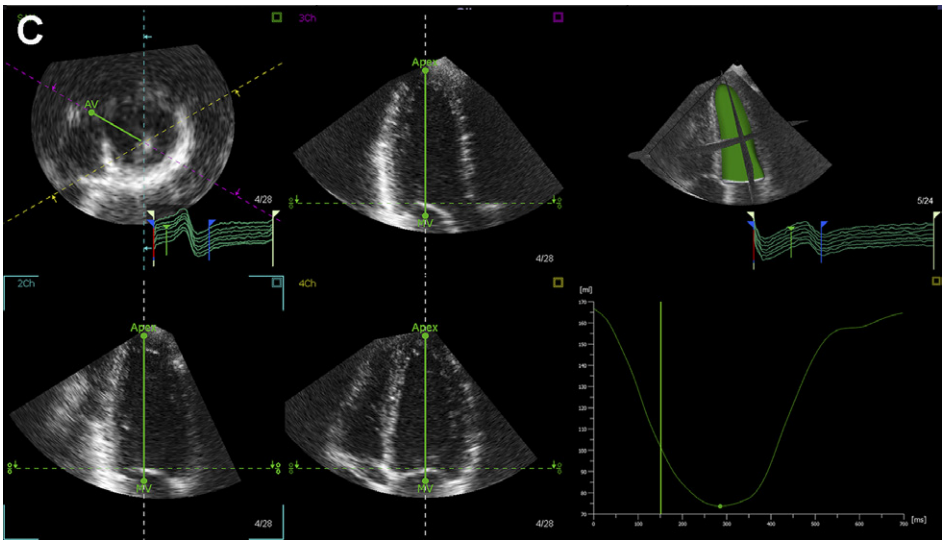

Figure 14 The 3D left ventricular volume analysis algorithms developed by different vendors. A, Philips QLAB 3DQA; B, Siemens LV analysis; C, TomTec 4D-LV analysis.

PVs[78,79]. As a result, the procedure initially targeted elimination of foci inside the triggering vein, but this strategy was not effective enough to prevent recurrences which originated from the same or other veins. Therefore, electrical disconnection of all four PVs from the atrium became the proposed treatment option. The circumferential isolation of the veins is the approach that is most frequently used nowadays[77,80]. As the atrium becomes more dilated and fibrotic, other structures in addition to PVs are increasingly being recognised as a possible source of AF initiation and/or are key in the perpetuation of AF. Non-PV triggers initiating AF can be identified in up to one third of unselected patients referred for catheter ablation for paroxysmal AF[78,79,81,82]. Typical locations of triggers and micro-reentry circuits in the LA are: left lateral ridge, left atrial isthmus (the area in the posterior-inferior wall of LA), left atrial appendage, fossa ovalis, and LA posterior wall. Other sites are superior vena cava, crista terminalis, coronary sinus and adjacent to the aortic annulus[81-84].

The ablation of AF is a complex procedure requiring a profound knowledge of the anatomy of the LA. Being the most posteriorly situated of the cardiac chambers, it is only separated from the oesophagus by the pericardium. The LA consists of three parts: the vestibule, the appendage and the venous component and shares the septum with the right atrium. The vestibule is the part of the LA surrounding the mitral valve orifice without distinctive anatomic characteristics. The left atrial appendage is a blind-ending multilobar structure located next to the left superior PV. The venous component receives the PVs. The most common pattern of entry is two veins from the hilum of each lung. The PVs enter the posterior part of the LA body with the ostia of left veins located

more superiorly than the right veins. The typical arrangement of four distinct pulmonary venous orifices is present in 20% to 60% of subjects, but it is also common to find the presence of a short or long common venous trunk on the left side, and supernumerary veins on the right side[85]. Where there are four PVs, the inferior venous ostia are situated more posteriorly than the superior venous ostia. The superior PV ostia tend to be larger and have longer distances from the ostium to the first-order branches than the inferior veins. The right superior PV passes behind the junction between the right atrium and the superior vena cava, whereas the inferior PV passes behind the intercaval area. The left PVs are separated from the left atrial appendage by the left lateral ridge, also known as the ligament of Marshall. Because the LA lies close to the transoesophageal transducer, specific internal atrial anatomy can be visualised clearly from different perspectives with 3D TOE.

Aims and outline of this thesis

3D echocardiography has been evaluated in multiple clinical studies for assessing cardiac valvular regurgitation, chamber function and facilitating catheter interventions. With its well-known strengths and drawbacks, the clinical application of 3D echocardiography in many field is still to be validated. In this thesis, the following research questions are addressed:

- How much error does the recommended 2D pulsed wave Doppler wave method make in calculating MR?
- How does LA function alter in patients with MR?
- How accurate is 3D echocardiography in automated analyses of LV function in real-world clinical conditions?
- Is 3D transoesophageal reconstruction of the LA accurate and can it facilitate the catheter ablation procedure of AF?

3D echocardiography in mitral valve regurgitation

For MR, quantification of the regurgitant volume and LA function are of great importance in diagnosis, treatment and prognosis. We have assessed 2D pulsed wave Doppler method in calculating the regurgitant volume by comparing with 3D echocardiographic measures of the MA and LVOT areas **(Chapter 2.1)**. The LA compliant function was assessed in asymptomatic and symptomatic patients with mitral regurgitation using 2D strain and strain rate imaging and the LA volumes were calculated using 3D echocardiography **(Chapter 2.2)**. The LA reservoir, conduit and contractile functions in patients with MR were also assessed using 3D echocardiography **(Chapter 2.3)**.

3D echocardiography in assessing left ventricular function

3D echocardiography has been validated against MRI in evaluating LV volumes and function in different patient populations. However, the manual or semiautomatic approach in the analyzing algorithm leads to time consuming analyses and observer variability. We have assessed the Siemens LV-Analysis **(Chapter 3.1 & 3.2)** and TomTec 4D-LV Analysis **(Chapter 3.3)** algorithms in the fully automated way in evaluating the LV function in patients in the real-world conditions.

3D echocardiography in LA reconstruction for facilitating the catheter ablation

Imaging of the LA is important in facilitating LA catheter ablation procedures. CT which is commonly used before the intervention has important limitations, e.g. radiation, high cost and non-real-time information. TOE can be a potential replacement of the pre-interventional CT. To overcome the limited field of view of one single 3D TOE dataset, we have developed a systematic imaging protocol in acquiring a minimal number of 3D datasets which could be registered and fused to reconstruct major parts of the LA **(Chapter 4.1)**. We have further assessed the accuracy of this 3D reconstruction by comparing with CT datasets **(Chapter 4.2)**. Finally, we have assessed the segmentation of multi-cavity from the wide-view fused 3D TOE datasets using a three-stage method by comparing with atlas based segmentation derived from CT angiographic images **(Chapter 4.3)**.

REFERENCES

1. Lang RM, Badano LP, Tsang W, Adams DH, Agricola E, Buck T, Faletra FF, Franke A, Hung J, de Isla LP, Kamp O, Kasprzak JD, Lancellotti P, Marwick TH, McCulloch ML, Monaghan MJ, Nihoyannopoulos P, Pandian NG, Pellikka PA, Pepi M, Roberson DA, Shernan SK, Shirali GS, Sugeng L, Ten Cate FJ, Vannan MA, Zamorano JL, Zoghbi WA. EAE/ASE recommendations for image acquisition and display using three-dimensional echocardiography. *J Am Soc Echocardiogr* 2012;25:3-46.
2. Iung B, Baron G, Butchart EG, Delahaye F, Gohlke-Barwolf C, Levang OW, Tornos P, Vanoverschelde JL, Vermeer F, Boersma E, Ravaud P, Vahanian A. A prospective survey of patients with valvular heart disease in Europe: The Euro Heart Survey on Valvular Heart Disease. *Eur Heart J* 2003;24: 1231-43.
3. Ling LH, Enriquez-Sarano M, Seward JB, Tajik AJ, Schaff HV, Bailey KR, Frye RL. Clinical outcome of mitral regurgitation due to flail leaflet. *N Engl J Med* 1996;335:1417-23.
4. Avierinos JF, Gersh BJ, Melton LJ, 3rd, Bailey KR, Shub C, Nishimura RA, Tajik AJ, Enriquez-Sarano M. Natural history of asymptomatic mitral valve prolapse in the community. *Circulation* 2002;106: 1355-61.
5. Zoghbi WA, Enriquez-Sarano M, Foster E, Grayburn PA, Kraft CD, Levine RA, Nihoyannopoulos P, Otto CM, Quinones MA, Rakowski H, Stewart WJ, Waggoner A, Weissman NJ, American Society of E. Recommendations for evaluation of the severity of native valvular regurgitation with two-dimensional and Doppler echocardiography. *J Am Soc Echocardiogr* 2003;16:777-802.
6. Enriquez-Sarano M, Avierinos JF, Messika-Zeitoun D, Detaint D, Capps M, Nkomo V, Scott C, Schaff HV, Tajik AJ. Quantitative determinants of the outcome of asymptomatic mitral regurgitation. *N Engl J Med* 2005;352:875-83.
7. Bargiggia GS, Tronconi L, Sahn DJ, Recusani F, Raisaro A, De Servi S, Valdes-Cruz LM, Montemartini C. A new method for quantitation of mitral regurgitation based on color flow Doppler imaging of flow convergence proximal to regurgitant orifice. *Circulation* 1991;84:1481-9.
8. Lewis JF, Kuo LC, Nelson JG, Limacher MC, Quinones MA. Pulsed Doppler echocardiographic determination of stroke volume and cardiac output: clinical validation of two new methods using the apical window. *Circulation* 1984;70:425-31.
9. Lancellotti P, Moura L, Pierard LA, Agricola E, Popescu BA, Tribouilloy C, Hagendorff A, Monin JL, Badano L, Zamorano JL, European Association of E. European Association of Echocardiography recommendations for the assessment of valvular regurgitation. Part 2: mitral and tricuspid regurgitation (native valve disease). *Eur J Echocardiogr* 2010;11:307-32.
10. Spencer KT, Mor-Avi V, Gorcsan J, 3rd, DeMaria AN, Kimball TR, Monaghan MJ, Perez JE, Weinert L, Bednarz J, Edelman K, Kwan OL, Glascock B, Hancock J, Baumann C, Lang RM. Effects of aging on left atrial reservoir, conduit, and booster pump function: a multi-institution acoustic quantification study. *Heart* 2001;85:272-7.
11. Benjamin EJ, D'Agostino RB, Belanger AJ, Wolf PA, Levy D. Left atrial size and the risk of stroke and death. The Framingham Heart Study. *Circulation* 1995;92:835-41.
12. Di Tullio MR, Sacco RL, Sciacca RR, Homma S. Left atrial size and the risk of ischemic stroke in an ethnically mixed population. *Stroke* 1999;30:2019-24.
13. Flaker GC, Fletcher KA, Rothbart RM, Halperin JL, Hart RG. Clinical and echocardiographic features of intermittent atrial fibrillation that predict recurrent atrial fibrillation. Stroke Prevention in Atrial Fibrillation (SPAF) Investigators. *Am J Cardiol* 1995;76:355-8.

14. Tsang TS, Gersh BJ, Appleton CP, Tajik AJ, Barnes ME, Bailey KR, Oh JK, Leibson C, Montgomery SC, Seward JB. Left ventricular diastolic dysfunction as a predictor of the first diagnosed nonvalvular atrial fibrillation in 840 elderly men and women. *J Am Coll Cardiol* 2002;40:1636-44.

15. Vaziri SM, Larson MG, Benjamin EJ, Levy D. Echocardiographic predictors of nonrheumatic atrial fibrillation. The Framingham Heart Study. *Circulation* 1994;89:724-30.

16. Beinart R, Boyko V, Schwammenthal E, Kuperstein R, Sagie A, Hod H, Matetzky S, Behar S, Eldar M, Feinberg MS. Long-term prognostic significance of left atrial volume in acute myocardial infarction. *J Am Coll Cardiol* 2004;44:327-34.

17. Moller JE, Hillis GS, Oh JK, Seward JB, Reeder GS, Wright RS, Park SW, Bailey KR, Pellikka PA. Left atrial volume: a powerful predictor of survival after acute myocardial infarction. *Circulation* 2003; 107:2207-12.

18. Dini FL, Cortigiani L, Baldini U, Boni A, Nuti R, Barsotti L, Micheli G. Prognostic value of left atrial enlargement in patients with idiopathic dilated cardiomyopathy and ischemic cardiomyopathy. *Am J Cardiol* 2002;89:518-23.

19. Quinones MA, Greenberg BH, Kopelen HA, Koilpillai C, Limacher MC, Shindler DM, Shelton BJ, Weiner DH. Echocardiographic predictors of clinical outcome in patients with left ventricular dysfunction enrolled in the SOLVD registry and trials: significance of left ventricular hypertrophy. Studies of Left Ventricular Dysfunction. *J Am Coll Cardiol* 2000;35:1237-44.

20. Rossi A, Cicoira M, Zanolla L, Sandrini R, Golia G, Zardini P, Enriquez-Sarano M. Determinants and prognostic value of left atrial volume in patients with dilated cardiomyopathy. *J Am Coll Cardiol* 2002;40:1425.

21. Sabharwal N, Cemin R, Rajan K, Hickman M, Lahiri A, Senior R. Usefulness of left atrial volume as a predictor of mortality in patients with ischemic cardiomyopathy. *Am J Cardiol* 2004;94:760-3.

22. Appleton CP, Galloway JM, Gonzalez MS, Gaballa M, Basnight MA. Estimation of left ventricular filling pressures using two-dimensional and Doppler echocardiography in adult patients with cardiac disease. Additional value of analyzing left atrial size, left atrial ejection fraction and the difference in duration of pulmonary venous and mitral flow velocity at atrial contraction. *J Am Coll Cardiol* 1993;22:1972-82.

23. Simek CL, Feldman MD, Haber HL, Wu CC, Jayaweera AR, Kaul S. Relationship between left ventricular wall thickness and left atrial size: comparison with other measures of diastolic function. *J Am Soc Echocardiogr* 1995;8:37-47.

24. Tsang TS, Barnes ME, Gersh BJ, Bailey KR, Seward JB. Left atrial volume as a morphophysiologic expression of left ventricular diastolic dysfunction and relation to cardiovascular risk burden. *Am J Cardiol* 2002;90:1284-9.

25. Loperfido F, Pennestri F, Digaetano A, Scabbia E, Santarelli P, Mongiardo R, Schiavoni G, Coppola E, Manzoli U. Assessment of left atrial dimensions by cross sectional echocardiography in patients with mitral valve disease. *Br Heart J* 1983;50:570-8.

26. Lester SJ, Ryan EW, Schiller NB, Foster E. Best method in clinical practice and in research studies to determine left atrial size. *Am J Cardiol* 1999;84:829-32.

27. Lang RM, Bierig M, Devereux RB, Flachskampf FA, Foster E, Pellikka PA, Picard MH, Roman MJ, Seward J, Shanewise JS, Solomon SD, Spencer KT, Sutton MS, Stewart WJ, Chamber Quantification Writing G, American Society of Echocardiography's G, Standards C, European Association of E. Recommendations for chamber quantification: a report from the American Society of Echocardiography's Guidelines and Standards Committee and the Chamber Quantification Writing Group, developed in conjunction with the European Association of Echocardiography, a branch of the European Society of Cardiology. *J Am Soc Echocardiogr* 2005;18:1440-63.

28. Wade MR, Chandraratna PA, Reid CL, Lin SL, Rahimtoola SH. Accuracy of nondirected and directed M-mode echocardiography as an estimate of left atrial size. *Am J Cardiol* 1987;60:1208-11.

29. Vandenberg BF, Weiss RM, Kinzey J, Acker M, Stark CA, Stanford W, Burns TL, Marcus ML, Kerber RE. Comparison of left atrial volume by two-dimensional echocardiography and cine-computed tomography. *Am J Cardiol* 1995;75:754-7.

30. Rodevan O, Bjornerheim R, Ljosland M, Maehle J, Smith HJ, Ihlen H. Left atrial volumes assessed by three- and two-dimensional echocardiography compared to MRI estimates. *Int J Card Imaging* 1999;15:397-410.

31. Khankirawatana B, Khankirawatana S, Porter T. How should left atrial size be reported? Comparative assessment with use of multiple echocardiographic methods. *Am Heart J* 2004;147:369-74.

32. Kircher B, Abbott JA, Pau S, Gould RG, Himelman RB, Higgins CB, Lipton MJ, Schiller NB. Left atrial volume determination by biplane two-dimensional echocardiography: validation by cine computed tomography. *Am Heart J* 1991;121:864-71.

33. Kataoka A, Funabashi N, Takahashi A, Yajima R, Takahashi M, Uehara M, Takaoka H, Saito M, Yamaguchi C, Lee K, Nomura F, Komuro I. Quantitative evaluation of left atrial volumes and ejection fraction by 320-slice computed-tomography in comparison with three- and two-dimensional echocardiography: a single-center retrospective-study in 22 subjects. *Int J Cardiol* 2011;153: 47-54.

34. Miyasaka Y, Tsujimoto S, Maeba H, Yuasa F, Takehana K, Dote K, Iwasaka T. Left atrial volume by real-time three-dimensional echocardiography: validation by 64-slice multidetector computed tomography. *J Am Soc Echocardiogr* 2011;24:680-6.

35. Rohner A, Brinkert M, Kawel N, Buechel RR, Leibundgut G, Grize L, Kuhne M, Bremerich J, Kaufmann BA, Zellweger MJ, Buser P, Osswald S, Handke M. Functional assessment of the left atrium by real-time three-dimensional echocardiography using a novel dedicated analysis tool: initial validation studies in comparison with computed tomography. *Eur J Echocardiogr* 2011;12: 497-505.

36. Buechel RR, Stephan FP, Sommer G, Bremerich J, Zellweger MJ, Kaufmann BA. Head-to-head comparison of two-dimensional and three-dimensional echocardiographic methods for left atrial chamber quantification with magnetic resonance imaging. *J Am Soc Echocardiogr* 2013;26: 428-35.

37. Delgado V, Vidal B, Sitges M, Tamborero D, Mont L, Berruezo A, Azqueta M, Pare C, Brugada J. Fate of left atrial function as determined by real-time three-dimensional echocardiography study after radiofrequency catheter ablation for the treatment of atrial fibrillation. *Am J Cardiol* 2008;101: 1285-90.

38. Marsan NA, Tops LF, Holman ER, Van de Veire NR, Zeppenfeld K, Boersma E, van der Wall EE, Schalij MJ, Bax JJ. Comparison of left atrial volumes and function by real-time three-dimensional echocardiography in patients having catheter ablation for atrial fibrillation with persistence of sinus rhythm versus recurrent atrial fibrillation three months later. *Am J Cardiol* 2008;102:847-53.

39. Fatema K, Barnes ME, Bailey KR, Abhayaratna WP, Cha S, Seward JB, Tsang TS. Minimum vs. maximum left atrial volume for prediction of first atrial fibrillation or flutter in an elderly cohort: a prospective study. *Eur J Echocardiogr* 2009;10:282-6.

40. Caselli S, Canali E, Foschi ML, Santini D, Di Angelantonio E, Pandian NG, De Castro S. Long-term prognostic significance of three-dimensional echocardiographic parameters of the left ventricle and left atrium. *Eur J Echocardiogr* 2010;11:250-6.

41. Russo C, Jin Z, Homma S, Rundek T, Elkind MS, Sacco RL, Di Tullio MR. Left atrial minimum volume and reservoir function as correlates of left ventricular diastolic function: impact of left ventricular systolic function. *Heart* 2012;98:813-20.

42. Russo C, Jin Z, Liu R, Iwata S, Tugcu A, Yoshita M, Homma S, Elkind MS, Rundek T, Decarli C, Wright CB, Sacco RL, Di Tullio MR. LA volumes and reservoir function are associated with subclinical cerebrovascular disease: the CABL (Cardiovascular Abnormalities and Brain Lesions) study. *JACC Cardiovasc Imaging* 2013;6:313-23.

43. Wu VC, Takeuchi M, Kuwaki H, Iwataki M, Nagata Y, Otani K, Haruki N, Yoshitani H, Tamura M, Abe H, Negishi K, Lin FC, Otsuji Y. Prognostic value of LA volumes assessed by transthoracic 3D echocardiography: comparison with 2D echocardiography. *JACC Cardiovasc Imaging* 2013;6:1025-35.

44. Kihara Y, Sasayama S, Miyazaki S, Onodera T, Susawa T, Nakamura Y, Fujiwara H, Kawai C. Role of the left atrium in adaptation of the heart to chronic mitral regurgitation in conscious dogs. *Circ Res* 1988;62:543-53.

45. Anwar AM, Geleijnse ML, Soliman OI, Nemes A, ten Cate FJ. Left atrial Frank–Starling law assessed by real-time, three-dimensional echocardiographic left atrial volume changes. *Heart* 2007;93: 1393-7.

46. Blondheim DS, Osipov A, Meisel SR, Frimerman A, Shochat M, Shotan A. Relation of left atrial size to function as determined by transesophageal echocardiography. *Am J Cardiol* 2005;96:457-63.

47. Matsuzaki M, Tamitani M, Toma Y, Ogawa H, Katayama K, Matsuda Y, Kusukawa R. Mechanism of augmented left atrial pump function in myocardial infarction and essential hypertension evaluated by left atrial pressure-dimension relation. *Am J Cardiol* 1991;67:1121-6.

48. Leitman M, Lysyansky P, Sidenko S, Shir V, Peleg E, Binenbaum M, Kaluski E, Krakover R, Vered Z. Two-dimensional strain-a novel software for real-time quantitative echocardiographic assessment of myocardial function. *J Am Soc Echocardiogr* 2004;17:1021-9.

49. Pirat B, Khoury DS, Hartley CJ, Tiller L, Rao L, Schulz DG, Nagueh SF, Zoghbi WA. A novel feature-tracking echocardiographic method for the quantitation of regional myocardial function: validation in an animal model of ischemia-reperfusion. *J Am Coll Cardiol* 2008;51:651-9.

50. Alharthi MS, Jiamsripong P, Calleja A, Sengupta PP, McMahon EM, Khandheria B, Tajik AJ, Belohlavek M. Selective echocardiographic analysis of epicardial and endocardial left ventricular rotational mechanics in an animal model of pericardial adhesions. *Eur J Echocardiogr* 2009;10: 357-62.

51. Jiamsripong P, Alharthi MS, Calleja AM, McMahon EM, Mookadam F, Khandheria BK, Belohlavek M. Quantification of left ventricular twisting mechanics by velocity vector imaging in an animal model of pericardial adhesions. *Ultrasound Med Biol* 2009;35:1963-72.

52. Kim DH, Kim HK, Kim MK, Chang SA, Kim YJ, Kim MA, Sohn DW, Oh BH, Park YB. Velocity vector imaging in the measurement of left ventricular twist mechanics: head-to-head one way comparison between speckle tracking echocardiography and velocity vector imaging. *J Am Soc Echocardiogr* 2009;22:1344-52.

53. Korinek J, Wang J, Sengupta PP, Miyazaki C, Kjaergaard J, McMahon E, Abraham TP, Belohlavek M. Two-dimensional strain--a Doppler-independent ultrasound method for quantitation of regional deformation: validation in vitro and in vivo. *J Am Soc Echocardiogr* 2005;18:1247-53.

54. Korinek J, Kjaergaard J, Sengupta PP, Yoshifuku S, McMahon EM, Cha SS, Khandheria BK, Belohlavek M. High spatial resolution speckle tracking improves accuracy of 2-dimensional strain measurements: an update on a new method in functional echocardiography. *J Am Soc Echocardiogr* 2007; 20:165-70.

55. Chen J, Cao T, Duan Y, Yuan L, Yang Y. Velocity vector imaging in assessing the regional systolic function of patients with post myocardial infarction. *Echocardiography* 2007;24:940-5.

56. Amundsen BH, Helle-Valle T, Edvardsen T, Torp H, Crosby J, Lyseggen E, Stoylen A, Ihlen H, Lima JA, Smiseth OA, Slordahl SA. Noninvasive myocardial strain measurement by speckle tracking echocardiography: validation against sonomicrometry and tagged magnetic resonance imaging. *J Am Coll Cardiol* 2006;47:789-93.

57. Cameli M, Caputo M, Mondillo S, Ballo P, Palmerini E, Lisi M, Marino E, Galderisi M. Feasibility and reference values of left atrial longitudinal strain imaging by two-dimensional speckle tracking. *Cardiovasc Ultrasound* 2009;7:6.

58. Vianna-Pinton R, Moreno CA, Baxter CM, Lee KS, Tsang TS, Appleton CP. Two-dimensional speckle-tracking echocardiography of the left atrium: feasibility and regional contraction and relaxation differences in normal subjects. *J Am Soc Echocardiogr* 2009;22:299-305.

59. Wang TJ, Evans JC, Benjamin EJ, Levy D, LeRoy EC, Vasan RS. Natural history of asymptomatic left ventricular systolic dysfunction in the community. *Circulation* 2003;108:977-82.

60. White HD, Norris RM, Brown MA, Brandt PW, Whitlock RM, Wild CJ. Left ventricular end-systolic volume as the major determinant of survival after recovery from myocardial infarction. *Circulation* 1987;76:44-51.

61. King DL, Harrison MR, King DL, Jr., Gopal AS, Martin RP, DeMaria AN. Improved reproducibility of left atrial and left ventricular measurements by guided three-dimensional echocardiography. *J Am Coll Cardiol* 1992;20:1238-45.

62. Gopal AS, Keller AM, Rigling R, King DL, Jr., King DL. Left ventricular volume and endocardial surface area by three-dimensional echocardiography: comparison with two-dimensional echocardiography and nuclear magnetic resonance imaging in normal subjects. *J Am Coll Cardiol* 1993;22:258-70.

63. Handschumacher MD, Lethor JP, Siu SC, Mele D, Rivera JM, Picard MH, Weyman AE, Levine RA. A new integrated system for three-dimensional echocardiographic reconstruction: development and validation for ventricular volume with application in human subjects. *J Am Coll Cardiol* 1993; 21:743-53.

64. Roelandt JR, ten Cate FJ, Vletter WB, Taams MA. Ultrasonic dynamic three-dimensional visualization of the heart with a multiplane transesophageal imaging transducer. *J Am Soc Echocardiogr* 1994;7:217-29.

65. Jiang L, Vazquez de Prada JA, Handschumacher MD, Vuille C, Guererro JL, Picard MH, Joziatis JT, Fallon JT, Weyman AE, Levine RA. Quantitative three-dimensional reconstruction of aneurysmal left ventricles. In vitro and in vivo validation. *Circulation* 1995;91:222-30.

66. Nosir YF, Fioretti PM, Vletter WB, Boersma E, Salustri A, Postma JT, Reijs AE, Ten Cate FJ, Roelandt JR. Accurate measurement of left ventricular ejection fraction by three-dimensional echocardiography. A comparison with radionuclide angiography. *Circulation* 1996;94:460-6.

67. Buck T, Hunold P, Wentz KU, Tkalec W, Nesser HJ, Erbel R. Tomographic three-dimensional echocardiographic determination of chamber size and systolic function in patients with left ventricular aneurysm: comparison to magnetic resonance imaging, cineventriculography, and two-dimensional echocardiography. *Circulation* 1997;96:4286-97.

68. Kuhl HP, Franke A, Merx M, Hoffmann R, Puschmann D, Hanrath P. Rapid quantification of left ventricular function and mass using transoesophageal three-dimensional echocardiography: validation of a method that uses long-axis cutplanes. *Eur J Echocardiogr* 2000;1:213-21.

69. Jenkins C, Bricknell K, Hanekom L, Marwick TH. Reproducibility and accuracy of echocardiographic measurements of left ventricular parameters using real-time three-dimensional echocardiography. *J Am Coll Cardiol* 2004;44:878-86.

70. Gutierrez-Chico JL, Zamorano JL, Perez de Isla L, Orejas M, Almeria C, Rodrigo JL, Ferreiros J, Serra V, Macaya C. Comparison of left ventricular volumes and ejection fractions measured by three-dimensional echocardiography versus by two-dimensional echocardiography and cardiac magnetic resonance in patients with various cardiomyopathies. *Am J Cardiol* 2005;95:809-13.

71. Jacobs LD, Salgo IS, Goonewardena S, Weinert L, Coon P, Bardo D, Gerard O, Allain P, Zamorano JL, de Isla LP, Mor-Avi V, Lang RM. Rapid online quantification of left ventricular volume from real-time three-dimensional echocardiographic data. *Eur Heart J* 2006;27:460-8.

72. Jenkins C, Chan J, Hanekom L, Marwick TH. Accuracy and feasibility of online 3-dimensional echocardiography for measurement of left ventricular parameters. *J Am Soc Echocardiogr* 2006; 19:1119-28.

73. Jenkins C, Leano R, Chan J, Marwick TH. Reconstructed versus real-time 3-dimensional echocardiography: comparison with magnetic resonance imaging. *J Am Soc Echocardiogr* 2007;20:862-8.

74. Chukwu EO, Barasch E, Mihalatos DG, Katz A, Lachmann J, Han J, Reichek N, Gopal AS. Relative importance of errors in left ventricular quantitation by two-dimensional echocardiography: insights from three-dimensional echocardiography and cardiac magnetic resonance imaging. *J Am Soc Echocardiogr* 2008;21:990-7.

75. Jenkins C, Moir S, Chan J, Rakhit D, Haluska B, Marwick TH. Left ventricular volume measurement with echocardiography: a comparison of left ventricular opacification, three-dimensional echocardiography, or both with magnetic resonance imaging. *Eur Heart J* 2009;30:98-106.

76. Marsan NA, Westenberg JJ, Roes SD, van Bommel RJ, Delgado V, van der Geest RJ, de Roos A, Klautz RJ, Reiber JC, Bax JJ. Three-dimensional echocardiography for the preoperative assessment of patients with left ventricular aneurysm. *Ann Thorac Surg* 2011;91:113-21.

77. Calkins H, Brugada J, Packer DL, Cappato R, Chen SA, Crijns HJ, Damiano RJ, Jr., Davies DW, Haines DE, Haissaguerre M, Iesaka Y, Jackman W, Jais P, Kottkamp H, Kuck KH, Lindsay BD, Marchlinski FE, McCarthy PM, Mont JL, Morady F, Nademanee K, Natale A, Pappone C, Prystowsky E, Raviele A, Ruskin JN, Shemin RJ, Heart Rhythm S, European Heart Rhythm A, European Cardiac Arrhythmia S, American College of C, American Heart A, Society of Thoracic S. HRS/EHRA/ECAS expert consensus statement on catheter and surgical ablation of atrial fibrillation: recommendations for personnel, policy, procedures and follow-up. A report of the Heart Rhythm Society (HRS) Task Force on Catheter and Surgical Ablation of Atrial Fibrillation developed in partnership with the European Heart Rhythm Association (EHRA) and the European Cardiac Arrhythmia Society (ECAS); in collaboration with the American College of Cardiology (ACC), American Heart Association (AHA), and the Society of Thoracic Surgeons (STS). Endorsed and approved by the governing bodies of the American College of Cardiology, the American Heart Association, the European Cardiac Arrhythmia Society, the European Heart Rhythm Association, the Society of Thoracic Surgeons, and the Heart Rhythm Society. *Europace* 2007;9:335-79.

78. Haissaguerre M, Jais P, Shah DC, Takahashi A, Hocini M, Quiniou G, Garrigue S, Le Mouroux A, Le Metayer P, Clementy J. Spontaneous initiation of atrial fibrillation by ectopic beats originating in the pulmonary veins. *N Engl J Med* 1998;339:659-66.

79. Chen SA, Hsieh MH, Tai CT, Tsai CF, Prakash VS, Yu WC, Hsu TL, Ding YA, Chang MS. Initiation of atrial fibrillation by ectopic beats originating from the pulmonary veins: electrophysiological characteristics, pharmacological responses, and effects of radiofrequency ablation. *Circulation* 1999;100:1879-86.

80. Pappone C, Rosanio S, Oreto G, Tocchi M, Gugliotta F, Vicedomini G, Salvati A, Dicandia C, Mazzone P, Santinelli V, Gulletta S, Chierchia S. Circumferential radiofrequency ablation of pulmonary vein ostia: A new anatomic approach for curing atrial fibrillation. *Circulation* 2000;102:2619-28.

81. Chen SA, Tai CT. Catheter ablation of atrial fibrillation originating from the non-pulmonary vein foci. *J Cardiovasc Electrophysiol* 2005;16:229-32.

82. Lee SH, Tai CT, Hsieh MH, Tsao HM, Lin YJ, Chang SL, Huang JL, Lee KT, Chen YJ, Cheng JJ, Chen SA. Predictors of non-pulmonary vein ectopic beats initiating paroxysmal atrial fibrillation: implication for catheter ablation. *J Am Coll Cardiol* 2005;46:1054-9.

83. Lin WS, Tai CT, Hsieh MH, Tsai CF, Lin YK, Tsao HM, Huang JL, Yu WC, Yang SP, Ding YA, Chang MS, Chen SA. Catheter ablation of paroxysmal atrial fibrillation initiated by non-pulmonary vein ectopy. *Circulation* 2003;107:3176-83.

84. Shah D, Haissaguerre M, Jais P, Hocini M. Nonpulmonary vein foci: do they exist? *Pacing Clin Electrophysiol* 2003;26:1631-5.

85. Kato R, Lickfett L, Meininger G, Dickfeld T, Wu R, Juang G, Angkeow P, LaCorte J, Bluemke D, Berger R, Halperin HR, Calkins H. Pulmonary vein anatomy in patients undergoing catheter ablation of atrial fibrillation: lessons learned by use of magnetic resonance imaging. *Circulation* 2003;107: 2004-10.

Part II

3D echocardiography in mitral valve regurgitation

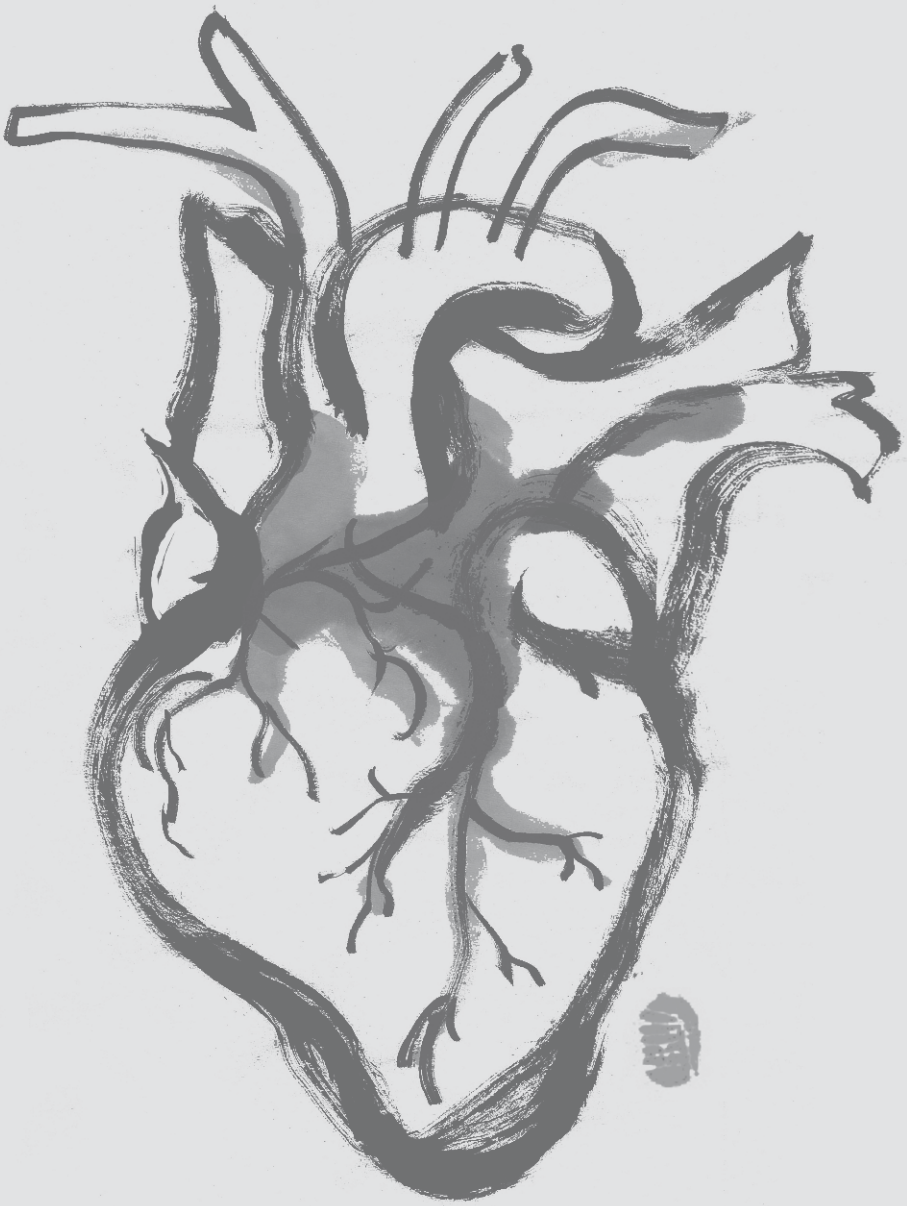

Chapter 2.1

Geometric Errors of the Pulsed Wave Doppler Flow Method in Quantifying Degenerative Mitral Valve Regurgitation: A Three-Dimensional Echocardiography Study

Ben Ren
Lotte E. de Groot - de Laat
Jacky McGhie
Wim B. Vletter
Folkert J. ten Cate
Marcel L. Geleijnse

J Am Soc Echocardiogr 2013;26:261-9.

ABSTRACT

Background The aim of this study was to estimate geometric errors made by the two-dimensional (2D) transthoracic echocardiographic (TTE) pulsed wave Doppler flow (PWDF) method in calculating regurgitant volume (R Vol) and effective regurgitant orifice area (EROA) in degenerative mitral regurgitation (MR) by comparison with the three-dimensional (3D) transesophageal echocardiographic (TEE) PWDF method.

Methods RVol and EROA were calculated in 22 patients with degenerative MR using the conventional 2D TTE PWDF method on the basis of monoplanar dimensions and a circular geometric assumption of the crosssectional areas (CSAs) of the mitral annulus (MA) and the left ventricular outflow tract (LVOT) and the 3D TEE PWDF method, in which the CSAs of the MA and LVOT were measured directly in "en face" views. Diameters of the MA and LVOT were also measured in similar views as with TTE imaging in 3D TEE data sets.

Results Both the MA and LVOT were oval. Mean MA diameters were 41 ± 4 mm (3D TEE major axis), 31 ± 4 mm (3D TEE minor axis), 39 ± 5 mm (2D TTE imaging), and 38 ± 5 mm (2D TEE imaging). Mean LVOT diameters were 29 ± 4 mm (3D TEE major axis), 21 ± 2mm (3D TEE minor axis), 22 ± 2 mm (2D TTE imaging), and 23 ± 2 mm (2D TEE imaging). Compared with 3D TEE measurements, mitral annular CSA was overestimated by 13 ± 12% on 2D TTE imaging and by 7 ± 14% on 2D TEE imaging, while LVOT CSA was underestimated by 23 ± 10% and 17 ± 10%, respectively. Mean values of RVol were 95 ± 43 mL (3D TEE PWDF), 137 ± 56 mL (2D TTE PWDF), 120 ± 45 mL (2D TEE PWDF), and 111 ± 49 mL (flow convergence). Mean EROAs were 69 ± 34 mm^2 (3D TEE PWDF), 98 ± 45 mm^2 (2D TTE PWDF), 88 ± 42 mm^2 (2D TEE PWDF), and 79 ± 36 mm^2 (flow convergence). Observer variability for 3D TEE imaging was better than for 2D imaging.

Conclusions The 2D TTE PWDF method overestimates mitral RVol and EROA significantly because monoplanar 2D measurements represent mitral annular major-axis diameter and LVOT minor-axis diameter, and assumed circular CSAs of the MA and LVOT are oval.

Keywords: mitral regurgitation, three-dimensional echocardiography, pulsed wave Doppler flow method

Quantification of mitral regurgitation (MR) is essential to determine the severity of MR[1] and clinical outcomes[2]. The two most used quantitative parameters are the regurgitant volume (R Vol) and effective regurgitant orifice area (EROA), which may be calculated by the flow convergence method and pulsed wave Doppler flow (PWDF) method as recommended[1,3]. However, both of these two methods suffer from geometric limitations of two-dimensional (2D) echocardiography. The flow convergence method potentially underestimates the R Vol and EROA in functional MR, because the shape of the flow convergence zone may be elliptic instead of hemispheric in this situation[4-11]. In the PWDF method, important geometric errors are made in calculating the cross-sectional areas (CSAs) of the mitral annulus (MA) and left ventricular outflow tract (LVOT)[12], because of the monoplanar measurements and assumption about the geometry. This study sought to ascertain the geometric errors the traditional 2D transthoracic ehchocardiography (TTE PWDF) method makes in calculating the R Vol and EROA in patients with degenerative MR, by comparing it with the 3D transesophageal echocardiography (TEE) PWDF method. Using the latter method, the CSAs of the MA and LVOT were measured directly in state-of-the-art "en face" views in 3D TEE.

PATIENTS AND METHODS

Study population

From November 2009 to September 2011, we enrolled prospectively 96 consecutive patients referred to our center for potential mitral valve (MV) repair and had undergone both baseline TTE and TEE examinations. In the present study, we included patients with: 1) degenerative MR according to the preoperative TTE; 2) P2 scallop prolapse confirmed by both the 3D TEE exam and surgery; 3) good 3D image quality with complete region of interest and without stitching artifacts. The exclusion criteria were: 1) MR due to other etiologies or mechanisms, e.g., endocarditis, functional MR, etc. (n = 39); 2) Prolapse of other scallops (n = 19); 3) severely calcified MA (n = 11); 4) more than trivial aortic valve regurgitation (n = 3); 5) poor general image quality (n = 2). Eventually, 22 patients (12 men, aged 64 ± 10 years) were included in the study. The protocols were approved by the institutional review board and informed consent was obtained from all patients.

Pulsed wave Doppler flow method

A. 2D TTE measurements

Two-dimensional TTE was performed using the iE33 ultrasound system (Philips Medical System) with the S5-1 transducer. The pulsed wave Doppler sample was carefully placed as parallel as possible (angle < 20°)[13] to the blood flow in the apical 4-chamber and

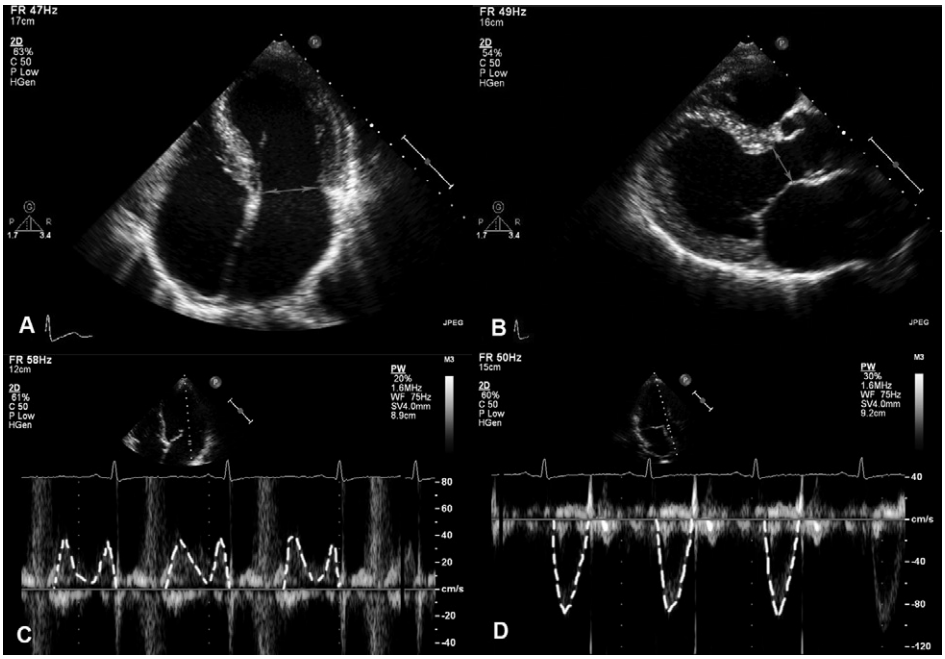

Figure 1 Measurements of the 2D transthoracic echocardiography pulsed wave Doppler flow method: A, the diameter of the mitral annulus was measured between the inner edges of the base of the posterior and anterior leaflets in early-to-mid diastole at the maximal opening of the mitral valve (2-3 frames after the mitral valve opens) in the apical 4-chamber view; B, the diameter of the left ventricular outflow tract was measured just below the aortic valve in early-to-mid systole in the parasternal long-axis view; C, mitral annulus inflow pulsed wave Doppler was traced to obtain the velocity–time integral of the mitral inflow; D, left ventricular outflow tract pulsed wave Doppler was traced to obtain the velocity–time integral of the ventricular outflow.

3-chamber views to obtain the Doppler spectral profiles of the MA and LVOT. The MA diameter was measured between the inner edges of the base of posterior and anterior leaflets in early-to-mid diastole at the maximal mitral valve opening in the apical 4-chamber view; the LVOT diameter was measured just below the aortic valve in early-to-mid systole in the parasternal long-axis view [3,13]. Both diameters were measured at the level at which the volume sample had been placed. The modal velocity profile on Doppler recordings was traced to obtain the velocity–time integral (VTI) (Figure 1). The regurgitant VTI was averaged from measurements in the apical 4-chamber and 3-chamber views. All measurements were averaged over three cardiac cycles.

B. 3D TEE measurements

Three-dimensional TEE was performed using the iE33 ultrasound system (Philips Medical System) with the X7-2t matrix-array transducer. Electrocardiographically gated full volume datasets (built from seven subvolumes) were acquired at the mid esophageal level during breath-hold with the ultrasound focus on the mitral valve in the 4-chamber

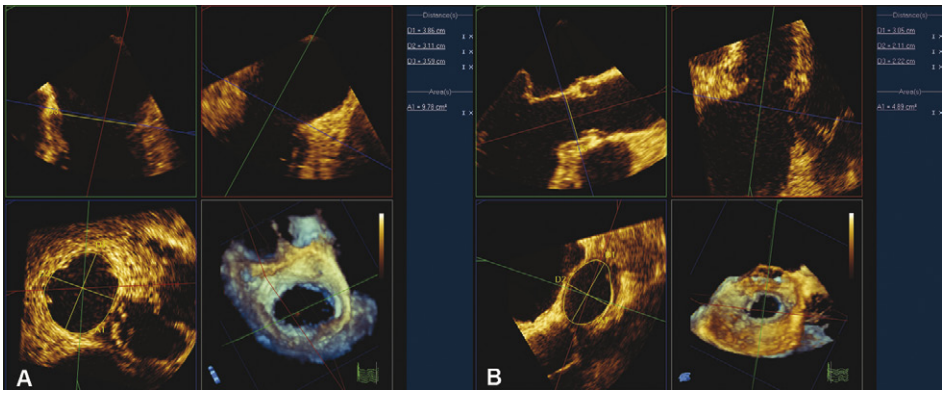

Figure 2 Measurements of the 3D and 2D transesophageal echocardiography pulsed wave Doppler flow methods: the 3D transoesopheageal echocardiographic datasets were displayed as three orthogonal images of the mitral annulus (A) and left ventricular outflow tract (B) and the visualization of the entire structures was optimized by adjusting the reference planes (the green, red and blue planes). The blue planes showed the "en face" views of the mitral annulus and left ventricular outflow tract, in which the inner border of the cross-sectional areas of the mitral annulus and left ventricular outflow tract were traced manually and the cross-sectional areas and major and minor diameters were measured directly. The green plane (A) was adjusted to 4-chamber view and the mitral annulus diameter was measured; the green plane (B) was adjusted to long-axis view and the left ventricular outflow tract diameter was measured. All measurements were performed at the level at which the sample volume of pulsed wave Doppler had been placed in the 2D transthoracic echocardiography examinations.

view and on the LVOT in the long-axis view. Care was taken to include the complete MA and LVOT circumferences throughout the acquisition. Each full volume dataset was digitally stored and exported to QLAB 8.0 3DQ software (Philips Medical System) for offline analysis. The "en face" views of the MA or LVOT were revealed at time points during the cardiac cycle similar as in the 2D TTE measurements and adjusted to the level at which the pulsed wave Doppler volume sample had been placed in 2D TTE. Subsequently, the inner border of the cross-sectional planes of the MA and LVOT as well as the major and minor axis diameters were measured (Figure 2).

C. 2D TEE measurements

By adjusting the orthogonal multiplanar reconstruction views of the 3D TEE datasets, the diameters of the MA was measured in the 4-chamber view in early-to-mid diastole at the maximal opening of the MV and that of the LVOT was measured in early systole in the long-axis view (Figure 2). Both diameters were measured at the level at which the volume sample had been placed.

Using the same VTI_{MR}, VTI_{MA}, and VTI_{LVOT} values obtained during the 2D TTE examinations, the 2D TTE, 3D TEE and 2D TEE measurements of the diameters or CSAs were taken into the following formulas to calculate the R Vol and EROA:

$$R\ Vol = SV_{MA} - SV_{LVOT} = \pi r_{MA}^2 \times VTI_{MA} - \pi r_{LVOT}^2 \times VTI_{LVOT}$$
$$EROA = R\ Vol / VTI_{MR}$$

where r = radius; SV = stroke volume

Flow convergence method

The flow convergence of MR was shown in a zoomed view of color flow Doppler aliasing at the Nyquist velocity limit (30–40cm/s) in the apical 4-chamber and 3-chamber views. The selected cine loop was reviewed stepwise and a clearly defined mid-to-late systolic maximal flow convergence zone was measured from the zenith to the regurgitant orifice. The averaged values measured in both views were used to calculate the R Vol and EROA from the following formulas:

$$EROA = 2\pi r^2 \times Va / PkV_{Regurg}$$
$$R\ Vol = EROA \times VTI_{MR}$$

where r = radius of the flow convergence; Va = aliasing velocity; PkV_{Regurg} = peak velocity of MR

Vena contracta (VC) width

The VC width of the MR jet was measured at narrowest portion of the regurgitant jet in a zoom mode with an adapted Nyquist limit (59.3 cm/s) and averaged from the measurements in the apical 4-chamber and 3-chamber views.

Statistical Methods

All values were expressed as median (minimum, maximum) or mean ± standard deviation. One-factorial repeated measures ANOVA or Friedman's analysis of variance was used to compare the diameters, CSAs, SVs, R Vols and EROAs calculated by the different methods. When differences were found, any two methods were compared using the paired *t* test or Wilcoxon signed-rank test with Bonferroni correction. Linear regression analysis was used to assess the correlation of variables of interest. Agreement between methods was assessed by Bland–Altman method, in which differences were plotted against the means of measurements. Inter- and intraobserver variabilities were tested by analyzing 2D and 3D images by two blinded observers (BR, LdGdL) and by the same observer (BR) at two difference times. The results were analyzed by the relative difference (expressed as the absolute difference divided by mean) and Bland–Altman method.

RESULTS

Baseline characteristics of the patient population

All patients included underwent the MV repair. The baseline TTE was to ascertain the severity of the MR and the TEE performed on the same day was to find out the exact mechanism of the MR and guide the selection of the cardiac surgeon. However, the preoperative TEE was declined or unsuccessful in eight patients and in one patient the image quality was inferior due to poor general image quality and 3D stitching artifacts. For these nine patients, the intraoperative TEE under general anesthesia was chosen as the baseline TEE study. The intraoperative TEE was performed within 24 hours of the baseline TTE in three patients and 6 to 35 days after the baseline TTE in six patients. Of the 13 patients who had both baseline TTE and TEE in the out-patient clinic, nine of them also underwent intraoperative TEE. The time period between the preoperative TEE and intraoperative TEE was 1 to 32 days. Although the hemodynamic characteristics of these nine patients changed significantly, the shape and size of the MA and LVOT remained relatively constant (Table 1).

Table 1 Comparisons of the patients' hemodynamic characteristics and mitral annulus and left ventricular outflow tract morphologies in the preoperative and intraoperative transesophageal echocardiography (TEE) examinations (n = 9).

	Preoperative TEE	Intraoperative TEE
Heart rate (bpm)	97 (71, 123)	68 (48, 99)
Blood pressure (mmHg)		
Systolic	140 (110, 163)	105 (80, 125)
Diastolic	80 (60, 88)	50 (40, 75)
Mitral annulus		
Major-minor axis diameter ratio	1.3 (1.0, 1.6)	1.4 (1.1, 1.5)
Cross-sectional area (mm^2)	1,058 (840, 1,542)	1,105 (747, 1,788)
Left ventricular outflow tract		
Major-minor axis diameter ratio	1.4 (1.2, 1.7)	1.4 (1.1, 1.5)
Cross-sectional area (mm^2)	497 (443, 723)	548 (424, 630)

All values were expressed as median (minimum, maximum).

Comparison of the 2D and 3D dimensions and cross-sectional areas of mitral annulus and left ventricular outflow tract

Frame and volume rates of the 2D and 3D datasets were of no differences (49 ± 6 vs. 46 ± 8). As shown in Table 2, the 2D TTE and 2D TEE diameters of the MA and LVOT were not significant different from each other. Both the MA and LVOT were oval in the 3D "en face" views with a significant difference between the major and minor axis diameters

Table 2 The diameters and cross-sectional areas of the mitral annulus and left ventricular outflow tract obtained with the 2D and 3D measurements.

	Diameter (mm)				Cross-sectional area (mm^2)		
	2D measurements		3D TEE measurements		2D measurements		3D TEE measurements
	TTE	TEE	Major axis	Minor axis	TTE	TEE	
Mitral annulus	39 ± 5*†	38 ± 5‡	41 ± 4φ	31 ± 4	1,185 ± 304*ψ	1,117 ± 254τ	1,050 ± 247
Left ventricular outflow tract	22 ± 2*†	23 ± 2‡	29 ± 4φ	21 ± 2	391 ± 73*ψ	426 ± 80‡	517 ± 110

*Non-significant (NS) for 2D TTE vs. 2D TEE measurements.
†$p < 0.05$ for 2D TTE vs. 3D TEE measurements.
‡$p < 0.001$ for 2D TEE vs. 3D TEE measurements.
φ$p < 0.001$ for 3D TEE major vs. minor axis measurements.
ψ$p < 0.001$ for 2D TTE vs. 3D TEE measurements.
τNS for 2D TEE vs. 3D TEE measurements.

(both $p < 0.001$). The major-minor diameter ratio of the MA was 1.3 ± 0.2 and that of the LVOT was 1.4 ± 0.2. The 2D diameters of the MA and LVOT were significantly different from both the major and minor axis diameter (all $p < 0.05$). The CSAs of the MA and LVOT calculated from 2D TTE and 2D TEE diameters were similar. For the CSA of the MA, the 2D TTE measurements were significantly different from the 3D TEE directly measurement ($p < 0.001$), and overestimated the CSA by 13% ± 12%; although the 2D TEE measurements were not significantly different from the 3D TEE measurements, the CSA was still overestimated by 7% ± 14%. For the CSA of the LVOT, both 2D TTE and 2D TEE measurements were significantly different from the 3D TEE direct measurements (both $p < 0.001$), and the CSAs was underestimated by 23% ± 10% by the 2D TTE measurements and 17% ± 10% by the 2D TEE measurements.

Comparison of the mitral regurgitant volume and effective regurgitant orifice area by the 2D and 3D pulsed wave Doppler flow and flow convergence methods

As a result of the differences in CSAs obtained by 2D and 3D measurements, the SV at the MA level was overestimated by 13% ± 12% by the 2D TTE measurements and 7% ± 14% by the 2D TEE measurements, while the SV at the LVOT level was underestimated by 23% ± 10% by the 2D TTE measurements and 17% ± 10% by the 2D TEE measurements. The R Vol and EROA obtained by the 3D TEE PWDF method were significantly smaller than those calculated by the 2D PWDF methods (all $p < 0.001$) (Table 3). Compared with the 3D TEE measurements, the R Vol and EROA were overestimated by 54% ± 39% by the 2D TTE PWDF method and 39% ± 40% by the 2D TEE PWDF method.

Compared with the flow convergence method, the R Vols obtained by the 3D PWDF methods correlated better with the R Vols obtained by using the flow convergence method than the 2D PWDF methods did (Figure 3: 2D TTE PWDF vs. flow convergence

Table 3 The stroke volumes at the level of the mitral annulus and left ventricular outflow tract, mitral regurgitation volume and effective regurgitant orifice area obtained by the flow convergence, 2D and 3D PWDF methods.

	Flow convergence method	Pulsed wave Doppler flow method		
		2D TTE	2D TEE	3D TEE
Stroke volume (ml)				
Mitral annulus	—	198 ± 55*†	186 ± 44‡	175 ± 42
Left ventricular outflow tract	—	61 ± 21*†	66 ± 20φ	80 ± 23
Regurgitant volume (ml)	111 ± 49	137 ± 56ψτ	120 ± 45φσ	95 ± 43ς
Effective regurgitant orifice area (mm²)	79 ± 36	98 ± 45*τ	88 ± 42φσ	69 ± 34ς

*Non significant (NS) for 2D TTE vs. 2D TEE pulsed wave Doppler flow methods.
†$p < 0.001$ for 2D TTE vs. 3D TEE pulsed wave Doppler flow methods.
‡NS for 2D TEE vs. 3D TEE pulsed wave Doppler flow methods.
φ$p < 0.001$ for 2D TEE vs. 3D TEE pulsed wave Doppler flow methods.
ψ$p < 0.05$ for 2D TTE vs. 2D TEE pulsed wave Doppler flow methods.
τ$p < 0.001$ for 2D TTE pulsed wave Doppler flow vs. flow convergence methods.
σNS for 2D TEE pulsed wave Doppler flow vs. flow convergence methods.
ς$p < 0.05$ for 3D TEE pulsed wave Doppler flow vs. flow convergence methods.

r = 0.91, 2D TEE PWDF vs. flow convergence r = 0.72, 3D PWDF vs. flow convergence r = 0.94). Comparisons with the flow convergence method revealed that the R Vol was overestimated by 24% ± 23% by the 2D TTE PWDF method (137 ± 56 ml vs. 111 ± 49 ml, $p < 0.001$) and 14% ± 40% by the 2D TEE PWDF method (120 ± 45 ml vs. 111 ± 49 ml), but underestimated by 17% ± 17% by the 3D TEE PWDF method (95 ± 43 ml vs. 111 ± 49 ml, $p < 0.05$). A very similar pattern was found for the EROA. Here too, the EROAs obtained by the 3D PWDF method correlated better with the EROAs obtained by using the flow convergence method that the 2D PWDF methods did (Figure 3: 2D TTE PWDF vs. flow convergence r = 0.92, 2D TEE PWDF vs. flow convergence r = 0.76, 3D PWDF vs. flow convergence r = 0.95). The magnitude of the overestimation and underestimation by comparison with the flow convergence method was the same as for the R Vol: the EROA was overestimated by 24% ± 23% by the 2D TTE PWDF method (98 ± 45 mm^2 vs. 79 ± 36 mm^2, $p < 0.001$) and by 14% ± 40% by the 2D TEE PWDF method (88 ± 42 mm^2 vs. 79 ± 36 mm^2), but underestimated by 17% ± 17% by the 3D PWDF method (69 ± 34 mm^2 vs. 79 ± 36 mm^2, $p < 0.05$).

Bland–Altman analysis plots for the agreement of the R Vol and EROA between the PWDF methods and flow convergence method are also depicted in Figure 3. For R Vol, the bias ± 2 standard deviations were 26 ± 48 ml (2D TTE PWDF vs. flow convergence), 9 ± 71 ml (2D TEE vs. flow convergence) and −16 ± 34 ml (3D TEE PWDF vs. flow convergence). For the EROA, the bias ± 2 standard deviations were 20 ± 38 mm^2 (2D TTE PWDF vs. flow convergence), 9 ± 56 mm2 (2D TEE PWDF vs. flow convergence) and −10 ± 23 mm^2 (3D TEE PWDF vs. flow convergence). There were a smaller bias and tighter limits

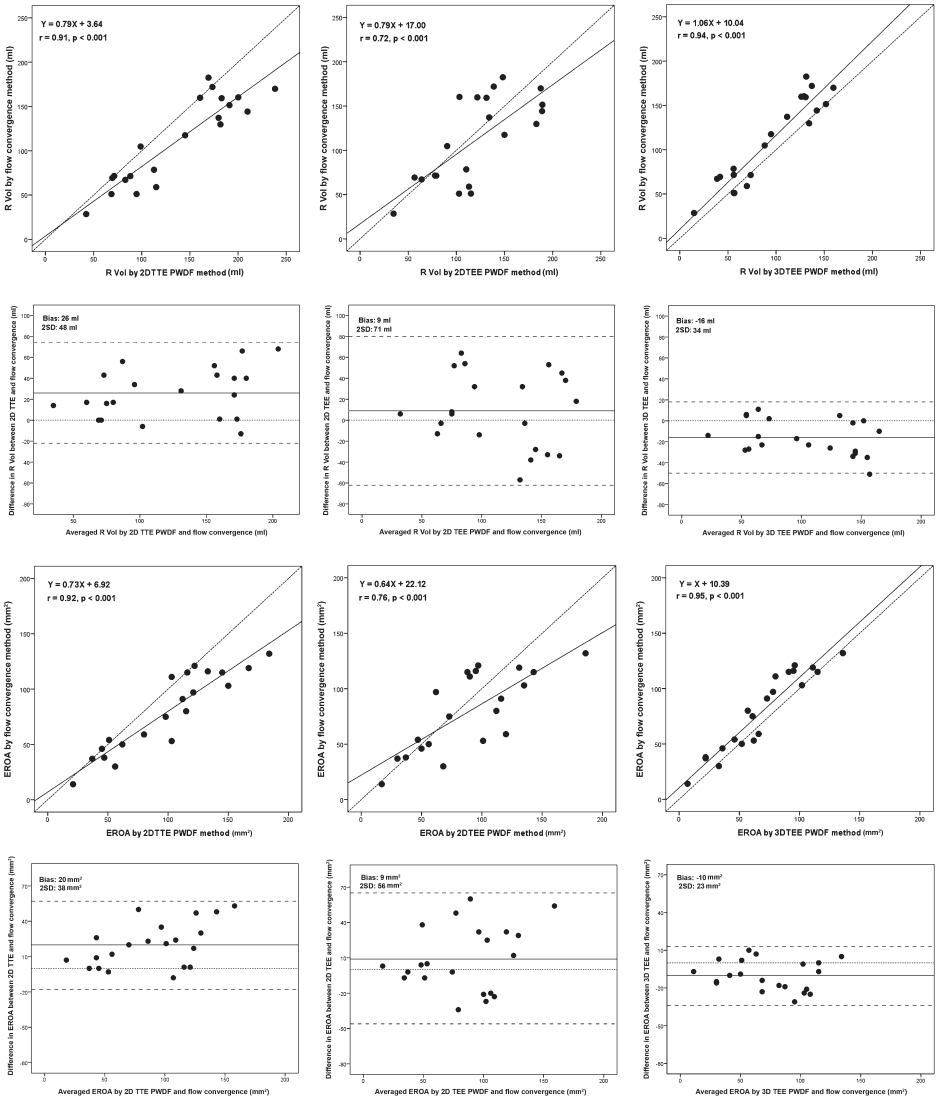

Figure 3 Linear regression and Bland–Altman analysis comparing the mitral regurgitant volume and effective regurgitant orifice area by the 2D transthoracic echocardiography (left column), 2D transesophageal echocardiography (middle column) and 3D transesophageal echocardiography (right column) pulsed wave Doppler flow methods with respective values by the flow convergence method.

of agreement between the 3D TEE PWDF and flow convergence methods than between the 2D PWDF and flow convergence methods.

Categorizations of the MR severity according to different methods

The MR severity of the patients included was categorized according to the R Vol and EROA calculated by 2D TTE, 2D TEE, 3D TEE PWDF and flow convergence methods and

VC width based on the American Society of Echocardiography recommendations for evaluation of the severity of native valvular regurgitation with two-dimensional and Doppler echocardiography[1]. The severity of MR was different in five patients (Table 4) and the same for the other 17 patients.

Table 4 The categorization of the MR severity of patients with discrepancy in MR severity using different methods (n = 5).

Patient No.	2D TTE PWDF	2D TEE PWDF	3D TEE PWDF	Flow convergence	Vena contracta
1	Severe	Severe	Moderate	Severe	Moderate
2	Severe	Severe	Moderate-to-severe	Moderate-to-severe	Moderate
3	Severe	Severe	Moderate-to-severe	Severe	Severe
4	Severe	Severe	Moderate-to-severe	Moderate-to-severe	Moderate
5	Severe	Severe	Moderate-to-severe	Severe	Severe

Intra- and interobserver variabilities of 2D and 3D measurements

For all measurements, Intra- and interobserver variabilities of the 3D TEE PWDF method were better in terms of the relative difference and limits of agreement (Table 5).

Table 5 The intra- and interobserver variabilities of the 2D and 3D pulsed wave Doppler flow methods in measurements of the diameters and cross-sectional areas of the mitral annulus and left ventricular outflow tract, mitral regurgitant volume and effective regurgitant orifice area.

	Intraobserver variability			Interobserver variability		
	2D TTE	**2D TEE**	**3D TEE**	**2D TTE**	**2D TEE**	**3D TEE**
Relative difference (%)						
MA diameter	6 ± 8	3 ± 2	—	13 ± 12	7 ± 8	—
MA cross-sectional area	12 ± 16	6 ± 4	10 ± 9	21 ± 20	14 ± 16	16 ± 11
LVOT diameter	6 ± 6	4 ± 3	—	8 ± 7	8 ± 6	—
LVOT cross-sectional area	11 ± 11	8 ± 6	6 ± 4	16 ± 13	16 ± 12	15 ± 9
Regurgitant volume	24 ± 31	19 ± 18	22 ± 21	46 ± 61	27 ± 31	33 ± 26
Effective regurgitant orifice area	24 ± 31	19 ± 18	22 ± 21	46 ± 61	27 ± 31	33 ± 26
Bias ± Limits of agreement						
MA diameter (mm)	−1 ± 6	0 ± 3	—	−3 ± 8	1 ± 7	—
MA cross-sectional area (mm²)	−21 ± 306	3 ± 174	−39 ± 271	−112 ± 325	55 ± 401	93 ± 228
LVOT diameter (mm)	−1 ± 3	0 ± 2	—	−1 ± 4	1 ± 4	—
LVOT cross-sectional area (mm²)	−24 ± 106	7 ± 90	−13 ± 68	−37 ± 117	52 ± 122	−60 ± 114
Regurgitant volume (ml)	1 ± 57	0 ± 30	−4 ± 49	−13 ± 91	12 ± 78	27 ± 73
Effective regurgitant orifice area (mm²)	1 ± 43	1 ± 23	−1 ± 36	−11 ± 69	10 ± 57	18 ± 50

Relative difference = absolute difference / mean × 100%; Bias = mean of differences; Limits of agreement = 2 standard deviations.

DISCUSSION

The main finding of this study is that compared with the 3D TEE PWDF method, the traditional 2D TTE PWDF method overestimated the mitral R Vol and EROA significantly. The overestimates were caused by the oversimplified 2D measurements and the geometry assumption of the CSAs of the MA and LVOT, which led to the CSA and SV being overestimated at the MA level and underestimated at the LVOT level.

Measurements of the cross-sectional areas of the mitral annulus and left ventricular outflow tract using the pulsed wave Doppler flow method

In the 2D TTE PWDF method, the preferred sites to calculate the SVs are the MA and LVOT, thus precise measurements of the MA and LVOT dimensions are crucial. Conventionally, the MA dimension is measured in the apical 4-chamber view and the LVOT dimension in the parasternal long-axis view[1,3,13]. These measurements have important limitations and lead to errors in calculating CSAs, because variable and unpredictable monoplanar cross-sections are made and circular geometry of the orifices is assumed. In reality, the CSAs of both the MA and LVOT are oval, with the major and minor diameters[14-18]. In this study, the 2D MA diameters approached the 3D major axis diameters and 2D LVOT diameters were close to the 3D minor axis diameters (Figure 4), which is consistent with previous findings[16-19]. The monoplanar measurements and false geometry assumption are important sources of error in measuring the MA and LVOT dimensions using the 2D PWDF method. And the error is even magnified because the diameter (radius) values are squared in the geometry assumption formula. The important geometric errors overestimated the CSA of the MA and corresponding SV by 13% ± 12% and underestimated the CSA of the LVOT and corresponding SV by 23% ± 10 % by the 2D TTE measurements, compared with the 3D CSAs measured directly in the "en face" views of the MA and LVOT at the level at which the velocity profiles had been recorded.

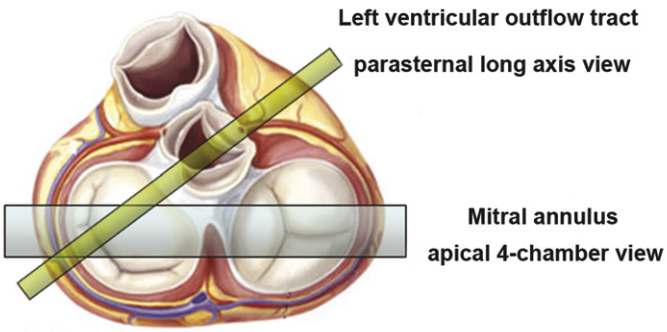

Figure 4 Orientations of the traditional 2D echocardiographic imaging planes of the mitral annulus (apical 4-chamber view) and left ventricular outflow tract (parasternal long-axis view).

The spatial resolution of the TEE images is better than the TTE images, thus allows a clearer identification of anatomical landmarks, e.g., the hinge points of the mitral leaflets. The difference in CSAs between 2D TEE and 3D TEE measurements was smaller (2D TEE overestimated MA CSA by 7% ± 14% and underestimated LVOT CSA by 17% ± 10%). The errors, however, especially for the CSA of the LVOT, were still considerable. Additionally, the errors of both 2D TTE and TEE measurements made in calculating the SVs were in different directions, i.e. overestimation at the MA level and underestimation at the LVOT level, thus the consequent impact in calculating the R Vol and EROA was even more significant, with an overestimate of 54% ± 39% by the 2D TTE PWDF method and 39% ± 40% by the 2D TEE PWDF method.

To measure the cardiac structures using the echocardiographic approaches, especially, the CSAs of the MA and LVOT, we believe that the 3D echocardiography improves the accuracy of measurements greatly because the structures of interest can be revealed in the en face views and measured directly without geometry assumption used in the 2D echocardiographic method. Additionally, the transesophageal imaging approach also contributes to improve the accuracy since the cardiac structures (e.g. the MA) lie in the near field of ultrasound field, thus a better spatial resolution. We assume that the observer variabilities of 3D TTE measurements would be higher than those of the 3D TEE measurements because of insufficient spatial resolution of the 3D TTE datasets.

The 2D and 3D pulsed wave Doppler flow methods in calculating the mitral regurgitant volume and effective regurgitant orifice area compared with the flow convergence method

The flow convergence method is one of the methods recommended for quantifying degenerative MR since the isovelocity surface is usually hemispheric[10,20-22]. The R Vol and EROA calculated by the 3D TEE PWDF method had a better correlation and agreement with the flow convergence method than the 2D PWDF methods did. The 2D PWDF methods overestimated the R Vol and EROA compared with both the 3D TEE PWDF and flow convergence methods. Surprisingly, the R Vol and EROA calculated by the 3D TEE PWDF method were smaller than those obtained by the flow convergence method. The probable reason is that the flow convergence method overestimates true R Vol and EROA as it estimates regurgitant flow from the "maximal" flow rate and thus overestimates the mean flow rates, especially in the situation of a dynamic orifice area change during systole seen in degenerative MR[23,24]. In our study, the flow convergence was measured in late systole in six cases because of the late systolic enhancement of MR due to prolapsed leaflets (Figure 5A). This overestimates the mean EROA because the timing of the flow convergence measurement and the peak velocity of the regurgitation are not synchronized. Additionally, the density of the continuous wave Doppler profile of MR in these cases was faint in early systole and became denser in late systole (Figure 5B),

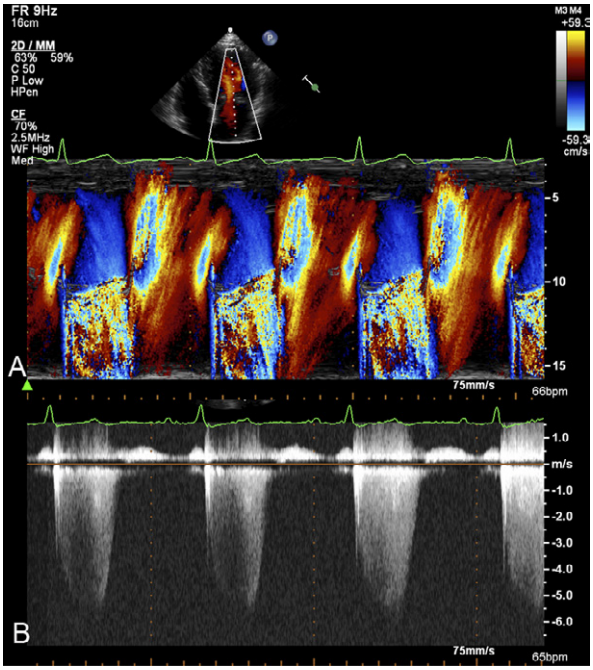

Figure 5 The "late systolic enhancement" of mitral regurgitation due to prolapsed P2 scallop. A, color M-mode echocardiography shows that the regurgitation increased progressively with a maximum in late systole; B, continuous wave Doppler echocardiography shows the density of the profile was faint in early systole and became denser in late systole.

probably overestimating the VTI of MR and thus further overestimating the R Vol. Other physiologic and technical factors can also substantially influence the flow quantification by this approach; they include the regurgitant orifice motion, aliasing velocity, and the ratio of the aliasing velocity to peak orifice velocity[3,24].

Noteworthily, it is crucial to understand the etiology and mechanism of MR and underlying principles and limitations of the flow convergence method when using this method to quantify the MR. The pitfalls of applying this method to the situations of non-hemispheric flow convergence zone and dynamically changing regurgitant orifice have been highlighted by extensive in vitro and clinical studies[4-11,23,25]. The major advantage of the PWDF method is the volumetric measures in which the stroke volume at the MA level is measured in diastole, thus not affected by the spatial or temporal homogeneity of the MR in systole.

The discrepancies in grading the severity of MR according to different methods

In five patients, the categorization of severity of MR was different according to different quantitative methods, and more specifically, it was less severe according to the 3D TEE PWDF method. For patient No.2 and No.4 (Table 4), the MR severity was probably

overestimated by the 2D TTE PWDF method which was confirmed by the 3D TEE PWDF method, flow convergence method and vena contracta width. For patient No.1 and No. 3, there was a late systolic enhancement of the MR, thus the severity was likely to be overestimated by the flow convergence method and vena contracta width as well. In only one patient, patient No.5, there were mismatches of MR severity according to different methods. Since all five patients had been symptomatic, although the MR severity was "less than severe" according to the 3D TEE PWDF method, the clinical management was not changed and all patients underwent the MV repair. There is no clinical evidence that the five patients benefited less from the MV repair.

Intra- and interobserver variabilities

The TEE PWDF method was generally more reproducible than TTE PWDF method mainly due to a better spatial resolution of TEE imaging. Additionally, when the 3D TEE PWDF method was used, the relative differences and limits of agreement of the intra- and interobserver measurements for the R Vol and EROA were smaller than those in the 2D PWDF methods. As expected, the major cause of variability in PWDF methods was the measurements of the CSAs of the MA and LVOT. For the 2D and 3D PWDF methods, the variabilities resulted from the differences in choosing image frames and locating sampling planes for measurements. Although the intra- and interobserver variabilities of 2D diameters of the MA and LVOT were relatively small, corresponding variabilities of the CSAs of the MA and LVOT were significantly higher because the 2D diameters (radiuses) are squared in the geometry assumption formula of the CSA.

Limitations

A true gold standard for calculating the R Vol and EROA was absent in the present study. The flow convergence method was used as the reference method, but underlying assumptions of this method is not entirely valid in the situations of eccentric regurgitant jet and dynamic regurgitant orfice change during systole as discussed above. We believe that a non-echocardiographic imaging modality, e.g., cardiac magnetic resonance imaging, would be much more helpful in validating our findings.

Mitral regurgitant jets due to prolapsed leaflets usually direct eccentrically and the flow convergence method is less accurate. In this study, most patients were with isolated P2 scallop prolapse and the flow convergence zones were visually smooth and measurable.

The sample size in this study was relatively small because only patients who had optimal available echocardiographic assessments of CSAs of the MA and LVOT by 3D TEE were included. Nevertheless, in all patients included, a consistent trend of overestimating the mitral R Vol and EROA using the 2D TTE PWDF method was obvious and therefore meaningful for clinical practice.

Since the MA and LVOT are dynamic structures, differences in timing of the measurements may produce different values. In this study, the 2D frame rate and 3D volume rate were comparable and the time points of measurements were set approximately equal in the cardiac cycle. We assume that the acquisition depth in 3D TEE exam, which was half of that in the 2D acquisition, contributed most to the high volume rate of the 3D datasets.

Finally, in some cases the Doppler sound beam was not perfectly parallel to the blood flow. However, small deviations (<20°) in angle produce mild (<10%) errors in velocity measurements and these errors may be acceptable for low-velocity flows[13].

CONCLUSIONS

The traditional 2D TTE PWDF method tends to overestimate mitral R Vol and EROA because the 2D measurements are monoplanar and it is assumed that the CSAs of the MA and LOVT are circular, which results in the SV being overestimated at the MA level and underestimated at the LVOT level.

REFERENCES

1. Zoghbi WA, Enriquez-Sarano M, Foster E, Grayburn PA, Kraft CD, Levine RA, Nihoyannopoulos P, Otto CM, Quinones MA, Rakowski H, Stewart WJ, Waggoner A, Weissman NJ, American Society of E. Recommendations for evaluation of the severity of native valvular regurgitation with two-dimensional and Doppler echocardiography. *J Am Soc Echocardiogr* 2003;16:777-802.
2. Enriquez-Sarano M, Avierinos JF, Messika-Zeitoun D, Detaint D, Capps M, Nkomo V, Scott C, Schaff HV, Tajik AJ. Quantitative determinants of the outcome of asymptomatic mitral regurgitation. *N Engl J Med* 2005;352:875-83.
3. Lancellotti P, Moura L, Pierard LA, Agricola E, Popescu BA, Tribouilloy C, Hagendorff A, Monin JL, Badano L, Zamorano JL, European Association of E. European Association of Echocardiography recommendations for the assessment of valvular regurgitation. Part 2: mitral and tricuspid regurgitation (native valve disease). *Eur J Echocardiogr* 2010;11:307-32.
4. Hopmeyer J, He S, Thorvig KM, McNeil E, Wilkerson PW, Levine RA, Yoganathan AP. Estimation of mitral regurgitation with a hemielliptic curve-fitting algorithm: in vitro experiments with native mitral valves. *J Am Soc Echocardiogr* 1998;11:322-31.
5. Hopmeyer J, Whitney E, Papp DA, Navathe MS, Levine RA, Kim YH, Yoganathan AP. Computational simulations of mitral regurgitation quantification using the flow convergence method: comparison of hemispheric and hemielliptic formulae. *Ann Biomed Eng* 1996;24:561-72.
6. Li X, Shiota T, Delabays A, Teien D, Zhou X, Sinclair B, Pandian NG, Sahn DJ. Flow convergence flow rates from 3-dimensional reconstruction of color Doppler flow maps for computing transvalvular regurgitant flows without geometric assumptions: An in vitro quantitative flow study. *J Am Soc Echocardiogr* 1999;12:1035-44.
7. Little SH, Igo SR, Pirat B, McCulloch M, Hartley CJ, Nose Y, Zoghbi WA. In vitro validation of real-time three-dimensional color Doppler echocardiography for direct measurement of proximal isovelocity surface area in mitral regurgitation. *Am J Cardiol* 2007;99:1440-7.
8. Matsumura Y, Saracino G, Sugioka K, Tran H, Greenberg NL, Wada N, Toyono M, Fukuda S, Hozumi T, Thomas JD, Yoshikawa J, Yoshiyama M, Shiota T. Determination of regurgitant orifice area with the use of a new three-dimensional flow convergence geometric assumption in functional mitral regurgitation. *J Am Soc Echocardiogr* 2008;21:1251-6.
9. Shiota T, Sinclair B, Ishii M, Zhou X, Ge S, Teien DE, Gharib M, Sahn DJ. Three-dimensional reconstruction of color Doppler flow convergence regions and regurgitant jets: an in vitro quantitative study. *J Am Coll Cardiol* 1996;27:1511-8.
10. Utsunomiya T, Ogawa T, Doshi R, Patel D, Quan M, Henry WL, Gardin JM. Doppler color flow "proximal isovelocity surface area" method for estimating volume flow rate: effects of orifice shape and machine factors. *J Am Coll Cardiol* 1991;17:1103-11.
11. Yosefy C, Levine RA, Solis J, Vaturi M, Handschumacher MD, Hung J. Proximal flow convergence region as assessed by real-time 3-dimensional echocardiography: challenging the hemispheric assumption. *J Am Soc Echocardiogr* 2007;20:389-96.
12. Little SH, Ben Zekry S, Lawrie GM, Zoghbi WA. Dynamic annular geometry and function in patients with mitral regurgitation: insight from three-dimensional annular tracking. *J Am Soc Echocardiogr* 2010;23:872-9.
13. Quinones MA, Otto CM, Stoddard M, Waggoner A, Zoghbi WA, Doppler Quantification Task Force of the N, Standards Committee of the American Society of E. Recommendations for quantification of Doppler echocardiography: a report from the Doppler Quantification Task Force of the

Nomenclature and Standards Committee of the American Society of Echocardiography. *J Am Soc Echocardiogr* 2002;15:167-84.

14. Anwar AM, Soliman OI, Nemes A, Germans T, Krenning BJ, Geleijnse ML, Van Rossum AC, ten Cate FJ. Assessment of mitral annulus size and function by real-time 3-dimensional echocardiography in cardiomyopathy: comparison with magnetic resonance imaging. *J Am Soc Echocardiogr* 2007; 20:941-8.

15. Anwar AM, Soliman OI, ten Cate FJ, Nemes A, McGhie JS, Krenning BJ, van Geuns RJ, Galema TW, Geleijnse ML. True mitral annulus diameter is underestimated by two-dimensional echocardiography as evidenced by real-time three-dimensional echocardiography and magnetic resonance imaging. *Int J Cardiovasc Imaging* 2007;23:541-7.

16. Doddamani S, Bello R, Friedman MA, Banerjee A, Bowers JH, Jr., Kim B, Vennalaganti PR, Ostfeld RJ, Gordon GM, Malhotra D, Spevack DM. Demonstration of left ventricular outflow tract eccentricity by real time 3D echocardiography: implications for the determination of aortic valve area. *Echocardiography* 2007;24:860-6.

17. Doddamani S, Grushko MJ, Makaryus AN, Jain VR, Bello R, Friedman MA, Ostfeld RJ, Malhotra D, Boxt LM, Haramati L, Spevack DM. Demonstration of left ventricular outflow tract eccentricity by 64-slice multi-detector CT. *Int J Cardiovasc Imaging* 2009;25:175-81.

18. Otani K, Takeuchi M, Kaku K, Sugeng L, Yoshitani H, Haruki N, Ota T, Mor-Avi V, Lang RM, Otsuji Y. Assessment of the aortic root using real-time 3D transesophageal echocardiography. *Circ J* 2010; 74:2649-57.

19. Foster GP, Dunn AK, Abraham S, Ahmadi N, Sarraf G. Accurate measurement of mitral annular dimensions by echocardiography: importance of correctly aligned imaging planes and anatomic landmarks. *J Am Soc Echocardiogr* 2009;22:458-63.

20. Okamoto M, Tsubokura T, Nakagawa H, Morichika N, Amioka H, Yamagata T, Hashimoto M, Tsuchioka Y, Matsuura H, Kajiyama G. [The suction signal detected by color Doppler echocardiography in patients with mitral regurgitation: its clinical significance]. *J Cardiol* 1988;18:739-46.

21. Rodriguez L, Anconina J, Flachskampf FA, Weyman AE, Levine RA, Thomas JD. Impact of finite orifice size on proximal flow convergence. Implications for Doppler quantification of valvular regurgitation. *Circ Res* 1992;70:923-30.

22. Utsunomiya T, Doshi R, Patel D, Mehta K, Nguyen D, Henry WL, Gardin JM. Calculation of volume flow rate by the proximal isovelocity surface area method: simplified approach using color Doppler zero baseline shift. *J Am Coll Cardiol* 1993;22:277-82.

23. Enriquez-Sarano M, Miller FA, Jr., Hayes SN, Bailey KR, Tajik AJ, Seward JB. Effective mitral regurgitant orifice area: clinical use and pitfalls of the proximal isovelocity surface area method. *J Am Coll Cardiol* 1995;25:703-9.

24. Simpson IA, Shiota T, Gharib M, Sahn DJ. Current status of flow convergence for clinical applications: is it a leaning tower of "PISA"? *J Am Coll Cardiol* 1996;27:504-9.

25. Buck T, Plicht B, Kahlert P, Schenk IM, Hunold P, Erbel R. Effect of dynamic flow rate and orifice area on mitral regurgitant stroke volume quantification using the proximal isovelocity surface area method. *J Am Coll Cardiol* 2008;52:767-78.

Chapter 2.2

Left Atrial Compliance in Asymptomatic versus Symptomatic Patients with Mitral Valve Regurgitation

Ben Ren
Lotte E. de Groot - de Laat
Marcel L. Geleijnse

Submitted

ABSTRACT

Objective the aim of this study was to assess left atrial (LA) compliance in asymptomatic and symptomatic patients with degenerative mitral regurgitation (MR) using strain (S) and strain rate (SR) parameters.

Methods forty-six patients with significant MR and normal lung function and left ventricular ejection fraction were divided according to NYHA class and mean pulmonary artery pressure (mPAP) in two groups matched with MR volume. LA strain and SR parameters were measured in 2D transthoracic echocardiographic apical views using vector velocity imaging. LA positive strain during LA filling was used as a parameter of LA compliance.

Results LA compliance was better in asymptomatic patients than that in the symptomatic patients: positive S was 23.2 ± 8.9% vs. 16.3 ± 4.9%, and SR was 1.4 (1.1, 2.0) s^{-1} vs. 1.0 (0.9, 1.2) s^{-1}, all $p < 0.02$. Positive S in asymptomatic patients was comparable to values in normal controls (22.4 ± 12.3%) as was SR 1.5 (1.2, 2.0) s^{-1}. The LA lateral and septal walls contributed most to the significant differences. Also, in patients with lower mPAP LA compliance was better: positive S was 20.3 (15.2, 30.0)% vs. 16.4 (12.2, 20.7)% and SR 1.4 (1.1-2.0) s^{-1} vs. 1.0 (0.8, 1.2) s^{1}.

Conclusions in patients with degenerative MR who were matched for MR volume, LA compliance was better in asymptomatic patients and in patients with lower mPAP. LA compliance may be an important mechanism in buffering LA pressure rise in patients with severe MR.

Keywords: left atrial compliance, mitral valve regurgitation, strain and strain rate imaging

Degenerative mitral regurgitation (MR) is the second most common valvular heart disease in Europe[1], and causes symptoms such as dyspnea, fatigue, orthopnea, and palpitations[2,3]. Although indeed most patients with severe MR have symptoms, surprisingly some patients with similar MR severity show no symptoms. Left atrial (LA) compliance defined as the ability of LA dilation during systolic filling may act as an important compensatory mechanism in buffering LA pressure rise and thus in preventing symptoms. According to our knowledge, however, the LA compliance in patients with and without symptoms with significant degenerative MR has not been evaluated. Therefore, we sought to assess LA compliance in asymptomatic and symptomatic patients with degenerative MR using strain (S) and strain rate (SR) parameters.

PATIENTS AND METHODS

Study population

Forty-six consecutive patients with degenerative MR referred to mitral valve surgery who had fulfilled the following inclusion criteria were included: 1) normal lung function (forced expiratory volume in one second > 80%), 2) left ventricular (LV) ejection fraction (EF) larger than 50% by three-dimensional transthoracic echocardiography (TTE), 3) sinus rhythm at the time of the baseline TTE examination, 4) no other significant cardiac abnormalities, and 5) adequate image quality. Two-dimensional echocardiographic images of 20 normal subjects matched with gender (60% male) and age (54 ± 11 years) were retrospectively included for analyses of LA compliant deformation properties. The protocol was approved by the institutional review board and informed consent was obtained from all patients.

All patients were graded according to the New York Heart Association (NYHA) Functional Classification[4] and patients in NYHA class I were categorized into an asymptomatic group (defined as absence of symptoms in active patients or negative stress testing in inactive patients) and patients of higher NYHA class into the symptomatic group. The 10 asymptomatic patients were referred for mitral valve surgery based on the European Society of Cardiology guideline of management of valvular heart disease, including end-systolic diameter ≥ 45mm (Class I) (n = 3), high likelihood of durable repair and low operative risk (Class IIa) (n = 6) and paroxymal atrial fibrillation (n = 1)[5]. The mean pulmonary artery pressure (mPAP) was measured by the right heart catheterization (n = 31). For patients who had not undergone the right heart catheterization (n = 15), the PAP was estimated by echocardiography[6].

Echocardiographic study

Transthoracic echocardiography was performed using the iE33 ultrasound system (Philips Medical System, Best, the Netherlands) with a S5-1 and a X3-1 or X5-1 transducers. Two-dimensional, color Doppler images and 3D datasets were acquired in standard views.

The MR regurgitant volume and effective regurgitant orifice severity was calculated by the proximal isovelocity surface area (PISA) method[7]. A clearly defined *maximal* flow convergence zone was measured from the zenith to the regurgitant orifice. The duration of the PISA was calculated as percentage in which the number of frames of visible PISA was divided by the total number of the systolic frames in the same color flow Doppler image.

The systolic PAP was calculated as the sum of the peak pressure gradient of tricuspid regurgitation calculated from the tricuspid regurgitation velocity using the simplified Bernoulli equation and right atrial pressure estimated based on the diameter and respiratory variation of the inferior vena cava[8]. The mPAP was than calculated as mPAP = 0.61 × systolic PAP + 2 mmHg[9].

Electrocardiographically gated full volume 3D datasets of the LA were built from 4 or 7 subvolumes and digitally stored and exported to QLAB 9.0 3DQA software (Philips Medical System) for offline analysis. After adding five atrial points, the anterior, inferior, lateral and septal mitral annuli and the LA roof, in the multiplanar reconstruction views, the endocardial surface was automatically traced[10]. The maximum LA volume was measured at end systole just before mitral valve opening and the minimum LA volume was measured at end diastole just before the mitral valve closure. The LA EF was determined as the difference between the maximum and minimum LA volumes divided by the maximum LA volume. The LA volume change index during atrial relaxation during LV systole was calculated as the LA volume difference at aortic valve opening and that just before mitral valve opening divided by the body surface area.

Left atrial strain and strain rate analyses

Two-dimensional images from the apical 4-chamber and 2-chamber views of the LA were analyzed using the Vector Velocity Imaging (VVI) (Siemens Medical Solutions, Mountain View, USA). The mean frame rate was 55 ± 10 frames/s. For each view, endocardial borders were traced manually in the end-systolic frame, and the software subsequently traced the borders in the other frames automatically. In segments with poor tracking (assessed subjectively), endocardial borders were readjusted until better tracking was achieved. Quantitative curves of deformation parameters for each segment were generated automatically. The software calculated the LA global S and SR values of each apical view which were the average S and SR values of three LA regions (Figure 1), and the LA average S and SR were the averages of the global values from six LA regions of the two

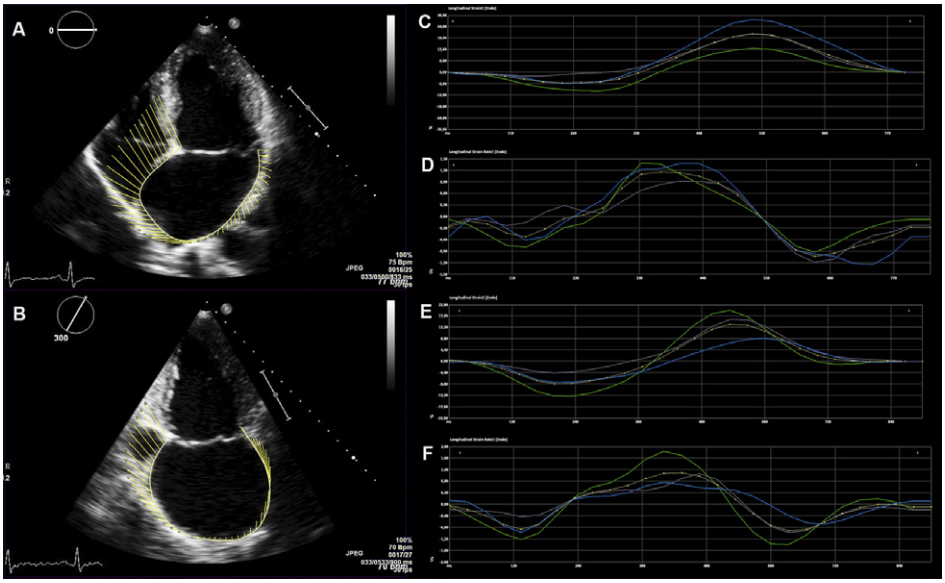

Figure 1 Using the velocity vector imaging, the apical 4-chamber view (A) and 2-chamber view (B) with the vectors of the velocities of the endocardial points were obtained; graphic displays of the left atrial regional (blue, purple and green lines) and global (yellow lines with dots) strain (C, E) and strain rate (D, F) throughout the cardiac cycle obtained from the 4-chamber and 2-chamber views were shown in the report.

apical views. The onset of the P wave was used as the reference point for calculating the S and SR, because it most relevantly represents the LA cavity just before its contraction[11,12]. Each regional LA S and SR curves were divided into component parts representing a different phase of the LA cardiac cycle. By definition, negative S designated as shortening represents LA contractile function, positive S as lengthening to LA compliance and total S (the absolute difference of the negative S and positive S) to LA reservoir[13,14]. The graphic display of the LA SR waveforms shows negative waves at atrial contraction and early diastolic LV filling and positive waves at atrial relaxation during LV systole.

Statistical Analysis

Continuous values were expressed as mean ± standard deviation, median (percentile 25 and 75), or number (percentage). Two-tailed *p* values were calculated and findings were considered statistically significantly when $p < 0.05$. To eliminate a significant difference in MR volume between asymptomatic and symptomatic patients, the statistical matching of the MR volume was performed between the asymptomatic and symptomatic patient groups with a 1:3 ratio (defined by the available number of patients). In the secondary analysis patients were divided into two groups with lower and higher mPAP according to the same ratio. The Kruskal–Wallis H test, Mann–Whitney *U*-test or independent *t*-test with Bonferroni's correction were used to compare parameters between differ-

ent groups. To analyze the inter- and intraobserver variabilities, 20 patients randomly selected were analyzed by two blinded observers (BR, LGL) and by the same observer (BR) at two difference times. The results were analyzed by Bland–Altman method.

RESULTS

Clinical and echocardiographic characteristics of the asymptomatic and symptomatic patients matched with mitral regurgitation volume

Of the total 46 patients, 10 were asymptomatic patients and 36 symptomatic. The MR volume was significantly different between the two groups: asymptomatic 88 (62, 107) ml vs. symptomatic 96 (62, 168) ml, $p = 0.01$ (Figure 2). After matching, measures of 10 asymptomatic and 30 symptomatic patients (1:3) whose MR volumes were comparable were taken into the data analyses. The baseline characteristics of these 40 patients are shown in Table 1. All baseline parameters were comparable between two groups of patients, except for the LV end diastolic volume index (95 ± 25 ml/m^2 vs. 75 ± 20 ml/m^2, $p = 0.02$) and LA volume change index during LV systole (30 ± 8 ml/m^2 vs. 21 ± 8 ml/m^2, $p = 0.024$).

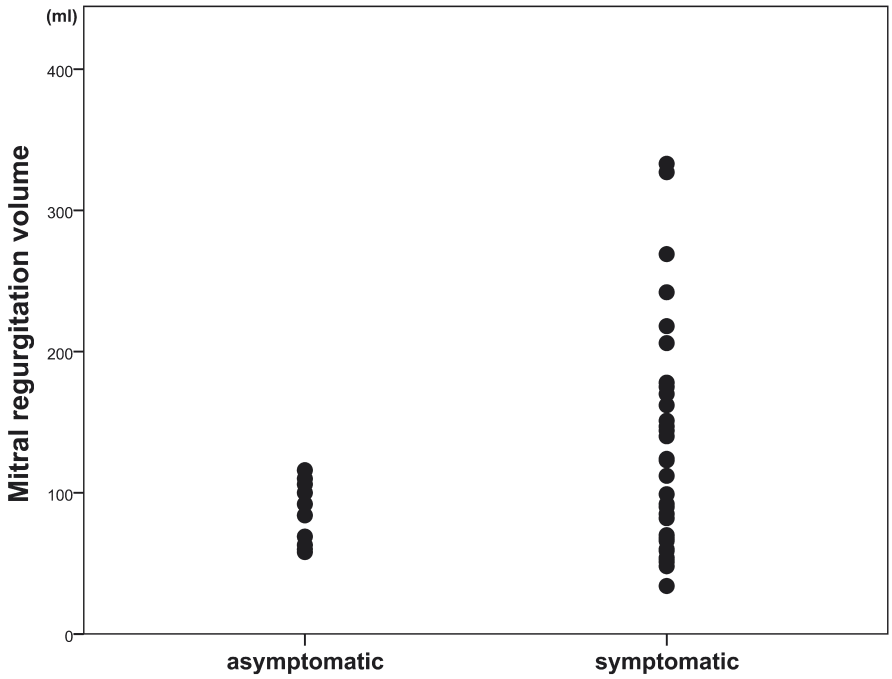

Figure 2 Mitral regurgitation volumes of 10 asymptomatic and 36 symptomatic patients included originally.

Table 1 Demographic and echocardiographic characteristics of the asymptomatic and symptomatic patients matched with mitral regurgitation volume.

	Asymptomatic patients (n = 10)	Symptomatic patients (n = 30)	*p* value
Age (years)	60 ± 9	58 ± 14	NS
Male (%)	70%	60%	NS
Body suface area (m^2)	2.0 ± 0.2	1.9 ± 0.2	NS
Paroxysmal AF	2 (20%)	5 (17%)	NS
Systolic blood pressure (mmHg)	135 (120, 155)	130 (124, 141)	NS
Diastolic blood pressure (mmHg)	80 (70, 86)	80 (74, 86)	NS
Heart rate (bpm)	67 ± 15	67 ± 12	NS
LV EDVi (ml/m^2)	95 ± 25	75 ± 20	0.020
LV ESVi (ml/m^2)	33 ± 12	28 ± 10	NS
LV EF (%)	66 ± 8	63 ± 6	NS
LAVi (ml/m^2)	84 (45, 110)	54 (41, 68)	0.038
LA EF (%)	49 (41, 58)	41 (33, 53)	NS
ΔLAVi	30 ± 8	21 ± 8	0.024
regurgitant volume (ml)	88 (62, 107)	88 (60, 145)	NS
EROA (cm^2)	0.61 (0.50, 0.95)	0.63 (0.50, 0.99)	NS
Visible PISA (%)	75 (62, 82)	75 (50, 82)	NS
Pulmonary vein S (m/s)	42.5 ± 24.9	48.1 ± 21.6	NS
Pulmonary vein D (m/s)	61.0 ± 15.5	62.9 ± 21.1	NS
Pulmonary vein S/D	0.7 ± 0.4	0.9 ± 0.5	NS
mPAP (mmHg)	16 (14, 19)	19 (13, 24)	NS

AF, atrial fibrillation; D, diastolic; EDVi, end diastolic volume index; EF, ejection fraction; EROA, effective regurgitant orifice area; ESDi, end systolic volume index; LAVi, left atrial volume index; ΔLAVi, LA volume change index at atrial relaxation during left ventricular systole; LV, left ventricular; mPAP, mean pulmonary artery pressure; NS, non-significant; PISA, proximal isovelocity surface area; S, systolic.

Strain analyses of asymptomatic and symptomatic patients matched by the mitral regurgitation volume

The LA average S and SR values of all 40 patients and 20 normal subjects are depicted in Table 2. All S and SR parameters were comparable between normal subjects and asymptomatic patients, except for the negative S and SR ($p < 0.02$). The average LA positive S, total S and positive SR were significantly higher in asymptomatic patients (all $p < 0.02$). The comparisons of the global and regional S and SR parameters are shown in Figure 3. The LA global positive S, total S and positive SR of the 4-chamber view were significantly higher in asymptomatic patients than those in the symptomatic patients (all $p < 0.02$). The LA global positive S and positive SR of the 2-chamber view were significantly higher in asymptomatic patients than those in the symptomatic patients (both $p < 0.05$), while the total S values were comparable between two groups. In the deformation analysis,

it is shown that the positive S, total S and positive SR of the lateral and septal walls were significantly higher in the asymptomatic patients than those in the symptomatic patients (all $p < 0.02$).

Table 2 Left atrial longitudinal strain and strain rate values in the asymptomatic and symptomatic patients with mitral regurgitation.

	Controls (n = 20)	Asymptomatic patients (n = 10)	Symptomatic patients (n = 30)
Strain (%)			
Negative	−15.2 ± 5.2*†	−10.9 ± 3.7	−8.7 ± 4.1
Positive	22.4 ± 12.3†	23.2 ± 8.9‡	16.3 ± 4.9
Total	36.8 ± 12.3†	34.1 ± 11.3‡	24.9 ± 6.7
Strain rate (s^{-1})			
Late negative	−1.7 (−2.0, −1.3)*†	−1.2 (−1.7, −0.9)	−1.0 (−1.2, −0.7)
Positive	1.5 (1.2, 2.0)†	1.4 (1.1, 2.0)‡	1.0 (0.9, 1.2)
Early negative	−1.4 (−1.7, −0.8)†	−1.1 (−1.7, −0.8)	−0.9 (−1.1, −0.8)

Abbreviation as in Table 1.
*$p \leq 0.017$, Controls vs. Asymptomatic patients;
†$p \leq 0.017$, Controls vs. Symptomatic patients;
‡$p < 0.017$, Asymptomatic vs. Symptomatic patients.

Comparisons between patients with lower and higher mean pulmonary artery pressures matched by mitral regurgitation volume

There were 11 patients in the group of lower mPAP (12 ± 1 mmHg) and 35 patients in the group of higher mPAP (25 ± 5 mmHg, $p < 0.001$). The MR volume was significantly different between the two groups: lower mPAP 90 (53, 112) ml vs. elevated mPAP 106 (62, 171) ml, $p < 0.05$. After matching, measures of 9 patients with lower mPAP and 27 patients with higher mPAP (1:3) whose MR volumes were comparable were taken into the data analyses. All baseline parameters were comparable between the two groups of patients, except for the LA EF (lower vs. higher mPAP: 59% ± 8% vs. 44% ± 13%, $p = 0.004$). The LA average S and SR values of all 36 patients are shown in Table 3. The average LA negative S and SR were significantly lower in patients in the lower mPAP group than those in patients in the higher mPAP group (all $p < 0.017$) and the average LA total S and positive SR were significantly higher in patients of lower mPAP (both $p < 0.017$). All S and SR parameters were comparable between the normal subjects and patients with lower mPAP except for the difference in the average LA late negative SR ($p = 0.017$).

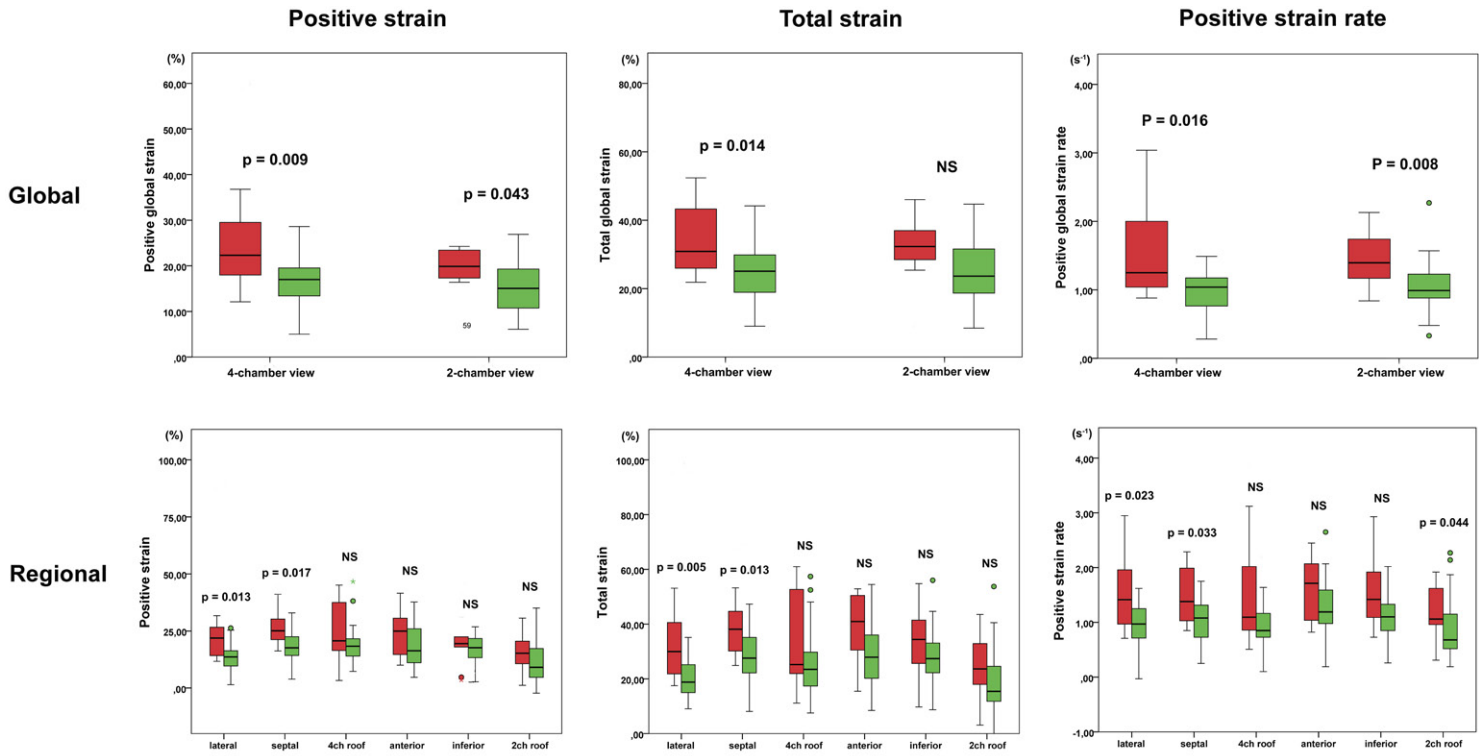

Figure 3 The global and regional positive strains, total strains and positive strain rates of asymptomatic (red) and symptomatic (green) patients matched with the mitral regurgitation volume. The global values of the 4-chamber view were the average values of the lateral wall, septal wall and roof; the global values of the 2-chamber view were the average values of the anterior wall, inferior wall and roof. Outliers were marked by an open circle and asterisk. The corresponding *p* values were indicated above each pair. NS, non-significant; 4ch, 4-chamber view; 2ch, 2-chamber view.

Table 3 Left atrial average strain and strain rate values in the patients with lower and higher mean pulmonary artery pressures.

	Patients with lower mPAP (n = 9)	Patients with higher mPAP (n = 27)
Strain (%)		
Negative	−12.0 (−14.1, −11.6)*	−8.5 (−9.1, −6.7)†
Positive	20.3 (15.2, 30.0)‡	16.4 (12.2, 20.7)†
Total	31.5 (27.2, 44.3)*	25.6 (17.9, 29.6)†
Strain rate (s^{-1})		
Late negative	−1.2 (−1.6, −1.2)‡§	−1.0 (1.2, −0.7)†
Positive	1.4 (1.1, 2.0)*	1.0 (0.8, 1.2)†
Early negative	−1.1 (−1.5, −1.0)*	−0.9 (−1.1, −0.8)†

Abbreviations as in Table 1. Controls' values as in Table 2.
*$p < 0.017$, patients with lower mPAP vs. patients with higher mPAP;
†$p < 0.017$, patients with higher mPAP vs. controls;
‡$p = 0.017$, patients with lower mPAP vs. patients with higher mPAP;
§$p = 0.017$, controls vs. patients with lower mPAP.

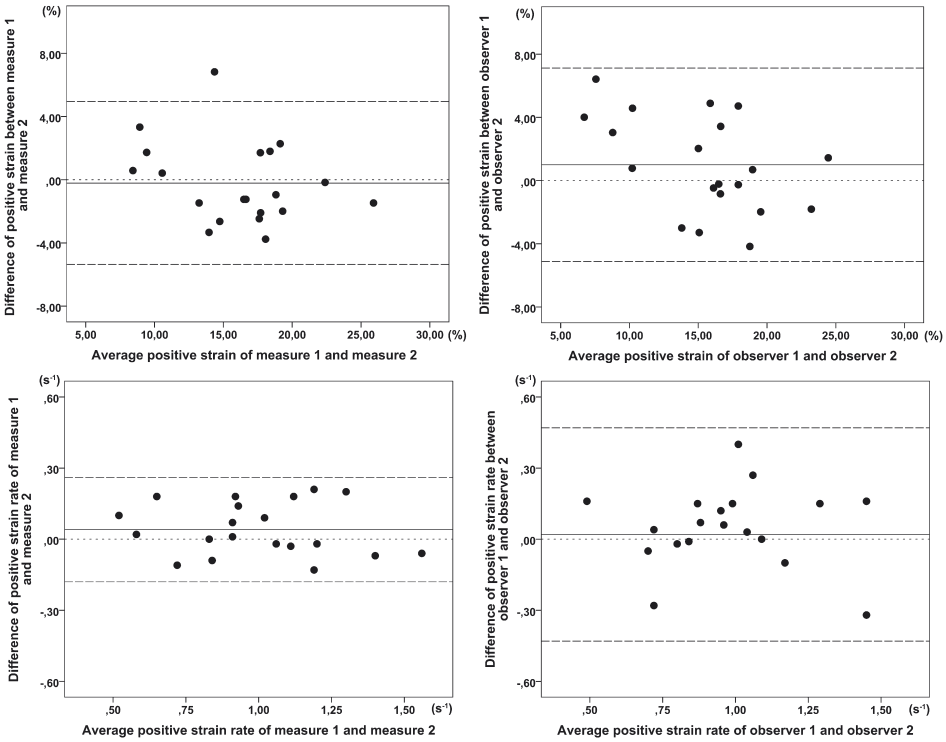

Figure 4 The Bland–Altman analyses of the intraobserver (left column) and interobserver (right column) variabilities of the average LA positive strain (upper row) and strain rate (lower row) measures where the differences were plotted against the average.

Intra-observer and inter-observer reproducibilities

The Bland–Altman analysis of the intra-observer and inter-observer variabilities of the average and regional S and SR measures are shown in Figure 4.

DISCUSSION

The major findings of our study were: 1) MR volumes were different in symptomatic versus asymptomatic patients, 2) in patients with matched MR volumes, asymptomatic patients showed better LA compliance, evidenced with higher positive atrial S and SR during LA filling; 3) the LA lateral and septal walls seemed to contribute most to the LA compliance differences between symptomatic and asymptomatic patients, and 4) in patients with matched MR volumes, patients with lower mPAP also showed better LA compliance.

Mitral regurgitation and left atrial compliance

Mitral regurgitation causes important morphological and hemodynamic changes. In acute MR, the pressure in the normal-sized LA rises abruptly, causing an acute increase in pulmonary venous pressure with pulmonary edema and sudden onset of dyspnea. In contrast, during chronic MR, as regurgitation worsens gradually, the volume overload leads to LA and LV dilatation. In an animal study, it has been shown that in the compensated phase of chronic MR, the LA becomes larger and more compliant with a more potent booster pump action[15]. The LA compliance plays an important role in buffering LA pressure rise[15]. However, LA remodelling may eventually cause chronic inflammatory changes, interstitial fibrosis, and decreased matrix metalloproteinase expression that may impair LA elastic properties and thus compliance[16-18].

Assessment of the left atrial compliance using velocity vector imaging

Vector Velocity Imaging (Syngo SC2000 Workplace, Siemens Medical Solutions, Mountain View, CA, USA) is a 2D speckle-tracking echocardiographic technique which is quite consistent in LA S and SR measurements with the more commonly applied standard 2D speckle tracking echocardiography techniques (EchoPAC, GE Healthcare, Waukesha, WI, USA) but has fewer difficulties in measuring longitudinal S in the thin LA wall[19].

The positive S and SR and total S values of the asymptomatic MR patients were comparable with those of the controls, indicating preserved LA compliance despite LA enlargement. In contrast, the symptomatic patients (with matched MR volumes) showed lower S and SR values, indicating impaired LA compliance. This difference in compliance between asymptomatic and symptomatic patients identified by S analysis was confirmed with a 3D echocardiographic analysis of LA volumes in which it was

shown that in asymptomatic patients a larger LA volume change index during LV systole was present. Interestingly, unlike the positive S and SR, the LA negative S and SR were comparable between asymptomatic and symptomatic patients, both of which were lower than those of the controls. The LA EF was also comparable between asymptomatic and symptomatic patients (66% ± 8% vs. 63% ± 6%). This indicates that although the asymptomatic patients still showed normal LA compliance, the LA contractile function may have already declined. One possible reason might be that in the transitional phase of severe MR, the Frank–Starling mechanism responds less to the chamber dilation and the chamber shortening diminishes. The maintained LA compliance but impaired contractile function indicated by normal LA positive S and SR and significantly reduced LA negative S and SR may have an important prognostic value in asymptomatic patients with severe MR. In a recent report of patient with primary MR and sinus rhythm, severe LA dilation (LAVi ≥ 60 ml/m^2) was associated with poor outcomes independently of known outcome predictors with MR, even in those without symptoms and with maintained LV EF[17]. In previous studies it has been shown that regional differences in atrial compliance exist with the LA inferior wall showing clearly higher positive[20]. In contrast, in our study the inferior wall showed the lowest values in the asymptomatic patients, which may relate to the jet direction in P2 prolapse that directed away from this wall.

Elevated LA pressure caused by chronic MR eventually leads to pulmonary hypertension, an important marker of adverse outcome[21]. A high LA compliance may sufficiently buffer the LA pressure rise and may thus prevent the systolic PAP rise. Marijon *et al.* reported a case presenting with a giant left atrium (73 cm^2 based on apical 4-chamber view) due to severe rheumatic MR in contrast to a normal systolic PAP (29 mmHg based on Doppler velocity of tricuspid regurgitation), testifying the effect of the high LA compliance[22]. Strictly speaking, an end-systolic LA volume is not an indicator of high LA compliance which can only be concluded by changes from minimal to maximal volume. However, in current literatures, very few data have been reported on LA compliance and systolic PAP in case of MR. In this study, the group with lower mPAP had higher positive S and SR values than the counterpart did.

Limitations

Due to the stringent inclusion criteria (excluding confounding factors that may cause symptoms such as impaired pulmonary or LV function), the sample size of the study was relatively small. Besides LA compliance, the LA original volume may also determine the magnitude and rate of rise in atrial pressure in response to the regurgitant volume. In a larger LA with a given compliance, the same MR volume will cause less pressure rise than in a smaller LA with a similar compliance. However, the LA volumes before the development of MR were obviously not available. Other factors such as pulmonary vein-atrium junction area and pulmonary inertance and their interactions with the LA

volume and compliance might also be important determinants of LA pressure rise[23,24]. Atrial fibrillation interacts with LA compliance: patients with atrial fibrillation are known to have lower S and SR values[24]. We controlled this factor by excluding patients with persistent atrial fibrillation and the number of patients with paroxysmal atrial fibrillation was comparable in the matched groups. It cannot be excluded that the LA compliance was better in the asymptomatic patients because of a less complex myxomatous valve disease. However, 97% of the symptomatic patients had also undergone valve repair, pointing to a similar extent of myxomatous lesion as in the asymptomatic patients.

Using the PISA method, the regurgitant volume is calculated from the maximal flow rate, which potentially makes errors in non-holosystolic MR[25]. We took this into account by comparing the time duration of visible PISA in systole, which was shown as comparable between groups. It should be understood that the MR volumes in valve prolapse are based also on the *maximal* PISA measurement (flow rate) and in reality should be much smaller, because in early systole, MR (and thus PISA) is usually absent and in the period of systole that the PISA was visible the maximal PISA was measured according to the guideline[7]. We did not use other quantitative methods to calculate the MR volumes since they also make significant errors[26].

Finally, compliance is usually defined as a change in volume divided by change in pressure. With the strain measurements, we obviously did not measure a change in volume but in dimension, but this is expected to relate directly to a change in the volume.

CONCLUSIONS

In patients with MR matched with MR volume LA compliance was better in asymptomatic patients and in patients with lower mPAP. LA compliance may be an important mechanism in buffering LA pressure rise in patients with MR.

REFERENCES

1. Iung B, Baron G, Butchart EG, Delahaye F, Gohlke-Barwolf C, Levang OW, Tornos P, Vanoverschelde JL, Vermeer F, Boersma E, Ravaud P, Vahanian A. A prospective survey of patients with valvular heart disease in Europe: The Euro Heart Survey on Valvular Heart Disease. *Eur Heart J* 2003;24: 1231-43.
2. Ling LH, Enriquez-Sarano M, Seward JB, Tajik AJ, Schaff HV, Bailey KR, Frye RL. Clinical outcome of mitral regurgitation due to flail leaflet. *N Engl J Med* 1996;335:1417-23.
3. Avierinos JF, Gersh BJ, Melton LJ, 3rd, Bailey KR, Shub C, Nishimura RA, Tajik AJ, Enriquez-Sarano M. Natural history of asymptomatic mitral valve prolapse in the community. *Circulation* 2002;106: 1355-61.
4. Association TCCotNYH. Nomenclature and Criteria for Diagnosis of Diseases of the Heart and Great Vessels Boston, Masschusettes: Little, Brown & Co, 1994:253-256.
5. Joint Task Force on the Management of Valvular Heart Disease of the European Society of C, European Association for Cardio-Thoracic S, Vahanian A, Alfieri O, Andreotti F, Antunes MJ, Baron-Esquivias G, Baumgartner H, Borger MA, Carrel TP, De Bonis M, Evangelista A, Falk V, Iung B, Lancellotti P, Pierard L, Price S, Schafers HJ, Schuler G, Stepinska J, Swedberg K, Takkenberg J, Von Oppell UO, Windecker S, Zamorano JL, Zembala M. Guidelines on the management of valvular heart disease (version 2012). *Eur Heart J* 2012;33:2451-96.
6. Galie N, Hoeper MM, Humbert M, Torbicki A, Vachiery JL, Barbera JA, Beghetti M, Corris P, Gaine S, Gibbs JS, Gomez-Sánchez MA, Jondeau G, Klepetko W, Opitz C, Peacock A, Rubin L, Zellweger M, Simonneau G, Guidelines ESCCfP. Guidelines for the diagnosis and treatment of pulmonary hypertension: the Task Force for the Diagnosis and Treatment of Pulmonary Hypertension of the European Society of Cardiology (ESC) and the European Respiratory Society (ERS), endorsed by the International Society of Heart and Lung Transplantation (ISHLT). *Eur Heart J* 2009;30:2493-537.
7. Zoghbi WA, Enriquez-Sarano M, Foster E, Grayburn PA, Kraft CD, Levine RA, Nihoyannopoulos P, Otto CM, Quinones MA, Rakowski H, Stewart WJ, Waggoner A, Weissman NJ, American Society of E. Recommendations for evaluation of the severity of native valvular regurgitation with two-dimensional and Doppler echocardiography. *J Am Soc Echocardiogr* 2003;16:777-802.
8. Rudski LG, Lai WW, Afilalo J, Hua L, Handschumacher MD, Chandrasekaran K, Solomon SD, Louie EK, Schiller NB. Guidelines for the echocardiographic assessment of the right heart in adults: a report from the American Society of Echocardiography endorsed by the European Association of Echocardiography, a registered branch of the European Society of Cardiology, and the Canadian Society of Echocardiography. *J Am Soc Echocardiogr* 2010;23:685-713; quiz 786-8.
9. Fisher MR, Forfia PR, Chamera E, Housten-Harris T, Champion HC, Girgis RE, Corretti MC, Hassoun PM. Accuracy of Doppler echocardiography in the hemodynamic assessment of pulmonary hypertension. *Am J Respir Crit Care Med* 2009;179:615-21.
10. Anwar AM, Geleijnse ML, Soliman OI, Nemes A, ten Cate FJ. Left atrial Frank–Starling law assessed by real-time, three-dimensional echocardiographic left atrial volume changes. *Heart* 2007;93: 1393-7.
11. Vianna-Pinton R, Moreno CA, Baxter CM, Lee KS, Tsang TS, Appleton CP. Two-dimensional speckle-tracking echocardiography of the left atrium: feasibility and regional contraction and relaxation differences in normal subjects. *J Am Soc Echocardiogr* 2009;22:299-305.
12. Teixeira R, Vieira MJ, Gonçalves L. Left atrial reservoir phase: deformation analysis. *Eur Heart J Cardiovasc Imaging* 2013;14:500-501.

13. Sirbu C, Herbots L, D'Hooge J, Claus P, Marciniak A, Langeland T, Bijnens B, Rademakers FE, Sutherland GR. Feasibility of strain and strain rate imaging for the assessment of regional left atrial deformation: a study in normal subjects. *Eur J Echocardiogr* 2006;7:199-208.

14. Mor-Avi V, Lang RM, Badano LP, Belohlavek M, Cardim NM, Derumeaux G, Galderisi M, Marwick T, Nagueh SF, Sengupta PP, Sicari R, Smiseth OA, Smulevitz B, Takeuchi M, Thomas JD, Vannan M, Voigt JU, Zamorano JL. Current and evolving echocardiographic techniques for the quantitative evaluation of cardiac mechanics: ASE/EAE consensus statement on methodology and indications endorsed by the Japanese Society of Echocardiography. *J Am Soc Echocardiogr* 2011;24:277-313.

15. Kihara Y, Sasayama S, Miyazaki S, Onodera T, Susawa T, Nakamura Y, Fujiwara H, Kawai C. Role of the left atrium in adaptation of the heart to chronic mitral regurgitation in conscious dogs. *Circ Res* 1988;62:543-53.

16. Anne W, Willems R, Roskams T, Sergeant P, Herijgers P, Holemans P, Ector H, Heidbuchel H. Matrix metalloproteinases and atrial remodeling in patients with mitral valve disease and atrial fibrillation. *Cardiovasc Res* 2005;67:655-66.

17. Le Tourneau T, Messika-Zeitoun D, Russo A, Detaint D, Topilsky Y, Mahoney DW, Suri R, Enriquez-Sarano M. Impact of left atrial volume on clinical outcome in organic mitral regurgitation. *J Am Coll Cardiol* 2010;56:570-8.

18. Verheule S, Wilson E, Everett Tt, Shanbhag S, Golden C, Olgin J. Alterations in atrial electrophysiology and tissue structure in a canine model of chronic atrial dilatation due to mitral regurgitation. *Circulation* 2003;107:2615-22.

19. Motoki H, Dahiya A, Bhargava M, Wazni OM, Saliba WI, Marwick TH, Klein AL. Assessment of left atrial mechanics in patients with atrial fibrillation: comparison between two-dimensional speckle-based strain and velocity vector imaging. *J Am Soc Echocardiogr* 2012;25:428-35.

20. Hoit BD, Walsh RA. Regional atrial distensibility. *Am J Physiol* 1992;262:H1356-60.

21. Crawford MH, Souchek J, Oprian CA, Miller DC, Rahimtoola S, Giacomini JC, Sethi G, Hammermeister KE. Determinants of survival and left ventricular performance after mitral valve replacement. Department of Veterans Affairs Cooperative Study on Valvular Heart Disease. *Circulation* 1990;81:1173-81.

22. Marijon E, Jani D, Voicu S, Ou P. Effect of left atrial compliance on pulmonary artery pressure: a case report. *Cardiovasc Ultrasound* 2006;4:31.

23. Leistad E, Christensen G, Ilebekk A. Effects of atrial fibrillation on left and right atrial dimensions, pressures, and compliances. *Am J Physiol* 1993;264:H1093-7.

24. Schneider C, Malisius R, Krause K, Lampe F, Bahlmann E, Boczor S, Antz M, Ernst S, Kuck KH. Strain rate imaging for functional quantification of the left atrium: atrial deformation predicts the maintenance of sinus rhythm after catheter ablation of atrial fibrillation. *Eur Heart J* 2008;29:1397-409.

25. Simpson IA, Shiota T, Gharib M, Sahn DJ. Current status of flow convergence for clinical applications: is it a leaning tower of "PISA"? *J Am Coll Cardiol* 1996;27:504-9.

26. Ren B, de Groot-de Laat LE, McGhie J, Vletter WB, Ten Cate FJ, Geleijnse ML. Geometric errors of the pulsed-wave Doppler flow method in quantifying degenerative mitral valve regurgitation: a three-dimensional echocardiography study. *J Am Soc Echocardiogr* 2013;26:261-9.

Chapter 2.3

Left Atrial Function in Patients with Mitral Valve Regurgitation

Ben Ren
Lotte E. de Groot - de Laat
Marcel L. Geleijnse

American Journal of Physiology - Heart and Circulatory Physiology.
Accepted.

ABSTRACT

Purpose The purpose of this study was to assess left atrial (LA) function and myocardial mechanics in patients with degenerative mitral regurgitation (MR).

Methods Eighty patients with degenerative MR and 20 controls were included prospectively. LA and right atrial (RA) volumes were measured with three-dimensional transthoracic echocardiography at three phases of the cardiac cycle as maximal volume (LAV_{max}/RAV_{max}), minimal volume (LAV_{min}/ RAV_{min}) and volume before atrial contraction ($LAV_{pre\text{-}A}$/ $RAV_{pre\text{-}A}$). From these volumes, active stroke volume (SV), distensibility and emptying fraction (EF) were calculated. LA strain and strain rate were measured with vector velocity imaging on 4-chamber and 2-chamber views.

Results Left ventricular (LV) filling pressures were increased in patients with severe MR (E/E' 16 ± 4 vs. 10 ± 3 in controls). LAV_{max}, LAV_{min} and $LAV_{pre\text{-}A}$ all increased with increasing MR volume. As $LAV_{pre\text{-}A}$ increased, both LA total SV ($r = 0.68$, $p < 0.001$) and passive filling volume ($r = 0.76$, $p < 0.001$) increased. LA active SV increased with $LAV_{pre\text{-}A}$ up to a certain point upon which it decreased despite further increased $LAV_{pre\text{-}A}$ ($r = 0.53$, $p < 0.001$). LA late negative strain decreased with increasing MR volume. A positive correlation existed between LA late negative strain and the LA active EF ($r = 0.55$, $p < 0.001$). In contrast, RA functions were comparable between groups.

Conclusion LA contractility (active SV) increased in response to an increase in LA preload ($LAV_{pre\text{-}A}$) up to a point beyond which LA contractility (active SV) decreased. Whether this was due to working of the LA at the descending limb of the Frank–Starling curve or mainly due to changes in afterload still remains unclear.

Keywords: left atrial function, myocardial mechanics, mitral valve regurgitation

In chronic degenerative mitral regurgitation (MR), the left ventricle (LV) and left atrium (LA) are subject to increased preload. In previous animal studies it has been shown that in the compensated phase of chronic MR, the LA becomes larger and more compliant with a more potent booster pump action as a result of the optimal use of the Frank–Starling mechanism of the LA muscle[1]. In accordance with animal studies, the Frank–Starling behaviour of the LA has been demonstrated in clinical studies including different patient populations[2-4], but not including patients with MR. As MR progressively increased, the extent of LA shortening and expansion is diminished, indicating that the extreme dilation no longer provokes the Frank–Starling response because LA myocardium may operate on the descending limb of the Frank–Starling curve. Two-dimensional echocardiographic assessment of LA size and function in patients with degenerative MR is of important prognostic value[5-7]. Nowadays, there are improved echocardiographic imaging techniques to study LA size and function. LA volume is a better index of LA size and may be best assessed by three-dimensional transthoracic echocardiography (3D TTE)[2,8-10]. Vector velocity imaging (VVI) can also quantitatively describe LA myocardial mechanics[11,12]. In this study, we sought to assess LA function and to confirm the Frank–Starling law of the LA in patients with degenerative MR by measuring LA volume using 3D TTE and myocardial mechanics using VVI.

METHODS

Study population

Eighty consecutive patients with degenerative MR referred for assessment of MR degree and potential mitral valve repair who had fulfilled the following criteria were included prospectively: 1) LV ejection fraction larger than 50% by 3D TTE, 2) sinus rhythm at the time of the baseline TTE examination, 3) no other significant cardiac abnormalities, and 4) adequate image quality. The patients were further divided into three groups based on the MR severity (based on regurgitant volume calculated by the proximal isovelocity surface area method) according to the American Society of Echocardiography recommendations[13]: mild (n = 15), moderate (n = 20) and severe (n = 45). Twenty age- and gender-matched patients referred for routine TTE examination without significant cardiac and systemic abnormalities were included as controls. The protocol was approved by the institutional review board and informed consent was obtained from all patients.

Left atrial volume by 3D tranthoracic echocardiography

Electrocardiographically gated full volume 3D TTE datasets of the LA built from four or seven subvolumes were acquired in apical views using the Philips iE33 ultrasound system (Philips Medical System, Best, the Netherlands) with the X3-1 or X5-1 transducer

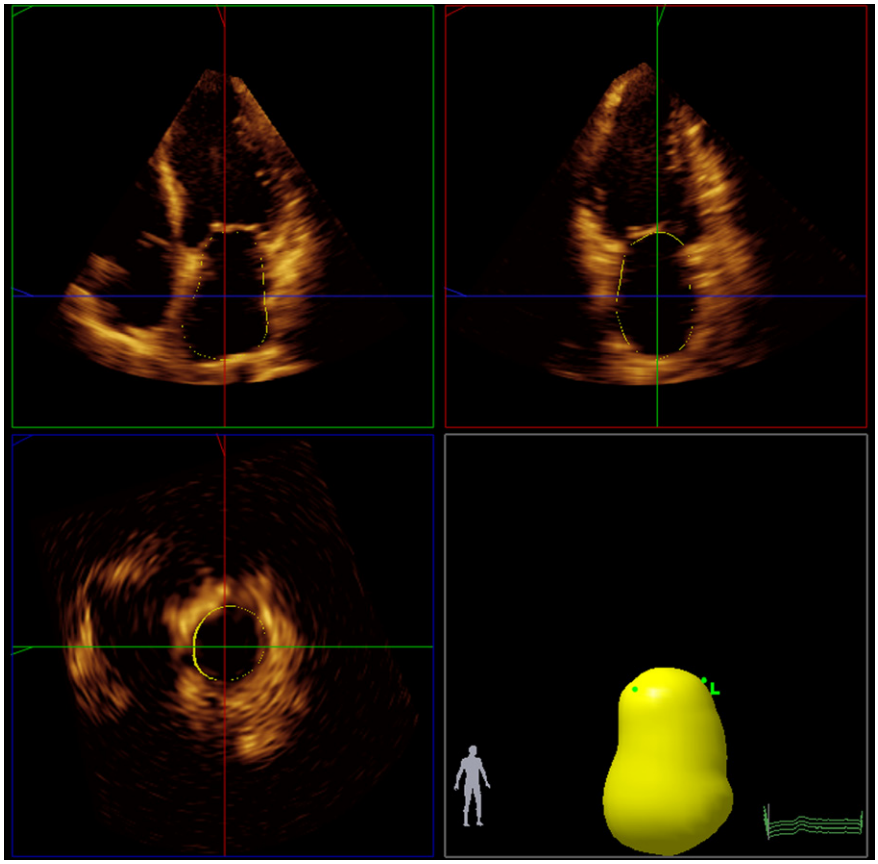

Figure 1 Left atrial 3D echocardiographic volume measures. Multiplanar reconstruction views and 3D model of the left atrium in QLAB 3DQA used for calculating the left atrial volumes.

and exported to QLAB 9.0 3DQA software (Philips Medical System) for offline analysis. To achieve a higher temporal resolution, the acquisition sector width was reduced to just include the complete LA. The average volume rate of the 3D TEE datasets were 31 ± 9 volumes per second. After adding five atrial points, the anterior, inferior, lateral and septal mitral annuli and the LA apex, in the multiplanar reconstruction views, the endocardial surface was automatically traced[2]. The LA 3D model was then built and LA volumes were obtained (Figure 1). Manual corrections of the contours were made to majority of the patients to optimize the tracings. The LA volume was measured at three phases of the cardiac cycle: the maximum LA volume (LAV_{max}) measured at end systole just before mitral valve opening, the minimum LA volume (LAV_{min}) measured at end diastole just before the mitral valve closure and volume before atrial contraction ($LAV_{pre\text{-}A}$) measured at the frame just before mitral valve reopening.

From the volumes, the following LA function indices were calculated:

- LA reservoir function

Total stroke volume (SV) = $LAV_{max} - LAV_{min}$
Distensibility = $(LAV_{max} - LAV_{min})/LAV_{min} \times 100\%$

- LA conduit function
  Passive filling volume = $LAV_{max} - LAV_{pre\text{-}A}$
  Passive emptying fraction (EF) = $(LAV_{max} - LAV_{pre\text{-}A})/LAV_{max} \times 100\%$
- LA contractile function
  Active SV = $LAV_{pre\text{-}A} - LAV_{min}$
  Active EF = $(LAV_{pre\text{-}A} - LAV_{min})/LAV_{pre\text{-}A} \times 100\%$

All volumes had been indexed by the body surface area before they were taken into further analyses.

Left atrial mechanics by velocity vector imaging

Two-dimensional images from the apical 4-chamber and 2-chamber views with proper depth to include the whole LA were acquired using the iE33 ultrasound system (Philips Medical System, Best, the Netherlands) with the S5-1 or X5-1 transducer and analyzed using the VVI (Siemens Medical Solutions, Mountain view, CA, USA). The average frame rate was 60 ± 10 frames per second. For each view, endocardial borders were traced manually in the end-systolic frame, and the software subsequently traced the borders in the other frames automatically. In segments with poor tracking (assessed subjectively), endocardial borders were readjusted until better tracking was achieved. Because all subjects were in sinus rhythm during the study, only one cardiac cycle was analysed. Quantitative curves of deformation parameters for each segment were then generated automatically. The software calculated the LA global strain and strain rate (SR) values of each apical view, which were the averages of three LA regions (in 4-chamber view, the lateral wall, septal wall and the roof were analysed; in 2-chamber view, the anterior wall, inferior wall and the roof were analysed.) (Figure 2). The LA average strain and SR were calculated as the averages of the global values of the two apical views. The onset of the P wave was used as the reference point for calculating the LA strain and SR, because it most relevantly represents the LA cavity just before its contraction[14,15]. Each regional LA strain and SR curves were divided into component parts representing a different phase of the LA cardiac cycle and the strain and SR were measured during LA contraction. By definition, negative strain designated as shortening represents LA contractile function, the positive strain as lengthening to LA distensibility, and the total strain (the absolute difference between the negative and positive strains) to LA reservoir[16,17]. In the graphic display of the LA SR waveforms, it showed negative peaks at atrial contraction (late diastolic negative SR) and early diastolic LV filling (early diastolic negative SR) and a positive peak at atrial relaxation during LV systole (positive SR). To study the Frank–Starling mechanism, the negative SR peak at atrial contraction (late diastolic negative SR) best represents the LA contractile function.

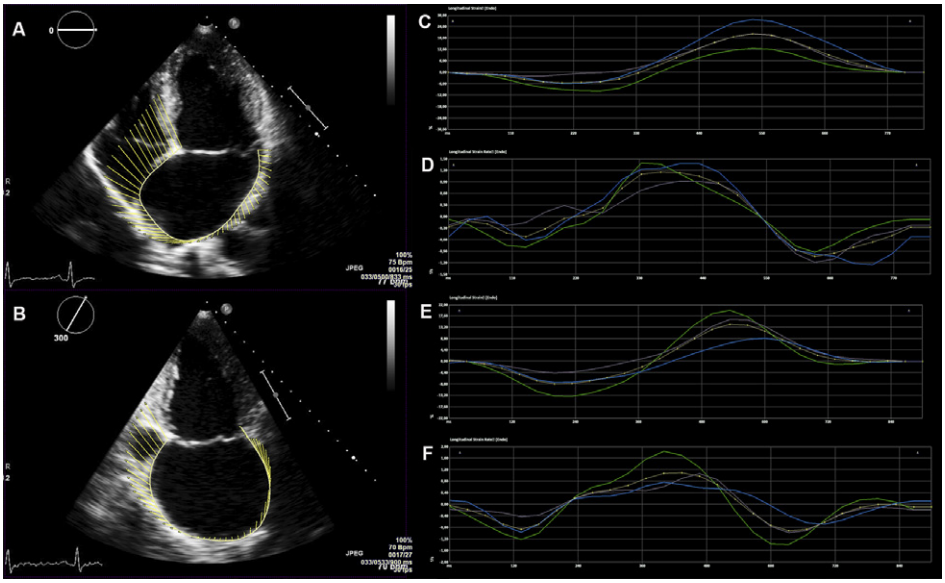

Figure 2 Left atrial longitudinal strain and strain rate obtained by Vector Velocity Imaging. Apical 4-chamber view (A) and 2-chamber view (B) with the vectors of the velocities of the endocardial points; graphic displays of the left atrial regional (blue, purple and green lines) and global (yellow lines with dots) strain (C) and strain rate (D) throughout the cardiac cycle obtained from the 4-chamber view and the strain (E) and strain rate (F) obtained from the 2-chamber view.

Right atrial volume by 3D tranthoracic echocardiography

To serve as a control atrium, 3D echocardiographic analysis of right atrial (RA) volumes was in a similar manner also performed on 3D datasets that retrospectively included the complete RA with sufficient image quality (eight subjects in the control group, seven in the mild MR group, ten in the moderate MR group and 13 in the severe MR group).

Statistical Analysis

Continuous values were expressed as mean ± standard deviation, median (percentile 25 and 75), or number (percentage). Two-tailed *p* values were calculated and findings were considered statistically significantly when $p < 0.05$. The Kruskal–Wallis H test and Mann–Whitney *U*-test with Bonferroni's correction or one-way ANOVA followed by *post hoc* testing were used to compare parameters between different groups. Curve estimation with linear, quadratic and cubic models was used to define the best regression model between LA function indices. For the analyses of the inter- and intraobserver variabilities of the LA volumes and mechanics, 20 patients were randomly selected as representative samples and analyzed by two blinded observers (BR, LGL) and by the same observer (BR) at two difference times. The results were analyzed by Bland–Altman method expressed as bias ± limits of agreement (2 standard deviations), Pearson's correlation analysis and relative difference where the absolute difference of two measurements was divided by

their mean. All statistical analyses were performed using IBM SPSS Statistics Version 21.0 (Armonk, NY: IBM Corp.).

RESULTS

Clinical characteristics and echocardiographic findings

The baseline and echocardiographic characteristics of the controls and three MR severity groups are shown in Table 1. The LV end-diastolic, end-systolic, and the volume at

Table 1 Demographic and echocardiographic characteristics of the study population.

	Controls	Mild MR	Moderate MR	Severe MR
	(n = 20)	(n = 15)	(n = 20)	(n = 45)
Age (years)	62 ± 9	66 ± 11	59 ± 17	58 ± 15
Male (%)	60	67	65	64
Paroxymal atrial fibrillation	0	3 (20%)	5 (25%)	9 (20%)
Body surface area (m^2)	1.8 ± 0.2	1.9 ± 0.3	1.9 ± 0.2	1.9 ± 0.2
Systolic blood pressure (mmHg)	140 ± 25	136 ± 19	128 ± 14	134 ± 16
Diastolic blood pressure (mmHg)	83 ± 12	81 ± 8	78 ± 8	79 ± 11
Heart rate (bpm)	65 (61, 81)	58 (50, 70)	67 (60, 80)	69 (65, 78)
LV EDVi (ml/m^2)[a]	51 ± 11[b,c]	65 ± 18[D]	72 ± 18	81 ± 22
LV ESVi (ml/m^2)[a]	20 ± 6[b,c]	27 ± 10	29 ± 10	29 ± 10
LV ejection fraction (%)	61 ± 7	59 ± 6	59 ± 7	64 ± 7
LV volume index before atrial contraction (ml/m^2)[a]	26 ± 8[b,c]	36 ± 11	39 ± 13	45 ± 17
MR volume (ml)	—	20 (8, 25)[d,e]	45 (32, 53)[f]	124 (91, 168)
EROA (cm^2)	—	0.14 (0.09, 0.18)[d,e]	0.30 (0.21, 0.49)[f]	0.93 (0.60, 1.25)
E wave (m/s)	0.7 ± 0.2[c]	0.7 ± 0.2[e]	0.9 ± 0.3[f]	1.1 ± 0.2
A wave (m/s)	0.7 ± 0.2	0.6 ± 0.2	0.6 ± 0.2	0.6 ± 0.2
E/A	1.0 (0.7, 1.3)[c]	1.2 (0.9, 1.5)[e]	1.3 (1.1, 1.8)[f]	1.8 (1.4, 2.5)
E′ (cm/s)	7.6 ± 3.2	7.3 ± 2.1	6.9 ± 1.5	7.3 ± 1.5
E/E′	10 ± 3[b,c]	10 ± 4[e]	13 ± 3	16 ± 4

[a] Indexed values were obtained by dividing the original values by the body surface area.
Significance (marked if $p < 0.05$): [b] controls vs. patients with moderate MR, [c] controls vs. patients with severe MR, [d] patients with mild MR vs. patients with moderate MR, [e] patients with mild MR vs. patients with severe MR, [f] patients with moderate MR vs. patients with severe MR.
A, peak late filling transmitral velocity; E, peak early filling transmitral velocity; E′, peak early diastolic velocity; EDVi, end diastolic volume index; EROA, effective regurgitant orifice area; ESDi, end systolic volume index; LV, left ventricular; MR, mitral regurgitation.

late diastole before atrial contraction increased with increasing MR volume, whereas the LV ejection fraction did not change. Mitral inflow E-wave velocity and E/A ratio also increased with increasing MR volume. However, the mitral inflow A-wave velocity was comparable between the controls and MR patients and between the MR groups. The E/E′ ratio increased significantly in patients with moderate and severe MR.

Left atrial volumes and function in patients with degenerative mitral regurgitation

LA volumes and EFs are shown in Table 2. Indexed LAV_{max}, LAV_{min} and $LAV_{pre\text{-}A}$ all increased with increasing MR volume.

Table 2 Left atrial volumes and function.

	Controls	Mild MR	Moderate MR	Severe MR
	(n = 20)	(n = 15)	(n = 20)	(n = 45)
LAV_{max}i (ml/m²)	27 (22, 35)[b,c,d]	39 (37, 61)[e]	49 (36, 61)	58 (47, 72)
LAV_{min}i (ml/m²)	14 (9, 18)[b,c,d]	24 (17, 34)	29 (18, 32)	34 (25, 45)
$LAV_{pre\text{-}A}$i (ml/m²)	23 ± 6[b,c,d]	33 ± 17	39 ± 15	44 ± 16
LA reservoir function				
Total SVi (ml/m²)[a]	15 (12, 17)[d]	16 (11, 19)[e]	19 (14, 22)[f]	24 (20, 32)
Distensibility (%)	121 ± 45[b,c,d]	75 ± 44	76 ± 34	76 ± 32
LA conduit function				
Passive filling volume index (ml/m²)[a]	5 (4, 8)[d]	7 (6, 10)[e]	9 (6, 13)[f]	14 (10, 19)
Passive emptying fraction (%)	20 ± 11	19 ± 10	19 ± 8	25 ± 9
LA contractile function				
Active SVi (ml/m²)[a]	8 ± 3	9 ± 3	11 ± 4	9 ± 5
Active emptying fraction (%)	36 (31, 47)[b,c,d]	26 (10, 37)	28 (17, 38)	20 (9, 31)

[a] Indexed values were obtained by dividing the original values by the body surface area.
Significance (marked if $p < 0.05$): [b] controls vs. patients with mild MR, [c] controls vs. patients with moderate MR, [d] controls vs. patients with severe MR, [e] patients with mild MR vs. patients with severe MR; [f] patients with moderate MR vs. patients with severe MR.
LAV_{max}i, maximal left atrial volume index; LAV_{min}i, minimal left atrial volume index; $LAV_{pre\text{-}A}$i, left atrial volume before atrial contraction; SVi, stroke volume index. Other abbreviations as in Table 1.

Left atrial reservoir function

In Table 2, it can be seen that the LA total SV index increased with increasing MR volume. However, the LA distensibility was decreased to a similar extent in all MR groups compared with that in the controls. In Figure 3A, it shows that the LA total SV index correlated positively with the LAV_{max} index ($r = 0.68$, $p < 0.001$), but the LA distensibility correlated negatively with the LAV_{max} index ($r = -0.53$, $p < 0.001$).

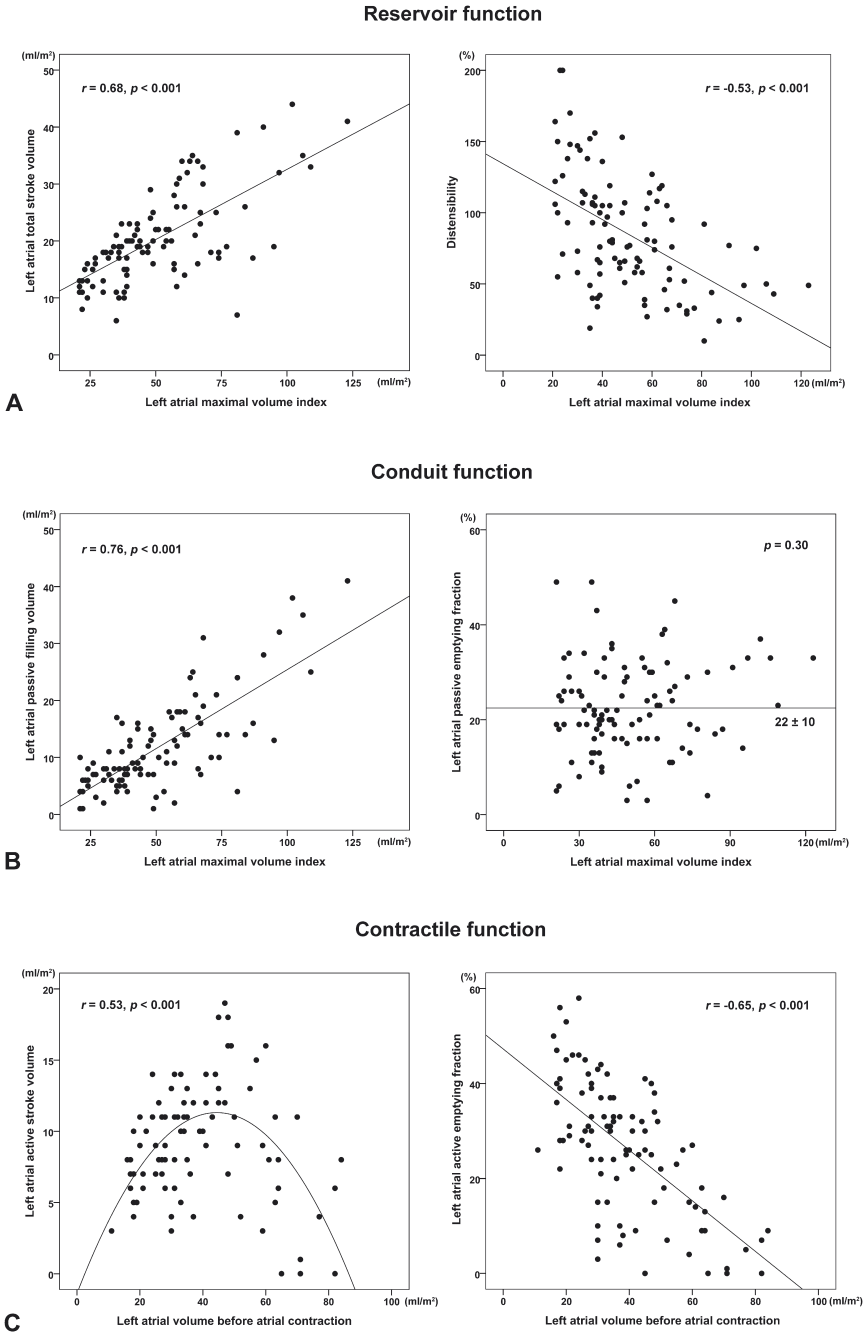

Figure 3 Left atrial functions demonstrated with volume measures. Correlation between (A) left atrial (LA) total stroke volume/distensibility and LA maximum volume; (B) LA passive filling volume/emptying fraction and LA maximum volume; (C) LA active stroke volume/emptying fraction and LA volume before atrial contraction.

Left atrial conduit function

In Table 2, it is shown the LA passive filling volume index increased with increasing MR volume. However, the passive EF was comparable between the controls and MR patients and between the MR groups. In Figure 3B, it shows that the LA passive filling volume index correlated positively with the LAV_{max} index ($r = 0.76$, $p < 0.001$). However, there was no linear correlation between the LA passive EF and the LAV_{max} index ($p = 0.30$).

Left atrial contractile function

In Table 2, it shows that the LA active SV was comparable between all groups but the LA active EF decreased in MR patients compared with that of the controls and tended to be lowest in the severe MR patients. In Figure 3C, it can be seen that LA active SV increased with indexed $LAV_{pre\text{-}A}$ up to a certain point upon which LA active SV decreased despite further increased indexed $LAV_{pre\text{-}A}$ ($r = 0.53$, $p < 0.001$). This curve was fitted with the quadratic model, which best interpreted the data. The LA active EF correlated negatively with the $LAV_{pre\text{-}A}$ index ($r = -0.65$, $p < 0.001$).

Correlation between left atrial deformation and function

The LA longitudinal negative strain and strain rate measures of all subjects are shown in Table 3. LA late negative strain decreased with increasing MR volume, and was highest

Table 3 Left atrial longitudinal myocardial deformation properties at atrial contraction.

	Controls	Mild MR	Moderate MR	Severe MR
	(n = 20)	(n = 15)	(n = 20)	(n = 45)
Negative Strain (%)	−12.5 ± 3.4*	−9.3 ± 4.2	−8.6 ± 4.5	−8.1 ± 3.6
Late negative strain rate (s^{-1})	−1.3 ± 0.4*	−0.9 ± 0.4	−1.0 ± 0.5	−0.9 ± 0.4

* $p < 0.05$ controls vs. patients with severe MR. Abbreviation as in Table 1.

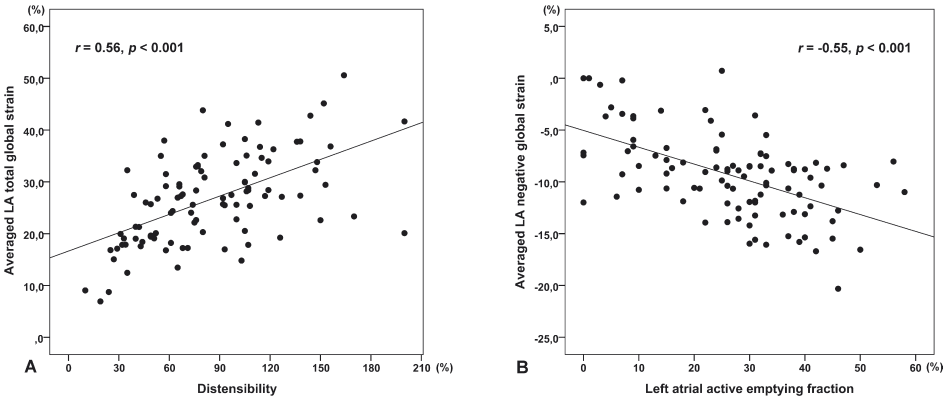

Figure 4 Correlation between (A) average left atrial (LA) total global strain and LA distensibility; (B) average LA negative global strain and LA active emptying fraction.

in the controls. As shown in Figure 4, there was a positive correlation between the average LA total strain and LA distensibility ($r = 0.56$, $p < 0.001$) and a negative correlation between the LA late negative strain and LA active EF ($r = -0.55$, $p < 0.001$).

Right atrial function

The RA volumes and functions are shown in Table 4. No significant differences were found between the groups (all $p > 0.05$).

Table 4 Right atrial volumes and function.

	Controls	Mild MR	Moderate MR	Severe MR
	(n = 8)	(n = 7)	(n = 10)	(n = 13)
$RAV_{max}i$ (ml/m²)	24 ± 6	27 ± 9	29 ± 12	27 ± 7
$RAV_{min}i$ (ml/m²)	13 (10, 17)	16 (13, 19)	13 (10, 17)	14 (10, 18)
$RAV_{pre\text{-}A}i$ (ml/m²)	20 (15, 22)	21 (18, 33)	22 (17, 26)	23 (18, 28)
RA reservoir function				
Total SVi (ml/m²)[a]	11 (7, 12)	8 (7, 20)	13 (12, 15)	12 (9, 17)
Distensibility (%)	78 (55, 122)	74 (45, 107)	105 (80, 118)	90 (49, 151)
RA conduit function				
Passive filling volume index (ml/m²)[a]	4 (3, 5)	2 (2, 5)	6 (3, 6)	4 (2, 7)
Passive emptying fraction (%)	17 ± 6	11 ± 5	16 ± 9	17 ± 10
RA contractile function				
Active SVi (ml/m²)[a]	7 ± 4	9 ± 6	9 ± 3	8 ± 4
Active emptying fraction (%)	33 (16, 47)	38 (27, 47)	43 (30, 53)	34 (24, 51)

No significant differences were found among measurements (all $p > 0.05$). RA, right atrial; $RAV_{max}i$, maximal right atrial volume index; $RAV_{min}i$, minimal right atrial volume index; $RAV_{pre\text{-}A}i$, right atrial volume before atrial contraction; Other abbreviations as in Table 1 and 2.

Observer variability

The Bland–Altman analysis, correlation coefficient and relative difference of the LA volumes, strains and strain rates are shown in Table 5.

Table 5 Intra-observer and inter-observer variabilities of the left atrial volumes and deformation parameters.

	Intra-observer variability	Inter-observer variability
Correlation coefficient (*r*)		
LAV_{max}	0.97	0.96
LAV_{min}	0.99	0.97
LAV_{pre-A}	0.98	0.98
Negative strain	0.97	0.94
Late negative strain rate	0.92	0.88
Relative difference (%)		
LAV_{max}	8 ± 9	10 ± 7
LAV_{min}	7 ± 7	14 ± 7
LAV_{pre-A}	9 ± 7	5 ± 4
Negative strain	9 ± 11	14 ± 10
Late negative strain rate	13 ± 15	14 ± 16
Bias ± 2SD		
LAV_{max} (ml)	−2 ± 19	5 ± 22
LAV_{min} (ml)	−2 ± 9	5 ± 14
LAV_{pre-A} (ml)	−6 ± 10	2 ± 10
Negative strain (%)	−0.4 ± 2.3	−0.0 ± 3.8
Late negative strain rate (s^{-1})	−0.1 ± 0.4	−0.0 ± 0.5

Relative difference = absolute difference/mean × 100% expressed as mean ± SD; Bias = mean of differences. SD, standard deviation; other abbreviations as in Table 2.

DISCUSSION

The main findings of this study in patients with MR were 1) LA contractility (active SV) increased in response to an increase in LA preload (LAV_{pre-A}) up to a point beyond which LA contractility (active SV) decreased; 2) LA late negative strain correlated negatively with the LA active EF and 3) the LA reservoir and conduit functions were augmented in significant MR, manifested by increased total SV and passive filling volume as the LAV_{max} increased.

Left atrial volumetric functions

In a normal heart, an increase in atrial preload, eg. during exercise, results in augmentation of the LA reservoir and booster functions, whereas conduit function is not augmented [18]. As shown in the present study, there was an increase in LAV_{max} from controls to more severe MR and a positive correlation between the LAV_{max} and total LA SV. The latter may be increased by both increased passive and active filling volumes. The LA passive filling volume (and E-wave velocity) increased with increasing MR volume and

was strongly positively correlated with LAV_{max}. This augmentation in LA conduit function was also shown by others[19] and is consistent with the restrictive filling pattern detected in the pulsed wave Doppler profile of mitral inflow of patients with severe MR[20]. Despite a substantially increasing MR volume from mild to severe MR, the increase in passive filling volume led to a damped increase in the $LAV_{pre\text{-}A}$ among the MR groups (which was actually statistically non-significant). LA contractile function may also help in LV filling. In our study, it is shown that active SV increased as the $LAV_{pre\text{-}A}$ increased up to a point around a volume of 40 ml/m^2, where the active SV decreased with increasing $LAV_{pre\text{-}A}$. The decreased active SV in the patients with severe MR may be due to a Frank–Starling mechanism with an ultimate functioning of the LA at the descending limb of the curve (see next paragraph), but more likely due to elevated LV filling pressures at late diastole before atrial contraction. LV filling pressure can be indirectly measured with the mitral inflow E/A and mitral annular E/E′ ratio[21]. In the severe MR group the E/A ratio was 1.8 (1.4, 2.5), indicating a moderately reduced LV compliance. The E/E′ ratio was 16 ± 4, consistent with a mean LV end-diastolic pressure of more than 15 mmHg[22]. Of note, the E/E′ ratio of the controls was 10 ± 3 which is a somewhat higher than the suggested normal value of < 8, implying a mildly decreased LV diastolic function commonly found in a normal population of about 60-year old. There are two possible main reasons for the elevated LV filling pressure. One is the increased LV volume before atrial contraction due to the increased passive filling volume and the other is increased LV stiffness caused by LV remodeling during MR progression.

In contrast, RA function seemed to remain normal even in patients with severe MR as no significant difference was found in any of the studied parameter. Although severe MR may cause an increase in pulmonary venous pressure which may eventually affect the right heart, subjects included in this study were without severe tricuspid regurgitation and symptoms of right heart failure.

Frank–Starling mechanism in the left atrium

In the compensated stage of MR, the LA enlarges in size and mass and becomes more compliant with a more potent booster action[1]. The Frank–Starling behavior of the atrium is manifested as an increased of contraction force after increasing the muscle stretch level controlled by intra-atrial pressure, when other factors remain constant. In animal studies, it was observed that the LA diameter suddenly increased following the onset of acute MR and the atrial shortening was initially augmented, as a result of optimal use of the Frank–Starling mechanism. However, progressive increase in MR was associated with further increases in atrial size but diminished atrial stroke volume[1,23], indicating this extreme dilation no long provokes Frank–Starling response and the atrial myocardium is made to operate on the descending limb of function. This diminished response may due to LA tissue structures disrupted by inflammatory cells and interstitial fibrosis[24].

However, it should be noted that as in our study, in this animal experiment, the afterload was not kept constant (due to increasing MR) and the Frank–Starling law can formally not be applied. In our patients with degenerative MR, the LA contractile function alterations may also present a Frank–Starling curve, in which the LA contraction augments in the early stage of MR and decreases in the later stage. Unfortunately, any animal model or patient study will be limited by a change in LA afterload due to the increased (regurgitant) volume in the LV.

Left atrial myocardial mechanics

In previous studies it has been shown that LA global and regional mechanics can be assessed by VVI[11,12], a 2D speckle-tracking echocardiographic technique quite consistent in LA strain and strain rate measurements compared with the more commonly applied standard 2D speckle-tracking echocardiography techniques[12]. Moustafa *et al.*[11] showed that in patients with chronic MR the reservoir and booster functions of LA were compromised in patients with significant MR manifested by decreased LA EF. However, this study was very small and did not subcategorize the MR severity. Also, the LA volumes (and thus EF) were measured in 2D images. For LA volume measures, the 3D technique used in our study has obvious advantage over the 2D echocardiography[2,8-10]. In the present study, we showed that the late negative longitudinal strain, the relative change in length of myocardial fibers in the longitudinal direction, correlated well with the change in LA volumes and LA EF.

Clinical implications

Chronic MR causes LA remodeling and alters LA function, which contributes to circulatory failure and atrial fibrillation[25]. In a recent report of patient with degenerative MR severe LA dilation (indexed $LAV_{max} \geq 60$ ml/m^2) was associated with poor outcome, independently of well-known outcome predictors like symptoms and LV EF[26]. It would be interesting to study whether the LA with depressed contractile function predicts poor outcome or poor reverse LA remodeling after surgery.

Limitations

As mentioned above, to study LA function changes during the progress of degenerative MR, a longitudinal study following the LA volume and function changes in individual patient would be ideal. However, this is admittedly difficult to perform in patients. For patients included in this study with mild MR, the follow-up clinical visit and TTE exam are undergoing and future studies should concentrate on the MR progress and LA function alteration. Atrial fibrillation may influence LV function and mechanics. As shown in Table 1, the percentages of patients with history of paroxysmal atrial fibrillation were comparable between different MR groups.

LA myocardial contour tracking might be problematic due to insufficient spatial resolution of 3D TTE, in particular because of the LA being in the far field of the ultrasound beam and echo loss because of the pulmonary vein-atrium junction area. For this reason, we included only subjects with adequate imaging quality (three patients were excluded from analyses). The temporal resolution of the 3D TTE should also be sufficient in order to catch the subtle movement of the mitral valve during systole. Although the depth of the acquisition sector was increased to include the LA lying in the far field, the sector width was minimized to compensate the potential drop in temporal resolution. Besides, the VVI algorithm is not designed specifically for LA mechanic analysis. However, it has been used in several clinical researches[11,12] and proved to produce comparable measures compared with the commonly used 2D speckle-tracking technique[12]. To our knowledge, there is so far no software algorithm specially developed for LA analysis. Additionally, the QLAB 3DQA algorithm is developed for LV rather than LA volume quantification. However, the purpose of this study was to study changes in LA volume and the algorithm produced measurements with good observer variabilities.

Three-dimemsional RA measurements were not available in all patients because acquisition of the RA images was not pre-defined in the protocol.

CONCLUSIONS

LA contractility (active SV) increased in response to an increase in LA preload ($LAV_{pre\text{-}A}$) up to a point beyond which LA contractility (active SV) decreased. Whether this is due to working of the LA at the descending limb of the Frank–Starling curve or mainly due to changes in afterload still remains unclear.

REFERENCES

1. Kihara Y, Sasayama S, Miyazaki S, Onodera T, Susawa T, Nakamura Y, Fujiwara H, Kawai C. Role of the left atrium in adaptation of the heart to chronic mitral regurgitation in conscious dogs. *Circ Res* 1988;62:543-53.
2. Anwar AM, Geleijnse ML, Soliman OI, Nemes A, ten Cate FJ. Left atrial Frank–Starling law assessed by real-time, three-dimensional echocardiographic left atrial volume changes. *Heart* 2007;93: 1393-7.
3. Blondheim DS, Osipov A, Meisel SR, Frimerman A, Shochat M, Shotan A. Relation of left atrial size to function as determined by transesophageal echocardiography. *Am J Cardiol* 2005;96:457-63.
4. Matsuzaki M, Tamitani M, Toma Y, Ogawa H, Katayama K, Matsuda Y, Kusukawa R. Mechanism of augmented left atrial pump function in myocardial infarction and essential hypertension evaluated by left atrial pressure-dimension relation. *Am J Cardiol* 1991;67:1121-6.
5. Reed D, Abbott RD, Smucker ML, Kaul S. Prediction of outcome after mitral valve replacement in patients with symptomatic chronic mitral regurgitation. The importance of left atrial size. *Circulation* 1991;84:23-34.
6. Grigioni F, Enriquez-Sarano M, Ling LH, Bailey KR, Seward JB, Tajik AJ, Frye RL. Sudden death in mitral regurgitation due to flail leaflet. *J Am Coll Cardiol* 1999;34:2078-85.
7. Avierinos JF, Gersh BJ, Melton LJ, 3rd, Bailey KR, Shub C, Nishimura RA, Tajik AJ, Enriquez-Sarano M. Natural history of asymptomatic mitral valve prolapse in the community. *Circulation* 2002;106: 1355-61.
8. Lester SJ, Ryan EW, Schiller NB, Foster E. Best method in clinical practice and in research studies to determine left atrial size. *Am J Cardiol* 1999;84:829-32.
9. Poutanen T, Jokinen E, Sairanen H, Tikanoja T. Left atrial and left ventricular function in healthy children and young adults assessed by three dimensional echocardiography. *Heart* 2003;89: 544-9.
10. Artang R, Migrino RQ, Harmann L, Bowers M, Woods TD. Left atrial volume measurement with automated border detection by 3-dimensional echocardiography: comparison with magnetic resonance imaging. *Cardiovascular Ultrasound* 2009;7.
11. Moustafa SE, Alharthi M, Kansal M, Deng Y, Chandrasekaran K, Mookadam F. Global left atrial dysfunction and regional heterogeneity in primary chronic mitral insufficiency. *Eur J Echocardiogr* 2011;12:384-93.
12. Motoki H, Dahiya A, Bhargava M, Wazni OM, Saliba WI, Marwick TH, Klein AL. Assessment of left atrial mechanics in patients with atrial fibrillation: comparison between two-dimensional speckle-based strain and velocity vector imaging. *J Am Soc Echocardiogr* 2012;25:428-35.
13. Zoghbi WA, Enriquez-Sarano M, Foster E, Grayburn PA, Kraft CD, Levine RA, Nihoyannopoulos P, Otto CM, Quinones MA, Rakowski H, Stewart WJ, Waggoner A, Weissman NJ, American Society of E. Recommendations for evaluation of the severity of native valvular regurgitation with two-dimensional and Doppler echocardiography. *J Am Soc Echocardiogr* 2003;16:777-802.
14. Vianna-Pinton R, Moreno CA, Baxter CM, Lee KS, Tsang TS, Appleton CP. Two-dimensional speckle-tracking echocardiography of the left atrium: feasibility and regional contraction and relaxation differences in normal subjects. *J Am Soc Echocardiogr* 2009;22:299-305.
15. Teixeira R, Vieira MJ, Gonçalves L. Left atrial reservoir phase: deformation analysis. *Eur Heart J Cardiovasc Imaging* 2013;14:500-501.

16. Sirbu C, Herbots L, D'Hooge J, Claus P, Marciniak A, Langeland T, Bijnens B, Rademakers FE, Sutherland GR. Feasibility of strain and strain rate imaging for the assessment of regional left atrial deformation: a study in normal subjects. *Eur J Echocardiogr* 2006;7:199-208.

17. Mor-Avi V, Lang RM, Badano LP, Belohlavek M, Cardim NM, Derumeaux G, Galderisi M, Marwick T, Nagueh SF, Sengupta PP, Sicari R, Smiseth OA, Smulevitz B, Takeuchi M, Thomas JD, Vannan M, Voigt JU, Zamorano JL. Current and evolving echocardiographic techniques for the quantitative evaluation of cardiac mechanics: ASE/EAE consensus statement on methodology and indications endorsed by the Japanese Society of Echocardiography. *J Am Soc Echocardiogr* 2011;24:277-313.

18. Toutouzas K, Trikas A, Pitsavos C, Barbetseas J, Androulakis A, Stefanadis C, Toutouzas P. Echocardiographic features of left atrium in elite male athletes. *Am J Cardiol* 1996;78:1314-7.

19. Borg AN, Pearce KA, Williams SG, Ray SG. Left atrial function and deformation in chronic primary mitral regurgitation. *Eur J Echocardiogr* 2009;10:833-40.

20. Lancellotti P, Moura L, Pierard LA, Agricola E, Popescu BA, Tribouilloy C, Hagendorff A, Monin JL, Badano L, Zamorano JL, European Association of E. European Association of Echocardiography recommendations for the assessment of valvular regurgitation. Part 2: mitral and tricuspid regurgitation (native valve disease). *Eur J Echocardiogr* 2010;11:307-32.

21. Lang RM, Bierig M, Devereux RB, Flachskampf FA, Foster E, Pellikka PA, Picard MH, Roman MJ, Seward J, Shanewise JS, Solomon SD, Spencer KT, Sutton MS, Stewart WJ, Chamber Quantification Writing G, American Society of Echocardiography's G, Standards C, European Association of E. Recommendations for chamber quantification: a report from the American Society of Echocardiography's Guidelines and Standards Committee and the Chamber Quantification Writing Group, developed in conjunction with the European Association of Echocardiography, a branch of the European Society of Cardiology. *J Am Soc Echocardiogr* 2005;18:1440-63.

22. Ommen SR, Nishimura RA, Appleton CP, Miller FA, Oh JK, Redfield MM, Tajik AJ. Clinical utility of Doppler echocardiography and tissue Doppler imaging in the estimation of left ventricular filling pressures: A comparative simultaneous Doppler-catheterization study. *Circulation* 2000; 102:1788-94.

23. Sasayama S, Takahashi M, Osakada G, Hirose K, Hamashima H, Nishimura E, Kawai C. Dynamic geometry of the left atrium and left ventricle in acute mitral regurgitation. *Circulation* 1979;60: 177-86.

24. Verheule S, Wilson E, Everett T, Shanbhag S, Golden C, Olgin J. Alterations in atrial electrophysiology and tissue structure in a canine model of chronic atrial dilatation due to mitral regurgitation. *Circulation* 2003;107:2615-2622.

25. Grigioni F, Avierinos JF, Ling LH, Scott CG, Bailey KR, Tajik AJ, Frye RL, Enriquez-Sarano M. Atrial fibrillation complicating the course of degenerative mitral regurgitation: determinants and long-term outcome. *J Am Coll Cardiol* 2002;40:84-92.

26. Le Tourneau T, Messika-Zeitoun D, Russo A, Detaint D, Topilsky Y, Mahoney DW, Suri R, Enriquez-Sarano M. Impact of left atrial volume on clinical outcome in organic mitral regurgitation. *J Am Coll Cardiol* 2010;56:570-8.

Part III

3D echocardiography in assessing left ventricular function

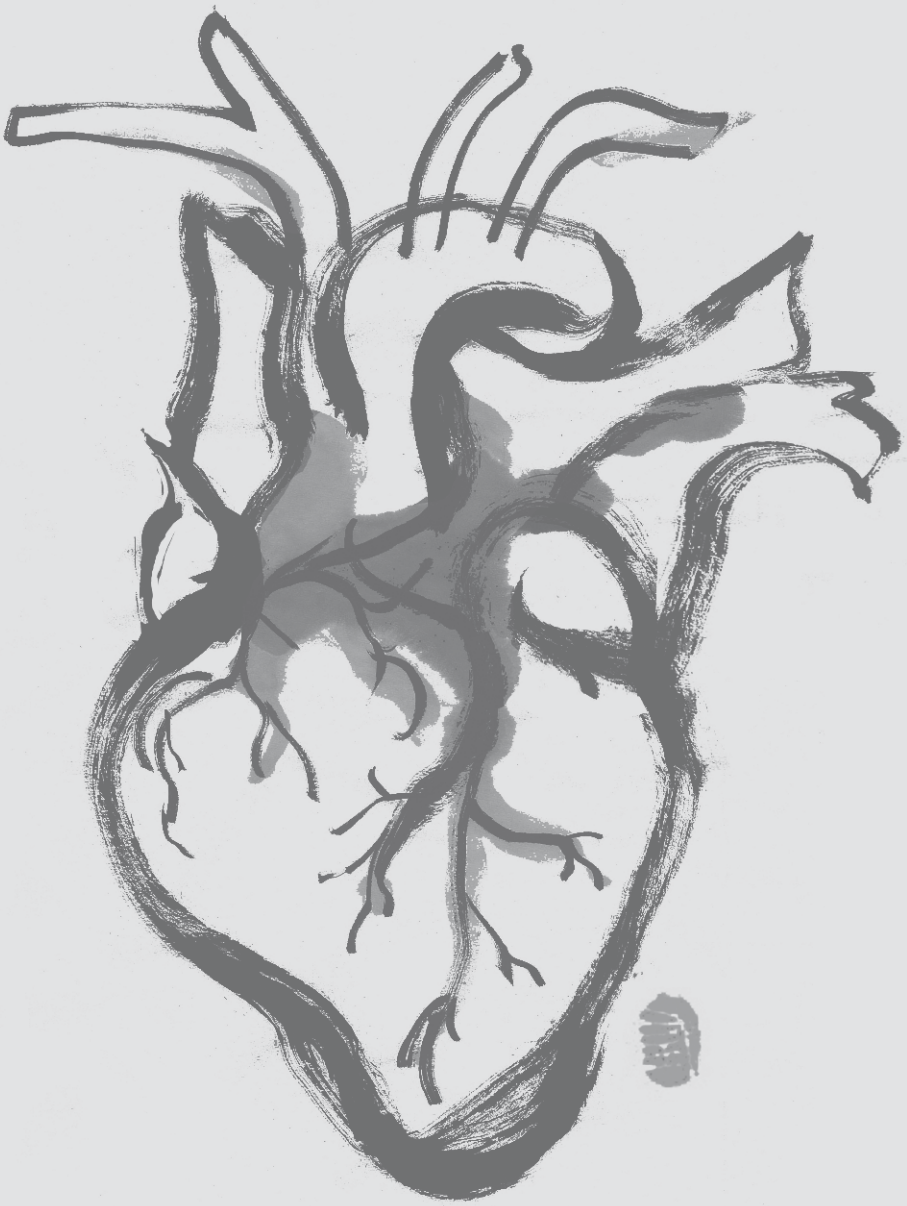

Chapter 3.1

Single-Beat Real-Time Three-Dimensional Echocardiographic Automated Contour Detection for Quantification of Left Ventricular Volumes and Systolic Function

Ben Ren
Wim B. Vletter
Jacky McGhie
Osama I.I. Soliman
Marcel L. Geleijnse

Int J Cardiovasc Imaging. 2014; 30(2):287-94.

ABSTRACT

Purpose To assess the feasibility and accuracy in measuring left ventricular (LV) end-diastolic volume (EDV), end-systolic volume (ESV) and ejection fraction (EF) with Siemens single-beat real-time 3D transthoracic echocardiography (RT-3DE).

Methods The LV volumes and EF were measured in 3D datasets acquired by six imaging modes (Time-1-Harmonic (T1H), Time-1-Fundamental, Time-2-Harmonic, Time-2-Fundamental, Space-1-Harmonic (S1H), and Space-1-Fundamental) in 41 patients using the automated contouring algorithm and compared with manually corrected 3DE QLAB measurements.

Results The main determinates of the temporal and spatial resolutions of 3D datasets acquired were the Fundamental and Harmonic modes. Consequently, the S1H mode had the lowest volume rate and highest spatial resolution. Compared with the 3DE QLAB analysis, the S1H mode resulted in the best LV volumes and EF estimates in all patients (0 ± 10% for EF, −7 ± 44 ml for EDV, −7 ± 39 ml for ESV) and in the 10 patients with correct LV contour tracking according to a visual assessment from the multiplanar reconstruction views in all six modes (0 ± 9% for EF, −3 ± 23 ml for EDV, −2 ± 14 ml for ESV). The T1H mode was the best alternative. Overall 28 patients (68%) could be analysed automatically and satisfyingly with the S1H and T1H modes: 0 ± 8% (EF), 0 ± 27 ml (EDV) and −1 ± 16 ml (ESV).

Conclusion The accuracy of the Siemens automated RT-3D algorithm in measuring LV volumes and EF was significantly influenced by the different imaging modes. The S1H mode may be the preferred 3D acquisition mode, supplemented by the T1H mode in enlarged LVs that do not fit in the S1H acquisition sector.

Keywords: Left ventricle, three-dimensional, echocardiography

Left ventricular (LV) volumes and ejection fraction (EF) are the most used parameters in assessing LV function and have important prognostic significance[1,2]. To assess these parameters, echocardiography is the most commonly applied imaging modality in routine clinical practice. Three-dimensional transthoracic echocardiography (3DE) has been considered as the optimal echocardiographic technique, mainly because of the absence of geometric assumptions. Although the accuracy of 3DE has been validated against cardiac magnetic resonance (CMR) imaging[3-8], it is still limited by the use of stitched LV subvolumes[3,4,7] and semiautomatic contouring of the endocardial border that may result in time-consumption and less reproducible data analysis[5,6,9,10]. Single-beat full volume real-time 3D transthoracic echocardiography (RT-3DE) is a new imaging technique capable in acquiring the LV from a single heartbeat and also allows fully automated contouring of the 3D LV endocardial surface. This imaging modality has been validated recently in different patient populations[11,12]. However, several acquisition imaging modes of the RT-3DE are available with significant differences in temporal and spatial resolutions of 3D datasets acquired. In this study we sought to assess the feasibility and accuracy in measuring LV volumes and EF in the different harmonic and fundamental imaging modes of the RT-3DE.

PATIENTS AND METHODS

Study population

Consecutive patients with sinus rhythm and non-hypertrophied LV scheduled for a routine echocardiographic examination for various indications were enrolled prospectively. Patients with severely distorted LV and inferior image quality were excluded from the study. All patients had undergone 3DE with the iE33 xMatrix ultrasound system (Philips Medical System) and RT-3DE with the Acuson SC2000 ultrasound system (Siemens Ultrasound). The protocols were approved by the institutional review board and informed consent was obtained from all patients.

3D transthoracic echocardiographic image acquisition and analysis

3DE was performed using the iE33 xMatrix ultrasound system (Philips Medical System) with the X5-1 transducer. Electrocardiographically gated full volume datasets of the LV (each built from four subvolumes) were acquired from the apical window during breath-hold with proper gain and depth (11 to 14 cm) to optimize the volume rate. Care was taken to include the complete LV within the imaging volume throughout the acquisition by adjusting the lateral and elevation widths of the acquisition sector. Each full volume dataset was digitally stored and exported to QLAB 8.0 3DQA software (Philips Medical System) for offline analysis by a highly experienced blinded investigator (WBV). The full

volume LV 3DE dataset was displayed as three orthogonal multiplanar reconstruction (MPR) views of the LV. After selecting the end-diastolic (ED) and end-systolic (ES) reference frames, five reference points (four on the mitral annulus and one on the LV apex) were added in two orthogonal MPR views of the reference frames. The software traced the LV endocardial border and calculated the volumes and EF automatically. The endocardial contours were corrected by the same investigator (WBV) manually if the QLAB automated contouring algorithm failed to trace the LV endocardium properly.

Single-beat full volume real-time 3D transthoracic echocardiographic image acquisition and analysis

The RT-3DE was performed using the Acuson SC2000 ultrasound system (Siemens Ultrasound) with the 4Z1c real-time full volume transducer. After the gain and depth (12 to 14 cm) were adjusted, real-time full volume datasets of LV were acquired in a single cardiac cycle from the apical window during breath-hold with six different imaging modes available: Time 1 Harmonic (T1H), Time 1 Fundamental (T1F), Time 2 Harmonic (T2H), Time 2 Fundamental (T2F), Space 1 Harmonic (S1H), and Space 1 Fundamental (S1F). The Space 2 modes were not used because the sector size was too small to include the complete LV. The maximum sector size of the T1H, T1F, T2H, T2F and S1F modes was 90° × 90° and that of the S1H modes was 69° × 66°. Care was taken to include the complete LV within the imaging volume throughout the acquisition. Each full volume RT-3DE dataset was digitally stored and exported to syngo SC2000 Workplace LV Analysis (Siemens Ultrasound). The offline analysis was done by an investigator (BR) blinded to the 3DE QLAB analysis. This custom algorithm traces the LV endocardial surface and selects the end-diastolic volume (EDV) from the electrocardiographic R-wave signal and the minimal systolic volume as the end-systolic volume (ESV) automatically. No manual corrections of the ED and ES frames and endocardial contour tracing were made. Three 2D MPR planes with the automated contour, the 3D mesh rendering of the LV cavity, as well as the LV volumes, EF measurements and volume-time curve were presented automatically (Figure 1). The correctness of segmental motion of the automated 3D LV endocardial contours during the cardiac cycle of all six imaging modes was evaluated by the same observer (BR) in two MPR views (4-chamber and 2-chamber views) of the 3D datasets. If the LV endocardium was not seen clearly in the MPR views, the LV automated contour was accessed by comparing the contours with the 2D images of the transthoracic apical 4-chamber and 2-chamber views.

Statistical methods

All values were expressed as mean ± standard deviation and number (percentage). Linear regression analysis was used to assess the correlation of the EF, EDV and ESV between Siemens RT-3DE and 3DE QLAB measurements. Bland–Altman method in which

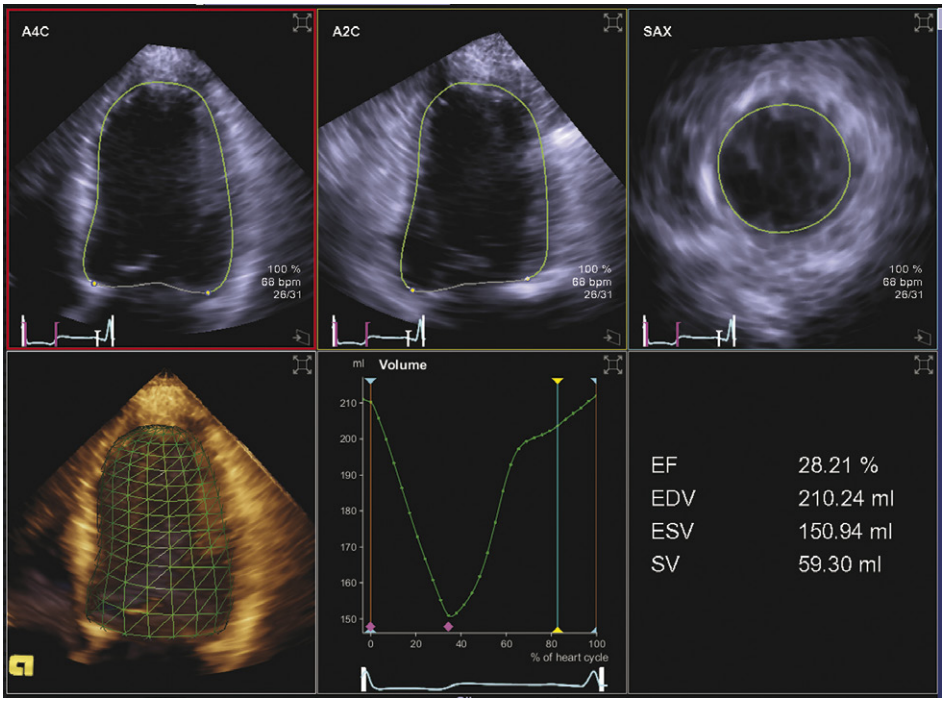

Figure 1 The result page of the automated contouring algorithm of Siemens single-beat full volume real-time 3D transthoracic echocardiography including three 2D multiplanar reconstruction planes with the automated contour, the 3D mesh rendering of the left ventricular cavity, left ventricular volumes and ejection fraction measures and volume-time curve.

differences were plotted against the 3DE QLAB measurements was used to assess the agreement between the two modalities. Differences were considered statistical significant when $p < 0.05$.

RESULTS

Patient characteristics and feasibility of the Siemens RT-3DE

Initially, 48 patients were included. The Siemens RT-3DE automated contouring algorithm failed to trace the LV endocardium in datasets acquired by all six imaging modes in three patients because of false data-acquisition triggering and in four patients due to inferior image quality. Finally, 41 patients were enrolled in the data analysis. The feasibility of the Siemens RT-3DE automated contouring algorithm in all patients included was therefore 85%.

In the 41 patients, the mean age was 56 ± 17 years and 73% were male. Most patients had degenerative valvular heart disease (39%) or non-hypertrophic cardiomyopathy (46%). The apical acquisition of one to two consecutive cardiac cycles of RT-3DE data-

sets took three to five seconds depending on the heart rate. The automated algorithm analysis required 25 ± 3 seconds for one cardiac cycle and 34 ± 4 seconds for two cardiac cycles depending on the imaging modes. In the 3DE QLAB analysis, the semiautomated LV contour was corrected manually in 40 patients (98%), and the manual correction in each case required 10 ± 5 minutes.

Temporal and spatial resolutions of the imaging modes of the RT-3DE

The average volume rate of the Philips 3DE datasets was 26 ± 6 volume per second (vps) and that of Siemens RT-3DE datasets was 49 ± 7 vps (T2F), 34 ± 4 vps (T1F), 24 ± 4 vps (S1F), 24 ± 4 vps (T2H), 17 ± 2 vps (T1H) and 14 ± 2 vps (S1H). In addition, the spatial resolution was different in the different Siemens RT-3DE imaging modes. The Siemens RT-3DE images were generally smoother in visualizing the myocardial tissue in the Harmonic modes than that in the Fundamental modes (Figure 2). According to the visualization of the cardiac structures and recognisability of the LV endocardial motion during the cardiac cycle, the 3D spatial resolution of the Space modes was better than that of the Time modes (Figure 2).

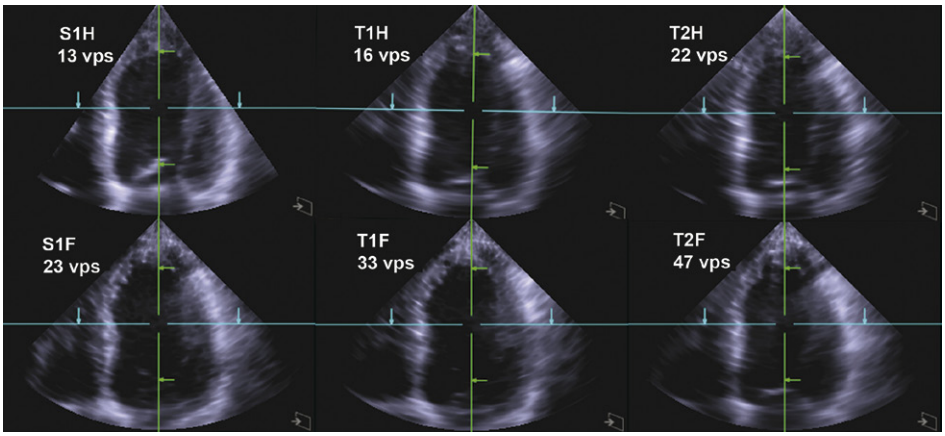

Figure 2 Sample 3DE datasets acquired by the six imaging modes with different temporal and spatial resolutions of Siemens single-beat full volume real-time 3D transthoracic echocardiography. S1H, Space 1 Harmonic; T1H, Time 1 Harmonic; T2H, Time 2 Harmonic; S1F, Space 1 Fundamental; T1F, Time 1 Fundamental; T2F, Time 2 Fundamental.

Accuracy of the automated LV contouring algorithm of the RT-3DTTE with six different imaging settings

The comparisons of the LV volumes and EF between six imaging modes of the Siemens RT-3DE and the 3DE QLAB in all patients are shown in Table 1. The volumes and EF of all six imaging settings calculated by the automated algorithm correlated well with the 3DE QLAB measurements (all $p < 0.001$). Bias of the EF was positive in S1H mode and

Table 1 Pearson correlation coefficient and Bland–Altman analysis of the EF and left ventricular volumes between six imaging modes of Siemens single-beat full volume real-time 3D transthoracic echocardiography (RT-3DE) and 3DE QLAB in all patients (n = 41).

	Siemens RT-3DE					
	T2F	**T1F**	**S1F**	**T2H**	**T1H**	**S1H**
EF (%)						
Pearson *r*	0.84	0.89	0.84	0.88	0.92	0.95
Bias	–7	–7	–6	–3	–1	0.4
Limits of agreement(2SD)	14	14	16	15	12	10
EDV (ml)						
Pearson *r*	0.88	0.91	0.88	0.93	0.91	0.92
Bias	21	20	21	11	6	–7
Limits of agreement(2SD)	40	46	46	42	46	44
ESV (ml)						
Pearson *r*	0.85	0.92	0.90	0.91	0.93	0.92
Bias	22	22	21	10	3	–7
Limits of agreement(2SD)	38	38	38	41	36	39

EF, ejection fraction; EDV, end diastolic volume, ESV, end systolic volume, SD, standard deviation; other abbreviations as in Fig. 2.

negative in all other imaging modes; biases of the EDV and ESV were negative in S1H mode and positive in all other imaging modes. The absolute bias values of EF, EDV and ESV from the S1H and T1H modes were smaller than those from the other modes.

Based on the visually assessed segmental motions of the LV contour during the cardiac cycle in the MPR views of the Siemens RT-3DE datasets, the automated LV contour was correct in all six imaging modes in 10 patients (24%). The comparisons of the EF and LV volumes between six imaging modes of the Siemens RT-3DE and the 3DE QLAB in these 10 patients are shown in Table 2. The EF, EDV and ESV of all six imaging settings calculated by the automated algorithm had excellent correlations with the 3DE QLAB measurements (all $p < 0.001$). Bias of the EF was positive in S1H and negative in other modes; bias of the EDV was negative in S1H and T1H modes and positive in other modes; bias of the ESV was negative in S1H modes and positive in other modes. The bias of the EF and limits of agreement of the EF and LV volumes were improved for all six imaging modes in these ten patients.

Use of the different imaging modes in routine clinical practice

Since the S1H mode led to the best results, this mode was selected as the primary imaging mode for potential use in routine clinical practice. In 23 patients (56%), the LV cavity fitted completely in the acquisition sector and the automated LV contour tracking was, based on the visual assessment, correct. The comparisons of the EF and LV volumes of the S1H mode and the 3DE QLAB measurements in these 23 patients are depicted in

Table 2 Pearson correlation coefficient and Bland–Altman analysis of the EF and left ventricular volumes between six imaging modes of Siemens RT-3DE and 3DE QLAB in the patients with (as assessed visually) correct automatic contour tracing of the Siemens RT-3DE (n = 10).

	Siemens RT-3DE					
	T2F	**T1F**	**S1F**	**T2H**	**T1H**	**S1H**
EF (%)						
Pearson *r*	0.95	0.96	0.88	0.92	0.89	0.95
Bias	−7	−6	−5	−5	−2	0.4
Limits of agreement(2SD)	9	10	14	11	13	9
EDV (ml)						
Pearson *r*	0.96	0.94	0.92	0.90	0.95	0.96
Bias	14	17	22	10	−1	−3
Limits of agreement(2SD)	21	30	39	34	25	23
ESV (ml)						
Pearson *r*	0.99	0.99	0.99	0.97	0.98	0.99
Bias	16	17	19	11	1	−2
Limits of agreement(2SD)	13	14	15	20	18	14

Abbreviations as in Table 1.

Figure 3A. Correlations between the S1H mode and 3DE QLAB were excellent for EF (r = 0.95), EDV (r = 0.97) and ESV (r = 0.99) (all $p < 0.001$), with biases and limits of agreement of 1% ± 9% (EF), −2 ± 26 ml (EDV) and −3 ± 16 ml (ESV). In the eight patients in whom the LV cavity did not fit completely into the acquisition sector of the S1H mode, the automated contour tracking of the T1H mode as the best alternative was correct in five patients based on the visual assessment. Thus, overall 28 of 41 patients (68%) could be analysed automatically and satisfyingly with the following results compared with the 3DE QLAB measurements (Figure 3B): correlation coefficient r = 0.95 (EF), r = 0.96 (EDV) and r = 0.98 (ESV); biases ± limits of agreement 0% ± 8% (EF), −0 ± 27 ml (EDV) and −1 ± 16 ml (ESV).

DISCUSSION

This is the first study to assess the feasibility and accuracy of the Siemens RT-3DE automated algorithm in measuring the LV volumes and EF of 3D datasets acquired with the six different available imaging modes. The main finding of this study was that the accuracy of the automated algorithm was influenced significantly by the different imaging modes. Compared with the manually optimized 3DE QLAB measurements, the automated measurements of the S1H mode were superior particularly in terms of the bias, and to a less extend in correlation and limits of agreement.

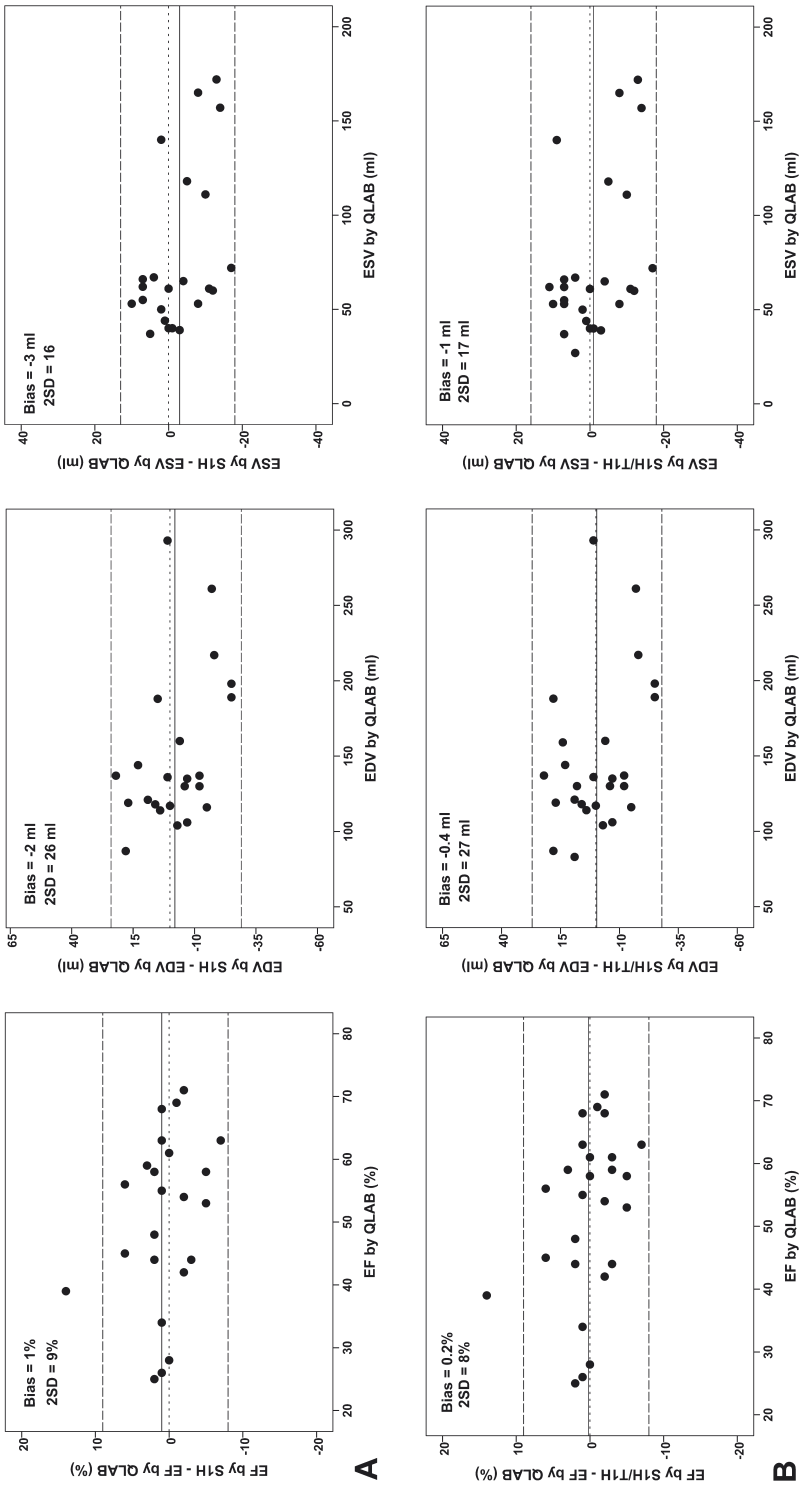

Figure 3 Bland–Altman analysis comparing the ejection fraction and left ventricular volumes in A, the Space 1 Harmonic mode with correct automated left ventricular contour tracking (n = 23); B, the Space 1 Harmonic mode or Time 1 Harmonic mode (if the LV cavity did not fit completely in the acquisition sector of the Space 1 Harmonic mode) with correct automated left ventricular contour tracking (n = 28). Abbreviations as in Table 1.

The temporal resolution of the different imaging modes

The major determinant of the temporal resolution was the Fundamental versus the Harmonic modes, i.e. the temporal resolution of the Fundamental mode was higher than that of the Harmonic mode. Besides, the Time and Space modes also influenced the temporal resolution, i.e. the temporal resolution of the Time mode was higher than that of the Space mode. Consequently, the 3DE datasets acquired by the S1H (Space 1 Harmonic) mode were of the lowest volume rate (14 ± 2 vps). Data acquisition was triggered by the R wave of the electrocardiogram and the Siemens automated contouring algorithm defined end diastole as the first (or occasionally the second) frame. Therefore, the EDV measure was independent of the volume rate. The ESV, however, was chosen from the smallest volume during the cardiac cycle. Since the normal time duration of the isovolumic relaxation period is 70 ± 12 ms (and will usually be even longer in pathological hearts) even the lowest volume rate in this study, i.e. the S1H mode, may be expected to be sufficient in capturing the smallest volume in the cardiac cycle.

The spatial resolution of the different imaging modes

By definition, the spatial resolution is inversely correlated to the temporal resolution (volume rate) because more time available per volume allows more ultrasound scan lines per volume. Therefore, spatial resolution was better in Harmonic and Space modes and best in the S1H (Space 1 Harmonic) mode.

The accuracy of the different imaging modes

There were significant differences in the LV volume and EF measurements between the six different imaging modes. Differences in the LV volume measures resulted from two main reasons: the general automated LV contour tracking and the near-field artifact. The automated LV contour was more toward the epicardium in the datasets acquired by the Fundamental modes, while more toward the LV cavity (particularly in the apex) in those acquired by the Harmonic modes. This might explain why the LV volumes of the Fundamental modes were larger than those of the Harmonic modes and the biases of the LV volumes compared with the 3DE QLAB measurements were positive in all Fundamental modes. The near-field artifact was very common, particularly in the T2H and T1H modes. In the datasets of the Fundamental modes, the near-field artifact was less common and the automated contour was more likely to cross over the near-field artefact and to track the stationary epicardium. Whereas in the datasets of the Harmonic modes, the apical contour was tracked better but seemed too much into the LV cavity (Figure 4). In fact, the LV apical endocardium contour should be more outward toward the compacted myocardium[13-15]. However, since the apical segment is only one out of the total number of 17 LV segments and has a relatively limited volume capacity, the variances of the global LV volumes may only to a limited extend be caused by the variances in the apical

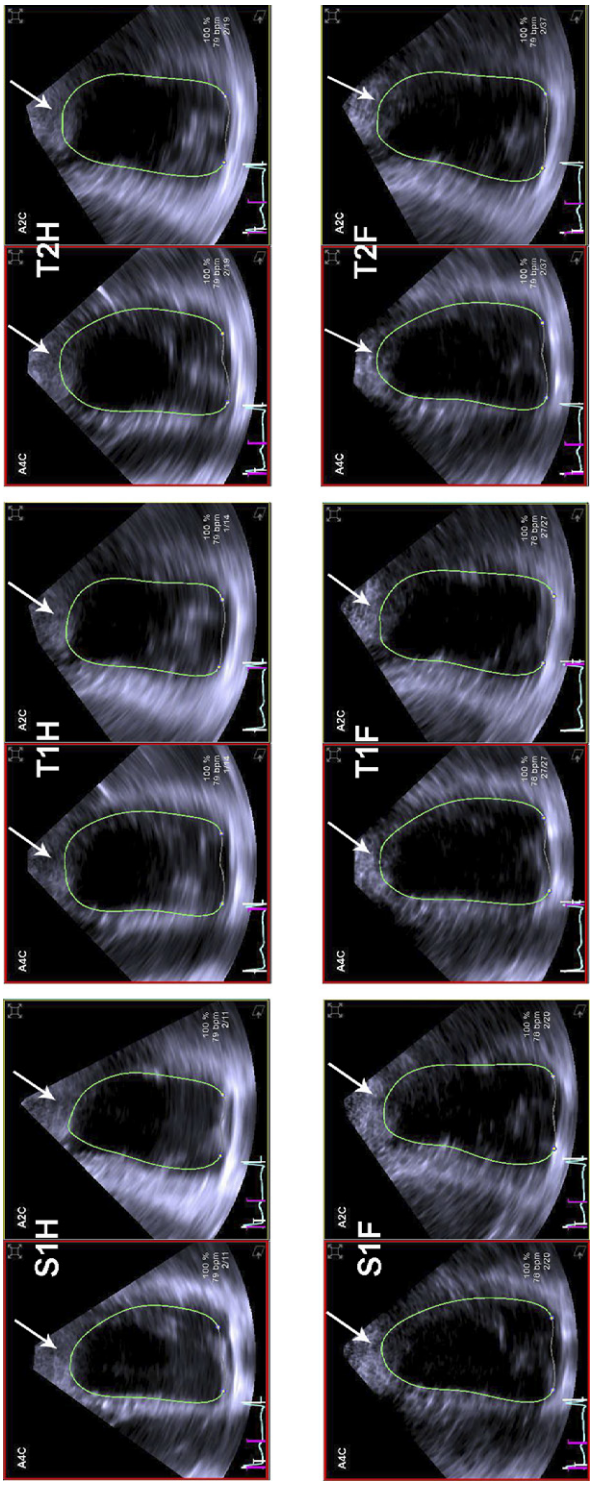

Figure 4 The near-field artefact (white arrows) and automated left ventricular contour in the multiplanar reconstruction views of the 3D datasets acquired with the six imaging modes. A4C, apical 4 chamber view; A2C, apical 2 chamber view; other abbreviations as in Figure 2.

volume alone. As shown in the overall patient population and 10 patients with correct LV contour tracking in all six imaging modes, the limits of agreement of LV volumes were, in contrast to the biases, quite comparable among the imaging modes.

In the previous studies it was reported that the Siemens RT-3DE automated contouring algorithm was accurate compared with CMR measurements[11,12]. However, these studies did not specify which imaging modes were used. In the study of Chang *et al.* a volume rate of 13 ± 1 vps was reported[11], so most likely this study was performed using the S1H mode. In the study of Thavendiranathan *et al.* a volume rate of 32 ± 20 vps was reported[12]. It is hard to establish what imaging mode they used, but it could not be the S1H mode because to achieve such a high volume rate in this mode it would require to decrease the maximal size of the S1H acquisition sector, which is impossible to include the complete LV cavity. As discussed above, the different imaging modes led to substantial differences in the temporal and spatial resolutions of datasets acquired and in the LV volume and EF estimates. Therefore, it is important to outline this issue in a scientific article.

Practical use of the different imaging modes

For the use of the Siemens system in the real-world, the S1H mode was chosen as the primary imaging mode because of the favourable bias, correlation and limits of agreement compared with the 3DE QLAB measurements, as shown in the overall patient population and in the 10 patients with correct automated LV contour in all six imaging modes. For similar reasons, the T1H mode was chosen as the best alternative if the LV cavity did not fit completely in the widest possible acquisition sector of the S1H mode. Using this approach, 28 patients out of 41 (68%) could be analysed automatically and satisfyingly (with the intraobserver and interobserver variabilities of 0% for analyzing the images acquired) with the automated algorithm; the S1H mode was used in 23 patients and the T1H mode in 5 patients. Compared with the 3DE QLAB measurements, the EF and LV volume estimates in these 28 patients were very accurate in terms of high correlation coefficient, small biases and tight limits of agreement. It should, however, also be recognized that due to false triggering of data acquisition and inferior echo quality, seven patients were not included in the data analysis of this study. Therefore, the true overall feasibility in the real-world of the Siemens RT-3DE automated algorithm was 28 of 48 patients (58%). Importantly, this study was performed in a research environment and the sonographer was highly experienced with more than 25 years in echocardiography. In the real world, the outcomes may actually be less favourable and should be investigated in a real-world clinical study.

In a previous study from our group, we have demonstrated that 3DE QLAB datasets acquired and analyzed by the same investigator who did the 3DE QLAB analysis in the present study led to a minimal underestimation of the LV volumes (−7 ± 20 ml for EDV

and −4 ± 8 ml for ESV) and EF (0% ± 6%), compared with the CMR[8]. Since the biases of the LV volumes between Siemens RT-3DE and 3DE QLAB in the 28 patients were less than 1 ml, the extent of underestimation of LV volumes by the Siemens RT-3DE automated algorithm may be expected to be of similar magnitude.

Limitations

One limitation could be the use of the manually corrected 3DE QLAB analysis as a gold standard for LV volumes and EF rather than CMR. As stated before, in a previous study from our group we have shown that 3DE QLAB measurements analyzed by the same investigator showed that the underestimation of LV volumes (−7 ± 20 ml for EDV and −4 ± 8 ml for ESV) and EF (0 ± 6%) was extremely small, compared with CMR[8]. However, it should be recognized that in the literature in general 3DE underestimated the LV volumes compared with CMR. From this respect, it cannot be excluded that the positive volume bias seen in Fundamental mode may be to some extent false positive. Nevertheless, the bias in EF will still remain inferior to that seen in the Harmonic modes.

In particular in the T1F and T2F modes the LV endocardial border was more difficult to see in the MPR views of the 3D datasets and therefore the visual assessment of correct contour tracking by the Siemens automated algorithm may have been biased by the imaging modes.

Finally, patients with abnormal LV shapes as seen in severely dilated and hypertrophic cardiomyopathy were not included in this study and the influence of the imaging modes on the EF and LV volume estimates in these patients is therefore not known.

CONCLUSIONS

The accuracy of the Siemens automated RT-3DE algorithm in measuring the LV volumes and EF is significantly influenced by the different imaging modes, caused by differences in temporal and spatial resolutions. The S1H mode may be the preferred 3D acquisition mode, supplemented by the T1H acquisition mode in enlarged LVs which cannot be included completely in the acquisition sector of the S1H mode. Using this method, the majority of patients could be analyzed automatically with excellent results.

REFERENCES

1. Wang TJ, Evans JC, Benjamin EJ, Levy D, LeRoy EC, Vasan RS. Natural history of asymptomatic left ventricular systolic dysfunction in the community. *Circulation* 2003;108:977-82.
2. White HD, Norris RM, Brown MA, Brandt PW, Whitlock RM, Wild CJ. Left ventricular end-systolic volume as the major determinant of survival after recovery from myocardial infarction. *Circulation* 1987;76:44-51.
3. Jenkins C, Bricknell K, Hanekom L, Marwick TH. Reproducibility and accuracy of echocardiographic measurements of left ventricular parameters using real-time three-dimensional echocardiography. *J Am Coll Cardiol* 2004;44:878-86.
4. Kuhl HP, Schreckenberg M, Rulands D, Katoh M, Schafer W, Schummers G, Bucker A, Hanrath P, Franke A. High-resolution transthoracic real-time three-dimensional echocardiography: quantitation of cardiac volumes and function using semi-automatic border detection and comparison with cardiac magnetic resonance imaging. *J Am Coll Cardiol* 2004;43:2083-90.
5. Soliman OI, Krenning BJ, Geleijnse ML, Nemes A, Bosch JG, van Geuns RJ, Kirschbaum SW, Anwar AM, Galema TW, Vletter WB, ten Cate FJ. Quantification of left ventricular volumes and function in patients with cardiomyopathies by real-time three-dimensional echocardiography: a head-to-head comparison between two different semiautomated endocardial border detection algorithms. *J Am Soc Echocardiogr* 2007;20:1042-9.
6. Soliman OI, Krenning BJ, Geleijnse ML, Nemes A, van Geuns RJ, Baks T, Anwar AM, Galema TW, Vletter WB, ten Cate FJ. A comparison between QLAB and TomTec full volume reconstruction for real time three-dimensional echocardiographic quantification of left ventricular volumes. *Echocardiography* 2007;24:967-74.
7. Mor-Avi V, Jenkins C, Kuhl HP, Nesser HJ, Marwick T, Franke A, Ebner C, Freed BH, Steringer-Mascherbauer R, Pollard H, Weinert L, Niel J, Sugeng L, Lang RM. Real-time 3-dimensional echocardiographic quantification of left ventricular volumes: multicenter study for validation with magnetic resonance imaging and investigation of sources of error. *JACC Cardiovasc Imaging* 2008;1:413-23.
8. Soliman OI, Kirschbaum SW, van Dalen BM, van der Zwaan HB, Mahdavian Delavary B, Vletter WB, van Geuns RJ, Ten Cate FJ, Geleijnse ML. Accuracy and reproducibility of quantitation of left ventricular function by real-time three-dimensional echocardiography versus cardiac magnetic resonance. *Am J Cardiol* 2008;102:778-83.
9. Dorosz JL, Lezotte DC, Weitzenkamp DA, Allen LA, Salcedo EE. Performance of 3-dimensional echocardiography in measuring left ventricular volumes and ejection fraction: a systematic review and meta-analysis. *J Am Coll Cardiol* 2012;59:1799-808.
10. Muraru D, Badano LP, Piccoli G, Gianfagna P, Del Mestre L, Ermacora D, Proclemer A. Validation of a novel automated border-detection algorithm for rapid and accurate quantitation of left ventricular volumes based on three-dimensional echocardiography. *Eur J Echocardiogr* 2010;11: 359-68.
11. Chang SA, Lee SC, Kim EY, Hahm SH, Jang SY, Park SJ, Choi JO, Park SW, Choe YH, Oh JK. Feasibility of single-beat full-volume capture real-time three-dimensional echocardiography and auto-contouring algorithm for quantification of left ventricular volume: validation with cardiac magnetic resonance imaging. *J Am Soc Echocardiogr* 2011;24:853-9.
12. Thavendiranathan P, Liu S, Verhaert D, Calleja A, Nitinunu A, Van Houten T, De Michelis N, Simonetti O, Rajagopalan S, Ryan T, Vannan MA. Feasibility, Accuracy, and Reproducibility of Real-Time Full-Volume 3D Transthoracic Echocardiography to Measure LV Volumes and Systolic Function: A

Fully Automated Endocardial Contouring Algorithm in Sinus Rhythm and Atrial Fibrillation. *JACC Cardiovasc Imaging* 2012;5:239-51.

13. Krenning BJ, Kirschbaum SW, Soliman OI, Nemes A, van Geuns RJ, Vletter WB, Veltman CE, Ten Cate FJ, Roelandt JR, Geleijnse ML. Comparison of contrast agent-enhanced versus non-contrast agent-enhanced real-time three-dimensional echocardiography for analysis of left ventricular systolic function. *Am J Cardiol* 2007;100:1485-9.

14. Malm S, Frigstad S, Sagberg E, Larsson H, Skjaerpe T. Accurate and reproducible measurement of left ventricular volume and ejection fraction by contrast echocardiography: a comparison with magnetic resonance imaging. *J Am Coll Cardiol* 2004;44:1030-5.

15. Thomson HL, Basmadjian AJ, Rainbird AJ, Razavi M, Avierinos JF, Pellikka PA, Bailey KR, Breen JF, Enriquez-Sarano M. Contrast echocardiography improves the accuracy and reproducibility of left ventricular remodeling measurements: a prospective, randomly assigned, blinded study. *J Am Coll Cardiol* 2001;38:867-75.

Chapter 3.2

Application of Siemens Automated Three-Dimensional Echocardiographic Algorithm for Assessing Left Ventricular Systolic Function in the Real World

Ben Ren
Ellen J.A. Wiegers – Groeneweg
Mariëtte Mijnlieff, Anja I. Seton
Lourus W. van Haveren
Debbie W. van Dongen
Linda de Jong
Kwaku Gyamfi
Beata M. Owsianska
Marcel L. Geleijnse

ABSTRACT

Objective The aim of this study was to assess the feasibility of the Siemens fully automated algorithm in assessing the LV function in real world clinical conditions.

Method Fifty-one consecutive patients referred for a routine echocardiographic examination for evaluation of LV function were included. The real-time 3D transthoracic echocardiography was performed by eight sonographers. The S1H mode was chosen as the primary imaging mode, and the T1H mode was used if the LV was not complete in the S1H mode acquisition sector. Each full volume 3D dataset was analysed using the custom automatic algorithm. The automatic contour was assessed in two MPR views with eye-balling.

Results In 51 patients, 43 patients (84%) a 3D dataset was acquired. In the 20 patients (47%) where the S1H mode was used, the automatic contour was correct in 15 patients (75%) and In 23 patients (53%) where the T1H mode was used, the automatic contour was correct in 11 patients (48%).

Conclusion In the real world, the Siemens fully automated 3D algorithm was useful in about half of the patients.

Keywords: Left ventricle, three-dimensional, echocardiography, real world

As stated in the previous chapter, the Space 1 Harmonic (S1H) mode of the Siemens SC2000 ultrasound system may be the preferred three-dimensional (3D) acquisition mode in routine clinical practice, supplemented by Time 1 Harmonic (T1H) mode in an enlarged left ventricle (LV) which cannot be included completely in the acquisition sector of the S1H mode. Using this approach, more than halve of patients can be analysed automatically with reasonable results[1]. However, the study was conducted in a research environment and 3D datasets were acquired by one highly-experienced (> 1000 3D studies) sonographer[2]. Therefore, in this chapter we sought to assess the feasibility of the Siemens fully automated algorithm in assessing the LV function in real-world clinical conditions, by implementing our recommendations in a routine echocardiographic examination carried out by eight sonographers with less experience in 3D echocardiography.

PATIENTS AND METHODS

Fifty-one consecutive patients with cancer planned for systemic chemotherapy and referred for a routine echocardiographic 2D/3D examination for evaluation of LV function in 2013 were included. Real-time 3D transthoracic echocardiography (TTE) was performed using the Acuson SC2000 ultrasound system (Siemens Ultrasound, Mountain View, USA) with the 4Z1c real-time full volume transducer. After the gain and depth were adjusted, real-time full volume LV datasets were acquired in a single cardiac cycle from the apical window during breath-hold for two to three cardiac cycles by eight sonographers (level of experience in 3D studies < 25 in 6, 10-50 in 1 and 50-100 in 1). The S1H mode was chosen as the primary imaging mode. In an enlarged LV, the T1H mode was used if the LV was not complete in the S1H mode acquisition sector. Each full volume RT-3DE dataset was digitally stored and exported to the syngo SC2000 Workplace LV Analysis (Siemens Ultrasound). The custom algorithm traces the LV endocardial surface and produces the LV contour throughout the cardiac cycle. The automatic contour was assessed by an observer (BR) in two MPR views (4-chamber and its orthogonal view) of the 3D datasets whether it traced the endocardial border correctly and whether it followed the movement of the endocardium throughout the cardiac cycle correctly.

RESULTS

As shown in the flow chart (Figure 1), in total 51 patients were examined with the Siemens SC2000 ultrasound system in 2013. In 43 patients (84%) a 3D dataset was acquired. In the 8 patients (16%) in whom the 3D TTE datasets were not acquired, four patients

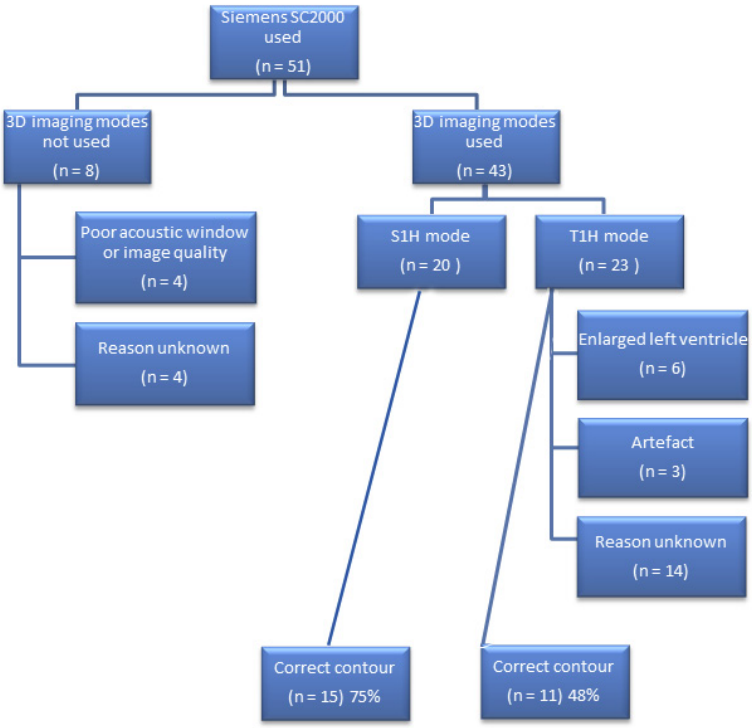

Figure 1 Flow chart of 3D datasets acquisition.

had a poor acoustic window precluding 3D analysis. In the remaining four patients the reason why a 3D dataset was not acquired was unknown. In the 43 patients in whom a 3D dataset was acquired, the S1H mode was applied in 20 patients (47%) and the T1H mode was applied in 23 patients (53%). In the 23 patients where the T1H modes was used, six had enlarged LV which could not be included compeletely in the small-sized S1H sector and in three patients the S1H mode produced strong artefact either in the LV apex or cavity. In the remaining 14 patients the S1H mode was not used without an apparent reason. 50% of these 14 patients were restricted to 2 specific sonographers.

In the 43 patients in whom the 3D datasets were acquired, the automatic LV contour tracking was generally acceptable in 26 patients (60%). Thus, the automatic algorithm was feasible and correct in at least 51% of all 51 patients where the Siemens SC2000 ultrasound system was used. Of the 26 patients with correct contours, the S1H mode was used in 15 patients (58%) and the T1H mode in 11 patients (42%). In the 20 patients where the S1H mode was used, the automatic contour was correct in 15 patients (75%) and not correct in 5 patients (25%). In 23 patients where the T1H mode was used, the automatic contour was correct in 11 patients (48%) and not correct in 12 patients (52%).

DISCUSSION

In this study, we assessed the Siemens automated 3D algorithm in assessing the LV function in consecutive clinical patients in real-world settings. The main findings were that 1) in the vast majority of clinical patients 3D imaging was done; 2) in about half of the patients the Siemens fully automated 3D algorithm generated correct LV contours.

In the vast majority of patients in whom image quality was not poor, 3D imaging was done (43 out of 47 patients, 91%). The true implementation of 3D LV analysis in the real world has often been debated because of the fear for a new technique or extra time consumption (because 3D analysis does not replace 2D analysis but merely supplements it). This study shows that implementation of the Siemens 3D fully automated algorithm is feasible since the experience of the sonographers with 3D LV analysis was limited and none had prior experience with the specific Siemens 3D acquisition or algorithm. In the previous chapter, the fully automated 3D algorithm generated correct LV contours in 58% of patients. That study was done by one highly-experienced sonographer. In the current study in consecutive patients referred for a routine echocardiographic 2D/3D examination for evaluation of LV function before application of systemic chemotherapy by less experienced sonographers, the overall feasibility was comparable (51%). In the patients in whom a 3D dataset was acquired the S1H mode was applied less frequently than the study in the previous chapter (47% vs. 82%). Apart from the known well-described reasons (enlarged LV and 3D artefacts), this was mainly due to two sonographers who apparently did not comply to the protocol.

Limitations

In this study, we did not compare the LV volume and ejection fraction (EF) measures calculated using the Siemens automatic LV algorithm with another imaging modality or echocardiographic algorithms. The aim of the study was to assess the feasibility of the Siemens automatic algorithm in the real-world clinical settings. The accuracy of the measures is assumed to be similar as presented in the previous chapter in terms of bias and limits of agreement compared to the Philips QLAB 3DQA manual measures, ie. 0% ± 8% (EF), −0 ± 27 ml (end-diastolic volume) and −1 ± 16 ml (end-systolic volume).

CONCLUSION

In the real world, the Siemens fully automated 3D algorithm was useful in about half of the patients.

REFERENCES

1. Ren B, Vletter WB, McGhie J, Soliman OI, Geleijnse ML. Single-beat real-time three-dimensional echocardiographic automated contour detection for quantification of left ventricular volumes and systolic function. *Int J Cardiovasc Imaging* 2014;30:287-94.
2. Ryan T, Armstrong WF, Khandheria BK, American Society of E. Task force 4: training in echocardiography endorsed by the American Society of Echocardiography. *J Am Coll Cardiol* 2008;51: 361-7.

Chapter 3.3

Accuracy of Fully Automated Left Ventricular Function Quantification by Three-Dimensional Echocardiography

Ben Ren
Sharon W.M. Kirschbaum
Wim B. Vletter
Jaco H. Houtgraaf
Marcel L. Geleijnse

Submitted

ABSTRACT

Purpose The aim of this study was to validate TomTec fully automated 3D-LV algorithm against cardiac magnetic resonance imaging (MRI) and echocardiographic QLAB manually corrected analysis.

Methods In 76 subjects (46 patients with cardiac diseases and 30 normal controls), left ventricular (LV) volumes and ejection fraction (EF) were calculated with TomTec 3D-LV algorithm automatically, QLAB manually and MRI.

Results The TomTec fully automated algorithm was feasible in all patients and the analysis required 30±5 seconds. In 49 patients (64%) the automated contour tracking was by expert consensus correct. In these patients, the bias and LOA were −38 ± 43 ml (EDV), −8 ± 34 ml (ESV) and −7 ± 11% (EF) compared with MRI and −1 ± 32 ml (EDV), 5 ± 26ml (ESV) and −4 ± 10% (EF) compared with QLAB manually corrected measures. Poor automated tracking was seen in patients with reduced image quality, in particular in the apex and mitral annulus. In these patients manually correction resulted in improvement in the bias but still wide LOAs compared with MRI: −72 ± 61 ml to −40 ± 58 ml (EDV), −31 ± 55 ml to −13 ± 44 ml (ESV) and −4 ± 15% to −4 ± 11% (EF).

Conclusions The TomTec 3D algorithm was feasible in assessing the LV volumes and EF in consecutive patients, independent of the vendor. In the real world, about two-thirds of echocardiograms can be analyzed fully automatically and accurately in a fast manner.

Keywords: left ventricular function, echocardiography, three-dimensional, magnetic resonance imaging

Left ventricular (LV) volumes and ejection fraction (EF) are the most used parameters in assessing LV function and have important prognostic significance[1,2]. Three-dimensional transthoracic echocardiography (3D TTE) has been validated against cardiac magnetic resonance imaging (MRI) as an accurate and reproducible imaging modality in measuring the LV volumes and EF in different patient populations[3-10]. However, compared with MRI, 3D TTE still underestimates the volumes and has wide limits of agreement (LOA)[11]. In addition, some manual input is still required and corrections are not infrequently necessary, which results in significant inter-observer variability, in particular between institutions[12], and variable time consumption. Therefore, the ultimate goal of assessment of LV volumes (and thus EF) in routine clinical practice should be a fast, fully automated system reducing observer variability to zero values. TomTec (Unterschleissheim, Germany) recently developed such an algorithm that is able to analyze datasets from all different echocardiographic machine vendors. In this study, we sought to assess the value of this fully automated analysis against MRI and manually corrected QLAB echocardiographic analysis in consecutive subjects.

PATIENTS AND METHODS

Patient population

The study included 76 subjects who had undergone both MRI and 3D TTE examinations within 24 hours from August 2008 to November 2011: 46 consecutive patients (37 men, 62 ± 12 years old) who were included in stem cell therapy, heart failure or hypertension trials, and 30 consecutive control subjects (15 men, 31 ± 7 years old) without cardiac and systemic abnormalities. Patient inclusion in these trials was independent on echocardiographic image quality. Thirty-four patients (45%) had suffered myocardial infarction treated with percutaneous coronary intervention, 7 patients (9%) were known with dilated cardiomyopathy, and 5 patients (6%) were known with hypertension. All imaging examinations were undertaken according to institutional trial protocols and written consents were obtained.

Three-dimensional transthoracic echocardiography

Electrocardiographically gated full volume 3D TTE datasets of the LV built from 4 or 7 subvolumes with breath-hold were acquired in apical views using Philips iE33 ultrasound system (Philips Medical System, Best, the Netherlands) with the X5-1 or X3-1 transducer. Efforts were taken to include the complete LV cavity into the datasets. The average volume rate of the 3D TTE datasets was 36 ± 6 vps. The 3D datasests were analyzed off-line using 4D LV-Analysis 3.1 (TomTec Imaging systems, Unterschleissheim, Germany) by one independent observer (BR). The 3D datasets were displayed as 3-chamber, 2-chamber,

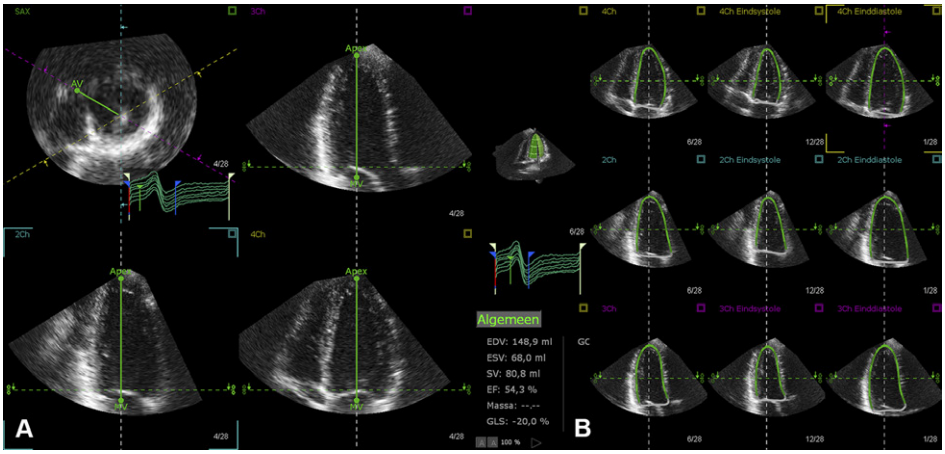

Figure 1 The TomTec 4D LV-Analysis automatic algorithm. A, two-dimensional reference views extracted from the 3D datasets; B, the left ventricular endocardial contour throughout the cardiac cycle which can be adjusted manually at end-diastolic and end-systolic frames.

4-chamber and short-axis views. The end-diastolic and end-systolic frames were defined automatically (Figure 1A). Then the endocardial border in end-diastolic frame was traced first as the beutel images. Subsequent frames including the end-systolic frame were then traced (Figure 1B). All contour trackings were performed automatically. In the report page, the LV volumes and EF as well as deformational analysis results were presented. Manual corrections of the automatic contours were applied only in cases where the automatic algorithm clearly failed to trace the endocardial border or to follow the motion of the LV endocardium.

In particular to analyze if any LV volume under- or overestimation compared with MRI was a specific TomTec algorithm problem or a non-specific echocardiographic problem, the same 3D datasets were also analyzed by a highly experienced blinded observer (WBV) using the 3DQA, QLAB 9.0 (Philips Medical System, Best, the Netherlands). The 3D dataset was displayed as 3 orthogonal multiplanar reconstruction views of LV. After selecting the end-diastolic and end-systolic reference frames, 5 reference points (four on the mitral annulus and one on the LV apex) were added manually in two orthogonal views of the reference frames. Although the software traced the LV endocardial border and calculated the volumes and EF automatically the contours were corrected manually in all patients to achieve optimal contour tracing and results.

Cardiac magnetic resonance imaging

A 1.5 Tesla scanner with a dedicated eight-element phased-array receiver coil was used for imaging (Signa CV/i, GE Medical systems, Milwaukee, Wisconsin USA). Cine MRI was performed using a steady-state free-precession technique (FIESTA). Imaging parameters were: 10-15 seconds breath hold (depending on the heart rate); repetition time, 3.4 ms;

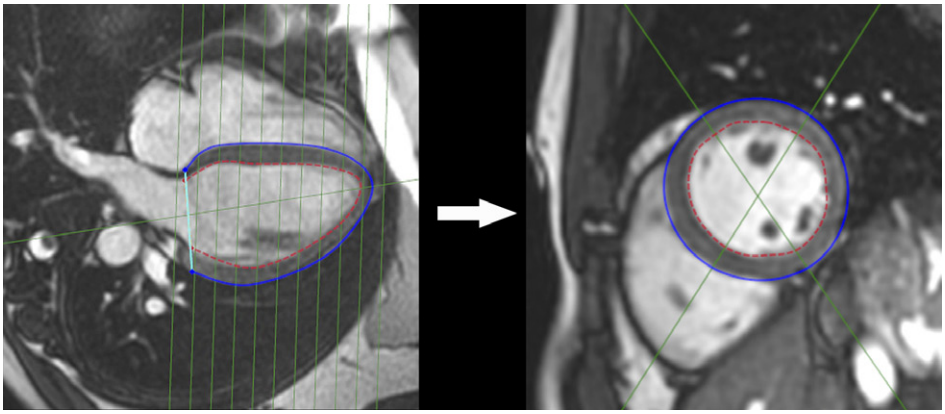

Figure 2 The magnetic resonance imaging analysis algorithm. The 4-chamber view with all short axis slices are first displayed. Four intersection points are then interpolated on the short axis view. According to the signal intensity, the software traces the endocardial border automatically.

echo time, 1.5 ms; flip angle, 45 degrees; slice thickness 8.0 mm with a 2.0 mm slice gap; field of view 36-40 x 28-36 cm; 12 views per segment and matrix size was 192 × 192. These parameters resulted in a temporal resolution per image of less than 41 ms. Repeated breath holds and gating to the electrocardiogram were applied to minimize the influence of cardiac and respiratory motion on data collection. Using standard techniques to identify the major cardiac axes, 2-chamber and 4-chamber cine MR images were obtained. The 2- and 4-chamber end diastolic images at end expiration provided the reference images to obtain a series of short axis views. The first slice was positioned at the basis covering the mitral valve and the last slice covering the apex. This resulted in 10-12 cine breath-hold short axis images to cover the entire left ventricle.

All images were transferred to a Microsoft Windows™ based personal computer for analysis using the CAAS-MRV program (Pie Medical Imaging version 3.2, Maastricht, The Netherlands) and analysed by the third independent observer (SWK) who was blinded to the echocardiographic analyses. Left ventricular volumes and EF were analysed using the additional information of the long axis to limit the extent of volume at the base and the apex of the heart[13]. Papillary muscles and trabeculations were considered as being part of the blood pool volume (Figure 2).

Statistical methods

All values were expressed as mean ± standard deviation and number (percentage). Linear regression analysis was used to assess the correlation of the EF, end-diastolic volume (EDV) and end-systolic volume (ESV) between echocardiographic and MRI measurements. The agreement between the TomTec analysis and MRI was assessed by Bland–Altman method in which differences were plotted against the average and the percentage error where the absolute difference between the echocardiographic and

MRI measures was divided by the MRI measures. The TomTec analysis was also compared with the QLAB analysis using the Bland–Altman method and the relative difference where the absolute difference between two measures was divided by the average value. Differences were considered statistical significant when $p < 0.05$.

RESULTS

Feasibility of the TomTec automated LV volumes algorithm

The automated TomTec 3D algorithm was feasible in all 76 patients (100%) and required 30 ± 5 seconds for one 3D dataset. In 14 patients (18%) the automated contour tracking was by visual assessment excellent. Although visually the contour seemed somewhat inward (not fully including the trabeculations in the volume) in 35 patients (46%) the contours were also accepted because the influence on the EF was expected to be minimal. Thus, in total in 49 patients (64%) the automated contour was generally considered correct and adjustments were not required or only expected to result in minor changes. In 27 patients (36%) with reduced image quality, the automated algorithm failed to trace the endocardial border correctly due to three main reasons : 1) the apical reference point was not set at the true apex but into the LV cavity resulting in to inner contour at the apex (Figure 3A); 2) the mitral valve reference plane was set below (ventricular side) the annular level (Figure 3B); 3) the contour traced an artifact or papillary muscle. In these latter 27 patients, manual correction was applied which took 3 ± 1 minutes and both the automated and manually corrected results were analyzed.

Accuracy of the automated TomTec LV volumes algorithm versus MRI

The comparisons between the 3D TomTec automated measures (in all patients) against the MRI measures in all patients are shown in Table 1 and Figure 4. The LV volumes and EFs were significantly different between 3D echocardiography and MRI. The volumes were respectively for EDV 132 ± 32 vs. 181 ± 44 ml, ESV 70 ± 29 vs. 86 ± 39 ml, and for EF 48 ± 11% vs. 54 ± 11% (all $p < 0.01$). The correlations of the LV volumes and EF between 3D echocardiography and MRI were all statistically significant (all $p < 0.001$).

Accuracy of the automated TomTec LV volumes algorithm versus manual QLAB

The manually corrected QLAB 3DQA analysis required 10 ± 5 minutes. The comparisons between the automated TomTec (in all patients) and manual QLAB analysis are also shown in Table 1 and Figure 4. The EDVs were significantly different between the automated TomTec and manual QLAB analysis (132 ± 32 vs. 138 ± 33 ml, $p < 0.02$). The ESVs between the automated TomTec and manual QLAB analysis were comparable (70 ± 29 vs. 68 ± 30 ml). The EFs were also significantly different from between the automated

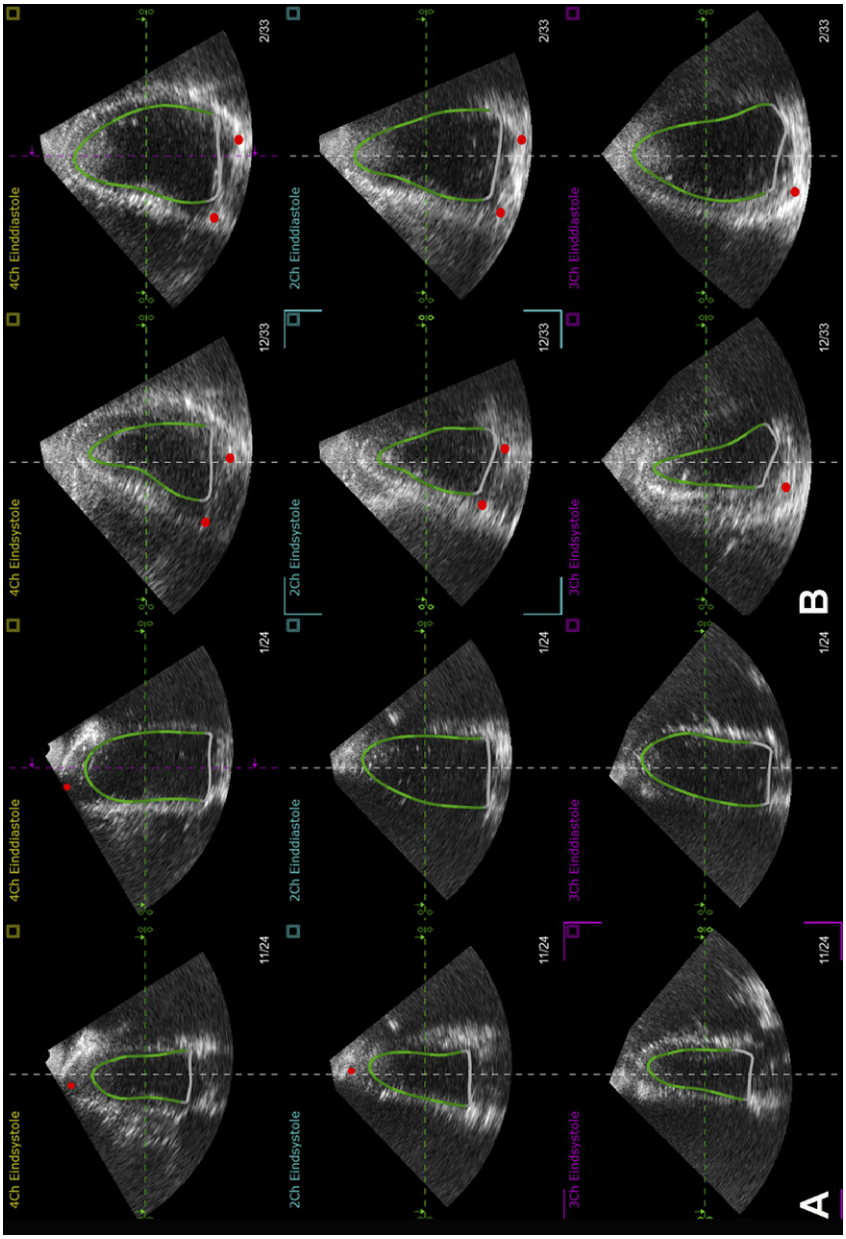

Figure 3 Failed LV automatic contour tracking requiring manual correction (left column: end-systole, right column: end-diastole, upper row: 4-chamber view, middle row: 2-chamber view, lower row: 3-chamber view). A, a too inner left ventricle contour at the apex; B, the mitral annular plane of the automatic left ventricle was below the annular level. The red dots indicate where true apex and mitral annular points should be.

Table 1 Accuracy of the automated TomTec LV volumes algorithm versus MRI and manual QLAB analyses in all patients (n = 76).

	MRI	QLAB manual
EDV		
Pearson *r*	0.74	0.81
Bias ± 2SD (ml)	−50 ± 60	−7 ± 40
Percentage error (%)	26 ± 12	12 ± 10
ESV		
Pearson *r*	0.80	0.84
Bias ± 2SD (ml)	−16 ± 48	2 ± 34
Percentage error (%)	22 ± 14	18 ± 14
EF		
Pearson *r*	0.83	0.84
Bias ± 2SD (%)	−6 ± 12	−5 ± 12
Percentage error (%)	14 ± 9	13 ± 10

Percentage error = absolute difference/MRI (QLAB manual) measures × 100% and presented as bias ± SD. EF, ejection fraction; EDV, end diastolic volume; ESV, end systolic volume; MRI, magnetic resonance imaging; SD, standard deviation.

Table 2 Accuracy of the automated TomTec LV volumes algorithm versus MRI and manual QLAB analyses in the subgroups defined by the quality of the generated automated contour.

		Good* (n = 14)	Fair† (n= 35)	Good / Fair‡ (n = 49)	Poor§ (n = 27)	Poor after manual correction‖ (n = 27)
MRI	**EDV (ml)**	−37 ± 32	−38 ± 47	−38 ± 43	−72 ± 61	−40 ± 58
	ESV (ml)	−9 ± 28	−8 ± 36	−8 ± 34	−31 ± 55	−13 ± 44
	EF (%)	−6 ± 9	−7 ± 12	−7 ± 11	−4 ± 15	−4 ± 11
QLAB Manual	**EDV (ml)**	4 ± 34	−3 ± 31	−1 ± 32	−18 ± 45	13 ± 47
	ESV (ml)	7 ± 20	4 ± 28	5 ± 26	−3 ± 43	15 ± 39
	EF (%)	−4 ± 7	−5 ± 11	−4 ± 10	−5 ± 15	−4 ± 12

*Good: no manual correction was required for the contour generated by the automatic algorithm;
†Fair: the automatic contour was generally correct and adjustments were only expected to result in minor changes of contour;
‡Good/Fair: mixed patients of the Good and Fair groups;
§Poor: the automatic contour failed to trace the endocardium correctly and manual correction thus seemed mandatory;
‖Poor after manual correction: the measures obtained after manual correction of the automatic contour failed to trace correctly in the 27 patients. Data presented as bias ± 2SD. Abbreviations as in Table 1.

TomTec and manual QLAB analysis (48 ± 11% vs. 53 ± 11%, $p < 0.001$). The correlations of the LV volumes and EF between the automated TomTec and manual QLAB analysis were all statistically significant (all $p < 0.001$).

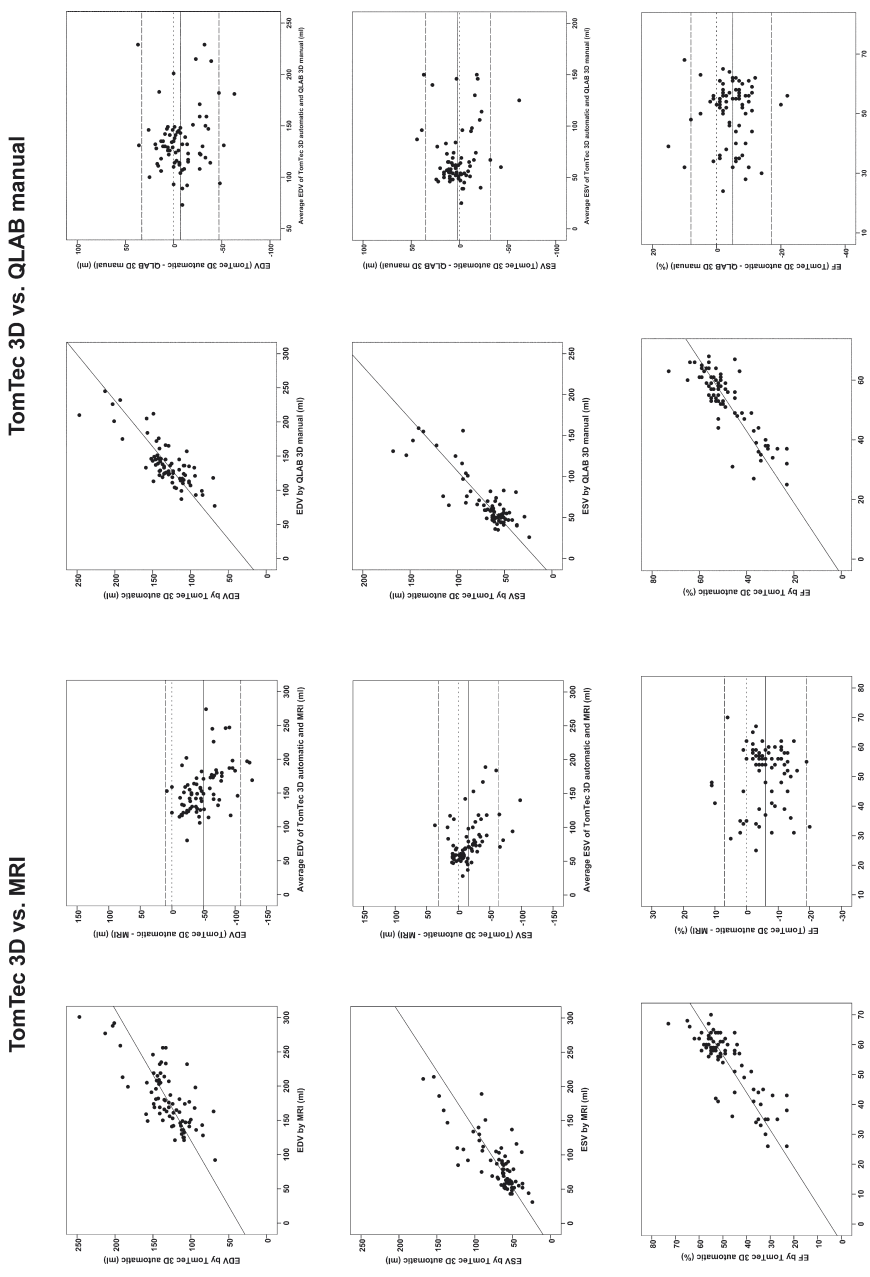

Figure 4 Linear regression and Bland–Altman analyses comparing the EDV, ESV and EF for TomTec versus MRI. EDV, end-diastolic volume; EF, ejection fraction; ESV, end-systolic volume; MRI, magnetic resonance imaging.

Subgroup analysis

As described before, the patients were divided into 3 subgroups according to the visual assessment of the quality of the automated contour tracking. The comparison of LV volumes and EF measures of patients in these 3 subgroups as well as the grouped good and fair quality patients with MRI and QLAB measurements are presented in Table 2 and Figure 5. The correlations of the LV volumes and EF between 3D echocardiography and MRI were all statistically significant (all $p < 0.001$). Both the biases and LOAs were smaller

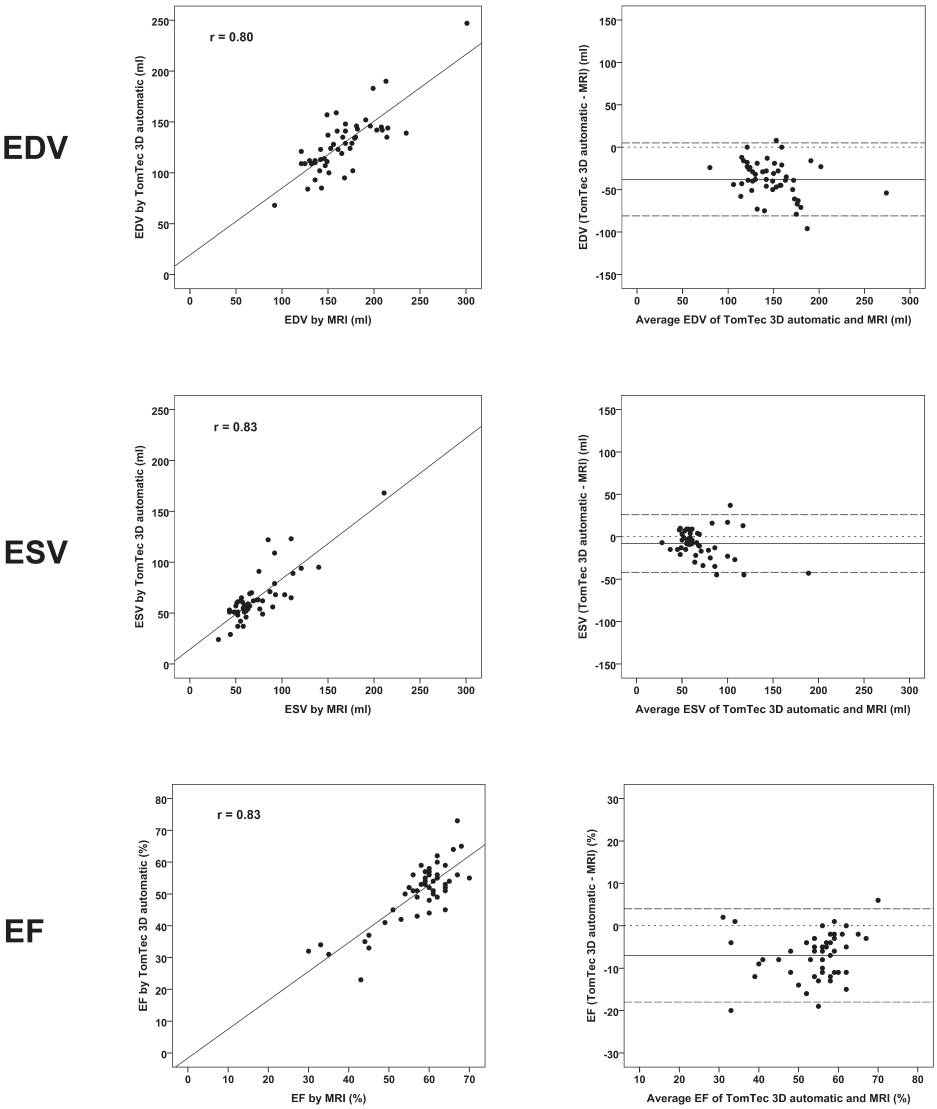

Figure 5 Linear regression and Bland–Altman analysis comparing the EDV, ESV and EF for TomTec versus MRI in patients with good/fair automated contour tracking contour. Abbreviations as in Figure 4.

in the grouped good and fair tracking group compared to the poor-tracking group. For the LV volumes, the biases in the combined TomTec good/fair group of patients almost reached zero values compared with the QLAB manual analysis (−1 ± 32 ml and, and 5 ± 26 ml for ESV). Additionally, manual corrections were made in the poor group (Table 2). Compared with MRI, the biases in the manually corrected poor group were comparable to the automated good/fair group. Compared with the QLAB manual measures, a positive bias was now seen (EDV: 13 ± 47 ml, ESV: 15 ± 39 ml).

DISCUSSION

This is the first clinical study validating the fully automated TomTec 4D-analysis algorithm against MRI and manually corrected QLAB measurements in consecutive patients. The main findings of this study were 1) the TomTec automatic algorithm was feasible in calculating LV volumes and EF in all consecutive patients; 2) the contour tracking was acceptable (not requiring major corrections) in about two thirds of patients (64%); 3) the biases and LOAs compared with the MRI measures in these acceptable analyses were comparable with published data on manually corrected 3D sets; and 4) the underestimation of LV volumes compared with the MRI was not seen when compared with the QLAB manual analysis.

Automated TomTec 4D-LV analysis compared with MRI

In the last decade, several vendors have developed different 3D algorithms for analysis of LV volumes. These 3D algorithms have been validated in different patient populations against MRI, and it has been shown that the assessment of 3D LV volumes is superior to 2D analyses[3,5,6,8,9]. However, it has also been recognized that 3D echocardiography is limited in spatial and temporal resolutions and still underestimates LV volumes compared with MRI. Additionally, apart from one recently developed algorithm[14,15], all but one software packages require manual input and in a substantial number of patients manual corrections. As a consequence, although improved compared with the standard 2D tracing, there is still a significant inter-observer and in particular inter-institutional[12] variability in measures[11].

In the present study the fully automated TomTec algorithm resulted in a zero inter-observer variability but significant differences in LV volumes and EF compared with MRI in terms of bias and LOA (−50 ± 60 ml for EDV, −16 ± 48 ml for ESV and −6 ± 12% for EF). However, it should be recognised that in one-third of the consecutive patients, the tracking software was not able to track the contours reliably according to a subjective interpretation. When these patients were excluded from the analysis, the biases and LOAs were improved in particular for the volumes (from −50 ± 60 ml to −38 ± 43 ml for

EDV and from −16 ± 48 ml to −8 ± 34 ml for ESV). These numbers were comparable to numbers recently reported by Dorosz *et al.* in a systemic review of studies comparing manually corrected 3D echocardiographic analysis with MRI[11]. The main reasons for the LV volume underestimation by the automated TomTec algorithm were (as shown in Figure 3) the LV contour was set to inward into the LV cavity at the LV apex, and the mitral annular plane was below the true annular level. In the poor automated tracking subset of patients, correction of the apical point led to an increase of 3-18% in EDV and correction of the mitral annular points led to a change of 10-28% in EDV.

In the literature, only one study was identified describing the results of a fully automated algorithm versus MRI. After excluding almost one-third of patients from analysis because of poor image quality, artefacts or technical problems in acquisition, Thavendiranathan *et al.* reported for the Siemens fully automated algorithm (eSie LVA, Siemens Ultrasound) volumes comparable to those in our study (−18 ± 54 ml for EDV and −10 ± 36 ml for ESV)[15].

In one-third of our patients the automated contour tracking was defined as not acceptable, thus requiring manual correction. This was mainly due to a poor echocardiographic window and artefacts especially in the near-field. As shown in Table 2, in these patients the biases were highest and LOAs were widest. Interestingly, manual correction improved the negative biases of the LV volumes substantially to a level approaching the numbers in the grouped good and fair quality patients. In contrast, the LOAs were improved only to a small extent.

TomTec 4D-LV analysis compared with QLAB manual analysis

Magnetic resonance imaging has been often used as the gold standard for measuring LV volumes and EF [16]. However, MRI itself is not perfect because it also has errors related to endocardial border-detection due to sub-optimal spatial resolution in particular for defining trabeculations and there may be controversy on the inclusion of basal LV planes. The difference in measuring LV volumes and EF using echocardiography and MRI may also be due to differences in the planimetric approach to LV contour tracing since the LV contour is generally traced in long-axis views using echocardiography but in short-axis views using MRI. As the QLAB software has been well established and validated in different patient populations in measuring LV volumes and EF with well-known advantages and drawbacks[5,6,10,12,17-19], we intended to compare the fully automated TomTec algorithm also with the manually corrected QLAB measures, in particular to investigate potential underestimation of volumes (that was indeed confirmed by MRI). When compared with the QLAB analysis, the TomTec "underestimation" of EDV was improved from −50 to −7 ml in the overall patient group and from −38 to −1 ml in the subgroup with visually acceptable contours. Thus, the "volume underestimation" seemed not a specific property of the automated TomTec algorithm but an inherent property of echocardiographic analysis.

Clinical application of the TomTec 4D-LV analysis

The greatest advantage of the TomTec 4D-LV analysis in routine clinical practice is the ability to analyze datasets from different vendors fully automatically in a fast manner, giving reasonable LV volume and EF measures in about two-thirds of routine clinical patients with a zero inter-observer variability. However, the assessment of the reliability of the automated contour tracking was performed with subjective eye-balling by expert consensus. An objective quality score system embedded in the program to show how reliable the automatic contour tracking might be very useful in particular for less experienced users. Additionally, the algorithm is included in the TomTec Image Arena platform and analysis is therefore only possible offline which could limit its application in routine practice. In the one-third of patients with less favourable image quality, although contour corrections were relatively easily made compared with other software packages, the results were still far from optimal.

Other limitations

In this study, we included consecutive patients who had undergone 3D TTE and MRI within 24 hours. Nevertheless, all patients included in the study were in sinus rhythm during image acquisition. For patients with permanent atrial fibrillation, the image quality of 3D datasets will be potentially further compromised by stitching artefacts, which may adversely affect this automatic algorithm. We did not report the observer variability of the QLAB manual analysis in this study. Based on previous studies by our group, the interobserver variability was maximal 12.2 ± 10.1% for EDV, 13.6 ± 11.2% for ESV, and 9.7 ± 8.8% for EF[18,20,21]. As mentioned before, the variability in the choice of the basal slice is a limitation of MRI, but this was controlled by the selection of the basal slice by referring to the long axis image[13].

CONCLUSIONS

The TomTec algorithm was feasible in assessing the LV volumes and EF in consecutive patients independent of the vendor. In the real world, about two-thirds of echocardiograms could be analyzed fully automatically and accurately in a very fast manner.

ACKNOWLEDGEMENT

Heleen B. van der Zwaan M.D., Ph.D., Admir Dedic M.D., Ph.D., and Joost Daemen M.D., Ph.D.'s contributions in the patients inclusion and echocardiographic and MRI data collections are gratefully acknowledged.

REFERENCES

1. Wang TJ, Evans JC, Benjamin EJ, Levy D, LeRoy EC, Vasan RS. Natural history of asymptomatic left ventricular systolic dysfunction in the community. *Circulation* 2003;108:977-82.
2. White HD, Norris RM, Brown MA, Brandt PW, Whitlock RM, Wild CJ. Left ventricular end-systolic volume as the major determinant of survival after recovery from myocardial infarction. *Circulation* 1987;76:44-51.
3. Jenkins C, Bricknell K, Hanekom L, Marwick TH. Reproducibility and accuracy of echocardiographic measurements of left ventricular parameters using real-time three-dimensional echocardiography. *J Am Coll Cardiol* 2004;44:878-86.
4. Gutierrez-Chico JL, Zamorano JL, Perez de Isla L, Orejas M, Almeria C, Rodrigo JL, Ferreiros J, Serra V, Macaya C. Comparison of left ventricular volumes and ejection fractions measured by three-dimensional echocardiography versus by two-dimensional echocardiography and cardiac magnetic resonance in patients with various cardiomyopathies. *Am J Cardiol* 2005;95:809-13.
5. Jacobs LD, Salgo IS, Goonewardena S, Weinert L, Coon P, Bardo D, Gerard O, Allain P, Zamorano JL, de Isla LP, Mor-Avi V, Lang RM. Rapid online quantification of left ventricular volume from real-time three-dimensional echocardiographic data. *Eur Heart J* 2006;27:460-8.
6. Jenkins C, Chan J, Hanekom L, Marwick TH. Accuracy and feasibility of online 3-dimensional echocardiography for measurement of left ventricular parameters. *J Am Soc Echocardiogr* 2006; 19:1119-28.
7. Jenkins C, Leano R, Chan J, Marwick TH. Reconstructed versus real-time 3-dimensional echocardiography: comparison with magnetic resonance imaging. *J Am Soc Echocardiogr* 2007;20:862-8.
8. Chukwu EO, Barasch E, Mihalatos DG, Katz A, Lachmann J, Han J, Reichek N, Gopal AS. Relative importance of errors in left ventricular quantitation by two-dimensional echocardiography: insights from three-dimensional echocardiography and cardiac magnetic resonance imaging. *J Am Soc Echocardiogr* 2008;21:990-7.
9. Jenkins C, Moir S, Chan J, Rakhit D, Haluska B, Marwick TH. Left ventricular volume measurement with echocardiography: a comparison of left ventricular opacification, three-dimensional echocardiography, or both with magnetic resonance imaging. *Eur Heart J* 2009;30:98-106.
10. Marsan NA, Westenberg JJ, Roes SD, van Bommel RJ, Delgado V, van der Geest RJ, de Roos A, Klautz RJ, Reiber JC, Bax JJ. Three-dimensional echocardiography for the preoperative assessment of patients with left ventricular aneurysm. *Ann Thorac Surg* 2011;91:113-21.
11. Dorosz JL, Lezotte DC, Weitzenkamp DA, Allen LA, Salcedo EE. Performance of 3-dimensional echocardiography in measuring left ventricular volumes and ejection fraction: a systematic review and meta-analysis. *J Am Coll Cardiol* 2012;59:1799-808.
12. Mor-Avi V, Jenkins C, Kuhl HP, Nesser HJ, Marwick T, Franke A, Ebner C, Freed BH, Steringer-Mascherbauer R, Pollard H, Weinert L, Niel J, Sugeng L, Lang RM. Real-time 3-dimensional echocardiographic quantification of left ventricular volumes: multicenter study for validation with magnetic resonance imaging and investigation of sources of error. *JACC Cardiovasc Imaging* 2008;1:413-23.
13. Kirschbaum SW, Baks T, Gronenschild EH, Aben JP, Weustink AC, Wielopolski PA, Krestin GP, de Feyter PJ, van Geuns RJ. Addition of the long-axis information to short-axis contours reduces interstudy variability of left-ventricular analysis in cardiac magnetic resonance studies. *Invest Radiol* 2008;43:1-6.

14. Ren B, Vletter WB, McGhie J, Soliman OI, Geleijnse ML. Single-beat real-time three-dimensional echocardiographic automated contour detection for quantification of left ventricular volumes and systolic function. *Int J Cardiovasc Imaging* 2013.

15. Thavendiranathan P, Liu S, Verhaert D, Calleja A, Nitinunu A, Van Houten T, De Michelis N, Simonetti O, Rajagopalan S, Ryan T, Vannan MA. Feasibility, accuracy, and reproducibility of real-time full-volume 3D transthoracic echocardiography to measure LV volumes and systolic function: a fully automated endocardial contouring algorithm in sinus rhythm and atrial fibrillation. *JACC Cardiovasc Imaging* 2012;5:239-51.

16. Alfakih K, Reid S, Jones T, Sivananthan M. Assessment of ventricular function and mass by cardiac magnetic resonance imaging. *Eur Radiol* 2004;14:1813-22.

17. Caiani EG, Coon P, Corsi C, Goonewardena S, Bardo D, Rafter P, Sugeng L, Mor-Avi V, Lang RM. Dual triggering improves the accuracy of left ventricular volume measurements by contrast-enhanced real-time 3-dimensional echocardiography. *J Am Soc Echocardiogr* 2005;18:1292-8.

18. Soliman OI, Krenning BJ, Geleijnse ML, Nemes A, Bosch JG, van Geuns RJ, Kirschbaum SW, Anwar AM, Galema TW, Vletter WB, ten Cate FJ. Quantification of left ventricular volumes and function in patients with cardiomyopathies by real-time three-dimensional echocardiography: a head-to-head comparison between two different semiautomated endocardial border detection algorithms. *J Am Soc Echocardiogr* 2007;20:1042-9.

19. Pouleur AC, le Polain de Waroux JB, Pasquet A, Gerber BL, Gerard O, Allain P, Vanoverschelde JL. Assessment of left ventricular mass and volumes by three-dimensional echocardiography in patients with or without wall motion abnormalities: comparison against cine magnetic resonance imaging. *Heart* 2008;94:1050-7.

20. Soliman OI, Kirschbaum SW, van Dalen BM, van der Zwaan HB, Mahdavian Delavary B, Vletter WB, van Geuns RJ, Ten Cate FJ, Geleijnse ML. Accuracy and reproducibility of quantitation of left ventricular function by real-time three-dimensional echocardiography versus cardiac magnetic resonance. *Am J Cardiol* 2008;102:778-83.

21. Soliman OI, Krenning BJ, Geleijnse ML, Nemes A, van Geuns RJ, Baks T, Anwar AM, Galema TW, Vletter WB, ten Cate FJ. A comparison between QLAB and TomTec full volume reconstruction for real time three-dimensional echocardiographic quantification of left ventricular volumes. *Echocardiography* 2007;24:967-74.

Part IV

3D echocardiography in reconstructing left atrium

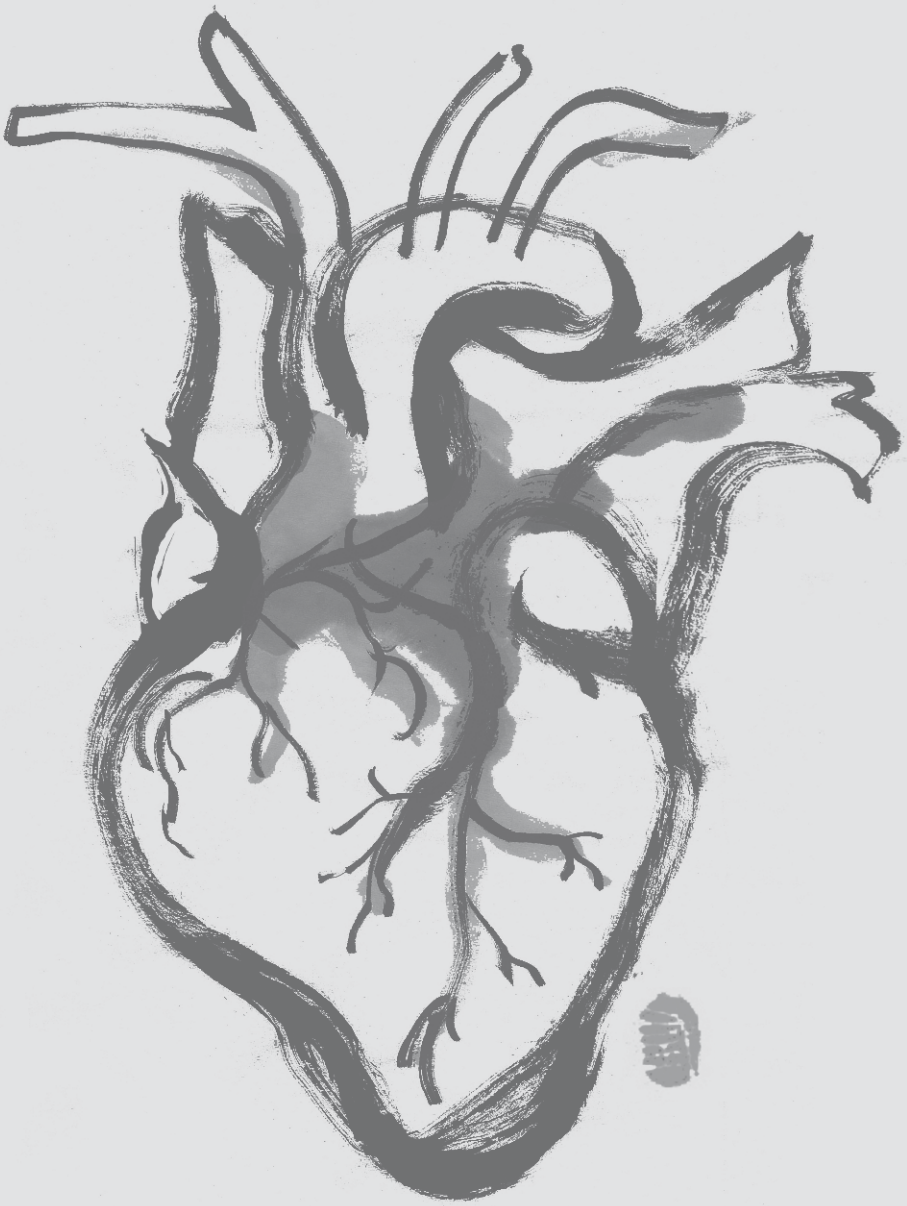

Chapter 4.1

A Transoesophageal Echocardiographic Image Acquisition Protocol for Wide-View Fusion of Three-Dimensional Datasets to Support the Atrial Fibrillation Catheter Ablation

Ben R
Harriët W. Mulder
Alexander Haak
Marijn van Stralen
Tamas Szili-Torok
Josien P.W. Pluim
Marcel L. Geleijnse
Johan G. Bosch

J Interv Card Electrophysiol. 2013; 37(1):21-6.

ABSTRACT

Purpose The aim of this study was to propose a transoesophageal echocardiography (TOE) image acquisition protocol which provided a systematic manner of acquiring a minimal number of overlapping 3D TOE datasets allowing the reconstruction of a wide 3D view of the left atrium (LA) with anatomical landmarks important for the atrial fibrillation catheter ablation.

Methods In eight cardiac surgical patients, 3D TOE datasets were acquired with a 6-step protocol. In the protocol, Step 1 aims to acquire the central view of the mitral valve (MV), aortic valve (AV) and left atrial appendage (LAA). Step 2 was developed to acquire the left pulmonary veins (PVs) and Step 3 to acquire the right PVs. Step 4, 5 and 6 were developed to create sufficient overlap between different datasets. 3D TOE datasets were registered and fused manually in end diastole.

Results The image acquisition protocol was feasible in all patients. In the fused 3D dataset, a wide 3D view of the LA was shown and left and right PVs could be seen simultaneously. The LAA, MV, AV, and fossa ovalis (FO) were visualised clearly in the 3D TOE datasets. The PV ostia located at the edges of the 3D datasets, suffered more from echo loss. The volume overlaps between neighbouring TOE datasets were 50–75%.

Conclusion The major part of the LA anatomy incorporating the PVs, LAA, MV, AV and FO as important anatomical landmarks could be reconstructed by registering and fusing 3D datasets acquired with the 6-step TOE image acquisition protocol.

Keywords: three-dimensional, transoesophageal echocardiography, wide-view fusion, atrial fibrillation, catheter ablation

Atrial fibrillation (AF) is increasingly treated by catheter ablation, during which circumferential lesions are created around the left and right pulmonary vein (PV) ostia to isolate the PVs, thus eliminating the triggers initiating AF[1]. To support the procedure, imaging the left atrium (LA) along with the PVs, left atrial appendage (LAA) and mitral valve (MV) is important. Several imaging modalities are commonly applied. Rotational angiography[2], computed tomography (CT), or magnetic resonance imaging (MRI) are often used before the ablation procedure, and the pre-acquired CT or MRI images are segmented and registered in the electro-anatomical surface mapping (EAM) system to the real time mapping space during the procedure[3]. However, the substantial dose of ionizing radiation of CT scans, rotational angiography and fluoroscopy required by the catheter ablation causes important delayed effects on patients[4-6]. As AF ablation procedures often need to be repeated, there is a consensus that every attempt should be taken to minimize radiation exposure[7]. Additionally, CT and MRI are of cumbersome logistics and high cost. Up till now, the contribution of pre-interventional CT or MRI to the efficacy of the AF catheter ablation procedure is still under debate.

Transoesophageal echocardiography (TOE) is used routinely to exclude LAA thrombus a few days or immediately before the catheter ablation. The anatomy of the LA and adjacent structures can be visualised in high resolution 2D and 3D TOE images[8-10]. However, the field of view of one single full volume 3D TOE dataset is not large enough to visualise all important cardiac structures simultaneously, and this holds particularly true for the PVs which are located at the left and right edges of the LA. In theory, it is possible to reconstruct a 3D anatomical surface of the LA using overlapping and fused 3D TOE datasets, potentially eliminating the need for pre-interventional CT or MRI [11]. In this study, we proposed a stepwise TOE image acquisition protocol which provided a fast and systematic manner of acquiring a minimal number of overlapping 3D TOE datasets which the reconstruction of a wide 3D view of the LA along with all important anatomical landmarks.

METHODS

Study population and ultrasound system

In eight cardiac surgical patients (five men, aged 59 ± 14 years), intraoperative TOE was performed with the iE33 xMatrix ultrasound system (Philips Medical System, the Netherlands) with the X7-2t matrix-array transducer under general anaesthesia. The protocol was approved by the institutional review board.

Transoesophageal echocardiography image acquisition protocol

The stepwise TOE image acquisition protocol with the rotation angle and probe manipulation is depicted in Table 1. All acquisitions were performed at the mid-oesophageal

Table 1 The 6-step transoesophageal echocardiographic image acquisition protocol.

Step	Angle	Manipulation of the probe
1	60–80°	First position the probe at the mid-oesophageal level at 0° and retroflex the probe tip slightly to develop the 4-chamber view; rotate the angle forward to 60–80° to develop the imaging plane parallel to the line intersecting the two commissures of the mitral valve[12].
2	60–80°	From Step 1, withdraw the probe by 1–2 cm and turn it anticlockwise about 15° to visualise the left PVs.
3	100–130°	Turn the probe back to the position in Step 1; rotate the angle forward to 100–130° and turn the probe clockwise until the left atrium appears in the upper part of the screen and right atrium in the lower part with the superior vena cava at the right side to develop the bicaval view; turn the probe further clockwise about 15° to reveal the right upper pulmonary vein at the right side of the screen and the superior vena cava is not seen.
4	120–160°	From Step 3, rotate the angle to 120–160° and turn the probe anticlockwise until the left ventricular outflow tract, aortic valve and proximal ascending aorta line up and the aortic valve appears in the centre of the image.[12]
5	120–160°	From Step 4, turn the probe clockwise by about 40°, half way back to the 2D view of Step 3.
6	120–160°	Turn the probe back to the position in Step 4; turn the probe further anticlockwise about 20°.

level. All structures of interest were first visualised in 2D images of each step (Figure 1A); then, the corresponding 3D datasets were acquired according with one cardiac cycle with a proper depth and the largest volume size to include the structures of interest. The 2D reference views and 3D datasets were acquired according to the ASE guidelines for performing the intraoperative TOE examination[12] and the latest EAE/ASE recommendations for image acquisition and display using 3D echocardiography[13]. In the protocol, Step 1 aims to acquire the central view of the MV, LAA and AV; Step 2 was developed to acquire the left PVs and Step 3 to acquire the right PVs (Figure 1B). Step 4, 5 and 6 were developed to create sufficient overlap between different datasets for image registration and fusion.

Image registration

To construct a wide 3D view of the LA including the left and right PVs, the datasets of the six different steps were registered manually in a pairwise fashion in end diastole in two stages. Firstly, three landmarks were indicated in each dataset. For all datasets, the tip of the pyramidal 3D datasets and the coaptation point of the aortic valve (AV) leaflets were used as soft landmarks. Depending on the view, the coaptation point of the MV leaflets or the fossa ovalis (FO) was chosen as the third landmark. Since corresponding time frames were registered, only rotational and translational differences between the volumes were expected and therefore a rigid transformation model was used. The landmarks were registered by a closed-form least squares optimization algorithm[14]. Secondly, the image alignment was improved manually by rotating and translating one volume with respect to the other, viewing the result in all three orthogonal views. Once an adequate transformation was found, the datasets were fused with maximum

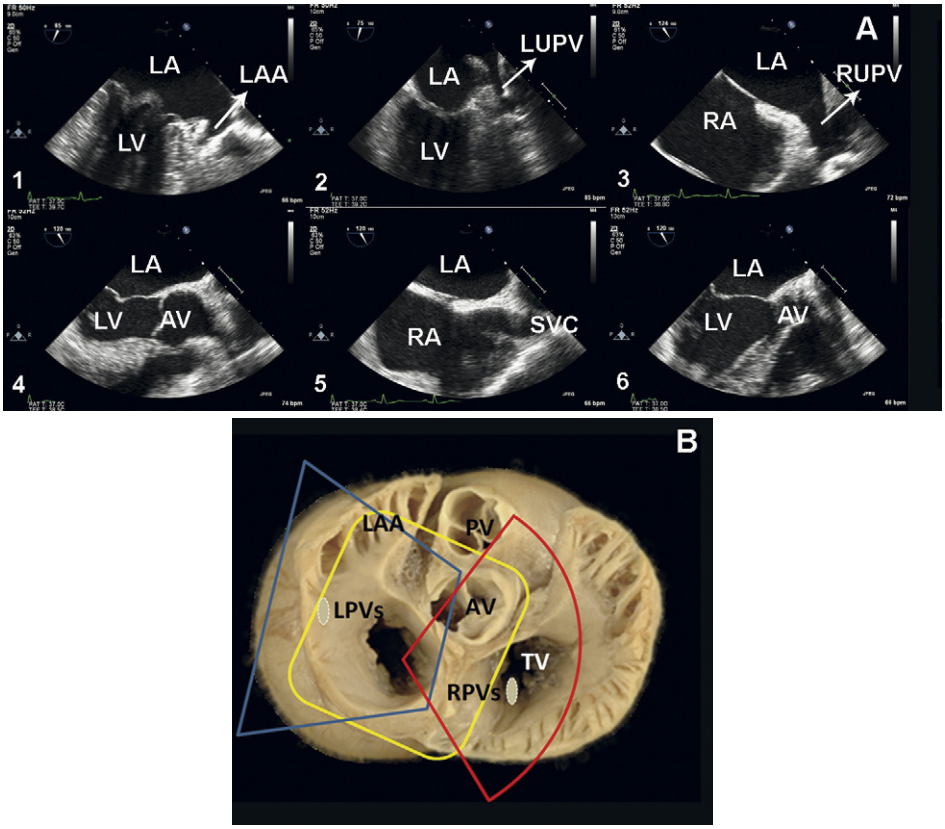

Figure 1 A, two-dimensional transoesophageal echocardiography reference views of the 6-step image acquisition protocol. 1, the mitral commissural view; 2, the superior commissural view including the left upper pulmonary vein; 3, the modified bicaval view including the right upper pulmonary vein; 4, the aortic valve long axis view; 5, the midpoint view between the aortic valve long axis and bicaval views; 6, Further left to the aortic valve long axis view. B, cardiac structures acquired in the 3D datasets of Step 1 (yellow), Step 2 (blue) and Step 3 (red). The grey areas represent the area of the pulmonary vein ostia projected to the cross-section of the anatomical view. AV, aortic valve; LA, left atrium; LAA, left atrial appendage; LPVs, left pulmonary veins; LUPV, left upper pulmonary vein; LV, left ventricle; MV, mitral valve; PV, pulmonary valve; RA, right atrium; RPVs, right pulmonary veins; RUPV, right upper pulmonary vein; SVC, superior vena cava; TV, tricuspid valve.

intensity fusion. Severe near-field artefacts were removed by cropping the ultrasound pyramid before the image fusion.

RESULTS

The clinical characteristics of all patients are depicted in Table 2. The image acquisition protocol was feasible in all eight patients and in total 48 3D TOE datasets were acquired.

Table 2 Clinical characteristics of the patients (n = 8).

No.	Age	Gender	BSA (m^2)	LA size*	Surgical indications	Rhythm	Hypertension	HR (bpm)†	BP (mmHg)†
1	76	F	1.96	Severely enlarged	Severe MR	Sinus	No	66	110/65
2	67	F	1.78	Normal	Severe MR	Sinus	Yes	87	115/60
3	30	M	1.99	Severely enlarged	Severe MR	Sinus	No	50	115/65
4	58	M	2.15	Normal	MI	Sinus	Yes	64	135/75
5	56	M	2.04	Normal	MI	Sinus	Yes	46	130/80
6	58	M	1.90	Severely enlarged	Paravalvular leak after mitral valve repair	Sinus	No	57	80/55
7	61	F	1.77	Severely enlarged	Severe MR, ventricle aneurysm,	Sinus	Yes	56	125/65
8	68	M	2.04	Severely enlarged	Severe MR, MI, tricuspid regurgitation	Pacemaker	Yes	60	125/65

BSA, body surface area; LA, left atrium; HR, heart rate; BP, blood pressure; F, female; M, male; MR, mitral regurgitation; MI, myocardial infarction.
*The grading of the LA size was based on LA volume index (LA volume divided by BSA) according to the ASE recommendations for chamber quantification[19].
†Heart rate and blood pressure were measured instantaneously during image acquisition.

For all full volume 3D datasets, the average volume size was 91° (lateral width) × 93° (elevation width). The average volume rate of the 3D TOE datasets was six volumes per second.

The cardiac structures captured in the 3D datasets of each step and the corresponding image qualities are shown in Table 3. The main 3D artefact was the echo loss. In general, the LAA, MV, AV, and FO were always visualised with good image quality, i.e. visualised

Table 3 Cardiac structures in and image quality of the 3D TOE datasets.

Step	Cardiac structures in 3D TOE datasets	Image quality
1	MV, AV, LAA	Good* in 8 patients.
2	part of MV, part of AV, LAA, ostia of left PVs	MV, AV and LAA: good* in 8 patients; left PVs: two ostia could be seen in 2 patients, one ostium could be seen in 2 patients, poor† in 4 patients.
3	part of AV, FO, ostia of right PVs	AV and FO: good* in 8 patients; right PVs: one ostium could be seen in 5 patients, poor† in 3 patients.
4	MV, AV	Good* in 8 patients.
5	part of AV, FO	Good* in 8 patients.
6	MV, AV	Good* in 8 patients.

TOE, transoesophageal echocardiography; MV, mitral valve; AV, aortic valve; LAA, left atrial appendage; PV, pulmonary vein; FO, fossa ovalis.
*Good: visualised clearly and distinguished easily in the 3D datasets without artefacts of echo loss.
†Poor: indistinguishable due to too much echo loss.

clearly and distinguished easily in the 3D datasets without artefacts of echo loss. The ostia of the PVs, which are located at the edges of the 3D datasets, suffered more from the artefact of echo loss.

Three orthogonal views of a fused 3D dataset and its orientation with respect to the heart are shown in Figure 2. The different colours represent the different steps. An example of a fused 3D TOE dataset in different orientations revealing the important anatomical structures is shown in Figure 3. It is clearly shown that the extension of the field of view gives a wider 3D view of the LA than the 3D TOE dataset of a single step does. Using the described protocol, the average volume overlap between neighbouring TOE datasets ranged from 50–75%.

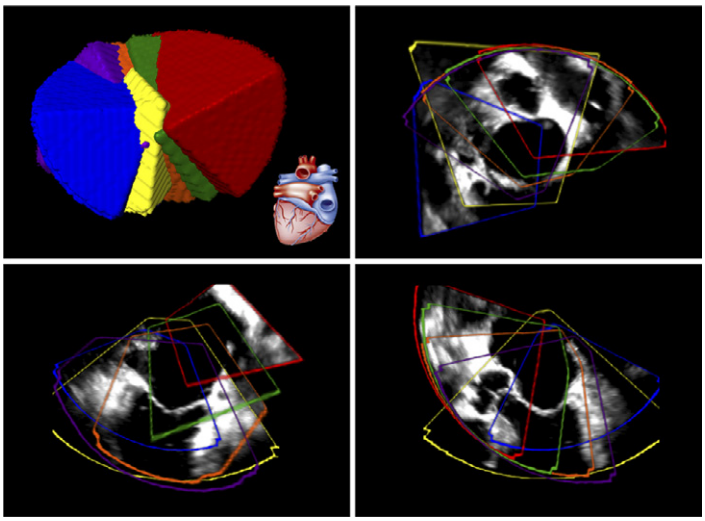

Figure 2 The orientation of 3D TOE datasets of each step with respect to the heart (the left upper quadrate) and orthogonal views of a fused 3D TOE dataset. Step 1 (yellow); Step2 (blue); Step 3 (red); Step 4 (orange); Step 5 (green); Step 6 (purple).

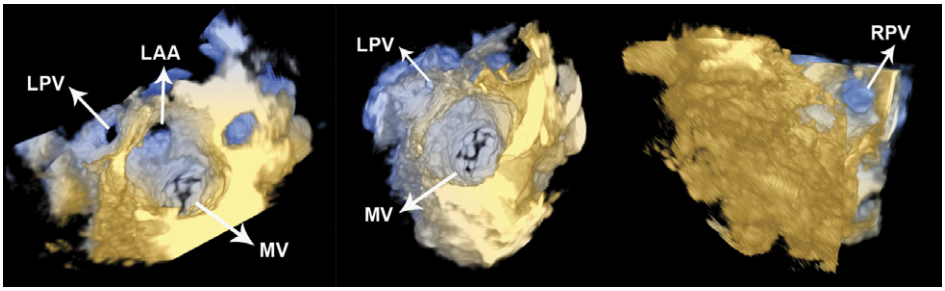

Figure 3 An example of a fused 3D TOE dataset and important cardiac structures are indicated. LAA, left atrial appendage; LPV, left pulmonary vein; MV, mitral valve; RPV, right pulmonary vein. Since the complete dataset was fused from six 3D TEE datasets, some part of the fused dataset was cropped to reveal the important anatomic landmarks.

DISCUSSION

In this study, we developed a systematic TOE image acquisition protocol with which six 3D TOE datasets were acquired and fused, providing a much wider reconstructed 3D view of the LA, incorporating the PVs, LAA, MV and AV. The protocol provides an important step towards using the pre- and/or intra-interventional 3D TOE to generate an anatomical map of LA for AF catheter ablation, potentially eliminating the need for pre-interventional CT or MRI.

The six steps of the protocol were chosen based on their feasibility and reproducibility in acquiring 3D TOE datasets which provide sufficient overlap among each step for registration.

Of all important anatomical landmarks, the LAA, MV, and AV were always of good image quality because they are located in the relative central part of the pyramidal 3D TOE datasets. Although the thin membranous area of the FO is likely to suffer from echo loss, its appositional muscular rim (limbus) can be distinguished easily in the 3D datasets. Since the PVs are adjacent to the lung and the 3D datasets are likely to suffer from the echo loss, the ostia of the PVs were less distinguishable than other cardiac structures, especially in those of inferior general image quality. The typical arrangement of four distinct pulmonary venous ostia is present in 20–60% of subjects, but it is also common to find the presence of a short or long common venous trunk on the left side, and supernumerary veins on the right side[15], The variances in the PVs' anatomy greatly influence the success rate of the AF catheter ablation if the variant PVs are treated inadequately. In this study, a short common venous stem of the left PVs was revealed in the 3D TOE datasets of one case and three right PVs in another case.

In this study, five patients had had severely enlarged LA due to severe mitral regurgitation. The relative positions of the PVs, lung and probe might be altered in this situation, which may compromise the general image quality. This might also be the case for patients with AF because they usually have an enlarged LA[16,17]. In addition, the patients' position during the acquisition may also influence the general image quality as the position of the heart relative to the lung might be changed. The lateral decubitus position tends to rotate the heart to the left of the sternum[18] and towards the chest wall. In this study, all patients were supine during the image acquisition.

Limitations

Although the major part of the LA including important anatomical structures was reconstructed successfully by registering the 3D TOE datasets, it was still not possible to reconstruct the whole LA. The roof of the LA was always lost in the 3D datasets, because the currently used matrix TOE probe (Philips X7-2t) is not capable of visualising the structures in the near field of the ultrasound beam. We tried to acquire 3D TOE datasets

in the transgastric view in which the LA roof lies in the far field of the ultrasound beam, but the spatial resolution dropped substantially and essential structures could hardly be distinguished. Nevertheless, we intend to carry out the 3D reconstructions also using images acquired by the Philips S8-3t micro-TOE probe which is of higher frequency (up to 6 MHz). According to our primary experience, the micro-TOE probe is able to visualise the LA roof in adults.

In this study, all 3D TOE datasets were registered manually, which requires specific expertise and relatively long time. However, the manual registration time consumption highly depends on the image quality of the 3D TOE datasets which determines the recognisability of the anatomical landmarks. Currently, we are developing an automatic registration method which will eliminate manual input and speed up the registration process. The automatic registration algorithm will take much less time than the manual registration and can be further incorporated into the ultrasound system, thus allows an on-line reconstruction. Therefore, the wide-view fused 3D TOE dataset can be made available to the electrophysiology physician during the ablation procedure.

All single full volume 3D datasets were free from 3D stitching artefacts because they were acquired from only one cardiac cycle, but as a result, the volume rates were very low. This limits temporal alignment and results in different positions of fast moving cardiac structures, thus influencing the quality of the fused dataset negatively. To acquire full volume 3D datasets from two or four cardiac cycles can greatly improve the volume rate (up to about 32 volumes per second) at the cost of longer acquisition time and stitching artefacts. Additionally, it should be noticed that the patients included in this study were under general anaesthesia and in non-anaesthetised patients stitching artefacts might be a bigger problem. These issues need to be investigated further.

Future clinical implications

The wide-view fused 3D TOE dataset will be very useful to reconstruct the LA anatomy; the segmented 3D surface could be imported to the EAM system. Additionally, intra-interventional 2D echocardiographic images can be matched to the pre-interventional 3D TOE images, preventing cumbersome multi-modality registration to CT or MRI images. The wide-view fused 3D TOE dataset may also serve as a substrate for registering and merging intra-interventional 2D echocardiographic images into the EAM system without errors from the probe position sensing.

CONCLUSION

The major part of the LA anatomy incorporating the PVs, LAA, MV, AV and FO as important anatomical landmarks could be reconstructed successfully by registering and fusing 3D datasets acquired with the proposed 6-step TOE image acquisition protocol.

REFERENCES

1. Marrouche NF, Martin DO, Wazni O, Gillinov AM, Klein A, Bhargava M, Saad E, Bash D, Yamada H, Jaber W, Schweikert R, Tchou P, Abdul-Karim A, Saliba W, Natale A. Phased-array intracardiac echocardiography monitoring during pulmonary vein isolation in patients with atrial fibrillation: impact on outcome and complications. *Circulation* 2003;107:2710-6.
2. Orlov MV, Hoffmeister P, Chaudhry GM, Almasry I, Gijsbers GH, Swack T, Haffajee CI. Three-dimensional rotational angiography of the left atrium and esophagus--A virtual computed tomography scan in the electrophysiology lab? *Heart Rhythm* 2007;4:37-43.
3. Dong J, Dickfeld T, Dalal D, Cheema A, Vasamreddy CR, Henrikson CA, Marine JE, Halperin HR, Berger RD, Lima JA, Bluemke DA, Calkins H. Initial experience in the use of integrated electro-anatomic mapping with three-dimensional MR/CT images to guide catheter ablation of atrial fibrillation. *J Cardiovasc Electrophysiol* 2006;17:459-66.
4. Rosenthal LS, Beck TJ, Williams J, Mahesh M, Herman MG, Dinerman JL, Calkins H, Lawrence JH. Acute radiation dermatitis following radiofrequency catheter ablation of atrioventricular nodal reentrant tachycardia. *Pacing Clin Electrophysiol* 1997;20:1834-9.
5. Kovoor P, Ricciardello M, Collins L, Uther JB, Ross DL. Risk to patients from radiation associated with radiofrequency ablation for supraventricular tachycardia. *Circulation* 1998;98:1534-40.
6. Perisinakis K, Damilakis J, Theocharopoulos N, Manios E, Vardas P, Gourtsoyiannis N. Accurate assessment of patient effective radiation dose and associated detriment risk from radiofrequency catheter ablation procedures. *Circulation* 2001;104:58-62.
7. Calkins H, Brugada J, Packer DL, Cappato R, Chen SA, Crijns HJ, Damiano RJ, Jr., Davies DW, Haines DE, Haissaguerre M, Iesaka Y, Jackman W, Jais P, Kottkamp H, Kuck KH, Lindsay BD, Marchlinski FE, McCarthy PM, Mont JL, Morady F, Nademanee K, Natale A, Pappone C, Prystowsky E, Raviele A, Ruskin JN, Shemin RJ, Heart Rhythm S, European Heart Rhythm A, European Cardiac Arrhythmia S, American College of C, American Heart A, Society of Thoracic S. HRS/EHRA/ECAS expert consensus statement on catheter and surgical ablation of atrial fibrillation: recommendations for personnel, policy, procedures and follow-up. A report of the Heart Rhythm Society (HRS) Task Force on Catheter and Surgical Ablation of Atrial Fibrillation developed in partnership with the European Heart Rhythm Association (EHRA) and the European Cardiac Arrhythmia Society (ECAS); in collaboration with the American College of Cardiology (ACC), American Heart Association (AHA), and the Society of Thoracic Surgeons (STS). Endorsed and approved by the governing bodies of the American College of Cardiology, the American Heart Association, the European Cardiac Arrhythmia Society, the European Heart Rhythm Association, the Society of Thoracic Surgeons, and the Heart Rhythm Society. *Europace* 2007;9:335-79.
8. Faletra FF, Castro S, Pandian NG, Kronzon I, Nesser HJ, Ho SY. Atlas of Real Time 3D Transesophageal Echocardiography. London: Springer, 2010:114-128.
9. Ho SY, McCarthy KP, Faletra FF. Anatomy of the left atrium for interventional echocardiography. *Eur J Echocardiogr* 2011;12:i11-5.
10. Vegas A, Meineri M, Jerath A. Real-Time Three-Dimensional Transesophageal Echocardiography: A Step-by-Step Guide. New York: Springer, 2012:218-9.
11. Szili-Torok T, Bosch JG. Transnasal transoesophageal ultrasound: the end of the intracardiac echocardiography age? *Europace* 2011;13:7-8.
12. Shanewise JS, Cheung AT, Aronson S, Stewart WJ, Weiss RL, Mark JB, Savage RM, Sears-Rogan P, Mathew JP, Quinones MA, Cahalan MK, Savino JS. ASE/SCA guidelines for performing a comprehensive intraoperative multiplane transesophageal echocardiography examination: recom-

mendations of the American Society of Echocardiography Council for Intraoperative Echocardiography and the Society of Cardiovascular Anesthesiologists Task Force for Certification in Perioperative Transesophageal Echocardiography. *J Am Soc Echocardiogr* 1999;12:884-900.

13. Lang RM, Badano LP, Tsang W, Adams DH, Agricola E, Buck T, Faletra FF, Franke A, Hung J, de Isla LP, Kamp O, Kasprzak JD, Lancellotti P, Marwick TH, McCulloch ML, Monaghan MJ, Nihoyannopoulos P, Pandian NG, Pellikka PA, Pepi M, Roberson DA, Shernan SK, Shirali GS, Sugeng L, Ten Cate FJ, Vannan MA, Zamorano JL, Zoghbi WA. EAE/ASE recommendations for image acquisition and display using three-dimensional echocardiography. *J Am Soc Echocardiogr* 2012;25:3-46.

14. Horn BKP. Closed-form solution of absolute orientation using unit quaternions. *J Opt Soc Am A Opt Image Sci Vis*;4:629-642.

15. Kato R, Lickfett L, Meininger G, Dickfeld T, Wu R, Juang G, Angkeow P, LaCorte J, Bluemke D, Berger R, Halperin HR, Calkins H. Pulmonary vein anatomy in patients undergoing catheter ablation of atrial fibrillation: lessons learned by use of magnetic resonance imaging. *Circulation* 2003;107: 2004-10.

16. Bangalore S, Yao SS, Chaudhry FA. Role of left atrial size in risk stratification and prognosis of patients undergoing stress echocardiography. *J Am Coll Cardiol* 2007;50:1254-62.

17. Henry WL, Morganroth J, Pearlman AS, Clark CE, Redwood DR, Itscoitz SB, Epstein SE. Relation between echocardiographically determined left atrial size and atrial fibrillation. *Circulation* 1976; 53:273-9.

18. Monaghan MJ. Practical echocardiography and doppler. West Sussex: John Wiley & Sons Ltd., 1990:11.

19. Lang RM, Bierig M, Devereux RB, Flachskampf FA, Foster E, Pellikka PA, Picard MH, Roman MJ, Seward J, Shanewise JS, Solomon SD, Spencer KT, Sutton MS, Stewart WJ, Chamber Quantification Writing G, American Society of Echocardiography's G, Standards C, European Association of E. Recommendations for chamber quantification: a report from the American Society of Echocardiography's Guidelines and Standards Committee and the Chamber Quantification Writing Group, developed in conjunction with the European Association of Echocardiography, a branch of the European Society of Cardiology. *J Am Soc Echocardiogr* 2005;18:1440-63.

Chapter 4.2

Fusion of Three-dimensional Transesophageal Echocardiographic Images of Left Atrium for Supporting Catheter Ablation Procedures: Comparison with Computed Tomography

Ben Ren
Harriët W. Mulder
Alexander Haak
Jackie McGhie
Tamas Szili-Torok
Koen Nieman
Marijn van Stralen
Josien P.W. Pluim
Marcel L. Geleijnse
Johan G. Bosch

Submitted

ABSTRACT

Objective The aim of the study was to evaluate wide-view fused 3D transesophageal echocardiography (TEE) datasets of the left atrium (LA) for supporting catheter ablation procedures by comparing with computed tomography (CT).

Methods Twenty-two patients undergoing transcatheter aortic valve implantation were included, who had had both CT and 3D TEE examinations. Six 3D TEE datasets were acquired according to the imaging protocol and were registered and fused manually in end diastole. Eight landmarks including mitral valve (MV), aortic valve (AV), left atrial appendage (LAA), fossa ovalis (FO), left superior pulmonary vein (LSPV), left inferior pulmonary vein, right superior pulmonary vein (RSPV), and right inferior pulmonary vein were marked in both fused 3D TEE and CT datasets. The Euclidean distances were calculated between corresponding landmarks.

Results The wide-view registration and fusion of the 3D TEE datasets was feasible in all patients. The MV, AV, and LAA were visualized in all cases and FO in 77% of cases. LSPV including the common ostium was visualized in 64% and RSPV including the common ostium in 77% of the patients. The inferior PVs were visualized with 3D TEE in only one patient. The distances between the landmarks marked in the fused 3D TEE and CT datasets were 5 ± 3 mm.

Conclusion Wide-view registration and fusion of the 3D TEE datasets were feasible and accurate in reconstructing the major part of the LA compared with the CT dataset. This technique can potentially replace the pre-interventional CT or MRI in complex LA catheter ablation procedures.

Keywords: transesophageal echocardiography, three-dimensional, wide-view fusion, left atrium, computed tomography

Atrial fibrillation (AF) is increasingly treated by catheter ablation, including pulmonary vein (PV) isolation and complex left atrial ablation for non-PV triggers, thus eliminating the triggers initiating AF[1]. Several imaging modalities are commonly applied before the intervention to visualize the left atrium (LA) along with the PVs, left atrial appendage (LAA) and mitral valve (MV), such as rotational angiography, computed tomography (CT), and magnetic resonance imaging (MRI)[2]. The pre-acquired CT or MRI images are segmented and registered within the electro-anatomical surface mapping (EAM) system to the real time mapping space during the procedure[3]. Since AF ablation procedures often need to be repeated and the substantial dose of ionizing radiation of CT scans, rotational angiography and fluoroscopy required by the procedures causes important delayed effects on patients[4-6], every attempt should be taken to minimize radiation exposure[1]. Additionally, CT and MRI are of cumbersome logistics and high cost.

Transesophageal echocardiography (TEE) is performed routinely to exclude LA/LAA thrombus before the catheter ablation. The anatomy of the LA and adjacent structures can be visualised in high resolution 2D and 3D TEE images[7-9]. However, the field of view of one single full volume 3D TEE dataset is not enough to visualize all important cardiac structures simultaneously, which is particularly true for the PVs at the left and right edges of the LA. We have shown in a previous study that it is feasible to reconstruct the majority of the LA with important anatomical landmarks with six single-view 3D TEE datasets acquired with a stepwise TEE image acquisition protocol[10]. In the present study, we sought to validate the wide-view fused 3D TEE dataset of the LA against CT by indicating the important anatomical landmarks in both fused 3D TEE and CT datasets. This is an important prerequisite in the process to replace pre-interventional CT by TEE in the catheter ablation procedures.

PATIENTS AND METHODS

Twenty-two patients (15 men, aged 79 ± 7 years old) who had undergone transcatheter aortic valve implantation (TAVI) for severe aortic valve stenosis were included in this study. These patients had undergone the CT examination three to five weeks before the procedure and 3D TEE examination during the procedure. The patients were under general anesthesia during the 3D TEE image acquisition. The protocol was approved by the institutional review board.

The TAVI patients were chosen as the study sample because they had had both CT and 3D TEE examinations. Although patients planned for catheter ablation all undertake the TEE exam a few days or immediately before the procedure, the TEE exam is always kept short and focused in our out-patient clinic in order to minimize patients' discomfort and 3D acquisition is not frequently performed. On contrary, the TAVI patients are under

general anesthesia during the procedure, which provides more time for 3D TEE acquisition and image optimization, thus are comparable ideal research subjects.

3D TEE image acquisition and registration

Intra-interventional TEE was performed with the Philips iE33 xMatrix ultrasound system (Philips Medical System, Best, the Netherlands) with the CX7-2t matrix-array transducer. All acquisitions were performed at the mid-esophageal level. The image acquisition was performed following the stepwise image acquisition protocol depicted in our

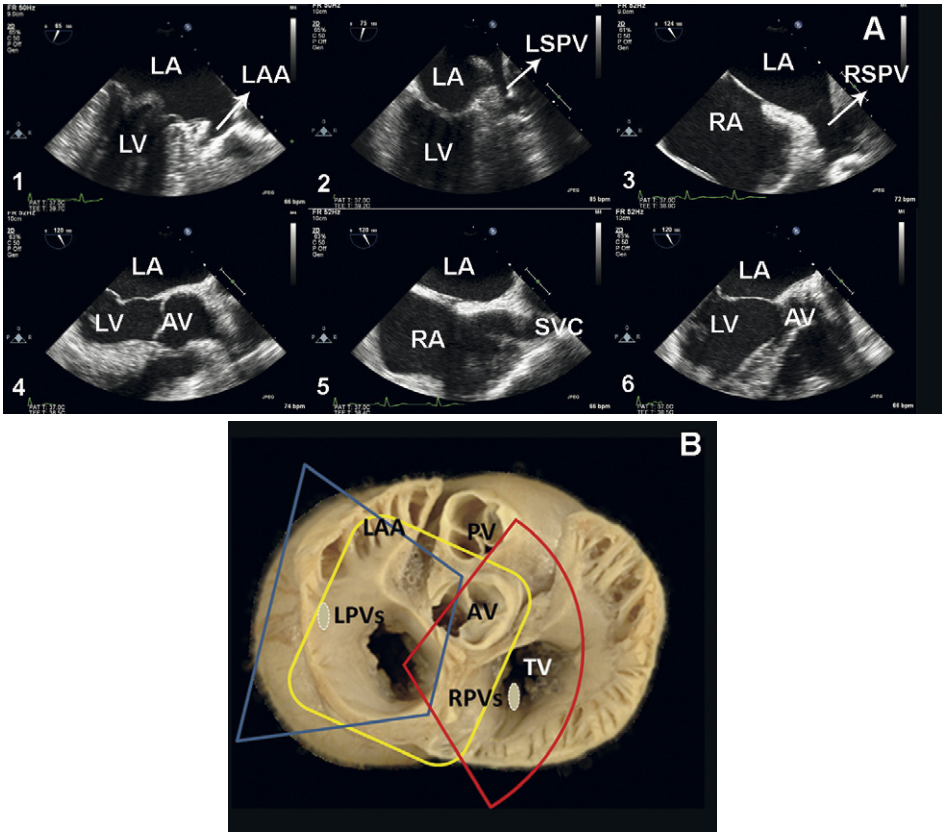

Figure 1 A, 2D transoesophageal echocardiography reference views of the 6-step image acquisition protocol[10]. 1, the mitral commissural view; 2, the superior commissural view including the left upper pulmonary vein; 3, the modified bicaval view including the right upper pulmonary vein; 4, the aortic valve long axis view; 5, the midpoint view between the aortic valve long axis and bicaval views; 6, Further left to the aortic valve long axis view. B, cardiac structures acquired in the 3D datasets of Step 1 (yellow), Step 2 (blue) and Step 3 (red). The grey areas represent the area of the pulmonary vein ostia projected to the cross-section of the anatomical view. AV, aortic valve; LA, left atrium; LAA, left atrial appendage; LPVs, left pulmonary veins; LSPV, left superior pulmonary vein; LV, left ventricle; MV, mitral valve; PV, pulmonary valve; RA, right atrium; RPVs, right pulmonary veins; RSPV, right superior pulmonary vein; SVC, superior vena cava; TV, tricuspid valve. Permission obtained from Springer (License no. 3441910283392).

previous study[10] (Figure 1). In the protocol, Step 1 aimed to acquire the central view of the MV, LAA and aortic valve (AV); Step 2 was developed to acquire the left PVs and Step 3 to acquire the right PVs. Step 4, 5 and 6 were mainly used to create sufficient overlap between different datasets for image registration and fusion. The 2D reference views and 3D datasets were acquired according to the ASE guidelines for performing a comprehensive TEE examination[11] and the latest EAE/ASE recommendations for image acquisition and display using 3D echocardiography[12]. The 3D datasets were acquired with the full volume mode during one cardiac cycle with a proper depth and the largest volume size to include the structures of interest.

To construct a wide 3D view of the LA, the datasets of the six different steps were registered manually to the CT image in end diastole by a single observer (HWM). Firstly, a minimum of three landmarks was indicated in both the TEE and CT datasets. Depending on the TEE view, the coaptation point of the AV leaflets, coaptation point of the MV leaflets, fossa ovalis (FO) and LAA were used as soft landmarks. Occasionally, some additional corresponding points were indicated to improve the initial alignment between the images. Since corresponding time frames were registered, only rotational and translational differences between the volumes were expected and therefore a rigid transformation model was used. The landmarks were registered by a closed-form least squares optimization algorithm[13]. Secondly, image alignment was improved manually by rotating and translating the TEE volume with respect to the CT, viewing the result in all three orthogonal views. Thirdly, all different TEE images were jointly displayed with respect to the CT image and each other, to optimize the image alignment between the different TEE views, thus minimizing TEE misalignment. Once an adequate transformation was found, the datasets belonging to step 1, 2, 3, and 4, the views that were required for coverage of the heart, were fused with maximum intensity fusion. Data of step 5 and 6 were used only in the registration process and not included in the fusion.

Multislice CT image acquisition

Contrast-enhanced cardiac CT was performed using a dual-source CT system (Somatom Definition, Siemens Medical Solutions, Forchheim, Germany), with the following acquisition parameters: two tube-detector systems with a detector collimation of 32 × 0.6 mm, Z-axis flying focal spot for double sampling in the longitudinal axis, rotation time 330 ms (temporal resolution 85 ms), tube voltage 120 kV. The pitch varied between 0.2 for low heart rates (<40 min^{-1}) and 0.53 for high heart rates (>100 min^{-1}). Each tube provided 412 mA/rot (625 mA), and full X-ray tube current (100%) was given during the 14–46% of the R – R interval. The scan ranged from the top of the aortic arch to the diaphragm. The radiation dose ranged from 8 to 20 mSv depending on body habitus and heart rate dependent table speed. The volume of iodinated contrast material (Iodixanol 320 mg/ml, GE Healthcare) was adapted to the expected scan duration. A contrast bolus (50–60

ml) was injected in an antecubital vein at a flow rate of 5.0 mL/s, followed by a second bolus of 30 – 40 at 3.0 ml/s. Bolus tracking was used to synchronize the start of the scan with opacification of the aortic root. Images were reconstructed at 5%-R-R intervals: slice thickness 1.5 mm; increment 0.4 mm; medium-to-smooth convolution kernel (B26f). In this study, we assessed CT datasets reconstructed during diastole, the same cardiac phase used in the TEE registration and fusion.

Indication of landmarks in the 3D TEE and CT datasets

Eight cardiac structures were chosen as the landmarks to be indicated in both fused 3D TEE and CT datasets: MV, AV, LAA, FO, left superior pulmonary vein (LSPV), left inferior pulmonary vein (LIPV), right superior pulmonary vein (RSPV), and right inferior pulmonary vein (RIPV). The common ostium of the PVs was defined if two PVs join each other and share a common stem before entering the LA or they enter the LA through the same ostium. All 3D TEE datasets were displayed as three orthogonal 2D views, which could be rotated and panned to locate the landmarks. The landmarks were indicated independently in the TEE and CT datasets at two different times in all 22 patients by one observer (BR) blinded to the image registration process. The landmarks were indicated in the following locations: 1) MV: in the center of the mitral annulus plane; 2) AV: in the center of the aortic annulus plane; 3) LAA: in the center of the ostium of the LAA; 4) FO: in the center of the thin fossa ovalis area; 5) LSPV: in the center of the ostium of the LSPV; 6) LIPV: in the center of the ostium of the LIPV; 7) RSPV: in the center of the ostium of the RSPV; 8) RIPV: in the center of the ostium of the RIPV. For a common ostium, only one landmark was marked in the center of the common ostium. If the cardiac structures were not visible in the datasets, the landmarks were skipped.

For correspondence evaluation, the differences between corresponding landmarks in the fused 3D TEE ($p_{TEE} = (x_{TEE}, y_{TEE}, z_{TEE})^T$) and CT ($p_{CT} = (x_{CT}, y_{CT}, z_{CT})^T$) datasets were calculated as Euclidean distances: $d = \sqrt{(x_{TEE} - x_{CT})^2 + (y_{TEE} - y_{CT})^2 + (z_{TEE} - z_{CT})^2}$

Intra- and interobserver variability analysis

The landmarks were indicated a second time by the same observer (BR) and independently by a second observer (JMG) in five patients randomly chosen. The distances of 40 corresponding landmarks of CT-CT, TEE-TEE and CT-TEE by the same observer and between two observers were calculated.

RESULTS

In Figure 2, a fused 3D TEE dataset of one patient are shown along with the CT dataset in different orientations to show important cardiac structures. In Figure 3, one fused 3D TEE dataset with the landmarks indicated for TEE and CT is shown.

Using CT as the gold standard, the visibility of eight landmarks in fused 3D TEE datasets in all patients is depicted in Table 1. As shown in Table 1, a left PV common ostium was observed in 14 cases using CT and seen in the fused 3D TEE datasets in 10 cases (71%). A right PV common ostium was seen in 2 patients using CT and also in the fused 3D TEE dataset (100%).

For the eight cardiac structures chosen as the landmarks, the distances between the corresponding landmarks placed in the fused 3D TEE and CT datasets are shown in Figure 4. The distances of the landmarks of the LIPV and RIPV were not calculated because they were seen in the fused 3D TEE dataset only in one patient. The distance between landmarks was 5 ± 2 mm for MV, 4 ± 2 mm for AV, 5 ± 2 mm for LAA, 6 ± 3 mm for FO, 9 ± 4 mm for LSPV, and 5 ± 3 mm for RSPV.

Table 1 The visibility of eight anatomic landmarks in the fused 3D TEE dataset compared with CT in 22 patients.

	CT	Fused 3D TEE	Visibility
MV	22	22	100%
AV	22	22	100%
LAA	22	22	100%
FO	22	17	77%
LPV common ostium	14	10	71%
LSPV	8	4	50%
LIPV	8	1	13%
RPV common ostium	2	2	100%
RSPV	20	15	75%
RIPV	20	0	0

Visibility was calculated as the number of fused 3D TEE divided by the number of CT. CT, computed tomography; TEE, transesophageal echocardiography; other abbreviations as in Figure 1, 2 and 3.

Table 2 Distances between 40 landmarks marked in CT and fused 3D TEE datasets, and distances between landmarks in CT and 3D TEE datasets in five patients from the same observer (intraobserver) and two observers (interobserver).

	Intraobserver	Interobserver
CT – CT (mm)	3 ± 2	5 ± 3
TEE – TEE (mm)	3 ± 2	7 ± 4
CT – TEE (mm)	6 ± 4	10 ± 5

Data presented as bias ± standard deviation. Abbreviations as in Table 1.

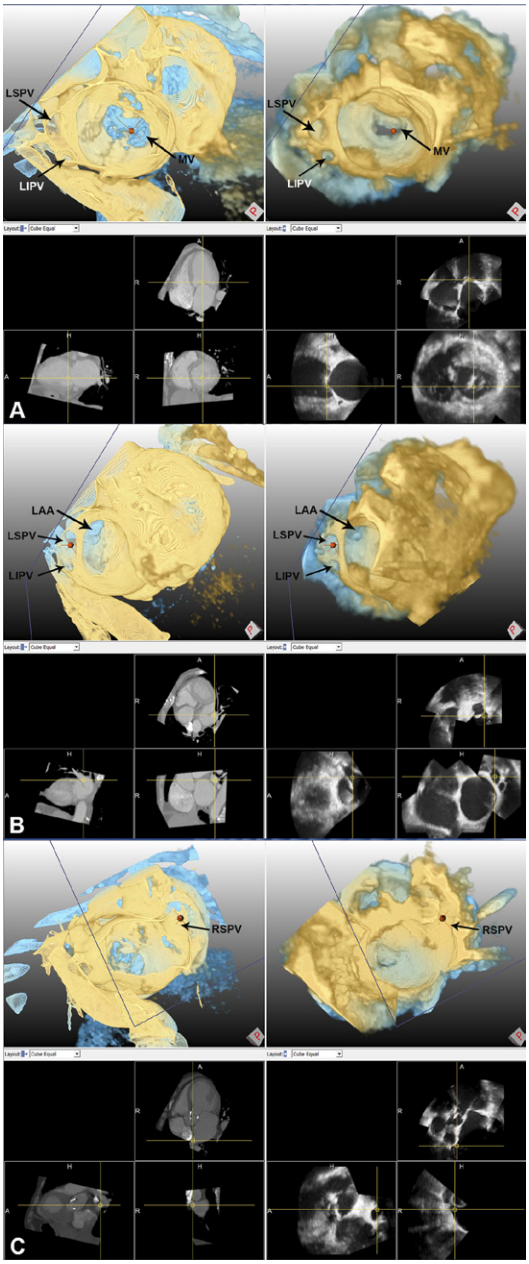

Figure 2 An example of a fused 3D transesophageal echocardiographic dataset and the corresponding CT dataset with important cardiac structures indicated. The 2D multiplanar reconstruction planes of both 3D echocardiographic and CT data are also shown. A, mitral valve en-face view with left pulmonary veins; B, left atrial appendage and left pulmonary veins; C, right inferior pulmonary vein. Some part of the fused 3D echocardiographic and CT datasets was cropped to reveal the anatomic landmarks. CT, computed tomography; LIPV, left inferior pulmonary vein; RSPV, right superior pulmonary vein; other abbreviations as in Figure 1.

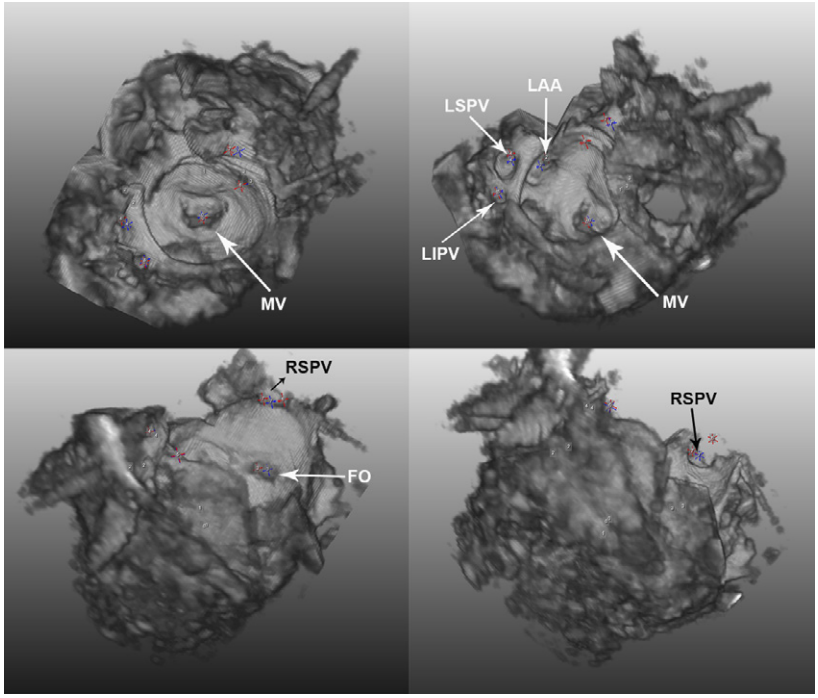

Figure 3 An example of a fused 3D transesophageal echocardiographic dataset with landmarks on the important cardiac structures. Red crosses are the landmarks marked in the CT dataset and blue crosses are the landmarks marked in the fused 3D TEE datasets. The right superior pulmonary vein ostium was not visible in the 3D TEE dataset. FO, fossa ovalis; other abbreviations as in Figure 1 and 2.

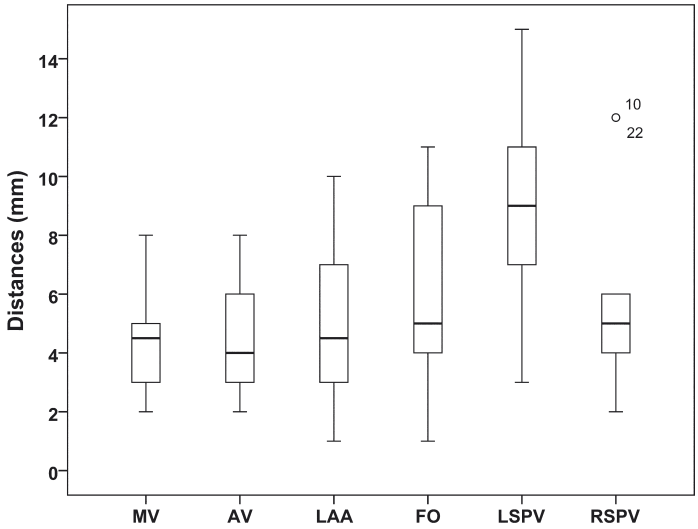

Figure 4 Boxplots showing the distance between corresponding landmarks. Open dot as outlier. Abbreviations as in Figure 1, 2 and 3.

The intra- and interobserver variabilities in landmarks are shown in Table 2. The intraobserver and interobserver variabilities of TEE-TEE and CT-CT distances were small, but were also shown to constitute a considerable part of the CT-TEE distances.

DISCUSSION

In this study, we compared the wide-view fused 3D TEE datasets of the LA with the CT data. The main findings were 1) the wide-view registration and fusion of the 3D TEE datasets was feasible in all patients and enabled the visualization of major parts of the LA; 2) important anatomical landmarks such as the MV, AV, LAA and FO could be clearly visualized in the fused 3D TEE in all (MV, AV and LAA) or almost all patients (FO); 3) LSPV including the common ostium could be visualized in 64% and RSPV including the common ostium in 77% of the patients. However, the LIPV and RIPV were very difficult to visualize with 3D TEE; 4) the registration and fusion of the 3D TEE datasets tended to be accurate as the average distances between the landmarks marked in the fused 3D TEE dataset and those made in the CT dataset were 5 ± 3 mm for the important cardiac structures.

The single view 3D TEE datasets were acquired with a systematic step-wise TEE image acquisition protocol as described in our previous study[10]. This image acquisition protocol provides a systematic and fast procedure for acquiring 3D TEE datasets which allows the manual registration and fusion. Important anatomical structures for the ablation procedure could be clearly visualized in the fused 3D TEE datasets. Centrally located structures such as MV, AV, LAA and FO were well visualized in the fused 3D TEE datasets in all (MV, AV, LAA) or the majority of the patients (FO in 77%). The reason why the FO was not visible in all patients was because it was not included in the 3D acquisition sector in some patients since the image protocol was set to focus on PVs. In fact, the atrial septum including the FO can be excellently visualized with 3D TEE[12,14], as this technique is commonly used to diagnose atrial septum defect[15,16]. Since the PVs are adjacent to the lung and the 3D datasets are likely to suffer from the echo drop-out, the ostia of the PVs were less distinguishable than other cardiac structures. This might be the main reason for the invisibility of the inferior PVs because the inferior veins tend to be smaller and have shorter distances from the ostia to the first-order branches than the superior veins and the LIPV is surrounded by descending aorta and lung. In addition, the superior veins enter the LA in an anterosuperior direction, whereas the inferior veins open into the LA perpendicular to the posterior wall[17]. The posterior wall of LA was always lost in the 3D TEE datasets, because the currently used matrix TEE probe (Philips CX7-2t) is not capable of visualizing the structures in the very near field of the ultrasound beam. Variances in the PV anatomy are commonly seen, such as a short or long common venous trunk or supernumerary veins[18]. These increase the difficulty in distinguishing the

PVs in the fused 3D TEE datasets. Additionally, the variable distance of the transducer placed into the esophagus and the PVs may also affect imaging. When the esophagus and transducer inside is close to the left PVs, imaging of right PVs can be easier, while imaging of the lower left PV is troublesome, and vice versa. There is quite a variance in the chance of visualizing the inferior PVs in the literature[19,20] and it should be noted that the visualization of PVs using TEE also depends on the operator's experience and apparently requires certain training.

As shown in the results, the distances between landmarks in the fused 3D TEE and CT datasets were around 5 mm, which is quite small for such cardiac structures compared with the reported inaccuracies in the EAM[21]. The reported distances were a combination of several inaccuracies: the TEE fusion and reconstruction inaccuracies, the observer variability in the landmarks, different physiological conditions between the CT and TEE images taken weeks apart and inherent differences between the CT and TEE images. Since the intraobserver and interobserver CT-CT and TEE-TEE distances were 3 to 7 mm (Table 2) , the CT-TEE distances could be largely attributed to observer variability, and the errors due to registration and modality differences were actually much smaller than suggested by the measurements. In order to investigate the cause of the distances between landmarks in 3D TEE and CT datasets, especially for the distances larger than 10 mm, we further calculated the distance vector in two directions: radial and circumferential (with respect to the centre of the LA). The results, however, showed no significant correlation between the absolute distance and the radial distance. On inspection, in all four cases where the landmark indicated in the fused 3D TEE datasets was not reliable, this was proven to be because of inferior 3D image quality, not because of registration errors.

Limitations

Although the major part of the LA was reconstructed accurately by registering the 3D TEE datasets, it was still not possible to reconstruct the whole LA as the posterior wall of the LA was always lost in the 3D datasets as discussed above. There may be several solutions for this, e.g., using a balloon standoff or using a probe of higher frequency. These solutions are subject of further study. In the imaging protocol, the inferior PVs are not visualized in the 2D reference views. Because of the close location between the superior and inferior PVs, we assumed that with sufficient image quality, both veins could be included in the $90^o \times 90^o$ 3D acquisition sector even if only one vein was seen in the 2D reference view. Different 2D views specially targeting at the inferior PVs could be used[12,20], yet the inferior PVs cannot always be visualized in certain views as the success rate reported largely varied[19,20], especially in diseased hearts whose orientations maybe changed due to chamber enlargement.

The study was carried out in patients undergoing the TAVI procedure, in whom both CT and TEE studies were available. Although the AV and MV annuli were often heav-

ily calcified in this patient population, the 3D TEE image quality in terms of structure recognition was not influenced by the strong echo of calcified annuli. Nevertheless, this study ultimately aims at facilitating the catheter ablation procedures in patients with AF. Thus, the ideal patient population would be patients undergoing the catheter ablation. However, the accuracy of fusing 3D TEE datasets acquired in the patients with AF compared with CT is assumed to be similar as shown in this study. Besides, patients with AF usually have enlarged LA as patients with aortic stenosis, but whether the degree of LA enlargement is comparable between the two patient populations and its influence on visualization, registration and fusion still need interrogation.

In this study, all 3D TEE datasets were registered manually, which requires specific expertise and relatively long time. An automatic registration method is highly desirable. This will eliminate manual input and speed up the registration process, which can be further incorporated into the ultrasound system, thus allowing an on-line reconstruction. In fact, this current study constitutes a proof of principle for the future case where such an automated registration will be available, and shows that TEE may support the ablation procedure as the fused 3D TEE dataset can be made available during the procedure. The parts that are not well visualized (atrial posterior wall and inferior PVs) should then be further elucidated during the simplified EAM procedure.

The temporal mismatch between the different TEE subsets may play an important role in the registration errors. The volume rates of the 3D TEE datasets were very low (4 Hz) because they were acquired from one cardiac cycle, which limited temporal alignment and resulted in different positions of fast moving cardiac structures. The volume rate can be improved if full volume 3D datasets are acquired from more cardiac cycles. However, it should be noted that the patients included in this study were under general anesthesia and had a stable heart rate. In non-anesthetized patients, the heart rate may vary more especially in patients with AF who usually have irregular R-R interval, thus stitching artefacts might adversely affect the registration.

The use of CT as the basis and aid for the manual TEE registration may provide a bias in the CT-TEE comparison, especially since some landmarks (MV, AV, FO) were used in both processes. However, the landmarks indicated in the TEE registration were not known to the observers performing the landmark indication. In fact, the TEE registration could also be performed without the CT and alignment of the TEE sets was finally performed between TEE datasets.

Clinical implications

The wide-view fused 3D TEE dataset can represent the atrial anatomy in a similar way as the preoperative CT does. Apart from some of the inferior PVs and the atrial posterior wall, the major structures are represented correctly. Regarding the poor visibility of the inferior PVs in the fused 3D TEE datasets, implementing 3D TEE in the PV isolation pro-

cedure may be limited. However, this technique might replace pre-interventional CT or MRI in facilitating ablation approaches not targeting the PVs, including ablation of peri-mitral flutter, LA tachycardia (post-ablational superior PVs and LAA tachycardias), septal atrial tachycardia, and LAA occlusion which is performed frequently during the catheter ablation procedure. In a separate study, we have shown that a multicavity anatomy can be successfully segmented from these TEE images[22]. This segmented 3D surface could be imported to the EAM system, which may obviate the need for preoperative CT. Additionally, intra-interventional 2D echocardiographic images can be matched to the pre-interventional 3D TEE images, preventing cumbersome multi-modality registration to CT or MRI images. TEE probes equipped with 3D position sensing or X-ray based position/orientation estimation[23] will fit this application even better. The wide-view fused 3D TEE dataset may also serve as a substrate for registering and merging intra-interventional 2D echocardiographic images into the EAM system without errors from the probe position sensing.

CONCLUSION

Wide-view registration and fusion of the 3D TEE datasets were feasible and accurate in reconstructing the major part of the LA compared with the CT dataset. This technique may replace the pre-interventional CT or MRI in complex LA catheter ablation procedures. When the visualization of the ostia of inferior PVs is improved, this technique could be applied in catheter ablations targeting at PVs as well.

ACKNOWLEDGEMENTS

The support of Gerard van Burken in data processing is gratefully acknowledged. We acknowledge MeVis Medical Solutions AG (Bremen, Germany) for the use of MeVisLab for analysis and visualization in this study. This research was supported by the Dutch Technology Foundation STW, which is the applied science division of NWO and the Technology Programme of the Ministry of Economic Affairs.

REFERENCES

1. Calkins H, Brugada J, Packer DL, Cappato R, Chen SA, Crijns HJ, Damiano RJ, Jr., Davies DW, Haines DE, Haissaguerre M, Iesaka Y, Jackman W, Jais P, Kottkamp H, Kuck KH, Lindsay BD, Marchlinski FE, McCarthy PM, Mont JL, Morady F, Nademanee K, Natale A, Pappone C, Prystowsky E, Raviele A, Ruskin JN, Shemin RJ, Heart Rhythm S, European Heart Rhythm A, European Cardiac Arrhythmia S, American College of C, American Heart A, Society of Thoracic S. HRS/EHRA/ECAS expert consensus statement on catheter and surgical ablation of atrial fibrillation: recommendations for personnel, policy, procedures and follow-up. A report of the Heart Rhythm Society (HRS) Task Force on Catheter and Surgical Ablation of Atrial Fibrillation developed in partnership with the European Heart Rhythm Association (EHRA) and the European Cardiac Arrhythmia Society (ECAS); in collaboration with the American College of Cardiology (ACC), American Heart Association (AHA), and the Society of Thoracic Surgeons (STS). Endorsed and approved by the governing bodies of the American College of Cardiology, the American Heart Association, the European Cardiac Arrhythmia Society, the European Heart Rhythm Association, the Society of Thoracic Surgeons, and the Heart Rhythm Society. *Europace* 2007;9:335-79.
2. Orlov MV, Hoffmeister P, Chaudhry GM, Almasry I, Gijsbers GH, Swack T, Haffajee CI. Three-dimensional rotational angiography of the left atrium and esophagus--A virtual computed tomography scan in the electrophysiology lab? *Heart Rhythm* 2007;4:37-43.
3. Dong J, Dickfeld T, Dalal D, Cheema A, Vasamreddy CR, Henrikson CA, Marine JE, Halperin HR, Berger RD, Lima JA, Bluemke DA, Calkins H. Initial experience in the use of integrated electro-anatomic mapping with three-dimensional MR/CT images to guide catheter ablation of atrial fibrillation. *J Cardiovasc Electrophysiol* 2006;17:459-66.
4. Rosenthal LS, Beck TJ, Williams J, Mahesh M, Herman MG, Dinerman JL, Calkins H, Lawrence JH. Acute radiation dermatitis following radiofrequency catheter ablation of atrioventricular nodal reentrant tachycardia. *Pacing Clin Electrophysiol* 1997;20:1834-9.
5. Kovoor P, Ricciardello M, Collins L, Uther JB, Ross DL. Risk to patients from radiation associated with radiofrequency ablation for supraventricular tachycardia. *Circulation* 1998;98:1534-40.
6. Perisinakis K, Damilakis J, Theocharopoulos N, Manios E, Vardas P, Gourtsoyiannis N. Accurate assessment of patient effective radiation dose and associated detriment risk from radiofrequency catheter ablation procedures. *Circulation* 2001;104:58-62.
7. Faletra FF, Castro S, Pandian NG, Kronzon I, Nesser HJ, Ho SY. Atlas of Real Time 3D Transesophageal Echocardiography. London: Springer, 2010:114-128.
8. Ho SY, McCarthy KP, Faletra FF. Anatomy of the left atrium for interventional echocardiography. *Eur J Echocardiogr* 2011;12:i11-5.
9. Vegas A, Meineri M, Jerath A. Real-Time Three-Dimensional Transesophageal Echocardiography: A Step-by-Step Guide. New York: Springer, 2012:218-9.
10. Ren B, Mulder HW, Haak A, van Stralen M, Szili-Torok T, Pluim JP, Geleijnse ML, Bosch JG. A transoesophageal echocardiographic image acquisition protocol for wide-view fusion of three-dimensional datasets to support atrial fibrillation catheter ablation. *J Interv Card Electrophysiol* 2013;37:21-6.
11. Shanewise JS, Cheung AT, Aronson S, Stewart WJ, Weiss RL, Mark JB, Savage RM, Sears-Rogan P, Mathew JP, Quinones MA, Cahalan MK, Savino JS. ASE/SCA guidelines for performing a comprehensive intraoperative multiplane transesophageal echocardiography examination: recommendations of the American Society of Echocardiography Council for Intraoperative Echo-

cardiography and the Society of Cardiovascular Anesthesiologists Task Force for Certification in Perioperative Transesophageal Echocardiography. *J Am Soc Echocardiogr* 1999;12:884-900.

12. Lang RM, Badano LP, Tsang W, Adams DH, Agricola E, Buck T, Faletra FF, Franke A, Hung J, de Isla LP, Kamp O, Kasprzak JD, Lancellotti P, Marwick TH, McCulloch ML, Monaghan MJ, Nihoyannopoulos P, Pandian NG, Pellikka PA, Pepi M, Roberson DA, Shernan SK, Shirali GS, Sugeng L, Ten Cate FJ, Vannan MA, Zamorano JL, Zoghbi WA. EAE/ASE recommendations for image acquisition and display using three-dimensional echocardiography. *J Am Soc Echocardiogr* 2012;25:3-46.

13. Horn BKP. Closed-form solution of absolute orientation using unit quaternions. *J Opt Soc Am A Opt Image Sci Vis*;4:629-642.

14. Faletra FF, Nucifora G, Ho SY. Imaging the atrial septum using real-time three-dimensional transesophageal echocardiography: technical tips, normal anatomy, and its role in transseptal puncture. *J Am Soc Echocardiogr* 2011;24:593-9.

15. van den Bosch AE, Ten Harkel DJ, McGhie JS, Roos-Hesselink JW, Simoons ML, Bogers AJ, Meijboom FJ. Characterization of atrial septal defect assessed by real-time 3-dimensional echocardiography. *J Am Soc Echocardiogr* 2006;19:815-21.

16. Melgarejo I, Orozco D, Nunez F, Rubio CM, Lang R. The role of real time 3D TEE in defining the anatomy of atrial septal defects and modifying the therapeutic approach. *Eur Heart J Cardiovasc Imaging* 2012;13:270.

17. Malouf JF, Edwards WD, Jamil Tajik A, Seward JB. Function anatomy of the heart. In: Fuster V, Wayne Alexander R, O'Rourke RA, eds. Hurst's the Heart. 10th Edition. McGraw-Hill: McGraw-Hill, 2001:49-51.

18. Kato R, Lickfett L, Meininger G, Dickfeld T, Wu R, Juang G, Angkeow P, LaCorte J, Bluemke D, Berger R, Halperin HR, Calkins H. Pulmonary vein anatomy in patients undergoing catheter ablation of atrial fibrillation: lessons learned by use of magnetic resonance imaging. *Circulation* 2003;107: 2004-10.

19. Artuso E, Stomaci B, Verlato R, Turrini P, Lafisca N, Baccillieri MS, Di Marco A, Piovesana P. Transesophageal echocardiographic follow-up of pulmonary veins in patients undergoing ostial radiofrequency catheter ablation for atrial fibrillation. *Ital Heart J* 2005;6:595-600.

20. Faletra FF, Ho SY, Regoli F, Acena M, Auricchio A. Real-time three dimensional transoesophageal echocardiography in imaging key anatomical structures of the left atrium: potential role during atrial fibrillation ablation. *Heart* 2013;99:133-42.

21. Heist EK, Perna F, Chalhoub F, Danik S, Barrett C, Houghtaling C, Tondo C, Mahapatra S, Ruskin J, Mansour M. Comparison of electroanatomical mapping systems: accuracy in left atrial mapping. *Pacing Clin Electrophysiol* 2013;36:626-31.

22. Haak A, Vegas-Sánchez-Ferrero G, Mulder H, Kirişli H, Baka N, Metz C, Klein S, Ren B, Burken G, Steen AW, Pluim JW, Walsum T, Bosch J. Segmentation of 3D Transesophageal Echocardiograms by Multi-cavity Active Shape Model and Gamma Mixture Model. In: Liao H, Linte C, Masamune K, Peters T, Zheng G, eds. Augmented Reality Environments for Medical Imaging and Computer-Assisted Interventions: Springer Berlin Heidelberg, 2013:19-26.

23. Szili-Torok T, Bosch JG. Transnasal transoesophageal ultrasound: the end of the intracardiac echocardiography age? *Europace* 2011;13:7-8.

Chapter 4.3

Segmentation of Multiple Cavities of the Heart in Fused Wide-View 3D Transesophageal Echocardiograms

Alexander Haak
Ben Ren
Harriët W. Mulder
Gonzalo Vegas-Sánchez-Ferrero
Gerard van Burken
Antonius F.W. van der Steen
Marijn van Stralen
Josien P.W. Pluim
Theo van Walsum
Johan G. Bosch

Submitted

ABSTRACT

Minimally-invasive interventions of the heart such as in electrophysiology (EP) are becoming more and more important in clinical practice. Currently, preoperative computed tomography angiography (CTA) is used to provide anatomical information during EP intervention, but this does not provide real-time feedback and burdens the patient with additional radiation and side effects of the contrast agent. Three-dimensional transesophageal echocardiography (3D TEE) is an excellent modality to visualize anatomical structures and instruments in real-time. However, especially the visualization of the left atrium (LA) suffers from the limited coverage of the 3D TEE volumes due to the close location of the TEE probe to the LA. This makes segmentation of the LA and therefore integration with electroanatomic maps difficult. Combining multiple rotated TEE volumes and creating a fused wide-view volume may overcome these shortcomings.

We propose in this paper to replace or complement preoperative CTA imaging by wide-view TEE. We tested this on twenty patients for which six overlapping 3D TEE image volumes covering the LA were acquired and CTA images were available. The TEE images were manually registered and combined based on minimum-intensity fusion to create wide-view volumes. Five heart cavities in single-view TEE and the wide-view TEE were segmented and compared with atlas based segmentations derived from the CTA images.

We could show that the segmentation accuracy (Dice coefficients) was improved by 5, 15, and 9 percent points for LA, right atrium, and aorta respectively. Average coverage was improved by 2, 29, 62, and 49 percent points for right ventricle, LA, right atrium, and aorta respectively. This demonstrates that the fusion of multiple views improves segmentation accuracy, especially for those cavities where the fusion improves the coverage. This finding confirms that wide-view 3D TEE can be useful for support of electrophysiology interventions.

Keywords: Transesophageal, echocardiography, segmentation, gamma mixture model, expectation maximization, three-dimensional, ultrasound, active shape model, electrophysiology

INTRODUCTION

With the aging population in the western world and improved survival of congenital diseases and infarcts, treatment of cardiac arrhythmias becomes more and more important. Cardiac electrophysiology (EP) is therefore a rapidly growing specialization in cardiac care. Atrial fibrillation (AF) is an unsynchronized or reduced contraction of the atria due to abnormal electrical activation patterns in the atria, and it is very common in elderly people. When pharmacological treatment is no longer effective, AF can be treated by interruption of the electrical pathways that induce the arrhythmia. Open heart surgery[1] is one way of isolating erroneous conduction sites but the involved risks are often too high for patients in this population[2].

In EP, AF is generally treated in a minimally invasive way by mapping the electrocardiographic (ECG) signals inside the atrium and ablating the culprit sites with radiofrequency ablation catheters. The ablation may sometimes be limited to a few points, but in many procedures continuous lines of ablation points need to be created to isolate a region on the atrial wall, leading to very lengthy and costly procedures. In the last decade, anatomical features became more important for treating AF; for instance, by creating circumferential lines around the pulmonary veins (PVs)[3,4]. The large anatomical variability in the PVs[5] and the high risk of complications[6] made 3D visualization of anatomical structures necessary.

Currently, the major means of real-time visualization during the intervention is X-ray fluoroscopy, which produces a 2D projection image only, has poor or no soft tissue contrast, and uses ionizing radiation[7]. The ablation and ECG catheters are equipped with 3D position sensors and their position is continuously tracked. By moving these catheters over the atrial wall, a rough 3D electro-anatomical map (EAM) of the atrium can be constructed[8]. This map is not very precise because of the limited number of contact points involved, influence of breathing and cardiac motion and the inaccuracy of 3D sensing. This led to the integration of preoperative computed tomography angiography (CTA) images into the EAM[9]. to supply a better impression of the patient's specific LA anatomy. These preoperative images are segmented and the resulting surfaces are imported into the EAM system. By indicating a number of anatomical landmarks in EAM and segmentation, the segmentation can be registered to the EAM. However, the preoperative CTA is a relatively costly, logistically cumbersome procedure, and burdens the patient with ionizing radiation. Moreover, these preoperative images are often acquired weeks before the intervention, and the current physiological state of the LA can be quite different from the preoperative images. Therefore, it is sometimes still difficult to ensure continuous ablation lines especially when dealing with abnormal anatomies. We believe that these shortcomings in the visualization of the anatomical structure are an important cause of the low success rate of the EP procedures: 52% without and 76% with the use of antiarrhythmic drugs[10]. In order to achieve these success rates in 27% of the patients multiple procedures were necessary.

Three-dimensional transesophageal echocardiography (TEE) with its good tissue-to-blood contrast could be an ideal real-time and preoperative modality to guide EP interventions. Preoperative TEE is generally performed shortly before the EP intervention to exclude the thrombus in atria and left atrial appendage. To complement or replace preoperative CTA, segmentation of the cardiac cavities in 3D TEE is required to allow the endocardial surfaces to be shown within the EAM system. We showed previously[11] that segmenting heart cavities in single TEE volumes is possible but may be limited by the narrow field of view (FoV). Wide-view image fusion is one way to increase the FoV[12] and we showed that by combining four TEE volumes we could cover most of the left atrium (LA), identify the main LA structures with accuracy similar to CTA and thus possibly replace preoperative CTA[13].

The purpose of this study is to investigate to what extent the wide-view fused TEE images can be segmented appropriately and that the segmentation accuracy improves with respect to single views. We hypothesize that the wide-view TEE will result in more accurate image segmentations. We tested our hypothesis on a set of twenty patients for whom CTA and TEE were available. We registered six TEE volumes aiming at different sites to generate wide-view TEE volumes. The preoperative CTA images were segmented using an atlas-based method[14]. These 3D segmentations covered the whole heart in 3D and served as the ground truth.

MATERIALS AND METHODS

A schematic outline of the used data and involved processing steps is shown in Figure 1. For each patient six TEE views were manually registered and fused to create a wide-view

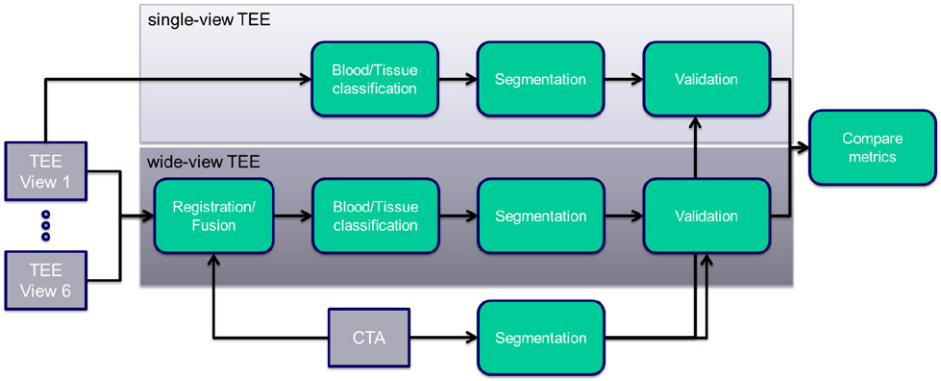

Figure 1 Block diagram of our methods and validation. For each patient six TEE images and one CTA image were acquired. We used a manual registration to align the six TEE views and subsequently a wide-view TEE image was created. A blood/tissue classifier was run on the single and wide-view images followed by a segmentation. The segmentations were validated with a ground truth derived from the CTA image.

image. A blood/tissue classifier and segmentation was applied to the wide-view images and the segmentation results were validated with CTA segmentations. We compared the segmentation results of the wide-view images with the results of a single-view image.

TEE Image Acquisition

Six 3D TEE image volumes were acquired at mid-esophageal level following the protocol described earlier[13]. There are three main volumes: 1) covering the central view including the mitral valve, the left atrial appendage, and the aortic valve; 2) aiming to the left including left PVs; 3) covering the atrial septum and the right PVs. The other three volumes are intermediate steps to ensure sufficient overlap of volumes 1 to 3. More details on the acquisition protocol can be found in the study of Ren *et al.*[13] and an example of the different views can be seen in Figure 2.

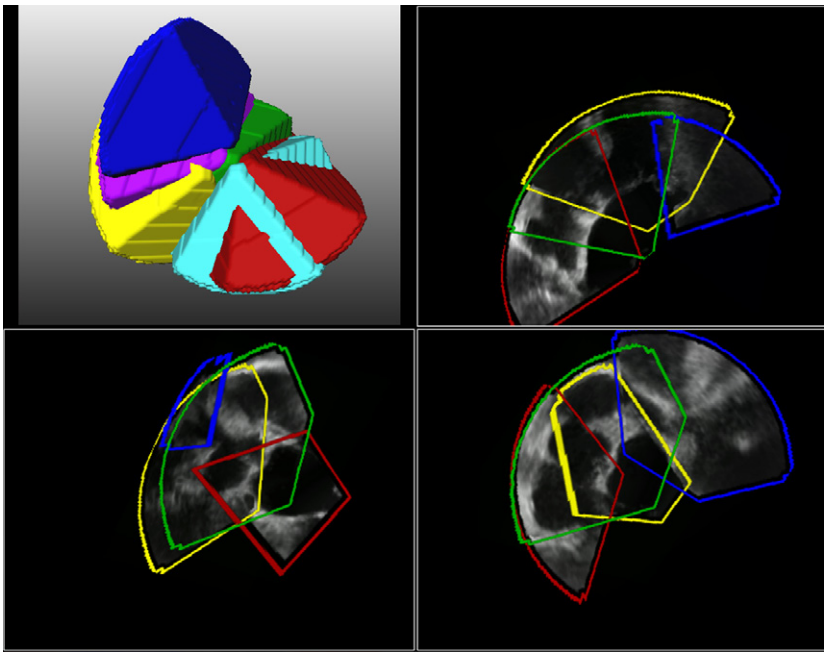

Figure 2 Display of the registered six TEE volumes. The center view (view 1) is shown in yellow, the view the furthest to the left (view 2) is shown in blue, and the view to the furthest to the right (view 3) is shown in red. The intermediate views four (green), five (turquoise), and six (purple) are recorded to ensure sufficient overlap between the center and the most right view. For image fusion views 1, 2, 3 , and 4 were used.

TEE Image Registration and Fusion

To build a 3D wide-view of the heart, the data sets of the six different volumes were registered manually to the corresponding CTA image and to each other. Since we aimed at a proof-of-principle for the segmentation of fused sets, we wanted to test our seg-

mentation on the best possible registration and fusion. Even though we expected that artifacts caused by registration errors and fusion in the wide-view images would only minimally affect our segmentation scheme, we did not want to mix the errors of the registration and segmentation and chose to evaluate our wide-view segmentation with the best possible registration. Therefore, we chose to use an elaborate manual registration in order to minimize the effect of registration errors on the segmentation results. First, a single observer picked in each of the six TEE images and the CTA image the end diastolic volume and indicated a minimum of three anatomical landmarks (from a set of 8) in all volumes. From corresponding landmarks an initial rigid transform (rotation and translation only) was computed. Second, image alignment was improved by manually refining the rotation and translation of the TEE volume with respect to the CTA image. The correct alignment of the anatomical structures was checked by slicing the volumes in three orthogonal cross-sections and overlaying the resulting 2D images. Third, after repeating step one to two for all 6 TEE views, all TEE images were jointly displayed with respect to the CTA image and each other. With small manipulations of the rotations and translations of the individual TEE volumes the alignment of the overall anatomical structures was optimized. The registered TEE volumes are shown in Figure 2. Once the adequate transformations were found, the volumes 1 to 4 were fused. We excluded view 5 and 6 from the fusion to minimize fusion artifacts. Furthermore, minimum-intensity fusion was chosen to suppress artifacts especially at the edge of the imaging cones.

The registration accuracy and the correspondence of anatomical landmarks in fused TEE volumes and CTA volumes was assessed previously[15]. The good correspondence between CTA and fused TEE can be visually appreciated in Figure 3.

Gamma Mixture Model

Classifying different tissues such as myocardium and blood can be done based on the differences in intensity distribution of the so-called ultrasound *speckle* for these tissues. Previously, Vegas-Sánchez-Ferrero *et al.*[16-18] showed that a Gamma Mixture Model (GMM) can accurately represent the intensity distribution ($X = \{X_i\}$, $i = 1 \ldots N$, with N denoting the number of voxels) of ultrasound images after beam-forming, post-processing, and interpolation. An Expectation Maximization algorithm[19] was used to estimate the parameters ($\Theta = \pi_1, \ldots, \pi_J, \alpha_1, \ldots, \alpha_J, \beta_1, \ldots, \beta_J$) of a two-class ($j = \{1, \ldots, J\}$, $J = 2$) mixture model with the probability density function

$$p(x|\Theta) = \sum_{j=1}^{2} \pi_j fx\,(x|\alpha_j, \beta_j) \tag{1}$$

where f_x denotes the Gamma density function. A 3D map showing the voxel-wise probability of blood versus tissue is then computed by applying Bayes' theorem. An example slice of a TEE volume and the computed tissue probability map is shown in Figure 4.

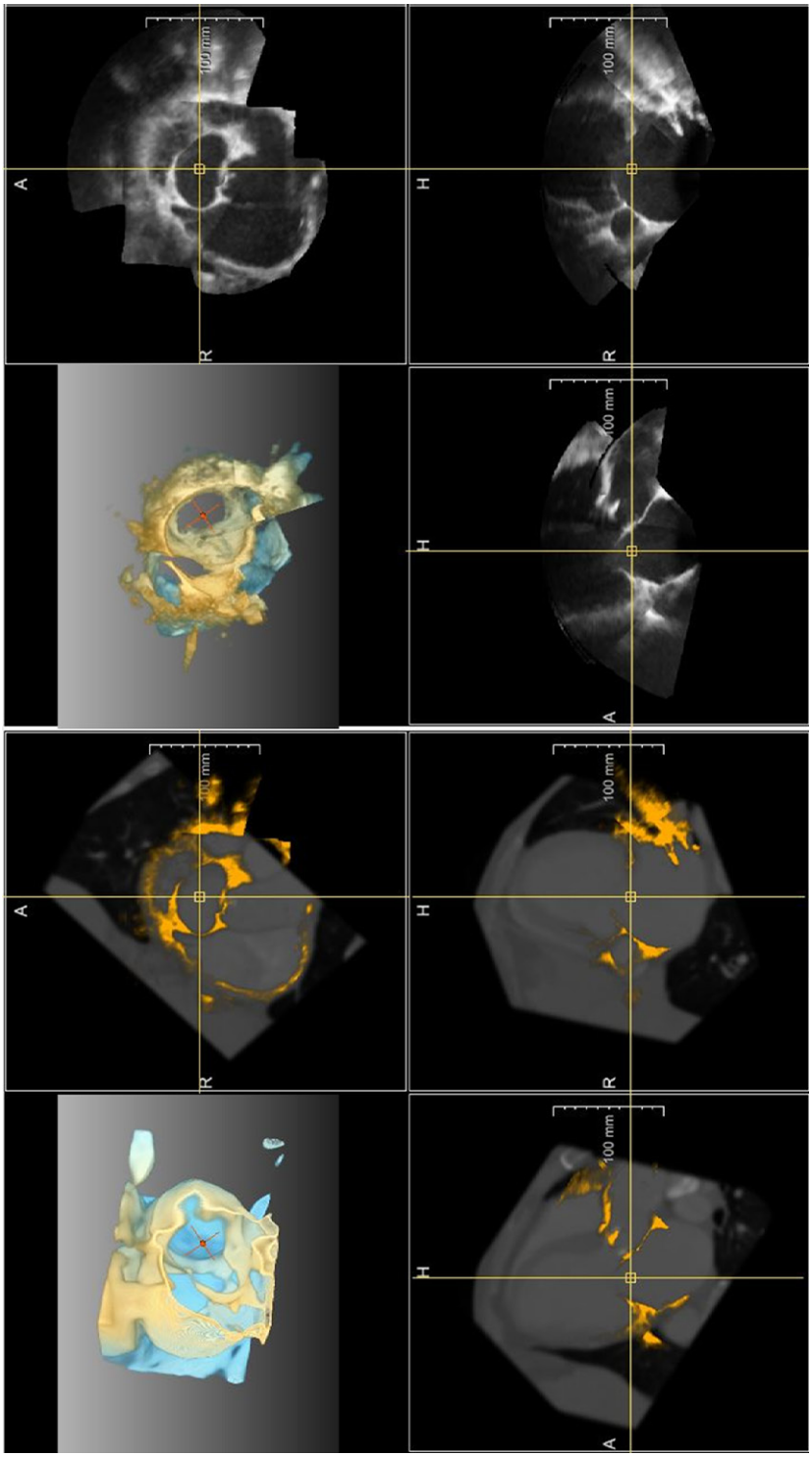

Figure 3 Rendered CTA volume (top left) and rendered fused TEE (top right). The three orthogonal cross sections of the CTA (left) and the fused TEE (right) are shown as well. The marker in the 2D views (yellow cross) indicates the center of the mitral valve. The same location is shown in the 3D rendering indicated by the red cross. Please note the good anatomical correspondence between CTA and TEE. This can be appreciated in the 2D CTA cross sections (left) where the fused TEE is overlaid in orange.

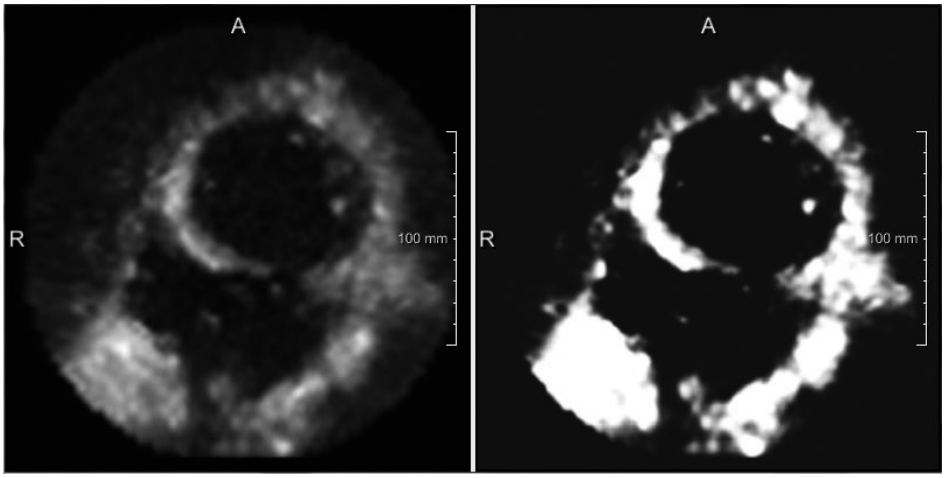

Figure 4 Short axis cross section through a TEE volume (left) and the corresponding tissue probability map (right). Note the suppression of speckle in the tissue probability map compared with the intensity map.

Active shape model

Active shape models (ASM)[20] employ statistical shape models (SSM) generated from a large training set to model all probable anatomical variations in organ shape. The SSMs used in this work were derived from 151 3D CTA segmentations[14,21] containing the left and right atria (LA and RA), left and right ventricles (LV and RV), and the aorta (Ao). We created SSMs for the complete heart keeping 90% and for the individual cavities keeping 98% of the shape variation. The CTA scans were made from a mixed population of patients covering a large variability in anatomy and pathology[21]. In our TEE segmentation scheme, update points (r′) are found along the surface normal of each shape vertex (r) in the tissue probability maps by minimizing an objective function as described by Van Ginneken *et al.*[22]. The pose and/or shape of the ASM is updated until convergence. The pose (scale, rotation and translation) is estimated with a weighted least square scheme which was described in[23,24]. Shape updates are estimated by a weighted projection to the shape parameter space as described by Cootes *et al.*[25]. The weights w used for the pose and shape updates are composed from a GMM based edge probability, $w_{GMM}(\mathrm{r}')$, a model distance term, $w_{ASM}(\mathrm{r}')$, and a term to disqualify points outside the pyramidal TEE volume, $w_{US}(\mathrm{r}')$. The weighting factor is computed as follows:

$$w(\mathrm{r}') = w_{ASM}(\mathrm{r}')\, w_{US}(\mathrm{r}')\, w_{GMM}(\mathrm{r}') \tag{2}$$

where

$$w_{ASM}(\mathrm{r}') = \exp\left(-\frac{\|\mathrm{r}-\mathrm{r}'\|^2}{\sigma^2}\right) \tag{3}$$

σ is used to adjust the model distance penalty term, and $\|\cdot\|$ indicates the Euclidean distance. The term w_{US} (r′), is derived by convolving the binary TEE mask with Gaussian kernel with a standard deviation of $\sqrt{20}$ voxels. The GMM term, w_{GMM} (r′), enhances update points being close to the blood/tissue transition zone (probability of 0.5) and is defined as

$$w_{GMM}(\mathrm{r}') = 1 - \frac{|p_2(I(\mathrm{r}')|\Theta) - 0.5|}{0.5} \tag{4}$$

where I (r′) is the intensity in the TEE image at r′.

Segmentation scheme

We used a three-stage segmentation scheme where the mean shape of the SSM is initialized by a rigid transform computed from three landmark points. Generally, each stage is initialized with the results of the previous stage while the model pose is more and more constrained and the shape is more and more relaxed. The different stages and their function are described by the flow chart in Figure 5.

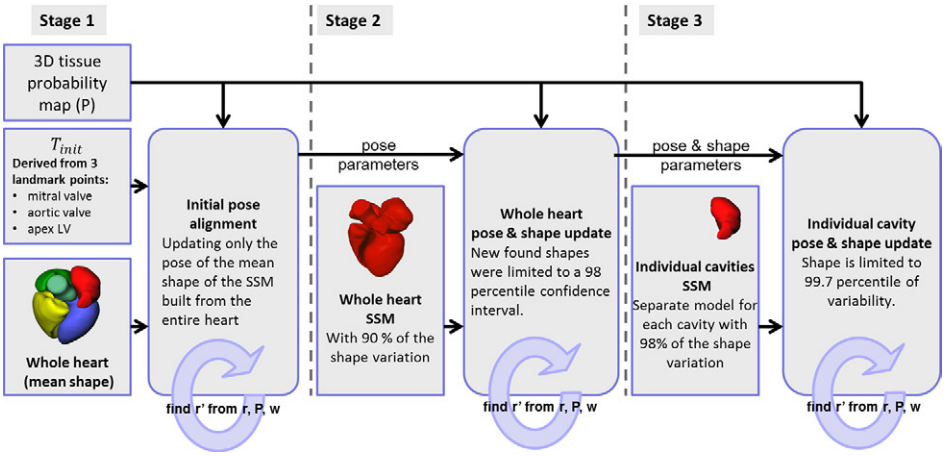

Figure 5 Three-stage segmentation scheme: At each stage the model is updated until convergence. Convergence criterion is a RMS difference between the current and previous shape of less than 0.1 mm. **First stage**, the mean shape of the SSM containing all five cavities is initialized using a rigid transform derived from three landmark point pairs. In this stage only the pose is updated and the resulting transform is passed to the next stage. **Second stage**, pose and shape of the complete heart SSM are simultaneously updated. **Third stage**, For each heart cavity a separate SSM is used and initialized based on the pose and shape of the previous stage. The shape estimates for stage 2 and 3 are limited to a hyper-ellipsoid defined by the 98th percentile of the shape parameters' χ^2 distribution[20]. Please note that in this segmentation scheme the pose is more and more constrained while the shape is more and more relaxed while propagating through the stages. The constraining and limiting parameters used for all stages are shown in Table 1.

To guarantee a high robustness of the segmentation scheme, the pose parameters and the shape are constrained and limited to a plausible range.

In the different stages we constrain the pose parameters (scale, rotation, and translation) and shape parameters to prevent large jumps of the model due to erroneous edge responses. Each of the parameters p at iteration *i* is constrained by

$$p_i = cp_{i-1} + (1-c)\hat{p}_i, \tag{5}$$

where $\hat{p}_i$ indicates the estimated unconstrained parameter at iteration *i*. The used constraints are shown in Table 1. These constraints are identical to those used in single TEE segmentations[11] for fair comparison.

The scale (a_{lim}), the rotation angles (θ_{lim}), the translation (t_{lim}) and the shape (b_{lim}) and their values for the different stages are shown in table 1 as well.

Table 1 Segmentation parameters: σ defines the range of w_{ASM}, c constrains $\boldsymbol{\theta}$, $\mathbf{t}$, $\mathbf{b}$, and c_a constrains a at each iteration. Upper and lower limits for the pose and shape parameters have the subscript *lim*.

parameters	stage 1 (S1)	stage 2 (S2)	stage 3 (S3)
c	0.0	0.2	0.6
c_a	0.0	0.2	0.3
σ (voxel)	44	20	20
a_{lim} (%)	±30 of a_{init}	±18 of a_{S1}	±15 of a_{S2}
$\boldsymbol{\theta}_{lim}$ (°)	±30 of $\boldsymbol{\theta}_{init}$	±20 of $\boldsymbol{\theta}_{S1}$	±5 of $\boldsymbol{\theta}_{S2}$
$\mathbf{t}_{lim}$ (mm)	±30 of $\mathbf{t}_{init}$	±20 of $\mathbf{t}_{S1}$	±5 of $\mathbf{t}_{S2}$
$\mathbf{b}_{lim}$ (%)	0.0	98.0	99.7

EXPERIMENTS

Data

The segmentation method was validated in 3D TEE data sets obtained from 20 patients (13 male, 7 female; mean age ± standard deviation: 80 ± 7) undergoing a transcatheter aortic valve implantation. Data were acquired in accordance with the hospital ethical regulations (MEC-2013-257). The protocols were approved by the institutional review board, and informed consent was obtained from all patients. All patients had severe aortic valve stenosis with different severity of valve regurgitation. This caused for all patients severe pathologies with different degrees of LV hypertrophy and enlargement as well as LA enlargement. All TAVI patients had 3D TEE data acquired with an iE33 system with a matrixTEE probe (CX7-2t, Philips Healthcare, The Netherlands) during the preparation of the intervention. The patients were anesthetized and in supine position.

One to three heart cycles were acquired in full volume mode with a volume rate of 4.3 ± 0.9 volumes/sec. The end-diastolic (ED) time frame was manually selected. All patients hadalso underwent a gated CTA three to five weeks before the intervention for preoperative planning. More details on the CTA acquisition protocol can be found in the study of Ren *et al.*[13].

Gold standard

Segmentations of CTA images from the same twenty patients served as the ground truth. We generated these using a multi-atlas based approach[14]. The CTA volumes were cropped so that only the heart was in the image volume. The ASM was generated earlier on 151 patients and did not include any of the CTA segmentations which were used for our validation. All CTA segmentations were visually inspected and considered of good quality. The CTA segmentations provide an independent ground truth of the cavity outline and are not limited to the TEE FoV. One should note that the CTA supplies the anatomy of the same patient but at a different time and with a different modality, so one cannot expect a perfect match with TEE.

Evaluation measures

For comparing the different segmentations, overlap in volume for each cavity was expressed as a Dice coefficient in 3D[26]. The distance between corresponding 3D segmentations was computed as average Euclidean point-to-surface distance ($P2S_{mean}$). Please note that the Dice coefficient and the $P2S_{mean}$ were computed for the whole heart and not limited to the FoV. Furthermore, the percentage of each cavity that was contained within the FoV was measured, both for the single-view segmentations and the wide-view. It was expected that the segmentation accuracy of each cavity was related to this coverage.

RESULTS

Spatial Coverage

The coverage of the FoV for each heart cavity for the single-view and wide-view images was computed based on the CTA segmentations and is shown in Figure 6. It is shown that the wide-view images contained a much larger portion of the different cavities. The median coverage increased by 2, 29, 62, and 49 percent points for RV, LA, RA, and Ao respectively. The FoV of the LV did not improve since it was captured already within the single-view volumes (view 1).

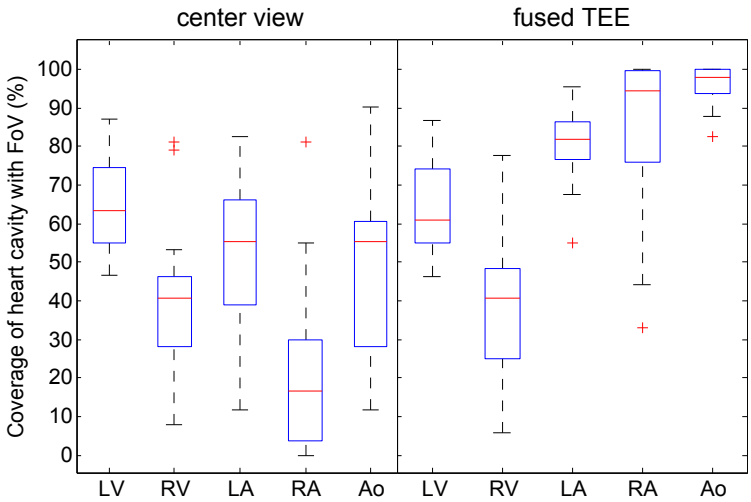

Figure 6 Coverage of the different heart cavities within the field of view (FoV) of the single-view TEE image (left) and of the fused wide-view TEE image (right). The red horizontal line indicates the median, the blue box indicates the 25 and 75 percentiles, and the whiskers indicate the range excluding outliers. Outliers are considered data points beyond mean ±2.7 times the standard deviation and plotted as red +. Note the improved coverage of the LA, RA, and Ao cavities compared with the single-view images.

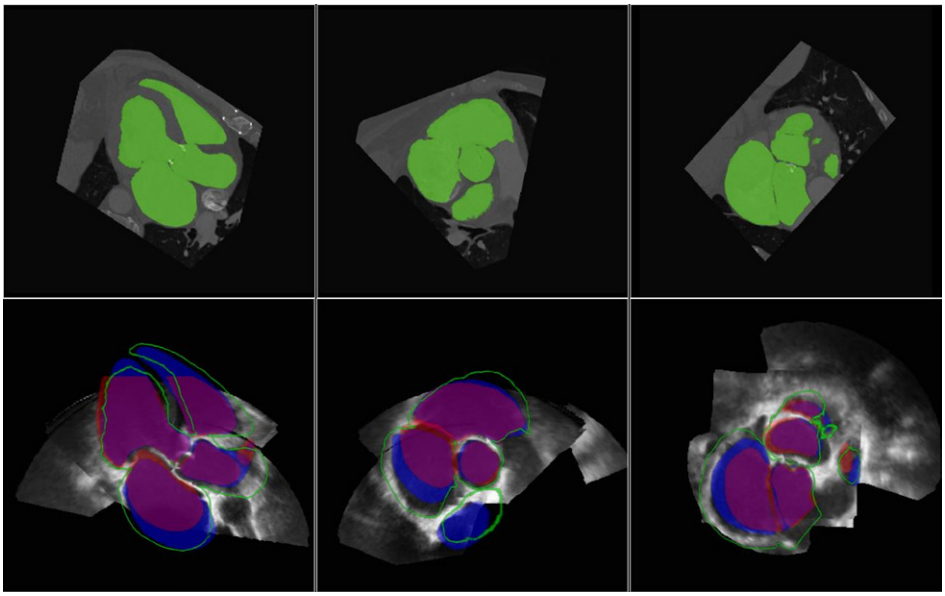

Figure 7 Three orthogonal cross sections of the CTA volume with the segmentation overlaid (top). The same cross sections are displayed for the fused TEE data set (bottom) together with the segmentation results based on the single-view (red) and the fused wide-view data (blue). The outline of the CTA based segmentation is shown in green.

Segmentation

A qualitative example of a wide-view TEE volume with corresponding CTA and their segmentations are shown in Figure 7. In Figure 8 the box-plots of the Dice coefficients and in Figure 9 the $P2S_{mean}$ distances for all cavities are shown. On the left of Figure 8 and 9 the segmentation results using only the central TEE volume (view 1) are shown,

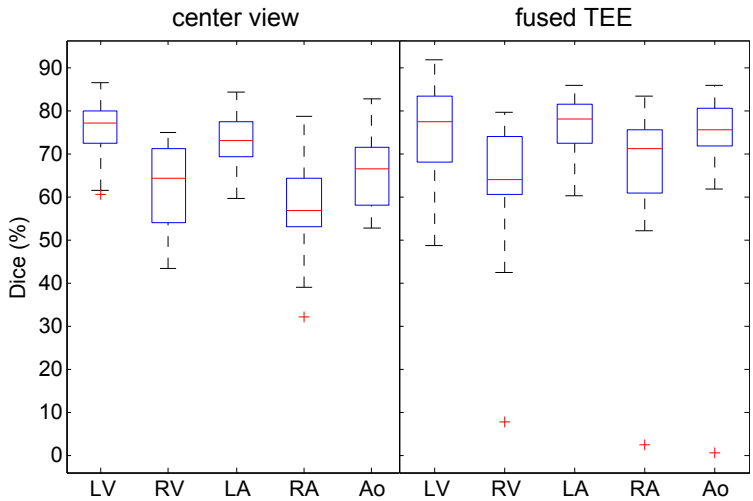

Figure 8 Comparison (Dice) of single-view segmentation (left) and fused TEE segmentation (right) vs. CTA segmentations. The computation of the Dice coefficients was not restricted to the FoV of the TEE images.

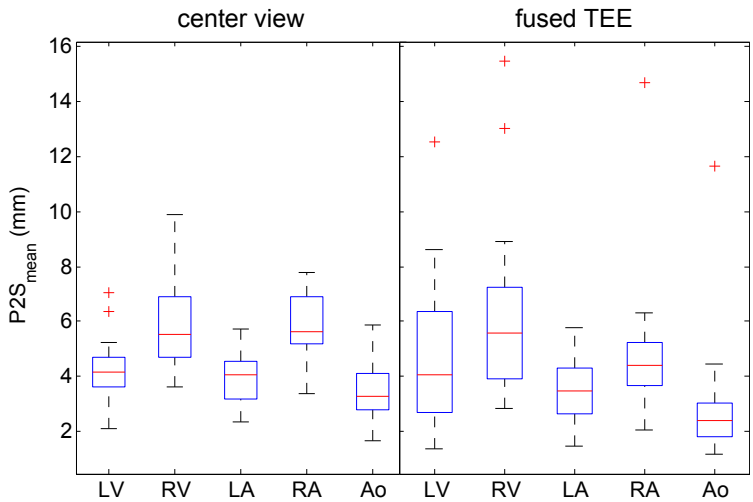

Figure 9 Comparison (Point-to-surface distance) of single-view segmentation and fused TEE segmentation vs. CTA segmentations. The computation of the mean point-to-surface distances was not restricted to the FoV of the TEE images.

whereas on the right the segmentation results using the fused TEE volumes are shown. It is shown that the cavities which had an improved coverage with the wide-view TEE FoV also had an improved segmentation accuracy.

DISCUSSION

We showed previously that wide-view TEE images can provide an alternative to preoperative CT images in clinical applications[15]. In this work we investigated to what extent wide-view TEE volumes could be used to improve segmentation accuracy. To that end, we segmented twenty single and wide-view patient data sets successfully with our segmentation scheme and compared them with CTA derived segmentations which served as ground truth.

Generally, the wide-view TEE images helped to improve the coverage of the FoV for the different heart cavities and fusion artifacts did not hamper the segmentation accuracy.

We obtained improvements of the segmentation results of LA, RA, and Ao which improved the median Dice coefficient by 5, 15, and 9 percent points respectively (see Figure 8). This may be mostly due to the improved field of view which resulted in a coverage of 82, 94, and 97 percent compared with the single-view coverage of 56, 17, and 56 for LA, RA, and Ao, respectively. For LV and RV, which had no improved FoV compared with the single-view TEE segmentations, the segmentation accuracy stayed the same. This implies that generally the segmentation accuracy was not deteriorated by the fusion.

For one fused patient data set segmentation failed (see Figure 8, outliers). Visual inspection of the fused image data and the segmentation indicated that for this patient the image data of the different views was quite noisy, had low SNR and the individual views seemed to have quite different mean intensities. This resulted in a wide-view image with considerable artifacts which misguided the segmentation.

Four registered TEE volumes were fused to a wide-view image utilizing a minimum-intensity fusion which creates in our opinion the least fusion artifacts. However, this method still created some fusion artifacts, such as propagating echo drop outs and edges of the single-view sectors, which will create false edges and may influence the segmentation scheme (see Figure 3). There could also be some temporal mismatches between the different single view volumes which also will influence the cavity borders in the fused image. With a higher volume rate these errors should be reduced.

We did not obtain a significant improvement of the segmentation results for LV and RV (see Figure 8 and 9). This may be due to the fact that the center view (view 1) contained most of the LV and RV and the wide-view fusion did not add much information. This is supported by the finding that the FoV did not improve for LV and RV, respectively (see Figure 6). Although it has been reported by others that multi-view fusion may improve

the image quality in transthoracic echocardiography[27], this is not very apparent in TEE. The effect of multi-angle compounding is small in TEE, since the position of the probe in the esophagus is almost the same for all views. Also, the minimum-intensity fusion that we applied is not improving local image quality, although it is good for reducing artifacts.

Limitations

Up to now our segmentation work is based on manual registration of the single TEE volumes. Our next step is to apply the segmentation in combination with an automated registration approach for TEE images. Our group previously reported good results for different registration metrics for transthoracic US/US registration[12] which is promising for replacement of CTA/MR. However, we chose to use an elaborate manual registration scheme since this is currently the most accurate method and will minimally deteriorate the results of our segmentation.

Our final goal is to replace or complement CTA/MR. For complementing CTA/MR with wide-view TEE, automatic intermodality registration would be desired. However, to our knowledge there is not yet a reliable standard method of registering ultrasound images to CT or MR and this is an ongoing research topic.

Another limitations is that the ground truth segmentations are derived from a different imaging modality (CTA) which uses different physical principles for image contrast formation. Furthermore, there are weeks between CTA and TEE image acquisitions which may have resulted in changes in anatomy and physiological state. Therefore, we cannot expect perfect correspondence between wide-view TEE and CTA. In a previous study[15] we investigated the correspondence between fiducial landmarks in CTA and wide-view TEE. We found an average Euclidean distance of about 6 mm between fused TEE and CTA landmarks. The intra-observer variability of repeated indications of the markers in CTA volumes proved to be already about 4 mm, which implies that correspondence between CTA and fused TEE was actually quite good. The $P2S_{mean}$ in our study included a similar intermodality difference error which means that the difference between TEE segmentations and anatomical reality may be considerably smaller than the values reported in Figure 9.

Future work

We expect that a more sophisticated fusion method than minimum-intensity fusion may improve the segmentation results further. The outer edges of ultrasound image volumes are usually hampered by artifacts and low SNR due to side lobes. Taking this information into account, a weighted-mean fusion with lower weights at the sides of the imaging pyramid than in the center portion may improve the image quality of the fused volumes. However, the fusion artifacts did not affect the segmentation scheme in all but

one extreme case. Also, the quality of our segmentation should still be investigated in combination with an automated registration approach, when this becomes available.

We are confident that our technique can improve the intra-operative visualization in EP procedures and may reduce the need of pre-operative imaging such as CT/MR and the use of X-ray fluoroscopy.

CONCLUSIONS

We showed that wide-view fusion could improve segmentation accuracy for TEE images by 5, 15, and 9 percent points for LA, RA, and Ao respectively. This proves that in principle 3D TEE is capable of visualizing large parts of the heart and that segmentation accuracy can be improved compared with single-view TEE, which makes this wide-view segmentation a good candidate for support of EP interventions.

ACKNOWLEDGEMENTS

This research is supported by the Dutch Technology Foundation STW (10847), which is the applied science division of NWO, and the Technology Programme of the Ministry of Economic Affairs.

REFERENCES

1. Cox JL, Schuessler R, D'Agostino HJJ, Stone CM, Chang BC, Cain ME, Corr PB, Boineau JP. The surgical treatment of atrial fibrillation. iii. Development of a definitive surgical procedure. *Journal of Thoracic and Cardiovascular Surgery* 1991;101:569-83.
2. Prasad SM, Maniar HS, Camillo CJ, Schuessler RB, Boineau JP, III TMS, Cox JL, Jr RJD. The cox maze {III} procedure for atrial fibrillation: long term efficacy in patients undergoing lone versus concomitant procedures. *The Journal of Thoracic and Cardiovascular Surgery* 2003;126:1822-1827.
3. Pappone C, Rosanio S, Oreto G, Tocchi M, Gugliotta F, Vicedomini G, Salvati A, Dicandia C, Mazzone P, Santinelli V, Gulletta S, Chierchia S. Circumferential radiofrequency ablation of pulmonary vein ostia: A new anatomic approach for curing atrial fibrillation. *Circulation* 2000;21:2619-28.
4. Pappone C, Oreto G, Rosanio S, Vicedomini G, Gugliotta F, Salvati A, Dicandia C, Calabro MP, Mazzone P, Ficarra E, Di Gioia C, Gulletta S, Nardi S, Santinelli V, Benussi S, Alfieri O. Atrial electroanatomic remodeling after circumferential radiofrequency pulmonary vein ablation: efficacy of an anatomic approach in a large cohort of patients with atrial fibrillation. *Circulation* 2001;104: 2539-2544.
5. Ghaye B, Szapiro D, Dacher JN, Rodriguez LM, Timmermans C, Devillers D, Dondelinger RF. Percutaneous ablation for atrial fibrillation: The role of cross-sectional imaging. *RadioGraphics* 2003;23: S19-S33.
6. Ravenel JG, McAdams HP. Pulmonary venous infarction after radiofrequency ablation for atrial fibrillation. *American Journal of Roentgenology* 2002;178:664-666.
7. Kovoor P, Ricciardello M, Collins L, Uther JB, Ross DL. Risk to patients from radiation associated with radiofrequency ablation for supraventricular tachycardia. *Circulation* 1998;98:1534-1540.
8. Shpun S, Gepstein L, Hayam G, Ben-Haim SA. Guidance of radiofrequency endocardial ablation with real-time three-dimensional magnetic navigation system. *Circulation* 1997;96:2016-2021.
9. Dong J, Calkins H, Solomon SB, Lai S, Dalal D, Lardo A, Brem E, Preiss A, Berger RD, Halperin H, Dickfeld T. Integrated electroanatomic mapping with three-dimensional computed tomographic images for real-time guided ablations. *Circulation* 2006;113:186-194.
10. Cappato R, Calkins H, Chen SA, Davies W, Iesaka Y, Kalman J, Kim YH, Klein G, Packer D, Skanes A. Worldwide survey on the methods, efficacy, and safety of catheter ablation for human atrial fibrillation. *Circulation* 2005;111:1100-1105.
11. Haak A, Vegas-Sánchez-Ferrero G, Mulder HM, Kirişli H, Baka N, Metz C, Klein S, Ren B, van Burken G, Pluim J, van der Steen A, van Walsum T, Bosch JG. Simultaneous segmentation of multiple heart cavities in 3d transesophageal echocardiograms. In: *Proc. Ultrasonic Symposium* 2013;659-662.
12. Mulder HW, van Stralen M, van der Zwaan H, Leung K, Bosch JG, Pluim J. Multi-frame registration of realtime 3d echocardiography time series. *Journal of Medical Imaging* 2014.
13. Ren B, Mulder HW, Haak A, van Stralen M, Szili-Torok T, Pluim J, Geleijnse ML, Bosch JG. A transoesophageal echocardiographic image acquisition protocol for wide-view fusion of three-dimensional datasets to support atrial fibrillation catheter ablation. *Journal of Interventional Cardiac Electrophysiology* 2013;37:21-26.
14. Kirişli H, Schaap M, Klein S, Papadopoulou S, Bonardi M, Chen C, Weustink A, Mollet N, Vonken EPA, van der Geest R, van Walsum T, Niessen W. Evaluation of a multi-atlas based method for segmentation of cardiac cta data: a large-scale, multi-center and multi-vendor study. *Medical Physics* 2010;37:6279-6292.
15. Ren B, Mulder HW, Haak A, McGhie J, Szili-Torok T, Nieman K, van Stralen M, Pluim J, Geleijnse ML, Bosch JG. Fusion of three-dimensional transesophageal echocardiographic images of left

atrium for supporting catheter ablation procedures: Comparison with computered tomography, unpublished observation.

16. Vegas-Sánchez-Ferrero G, Tristan-Vega A, Aja-Fernandez S, Martin-Fernandez M, Palencia C, Deriche R. Anisotropic LMMSE denoising of MRI based on statistical tissue models. *International Symposium on Biomedical Imaging* 2012;1519-1522.

17. Vegas-Sánchez-Ferrero G, Seabra J, Rodriguez-Leor O, Serrano-Vida A, Aja-Fernandez S, Palencia C, , Martin-Fernandez M, Sanches J. Gamma mixture classifier for plaque detection in intravascular ultrasonic images. *IEEE Transactions on Ultrasonics Ferroelectrics and Frequency Control* 2014b; In press.

18. Vegas-Sánchez-Ferrero G, Martin-Fernandez M, Miguel-Sanches J. Multi-Modality Atherosclerosis Imaging and Diagnosis. Springer Verlag, Ch. A Gamma Mixture Model for IVUS Imaging 2014a; 155-171.

19. Moon T. The expectation-maximization algorithm. *IEEE Signal Processing Magazine* 1996;13:47-60.

20. Cootes T, Cooper D, Taylor C, Graham J. Active shape models – their training and application. *Computer Vision and Image Understanding* 1995;61:38-59.

21. Metz C, Baka N, Kirişli H, Schaap M, Klein S, Neefjes L, Mollet N, Lelieveldt B, de Bruijne M, Niessen W, van Walsum T. Regression-based cardiac motion prediction from single-phase cta. *IEEE Transactions on Medical Imaging* 2012;31:1311-1325.

22. van Ginneken B, Frangi A, Staal J, ter Haar Romeny B, Viergever M. Active shape model segmentation with optimal features. *IEEE Transactions on Medical Imaging* 2002;21:924-933.

23. Arun KS, Huang TS, Blostein SD. Least-squares fitting of two 3-d point sets. *IEEE Transactions on Pattern Analysis and Machine Intelligence* 1987;PAMI-9:698-700.

24. Horn BKP, Hilden H, Negahdaripour S. Closed-form solution of absolute orientation using orthonormal matrices. *Journal of the Optical Society America* 1988;5:1127-1135.

25. Cootes TF, Hill A, Taylor CJ, Haslam J. Use of active shape models for locating structures in medical images. *Image and vision computing* 1994;12:355-365.

26. Dice LR. Measures of the amount of ecologic association between species. *Ecology* 1945;26: 297-302.

27. Rajpoot K, Grau V, Noble JA, Szmigielski C, Becher H. Multiview fusion 3-d echocardiography: Improving the information and quality of real-time 3-d echocardiography. *Ultrasound in Medicine & Biology* 2011;37:1056-1072.

Part V

Discussion

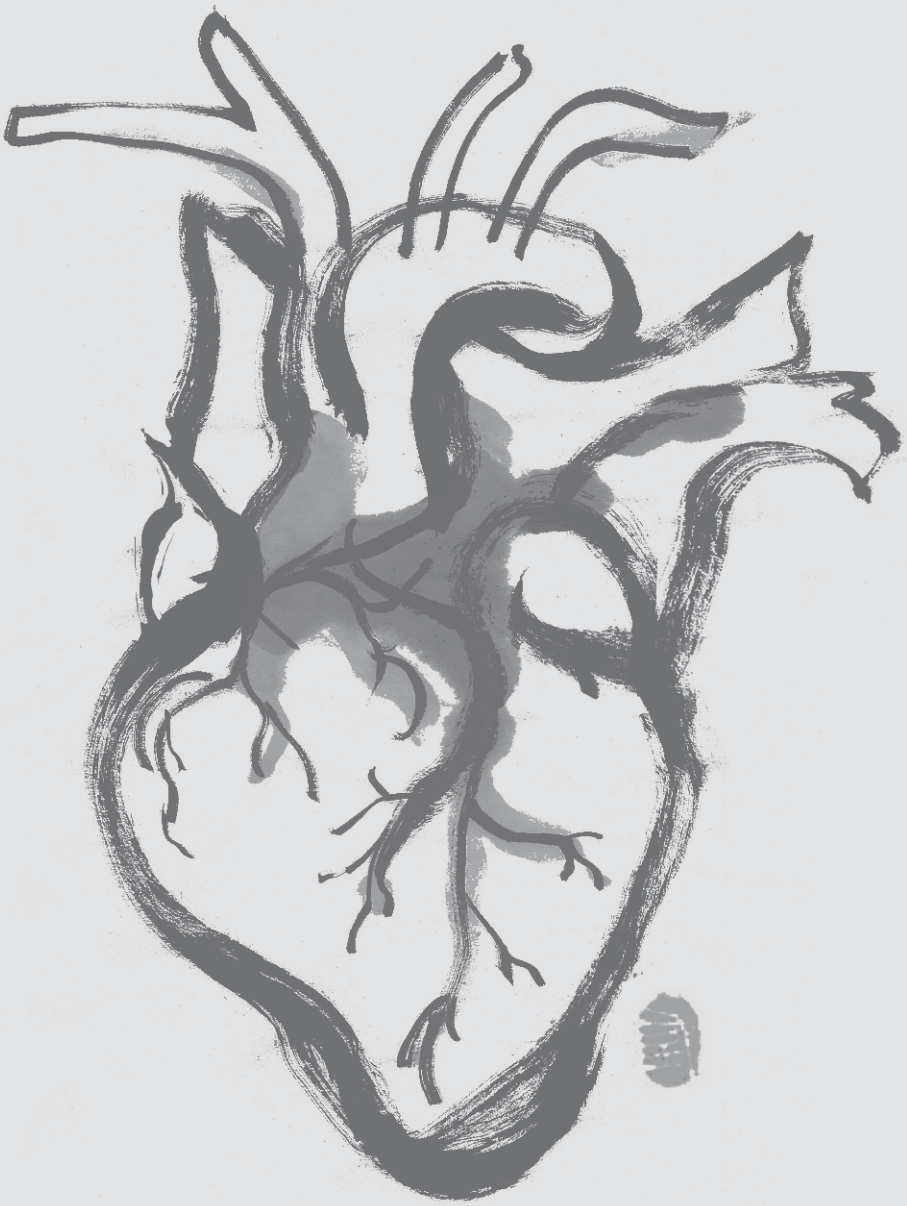

Chapter 5.1

Summary

SUMMARY

The main goal of this thesis was to investigate the clinical implications of advanced three-dimensional (3D) echocardiography in assessing mitral valve regurgitation, left atrial (LA) function, left ventricular (LV) function and reconstructing the LA. Chapter 1 is the introduction to this thesis, in which the techniques to study mitral regurgitation (MR) quantification, LA and LV volume and function assessment and LA anatomy for catheter ablation are introduced. Thereafter, the feasibility and accuracy in applying 3D echocardiography in the mentioned topics are described.

3D echocardiography in quantification of mitral valve regurgitation

Quantification of MR is essential to determine the severity of MR and clinical outcome. In Chapter 2.1 the error made by the traditional 2D transthoracic echocardiographic (TTE) pulsed wave Doppler flow method in calculating regurgitant volume was estimated. In particular, the circular geometric assumption of the mitral annulus (MA) and left ventricular outflow tract (LVOT) was analyzed. This was done by comparing this method with a 3D transoesophageal echocardiographic (TOE) method in which the cross-sectional areas of the MA and LVOT were measured directly in "en face" views. In this study it is shown that both the MA and LVOT are oval with significantly different major and minor axis diameters. It is also shown that the MA cross-sectional area is overestimated by about 13% and the LVOT cross-sectional area is underestimated by about 23% by the 2D method. Moreover, since the errors are in different directions, the error in calculating the regurgitant volumes is even more significant, with an overestimate of about 54% by the 2D method.

3D echocardiography in assessing left atrial function in mitral valve regurgitation

Chronic degenerative MR causes important remodeling of the LA. LA compliance may play an important role in buffering LA pressure rise. In Chapter 2.2 we sought to assess LA compliance in asymptomatic versus symptomatic patients with degenerative MR using strain and strain rate imaging. In patients with matched MR volumes, asymptomatic patients show better LA compliance, evidenced by higher positive atrial strain and strain rate during LA filling comparable to the values of normal controls. The difference in positive strain and strain rate values between asymptomatic and symptomatic patients is further confirmed with a 3D echocardiographic analysis of LA volumes in which a larger LA volume change index during LV systole is found in the asymptomatic patients. Finally, patients with lower mean pulmonary arterial pressure also have better LA compliance.

In previous animal studies it has been shown that in the compensated phase of chronic MR, the LA becomes larger and more compliant with a more potent booster

pump action as a result of the optimal use of the Frank–Starling mechanism of the LA muscle. In Chapter 2.3 we aim to investigate the LA function changes in patients with chronic MR and preserved LV function by calculating the LA volumes using 3D TTE and myocardial mechanics using strain and strain rate imaging. In this study it is demonstrated that the LA contractile function decreased significantly in patients with severe MR, while did not show significant decrease in patients with mild and moderate MR. Additionally, the LA reservoir and conduit functions are augmented in significant MR, manifested by increased total stroke volume and passive filling volume as the maximal LA volume increased. By deformation analysis, we also find that LA late negative strain correlated well with LA active EF.

3D echocardiography in assessing the ventricular function

Left ventricular volumes and ejection fraction (EF) are the most commonly used parameters in assessing LV function and have important prognostic significance. In the 3rd part of this thesis, we sought to evaluate the accuracy of two automated algorithms in calculating LV volumes and EF. In Chapter 3.1 we apply the single-beat 3D echocardiographic automatic LV Analysis (Siemens Medical Solutions, Mountain view, USA) in calculating LV volumes and EF in datasets acquired with six different imaging modes and the measurements were compared with 3DQA QLAB manual analysis (Philips Medical System, Best, the Netherlands). In this study, it is shown that the accuracy of the Siemens automated 3D algorithm in measuring LV volumes and EF is significantly influenced by the different imaging modes, caused by differences in temporal and spatial resolutions. The Space 1 Harmonic (S1H) mode may be the preferred 3D acquisition mode, supplemented by the Time 1 Harmonic (T1H) acquisition mode in enlarged LVs which cannot be included completely in the acquisition sector of the S1H mode. Using this method, about two-thirds of the patients can be analysed automatically with favourable results compared with the QLAB manual analysis. In order to evaluate this algorithm in a real-world setting, we further apply this algorithm in consecutive patients with cancer planned for systemic chemotherapy and referred for routine echocardiographic examination for evaluation of LV function as shown in Chapter 3.2. The S1H mode was chosen as the primary imaging mode and the T1H mode as the first alternative in enlarged LV. The 3D imaging modes are applicable in a majority of clinical patients. The results in this study were in line with the previous study conducted in a scientific research condition.

In Chapter 3.3 we evaluate the TomTec 4D LV-Analysis (TomTec Imaging systems, Unterschleissheim, Germany) against cardiac magnetic resonance imaging (MRI) and QLAB manual analysis in consecutive subjects. The TomTec automatic algorithm is feasible in calculating LV volumes and EF in all consecutive patients and the contour tracking is acceptable (not requiring major corrections) in about two thirds of patients. In these patients with acceptable automatic contours, negative biases and quite considerable

limits of agreements compared with the MRI measures are found, which are comparable to previously published data using a manual approach. Furthermore, when compared with the QLAB manual measures, the negative biases especially in LV volumes are not seen. This indicates that the "volume underestimation" seems not a specific property of the automated TomTec algorithm but an inherent property of echocardiographic analysis.

3D echocardiography in reconstruction of the left atrium

Imaging of the LA is critical for catheter ablation of atrial fibrillation. Computed tomography (CT) is commonly used before the procedure and the images are segmented and registered by the electro-anatomical surface mapping (EAM) system to the real time mapping space during the procedure. However, the drawbacks of CT such as ionizing radiation are well recognized. In part 4 of the thesis, the aims are to develop a TOE imaging protocol in order to acquire a minimal number of overlapping 3D TOE datasets, allowing reconstruction of a wide 3D view of the LA with important anatomical structures and to validate the fused 3D TOE dataset with CT. In Chapter 4.1 the six-step TOE imaging protocol is described. The acquired datasets are registered and fused, providing a much wider reconstructed 3D view of the LA, incorporating the pulmonary veins, LA appendage, and the mitral and aortic valves. The protocol provides an important step towards using the pre- and/or intra-interventional 3D TOE to generate an anatomical map of LA for AF catheter ablation, eliminating the need for pre-interventional CT or MRI.

In Chapter 4.2, the accuracy of the image registration and fusion of the 3D TOE datasets is assessed by calculating the absolute distances between eight corresponding landmarks indicated in the fused 3D TOE and CT datasets. It is shown that the wide-view registration and fusion of the 3D TOE datasets are feasible in all patients and enabled the visualisation of major parts of the LA. The comparably central located structures such as the mitral and aortic valves, LA appendage and fossa ovalis can be clearly visualised in the fused 3D TOE in almost all patients. The superior pulmonary veins including common ostia are less well visible and the inferior pulmonary veins are very difficult to visualise in the fused 3D TOE datasets. The distances between landmarks in 3D TOE and CT datasets are 5 ± 3 mm for the important cardiac structures, which indicates the registration and fusion of the 3D TOE datasets tend to be accurate as compared with the routinely used EAM system.

In Chapter 4.3, the segmentation of multi-cavity anatomy from the wide-view fused 3D TOE datasets is further assessed in patients using a three-stage segmentation by comparing with a ground truth provided by atlas based segmentations derived from the CT angiographic images. The segmentation accuracy of single view TOE volumes and wide-view volumes is compared. It is shown that the segmentation accuracy is improved for LA, right atrium, and the aortic valve and is equally good in right ventricle

and LV. This implies that the automated segmentation is feasible in wide-view fused datasets and that the segmentation accuracy is improved for most cardiac cavities. This segmented 3D surface could be imported into the EAM system for supporting the electrophysiology interventions.

Chapter 5.2

General discussion

GENERAL DISCUSSION

To investigate the clinical implications of three-dimensional (3D) echocardiography, this thesis focuses on using 3D echocardiography in assessing cardiac geometry, cardiac chamber function and left atrium (LA) anatomical reconstruction. This chapter provides a brief summary of the main findings presented in the previous chapters and a general discussion in perspective of the published literature. Additionally, limitations of current studies and future perspectives in clinical application of 3D echocardiography are also suggested.

Can 3D echocardiography improve the assessment of mitral regurgitation severity?

It is of paramount importance to quantify mitral regurgitation (MR) because it is a critical parameter in determining clinical prognosis[1]. In both the American and European Society of Echocardiography guidelines on quantification of MR severity, an integral approach combining 2D/3D imaging of the valve and ventricle as well as Doppler measures of regurgitation severity is recommended. Two quantitative methods, the pulsed wave Doppler flow (PWDF) and proximal isovelocity surface area (PISA) methods are specifically described[2,3]. In order to use the measurements obtained with 2D echocardiography, important geometry assumptions are assumed in both methods: circular cross-sectional area (CSA) of the mitral annulus (MA) and left ventricular outflow tract (LVOT) in the PWDF method and hemispherical isovelocity surface in the PISA method. These assumptions bring essential errors in calculating the stroke volume or regurgitant volume because the target structures are not necessarily circular or hemispherical and the error of the monoplane diameter (radius) is further squared in the formulas.

Both the MA and LVOT have been confirmed to be oval in multiple studies with different imaging modalities[4-10]. In our study (Chapter 2.1), similar findings are presented. In state-of-the-art "en face" views in 3D transoesophageal echocardiography (TOE), both the MA and LVOT are oval with a major and minor diameters. However, in the 2D PWDF method, the MA dimension is measured only in the apical 4-chamber view and the LVOT dimension in the parasternal long-axis view[2,3,11]. As shown in our study, the 2D MA diameters approached the 3D major axis diameters and 2D LVOT diameters were close to the 3D minor axis diameters, which led to an overestimation of the CSA of the MA by 13 ± 12% and underestimation of the CSA of the LVOT by 23 ± 10%. The same extent of errors was made in calculating the SVs at the mitral annular and LVOT levels. Because the errors were in different directions (overestimation at the MA level and underestimation at the LVOT level), the consequent error (overestimation) in calculating the regurgitant volume was even more significant. Although in our study, the correction of regurgitant volume using 3D TOE did not change the clinical management of the patients because

all patients were symptomatic, it may have serious consequences in patients without symptoms who are referred for surgery solely on the basis of echocardiographic parameters.

In our study, we used the 2D PISA method as a reference method due to a lack of a golden standard in calculating the regurgitant volume. The underlying concepts in calculating the regurgitant volume using the PWDF method and PISA method are basically different. In the latter method, both spatial and temporal homogeneities of MR in systole are required, i.e. hemispherical isovelocity surface and holo-systolic regurgitant jet. In our study, the assumption that the isovelocity surface is hemispherical[12-15] was usually valid in degenerative MR, while the requirement of temporal homogeneity was not entirely met. In mitral valve (MV) prolapse, a dynamic orifice area change during systole typically presented as "late-systolic enhancement" is commonly seen. In the PISA method, the regurgitant volume is calculated from the maximal flow rate obtained by measuring the largest PISA radius, which is likely to overestimate regurgitant volume[16-18]. In contrast, in the PWDF method, the stroke volume at the MA level is measured in diastole, thus not affected by the dynamics of the MR in systole. The other crucial point, the hemispherical assumption in the PISA method, has been studied extensively (especially in functional MR because of its ellipsoid isovelocity surface as visualised with 3D echocardiography), and it has been demonstrated that it potentially underestimates the regurgitant volume[19-24]. Many studies proposed a direct measurement of the vena contracta area as it can be measured in the en-face view in 3D colour echocardiography[25-28]. The major advantages of this approach are the absence of geometric assumptions, relative independence of hemodynamic conditions and the capability of assessing multiple jets. The limitations are artefacts and comparably lower spatial and temporal resolutions than 2D echocardiography, which potentially causes considerable observer variability. Recently, an automated algorithm (Siemens 3D PISA) capable of measuring 3D PISA has been studied[29-31], and it was claimed to be more accurate than the 2D PISA method. The limitations of those studies, however, are also noted, being the lack of a golden standard and low temporal resolution. More investigations are needed before this new technique can be implemented in clinical practice.

Can 3D echocardiography improve the assessment of left atrial function in degenerative mitral regurgitation?

Mitral regurgitation causes important morphological and hemodynamic changes. During chronic MR, as regurgitation worsens gradually, the volume overload leads to LA and left ventricular (LV) dilatation. Many patients with chronic severe degenerative MR show symptoms such as dyspnoea, fatigue, and orthopnoea[32,33], while some patients with similar MR severity surprisingly show no symptoms. Left atrial compliance, defined as the ability of LA dilation during systolic filling, may act as an important compensatory

mechanism in buffering LA pressure rise and thus in preventing symptoms. Whereas in end-stage MR, LA compliance may eventually be compromised due to impaired LA elastic properties caused by chronic inflammatory changes, interstitial fibrosis, and decreased matrix metalloproteinase expression[34-36].

2D speckle tracking echocardiography techniques has been used to analyse myocardial mechanics in different patient populations[37-44]. In our study (Chapter 2.2), the positive strain and strain rate (SR) parameters were used to represent LA compliant function. The positive strain and SR and total strain values of the asymptomatic MR patients were found to be comparable with those of normal controls, indicating preserved LA compliance despite LA enlargement. In contrast, symptomatic patients with matched MR volumes showed lower strain and SR values, indicating impaired LA compliance. Moreover, the LA volume change index during LV systole obtained using 3D TTE was larger in the asymptomatic patients than in the symptomatic patients, which confirmed the difference in compliance between asymptomatic and symptomatic patients identified by the strain analysis. The main limitations of the 2D speckle tracking echocardiography in assessing the LA are that 1) it is dependent on image quality and suffers from errors due to the loss of some speckles that move out of the image plane, i.e. through-plane motion[45]; and 2) it assesses the LA function only in the longitudinal direction which might overlook some LA dysfunction because LA myocardial fibres are arranged in both longitudinal and circumferential directions[46]. 3D speckle tracking echocardiography has recently been developed and evaluated in assessing the LA mechanics in different subjects[47-49]. The major advantages of 3D over 2D speckle tracking have been reported as a more comprehensive assessment of LA function including LA synchrony with better reproducibility. The limitations of this new technique are also noted. First of all, the current 3D speckle tracking software was designed for LV analysis and there is no such software specific to LA strain analysis. Secondly, as a common drawback of 3D TTE, the 3D datasets are limited in temporal and spatial resolutions, especially for structures like the LA which lies in the far field of the ultrasound beam and has a thin wall. The relatively low volume rate would limit the accurate identification of the peak LA strain[50] and the echo drop-out on the LA wall adversely affects the image analysis.

In our study, although symptomatic patients showed reduced positive strain and SR, the LA negative strain and SR were comparable between asymptomatic and symptomatic patients, both of which were lower than those of the controls. This indicates that even though the asymptomatic patients still showed normal LA compliance, the LA contractile function may have already declined. This may have an important prognostic value in asymptomatic patients with severe MR. The possible reason for the maintained LA compliance but impaired contractile function might be probably due to an elevated LV filling pressure at late diastole before the atrial contraction caused by increased LV volume before atrial contraction due to the increased passive filling volume and

increased LV stiffness during LV remodeling due to MR progression. In animal studies, Frank–Starling behavior of the atrium was shown. In patients with degenerative MR, the LA contractile function alterations may also present a Frank–Starling curve, in which the LA contraction augments in the early stage of MR and decreases in the later stage. In our study (Chapter 2.3), the LA active stroke volume calculated using 3D TTE presented a curve similar as the Frank–Starling curve. However, this can be best appreciated by a longitudinal study following individual patients as MR progresses and assessing the LA contractile function change as regurgitant volume and LA volume increase when the after-load remains constant.

Traditionally, LA volumes are calculated with either an ellipsoid model or the modified bi-plane Simpson's rule using 2D echocardiography[51]. However, insights from cardiac computed tomography (CT) and anatomic studies showed that the LA has a complex shape with an irregular ellipsoid LA free wall and oblique planar interatrial septal wall[52,53]. Pitfalls exist in 2D echocardiographic determination of LA volumes because 1) the LV long axis does not necessarily cut through the long axis of the LA; 2) the apical 4-chamber and 2-chamber views are not exactly 90° perpendicular to each other; and 3) the 2D cutting plane does not always bisect the centre of the LA short axis view[54]. For these reasons, the observer variabilities of 2D echocardiographic measurements were reported to be larger than those of 3D echocardiographic measurements[54-56]. In 3D echocardiographic studies, also LA volume underestimation was consistently lower than that of 2D echocardiography[56,57]. In addition, it has been shown that 3D LA volumes better predicted cardiac outcome[58-62]. A recent report on patients with MR showed that even in those without symptoms and with maintained LV ejection fraction (EF), severe LA dilation was associated with poor outcomes independently of known outcome predictors with MR[36]. Thus, further 3D echocardiographic studies concentrating on whether a depressed LA contractile function may predict poor outcome or poor reverse LA remodeling after MV surgery would be interesting.

Is 3D echocardiography ready for routine clinical practice in evaluating left ventricular function?

Accurate and reproducible quantitative assessment of LV size and function are pivotal for diagnosis, treatment, and prediction of prognosis in structural heart disease. Despite the utility and established role of 2D echocardiography to assess LV function, it has a number of important limitations for LV imaging, including foreshortening, malrotation and angulation. Because of the geometric assumptions of 2D echocardiography, volumetric measurements may be inaccurate if the acquisition of 2D images is suboptimal. In this regard, the most important contribution of 3D echocardiography may be in LV quantification, in which volumes and EF are measured independent of geometric assumptions regarding LV shape[63]. The matrix transducers which can acquire "live" 3D datasets with

minimal post-processing, together with improvements in semiautomated/automated volumetric analysis, have allowed 3D echocardiography to evolve from a complicated and time consuming research tool into a simple and fast imaging modality suitable for everyday clinical use.

Multiple studies have investigated the performance of 3D echocardiography in measuring the LV volumes and EF against MRI in different populations[64-73] and recently a meta-analysis was undertaken to evaluate published studies on performance of 3D echocardiography against MRI and its advantages over 2D echocardiography[74]. In this systematic review, it was shown that under controlled study settings in patients with adequate image quality, 3D echocardiography offers better accuracy and precision in measuring LV volumes and EF than 2D echocardiography does. However, compared with MRI, 3D echocardiography still consistently underestimated LV volumes, and more importantly, there is substantial variability (limits of agreement) in 95% confidence intervals (±38 ml for EDV, ±34 ml for ESV, and ±15% for EF) if datasets were not selected for higher image quality. All studies included in the systematic review were conducted in a manual way in which the LV contour generated in the (semi)automated algorithm was corrected manually. The manual correction seemed to improve the contour tracking, yet resulted in significant inter-observer variability, in particular between institutions[75].

In our studies (Part III), we have evaluated two fully automated algorithms (Siemens LV-analysis and TomTec 4D-LV analysis). The main purpose of those two studies was to evaluate the feasibility and accuracy of the fully automated 3D echocardiographic algorithms in calculating the LV volumes and EF in the real-world settings. We found that (excluding patients with ECG triggering problems in acquisition) about two-thirds of patients could be analysed automatically and reasonably with the Siemens Space 1 Harmonic mode (or the Time 1 Harmonic mode in case of a large LV). In the real clinical world of consecutive cancer patients referred for evaluation of EF, the results were slightly less favourable (50%). Similar results were found in the TomTec 4D-LV analysis. Compared with the MRI measures, the same extent of volume underestimation and variability were found as shown in the previous studies with manual input. By comparing with QLAB manual measures, we further concluded that the volume underestimation is most likely an inherent property of echocardiographic analysis as the biases compared with the manually corrected 3D datasets were quite small. The common merit of both automated algorithms is the ability to analyse datasets fully automatically in a fast manner, giving reasonable LV volume and EF measures in about two-thirds of routine clinical patients with a zero inter-observer variability. The major advantages of the Siemens LV-analysis are that 1) this algorithm works on datasets acquired with the single-beat 3D full volume mode (Siemens SC2000 ultrasound system) which eliminates the subvolume stitching and would be particularly useful for patients with permanent atrial fibrillation (AF); and 2) this software is embedded in the ultrasound system allowing a fast online

analysis. The major advantages of the TomTec 4D-LV analysis are that 1) it accepts 3D datasets regardless of the vendors; and 2) the contour correction if needed is relatively easy compared with software packages from other vendors. However, both algorithm share similar drawbacks in producing correct LV contours. Firstly, the most problematic areas for the automatic contours are the LV apex and mitral annulus. The contour at the apex is commonly set too much into the cavity and the mitral annulus points are often mistracked. The possible reason could be insufficient image quality due to artefacts in particular at the apex. Secondly, the LV contour was generally set inwardly into the cavity rather than along the compacted myocardium. According to the contrast echocardiographic studies, the LV contour should be set along the most compacted myocardium seen in the 3D echocardiographic datasets[76-78]. Lastly, an objective quality score system assessing how reliable the automatic contour tracking is, is currently lacking in both algorithms. This might be very useful especially for less experienced users. Beside the common drawbacks, the Siemens LV-analysis is also limited by only accepting 3D datasets acquired with Siemens machines.

In both studies, the QLAB manual analysis was used as a reference method besides the golden standard MRI analysis because the QLAB 3DQA software has been well established and validated in different patient populations in measuring LV volumes and EF with well-known advantages and drawbacks[66,67,70,73,75,79,80] and is considered as the echocardiographic golden standard. The main limitation of this algorithm is its semiautomatic approach in which time consuming manual input is mandatory. This hampers its application in the routine clinical practice.

On base of current studies, 3D echocardiography with automatic volumetric analysis provides a fast and accountable approach in assessing LV function in routine clinical practice. However, regarding the substantial volume underestimation and degree of variance, especially in patients with poor image quality and large ventricles, a degree of scepticism is still warranted.

Can 3D transoesphageal echocardiography replace computed tomography in catheter ablation of atrial fibrillation?

During the catheter ablation procedure of AF, either pulmonary vein (PV) isolation or complex LA ablation for non-PV triggers is performed. Therefore, imaging of the LA and especially the PVs is crucial. The pre-interventional CT is commonly used for imaging the anatomic features of the PVs and LA[81]. The pre-acquired images can be registered to the real time mapping space in the electro-anatomic mapping (EAM) systems during the procedures[82,83]. However, because of the time interval between the CT examination and the ablation procedure, the differences in the volume status and cardiac rhythm might be potential sources of error which influence the accuracy of the registration process. Additionally, the substantial dose of ionizing radiation of CT scans, rotational

angiography and fluoroscopy required by the catheter ablation causes important delayed effects on patients[84-86]. As AF ablation procedures often need to be repeated, it is a consensus that every attempt should be taken to minimize radiation exposure[81]. In our studies (Part IV), we assessed the feasibility and accuracy of 3D TOE registration, fusion and segmentation of the LA. The major advantages of implementing TOE in the ablation procedure are that it may ultimately provide real-time data and continuous assessment of catheter-tissue contact and is radiation free. In addition, coagulum/thrombus formed on the catheter during ablation and air bubble formation can also be detected. Nevertheless, several questions need to be answered in order to investigate the possibility of replacing pre-interventional CT with intra-interventional TOE.

First of all, is it possible to acquire the whole LA with 3D TOE? Limited by the field of view of the 3D acquisition sector, it is impossible to acquire the whole LA in one single 3D dataset, especially for the PVs. For this reason, we have developed a TOE image acquisition protocol with which the acquired 3D datasets cover the major part of the LA, except for the posterior wall. As explained in Part IV, the currently used matrix TOE probe (Philips CX7-2t) is not capable of visualising the structures in the near field of the ultrasound beam, e.g. the LA posterior wall. Possible solutions may be the use of a balloon standoff or a higher frequency probe. In a future study, we intend to carry out the 3D reconstructions with images acquired by the Philips S8-3t micro-TOE probe with a frequency up to 6 MHz. According to our initial experience, the micro-TOE probe is able to visualise the LA posterior wall in adults. The PVs, especially the inferior veins seem to be the most difficult task for 3D TOE. As discussed in detail in Chapter 4.2, the main reason of the invisibility of the PVs is the 3D echo loss because of the short distance between the PV ostia and the lung. Additionally, the visualisation also depends on the operator's experience and an experienced cardiac imaging physician may be required during PV ablation. Therefore, the application of 3D TOE in PV isolation procedure is still limited and a research focus. However, 3D TOE is excellent in visualising cardiac structures such as the MV, aortic valve, left atrial appendage and foramen ovale. For non-PV triggered AF which is identified in up to one-third of unselected patients referred for catheter ablation for paroxysmal AF[87-89], this technique may actually replace CT in facilitating the complex LA catheter ablation and also ablation of peri-mitral flutter, LA tachycardia (post-ablational superior PVs and LAA tachycardias), septal atrial tachycardia, and LAA occlusion which is performed frequently during the catheter ablation procedure.

Secondly, how accurate is the registration and fusion of 3D TOE datasets? As shown in Chapter 4.2, Euclidean distances between TOE landmarks and corresponding CT landmarks was in average 5 ± 3 mm for cardiac structures important to the catheter ablation procedures, which can be considered as accurate, compared with inaccuracies reported for the EAM system[90]. Two reasons that contribute most to the inaccuracies of the fused 3D TOE datasets are the less optimal 3D spatial resolution which leads to

unreliable landmarks, and observer variability which was shown to constitute a considerable part of the CT-TOE distance. Other sources of the inaccuracy might be the TOE fusion and reconstruction inaccuracies, different physiological conditions between the CT and TOE images taken weeks apart and inherent differences between the CT and TOE images. Considering the observer variability, the errors due to registration and modality differences are actually much smaller than the suggested 5 mm.

Thirdly, can the 3D TOE images be segmented and registered within the EAM system? Currently, the pre-acquired CT or MRI data is segmented and the surfaces are imported into the EAM system to improve the guidance of the catheter position. Considering the limitation of pre-interventional CT, ideally the live 3D TOE data should be segmented, which allows real-time guidance of the catheter with respect to the EAM. In general, the segmentation of the cardiac echocardiographic data is challenging because of the multiple and complex cardiac structures involved. In Chapter 4.3, we have segmented five heart chambers in the wide-view fused 3D TOE datasets using a three-stage segmentation scheme, which has been proven to be robust and accurate compared with the atlas based segmentations CT angiographic images. By comparing the segmentation accuracy of single-view and wide-view 3D TOE volumes, the accuracy was shown improved for LA, right atrium and aoritic valve in the wide-view 3D TOE datasets. Even though the study population all had dilated LA (similar as patients with AF), which sets a challenge for the statistical shape model coverage, the achieved segmentation is still considered to be very acceptable.

Finally, how fast is the whole process, i.e. data acquisition, registration, fusion and segmentation? This question is important for implementing intra-interventional TOE to provide real-time anatomical information. The TOE imaging protocol described in Chapter 4.1 provides a fast and systematic manner of acquiring a minimal number of 3D TOE datasets for registration and fusion. The acquisition procedure usually takes about 5 minutes. One should note that a learning curve exists in TOE practice and a certain training is required for identifying and acquiring the PVs as they are more difficult to be visualised in TOE images than other cardiac structures. Currently, the registration and fusion of 3D TOE datasets are done in a manual approach, requiring expertise and relatively long time. However, this current study constitutes a proof of principle for the future case where an automated registration will be available. The automatic registration method will eliminate manual input and speed up the registration process. More importantly, it can be incorporated into the ultrasound system, thus allowing an on-line reconstruction. Finally, the segmentation of multiple heart chambers in the 3D TOE images can be done within minutes.

Besides strengths and limitations of 3D TOE mentioned above, there are other limitations that need to be addressed. First of all, TOE requires general anaesthesia which adds additional cost to the procedure. It is almost impossible for patients to stand the

whole procedure with TOE examination without general anaesthesia. Secondly, The temperature of the probe and the contact tissue temperature during visualisation of PVs is about 38°C. However, the prolonged and continuous use of 3D imaging may cause an increase in the temperature of the probe up to 40°C. Whether this temperature interferes with or adds to the heating produced by radiofrequency ablation remains an open question. Finally, artefacts created by ablation catheters may produce disturbing reverberations and artificial dropout beyond the catheter. Whenever the catheter is parallel to the ultrasound beam, the reverberation appears to prolong the catheter and can be misinterpreted as the catheter tip[91]. The new cryoballoon catheter, by covering the PV's ostium, may limit artefacts while maintaining interpretable images.

Conclusions and prospects

3D echocardiography provides a more accurate method in quantitative analysis of valvular regurgitation and cardiac chamber volumes mainly because it eliminates the geometric assumptions applied in 2D echocardiography. Additionally, it is a low cost and safer image technique compared with cardiac CT or MRI. Exciting new developments are currently available or at the horizon such as automated 3D PISA and fully automated assessment of all four cardiac chamber volumes. To achieve optimal results, improvements particularly in near-field artifacts (for LV analysis) and volume rate (for PISA analysis) are essential.

REFERENCES

1. Enriquez-Sarano M, Avierinos JF, Messika-Zeitoun D, Detaint D, Capps M, Nkomo V, Scott C, Schaff HV, Tajik AJ. Quantitative determinants of the outcome of asymptomatic mitral regurgitation. *N Engl J Med* 2005;352:875-83.
2. Lancellotti P, Moura L, Pierard LA, Agricola E, Popescu BA, Tribouilloy C, Hagendorff A, Monin JL, Badano L, Zamorano JL, European Association of E. European Association of Echocardiography recommendations for the assessment of valvular regurgitation. Part 2: mitral and tricuspid regurgitation (native valve disease). *Eur J Echocardiogr* 2010;11:307-32.
3. Zoghbi WA, Enriquez-Sarano M, Foster E, Grayburn PA, Kraft CD, Levine RA, Nihoyannopoulos P, Otto CM, Quinones MA, Rakowski H, Stewart WJ, Waggoner A, Weissman NJ, American Society of E. Recommendations for evaluation of the severity of native valvular regurgitation with two-dimensional and Doppler echocardiography. *J Am Soc Echocardiogr* 2003;16:777-802.
4. Anwar AM, Soliman OI, Nemes A, Germans T, Krenning BJ, Geleijnse ML, Van Rossum AC, ten Cate FJ. Assessment of mitral annulus size and function by real-time 3-dimensional echocardiography in cardiomyopathy: comparison with magnetic resonance imaging. *J Am Soc Echocardiogr* 2007; 20:941-8.
5. Anwar AM, Soliman OI, ten Cate FJ, Nemes A, McGhie JS, Krenning BJ, van Geuns RJ, Galema TW, Geleijnse ML. True mitral annulus diameter is underestimated by two-dimensional echocardiography as evidenced by real-time three-dimensional echocardiography and magnetic resonance imaging. *Int J Cardiovasc Imaging* 2007;23:541-7.
6. Doddamani S, Bello R, Friedman MA, Banerjee A, Bowers JH, Jr., Kim B, Vennalaganti PR, Ostfeld RJ, Gordon GM, Malhotra D, Spevack DM. Demonstration of left ventricular outflow tract eccentricity by real time 3D echocardiography: implications for the determination of aortic valve area. *Echocardiography* 2007;24:860-6.
7. Doddamani S, Grushko MJ, Makaryus AN, Jain VR, Bello R, Friedman MA, Ostfeld RJ, Malhotra D, Boxt LM, Haramati L, Spevack DM. Demonstration of left ventricular outflow tract eccentricity by 64-slice multi-detector CT. *Int J Cardiovasc Imaging* 2009;25:175-81.
8. Foster GP, Dunn AK, Abraham S, Ahmadi N, Sarraf G. Accurate measurement of mitral annular dimensions by echocardiography: importance of correctly aligned imaging planes and anatomic landmarks. *J Am Soc Echocardiogr* 2009;22:458-63.
9. Otani K, Takeuchi M, Kaku K, Sugeng L, Yoshitani H, Haruki N, Ota T, Mor-Avi V, Lang RM, Otsuji Y. Assessment of the aortic root using real-time 3D transesophageal echocardiography. *Circ J* 2010; 74:2649-57.
10. Gordic S, Nguyen-Kim TD, Manka R, Sundermann S, Frauenfelder T, Maisano F, Falk V, Alkadhi H. Sizing the mitral annulus in healthy subjects and patients with mitral regurgitation: 2D versus 3D measurements from cardiac CT. *Int J Cardiovasc Imaging* 2014;30:389-98.
11. Quinones MA, Otto CM, Stoddard M, Waggoner A, Zoghbi WA, Doppler Quantification Task Force of the N, Standards Committee of the American Society of E. Recommendations for quantification of Doppler echocardiography: a report from the Doppler Quantification Task Force of the Nomenclature and Standards Committee of the American Society of Echocardiography. *J Am Soc Echocardiogr* 2002;15:167-84.
12. Utsunomiya T, Ogawa T, Doshi R, Patel D, Quan M, Henry WL, Gardin JM. Doppler color flow "proximal isovelocity surface area" method for estimating volume flow rate: effects of orifice shape and machine factors. *J Am Coll Cardiol* 1991;17:1103-11.

13. Utsunomiya T, Doshi R, Patel D, Mehta K, Nguyen D, Henry WL, Gardin JM. Calculation of volume flow rate by the proximal isovelocity surface area method: simplified approach using color Doppler zero baseline shift. *J Am Coll Cardiol* 1993;22:277-82.
14. Rodriguez L, Anconina J, Flachskampf FA, Weyman AE, Levine RA, Thomas JD. Impact of finite orifice size on proximal flow convergence. Implications for Doppler quantification of valvular regurgitation. *Circ Res* 1992;70:923-30.
15. Okamoto M, Tsubokura T, Nakagawa H, Morichika N, Amioka H, Yamagata T, Hashimoto M, Tsuchioka Y, Matsuura H, Kajiyama G. [The suction signal detected by color Doppler echocardiography in patients with mitral regurgitation: its clinical significance]. *J Cardiol* 1988;18:739-46.
16. Enriquez-Sarano M, Miller FA, Jr., Hayes SN, Bailey KR, Tajik AJ, Seward JB. Effective mitral regurgitant orifice area: clinical use and pitfalls of the proximal isovelocity surface area method. *J Am Coll Cardiol* 1995;25:703-9.
17. Simpson IA, Shiota T, Gharib M, Sahn DJ. Current status of flow convergence for clinical applications: is it a leaning tower of "PISA"? *J Am Coll Cardiol* 1996;27:504-9.
18. Buck T, Plicht B, Kahlert P, Schenk IM, Hunold P, Erbel R. Effect of dynamic flow rate and orifice area on mitral regurgitant stroke volume quantification using the proximal isovelocity surface area method. *J Am Coll Cardiol* 2008;52:767-78.
19. Hopmeyer J, He S, Thorvig KM, McNeil E, Wilkerson PW, Levine RA, Yoganathan AP. Estimation of mitral regurgitation with a hemielliptic curve-fitting algorithm: in vitro experiments with native mitral valves. *J Am Soc Echocardiogr* 1998;11:322-31.
20. Li X, Shiota T, Delabays A, Teien D, Zhou X, Sinclair B, Pandian NG, Sahn DJ. Flow convergence flow rates from 3-dimensional reconstruction of color Doppler flow maps for computing transvalvular regurgitant flows without geometric assumptions: An in vitro quantitative flow study. *J Am Soc Echocardiogr* 1999;12:1035-44.
21. Little SH, Igo SR, Pirat B, McCulloch M, Hartley CJ, Nose Y, Zoghbi WA. In vitro validation of real-time three-dimensional color Doppler echocardiography for direct measurement of proximal isovelocity surface area in mitral regurgitation. *Am J Cardiol* 2007;99:1440-7.
22. Matsumura Y, Saracino G, Sugioka K, Tran H, Greenberg NL, Wada N, Toyono M, Fukuda S, Hozumi T, Thomas JD, Yoshikawa J, Yoshiyama M, Shiota T. Determination of regurgitant orifice area with the use of a new three-dimensional flow convergence geometric assumption in functional mitral regurgitation. *J Am Soc Echocardiogr* 2008;21:1251-6.
23. Shiota T, Sinclair B, Ishii M, Zhou X, Ge S, Teien DE, Gharib M, Sahn DJ. Three-dimensional reconstruction of color Doppler flow convergence regions and regurgitant jets: an in vitro quantitative study. *J Am Coll Cardiol* 1996;27:1511-8.
24. Yosefy C, Levine RA, Solis J, Vaturi M, Handschumacher MD, Hung J. Proximal flow convergence region as assessed by real-time 3-dimensional echocardiography: challenging the hemispheric assumption. *J Am Soc Echocardiogr* 2007;20:389-96.
25. Buck T, Plicht B, Kahlert P, Erbel R. Understanding the asymmetrical vena contracta area: the difficult relationship between 2D and 3D measurements. *JACC Cardiovasc Imaging* 2013;6:744.
26. Hyodo E, Iwata S, Tugcu A, Arai K, Shimada K, Muro T, Yoshikawa J, Yoshiyama M, Gillam LD, Hahn RT, Di Tullio MR, Homma S. Direct measurement of multiple vena contracta areas for assessing the severity of mitral regurgitation using 3D TEE. *JACC Cardiovasc Imaging* 2012;5:669-76.
27. Song JM, Jang MK, Choi YS, Kim YJ, Min SY, Kim DH, Kang DH, Song JK. The vena contracta in functional tricuspid regurgitation: a real-time three-dimensional color Doppler echocardiography study. *J Am Soc Echocardiogr* 2011;24:663-70.

28. Zeng X, Levine RA, Hua L, Morris EL, Kang Y, Flaherty M, Morgan NV, Hung J. Diagnostic value of vena contracta area in the quantification of mitral regurgitation severity by color Doppler 3D echocardiography. *Circ Cardiovasc Imaging* 2011;4:506-13.

29. de Agustin JA, Marcos-Alberca P, Fernandez-Golfin C, Goncalves A, Feltes G, Nunez-Gil IJ, Almeria C, Rodrigo JL, Perez de Isla L, Macaya C, Zamorano J. Direct measurement of proximal isovelocity surface area by single-beat three-dimensional color Doppler echocardiography in mitral regurgitation: a validation study. *J Am Soc Echocardiogr* 2012;25:815-23.

30. Son JW, Chang HJ, Lee JK, Chung HJ, Song RY, Kim YJ, Datta S, Heo R, Shin SH, Cho IJ, Shim CY, Hong GR, Chung N. Automated quantification of mitral regurgitation by three dimensional real time full volume color Doppler transthoracic echocardiography: a validation with cardiac magnetic resonance imaging and comparison with two dimensional quantitative methods. *J Cardiovasc Ultrasound* 2013;21:81-9.

31. Thavendiranathan P, Liu S, Datta S, Rajagopalan S, Ryan T, Igo SR, Jackson MS, Little SH, De Michelis N, Vannan MA. Quantification of chronic functional mitral regurgitation by automated 3-dimensional peak and integrated proximal isovelocity surface area and stroke volume techniques using real-time 3-dimensional volume color Doppler echocardiography: in vitro and clinical validation. *Circ Cardiovasc Imaging* 2013;6:125-33.

32. Ling LH, Enriquez-Sarano M, Seward JB, Tajik AJ, Schaff HV, Bailey KR, Frye RL. Clinical outcome of mitral regurgitation due to flail leaflet. *N Engl J Med* 1996;335:1417-23.

33. Avierinos JF, Gersh BJ, Melton LJ, 3rd, Bailey KR, Shub C, Nishimura RA, Tajik AJ, Enriquez-Sarano M. Natural history of asymptomatic mitral valve prolapse in the community. *Circulation* 2002;106:1355-61.

34. Verheule S, Wilson E, Everett Tt, Shanbhag S, Golden C, Olgin J. Alterations in atrial electrophysiology and tissue structure in a canine model of chronic atrial dilatation due to mitral regurgitation. *Circulation* 2003;107:2615-22.

35. Anne W, Willems R, Roskams T, Sergeant P, Herijgers P, Holemans P, Ector H, Heidbuchel H. Matrix metalloproteinases and atrial remodeling in patients with mitral valve disease and atrial fibrillation. *Cardiovasc Res* 2005;67:655-66.

36. Le Tourneau T, Messika-Zeitoun D, Russo A, Detaint D, Topilsky Y, Mahoney DW, Suri R, Enriquez-Sarano M. Impact of left atrial volume on clinical outcome in organic mitral regurgitation. *J Am Coll Cardiol* 2010;56:570-8.

37. Todaro MC, Choudhuri I, Belohlavek M, Jahangir A, Carerj S, Oreto L, Khandheria BK. New echocardiographic techniques for evaluation of left atrial mechanics. *Eur Heart J Cardiovasc Imaging* 2012;13:973-84.

38. Motoki H, Dahiya A, Bhargava M, Wazni OM, Saliba WI, Marwick TH, Klein AL. Assessment of left atrial mechanics in patients with atrial fibrillation: comparison between two-dimensional speckle-based strain and velocity vector imaging. *J Am Soc Echocardiogr* 2012;25:428-35.

39. Moustafa SE, Alharthi M, Kansal M, Deng Y, Chandrasekaran K, Mookadam F. Global left atrial dysfunction and regional heterogeneity in primary chronic mitral insufficiency. *Eur J Echocardiogr* 2011;12:384-93.

40. Cameli M, Lisi M, Giacomin E, Caputo M, Navarri R, Malandrino A, Ballo P, Agricola E, Mondillo S. Chronic mitral regurgitation: left atrial deformation analysis by two-dimensional speckle tracking echocardiography. *Echocardiography* 2011;28:327-34.

41. Boyd AC, Richards DA, Marwick T, Thomas L. Atrial strain rate is a sensitive measure of alterations in atrial phasic function in healthy ageing. *Heart* 2011;97:1513-9.

42. Saraiva RM, Demirkol S, Buakhamsri A, Greenberg N, Popovic ZB, Thomas JD, Klein AL. Left atrial strain measured by two-dimensional speckle tracking represents a new tool to evaluate left atrial function. *J Am Soc Echocardiogr* 2010;23:172-80.

43. Vianna-Pinton R, Moreno CA, Baxter CM, Lee KS, Tsang TS, Appleton CP. Two-dimensional speckle-tracking echocardiography of the left atrium: feasibility and regional contraction and relaxation differences in normal subjects. *J Am Soc Echocardiogr* 2009;22:299-305.

44. Borg AN, Pearce KA, Williams SG, Ray SG. Left atrial function and deformation in chronic primary mitral regurgitation. *Eur J Echocardiogr* 2009;10:833-40.

45. Geyer H, Caracciolo G, Abe H, Wilansky S, Carerj S, Gentile F, Nesser HJ, Khandheria B, Narula J, Sengupta PP. Assessment of myocardial mechanics using speckle tracking echocardiography: fundamentals and clinical applications. *J Am Soc Echocardiogr* 2010;23:351-69; quiz 453-5.

46. Wang K, Ho SY, Gibson DG, Anderson RH. Architecture of atrial musculature in humans. *Br Heart J* 1995;73:559-65.

47. Mochizuki A, Yuda S, Oi Y, Kawamukai M, Nishida J, Kouzu H, Muranaka A, Kokubu N, Shimoshige S, Hashimoto A, Tsuchihashi K, Watanabe N, Miura T. Assessment of left atrial deformation and synchrony by three-dimensional speckle-tracking echocardiography: comparative studies in healthy subjects and patients with atrial fibrillation. *J Am Soc Echocardiogr* 2013;26:165-74.

48. Nemes A, Domsik P, Kalapos A, Lengyel C, Orosz A, Forster T. Comparison of Three-Dimensional Speckle Tracking Echocardiography and Two-Dimensional Echocardiography for Evaluation of Left Atrial Size and Function in Healthy Volunteers (Results from the MAGYAR-Healthy Study). *Echocardiography* 2013.

49. Onishi N, Kawasaki M, Tanaka R, Sato H, Saeki M, Nagaya M, Sato N, Minatoguchi S, Watanabe T, Ono K, Arai M, Noda T, Amano K, Goto K, Watanabe S, Minatoguchi S. Comparison between left atrial features in well-controlled hypertensive patients and normal subjects assessed by three-dimensional speckle tracking echocardiography. *J Cardiol* 2013.

50. Mor-Avi V, Lang RM, Badano LP, Belohlavek M, Cardim NM, Derumeaux G, Galderisi M, Marwick T, Nagueh SF, Sengupta PP, Sicari R, Smiseth OA, Smulevitz B, Takeuchi M, Thomas JD, Vannan M, Voigt JU, Zamorano JL. Current and evolving echocardiographic techniques for the quantitative evaluation of cardiac mechanics: ASE/EAE consensus statement on methodology and indications endorsed by the Japanese Society of Echocardiography. *J Am Soc Echocardiogr* 2011;24:277-313.

51. Lang RM, Bierig M, Devereux RB, Flachskampf FA, Foster E, Pellikka PA, Picard MH, Roman MJ, Seward J, Shanewise JS, Solomon SD, Spencer KT, Sutton MS, Stewart WJ, Chamber Quantification Writing G, American Society of Echocardiography's G, Standards C, European Association of E. Recommendations for chamber quantification: a report from the American Society of Echocardiography's Guidelines and Standards Committee and the Chamber Quantification Writing Group, developed in conjunction with the European Association of Echocardiography, a branch of the European Society of Cardiology. *J Am Soc Echocardiogr* 2005;18:1440-63.

52. O'Brien JP, Srichai MB, Hecht EM, Kim DC, Jacobs JE. Anatomy of the heart at multidetector CT: what the radiologist needs to know. *Radiographics* 2007;27:1569-82.

53. Ho SY, McCarthy KP, Faletra FF. Anatomy of the left atrium for interventional echocardiography. *Eur J Echocardiogr* 2011;12:i11-5.

54. Iwataki M, Takeuchi M, Otani K, Kuwaki H, Haruki N, Yoshitani H, Tamura M, Abe H, Otsuji Y. Measurement of left atrial volume from transthoracic three-dimensional echocardiographic datasets using the biplane Simpson's technique. *J Am Soc Echocardiogr* 2012;25:1319-26.

55. Anwar AM, Soliman OI, Geleijnse ML, Nemes A, Vletter WB, ten Cate FJ. Assessment of left atrial volume and function by real-time three-dimensional echocardiography. *Int J Cardiol* 2008;123: 155-61.

56. Miyasaka Y, Tsujimoto S, Maeba H, Yuasa F, Takehana K, Dote K, Iwasaka T. Left atrial volume by real-time three-dimensional echocardiography: validation by 64-slice multidetector computed tomography. *J Am Soc Echocardiogr* 2011;24:680-6.

57. Mor-Avi V, Yodwut C, Jenkins C, Kuhl H, Nesser HJ, Marwick TH, Franke A, Weinert L, Niel J, Steringer-Mascherbauer R, Freed BH, Sugeng L, Lang RM. Real-time 3D echocardiographic quantification of left atrial volume: multicenter study for validation with CMR. *JACC Cardiovasc Imaging* 2012;5: 769-77.

58. Fatema K, Barnes ME, Bailey KR, Abhayaratna WP, Cha S, Seward JB, Tsang TS. Minimum vs. maximum left atrial volume for prediction of first atrial fibrillation or flutter in an elderly cohort: a prospective study. *Eur J Echocardiogr* 2009;10:282-6.

59. Caselli S, Canali E, Foschi ML, Santini D, Di Angelantonio E, Pandian NG, De Castro S. Long-term prognostic significance of three-dimensional echocardiographic parameters of the left ventricle and left atrium. *Eur J Echocardiogr* 2010;11:250-6.

60. Russo C, Jin Z, Homma S, Rundek T, Elkind MS, Sacco RL, Di Tullio MR. Left atrial minimum volume and reservoir function as correlates of left ventricular diastolic function: impact of left ventricular systolic function. *Heart* 2012;98:813-20.

61. Russo C, Jin Z, Liu R, Iwata S, Tugcu A, Yoshita M, Homma S, Elkind MS, Rundek T, Decarli C, Wright CB, Sacco RL, Di Tullio MR. LA volumes and reservoir function are associated with subclinical cerebrovascular disease: the CABL (Cardiovascular Abnormalities and Brain Lesions) study. *JACC Cardiovasc Imaging* 2013;6:313-23.

62. Wu VC, Takeuchi M, Kuwaki H, Iwataki M, Nagata Y, Otani K, Haruki N, Yoshitani H, Tamura M, Abe H, Negishi K, Lin FC, Otsuji Y. Prognostic value of LA volumes assessed by transthoracic 3D echocardiography: comparison with 2D echocardiography. *JACC Cardiovasc Imaging* 2013;6:1025-35.

63. Monaghan MJ. Role of real time 3D echocardiography in evaluating the left ventricle. *Heart* 2006; 92:131-6.

64. Jenkins C, Bricknell K, Hanekom L, Marwick TH. Reproducibility and accuracy of echocardiographic measurements of left ventricular parameters using real-time three-dimensional echocardiography. *J Am Coll Cardiol* 2004;44:878-86.

65. Gutierrez-Chico JL, Zamorano JL, Perez de Isla L, Orejas M, Almeria C, Rodrigo JL, Ferreiros J, Serra V, Macaya C. Comparison of left ventricular volumes and ejection fractions measured by three-dimensional echocardiography versus by two-dimensional echocardiography and cardiac magnetic resonance in patients with various cardiomyopathies. *Am J Cardiol* 2005;95:809-13.

66. Jacobs LD, Salgo IS, Goonewardena S, Weinert L, Coon P, Bardo D, Gerard O, Allain P, Zamorano JL, de Isla LP, Mor-Avi V, Lang RM. Rapid online quantification of left ventricular volume from real-time three-dimensional echocardiographic data. *Eur Heart J* 2006;27:460-8.

67. Jenkins C, Chan J, Hanekom L, Marwick TH. Accuracy and feasibility of online 3-dimensional echocardiography for measurement of left ventricular parameters. *J Am Soc Echocardiogr* 2006; 19:1119-28.

68. van den Bosch AE, Robbers-Visser D, Krenning BJ, Voormolen MM, McGhie JS, Helbing WA, Roos-Hesselink JW, Simoons ML, Meijboom FJ. Real-time transthoracic three-dimensional echocardiographic assessment of left ventricular volume and ejection fraction in congenital heart disease. *J Am Soc Echocardiogr* 2006;19:1-6.

69. Jenkins C, Leano R, Chan J, Marwick TH. Reconstructed versus real-time 3-dimensional echocardiography: comparison with magnetic resonance imaging. *J Am Soc Echocardiogr* 2007;20:862-8.

70. Soliman OI, Krenning BJ, Geleijnse ML, Nemes A, Bosch JG, van Geuns RJ, Kirschbaum SW, Anwar AM, Galema TW, Vletter WB, ten Cate FJ. Quantification of left ventricular volumes and function in patients with cardiomyopathies by real-time three-dimensional echocardiography: a head-to-head comparison between two different semiautomated endocardial border detection algorithms. *J Am Soc Echocardiogr* 2007;20:1042-9.

71. Chukwu EO, Barasch E, Mihalatos DG, Katz A, Lachmann J, Han J, Reichek N, Gopal AS. Relative importance of errors in left ventricular quantitation by two-dimensional echocardiography: insights from three-dimensional echocardiography and cardiac magnetic resonance imaging. *J Am Soc Echocardiogr* 2008;21:990-7.

72. Jenkins C, Moir S, Chan J, Rakhit D, Haluska B, Marwick TH. Left ventricular volume measurement with echocardiography: a comparison of left ventricular opacification, three-dimensional echocardiography, or both with magnetic resonance imaging. *Eur Heart J* 2009;30:98-106.

73. Marsan NA, Westenberg JJ, Roes SD, van Bommel RJ, Delgado V, van der Geest RJ, de Roos A, Klautz RJ, Reiber JC, Bax JJ. Three-dimensional echocardiography for the preoperative assessment of patients with left ventricular aneurysm. *Ann Thorac Surg* 2011;91:113-21.

74. Dorosz JL, Lezotte DC, Weitzenkamp DA, Allen LA, Salcedo EE. Performance of 3-dimensional echocardiography in measuring left ventricular volumes and ejection fraction: a systematic review and meta-analysis. *J Am Coll Cardiol* 2012;59:1799-808.

75. Mor-Avi V, Jenkins C, Kuhl HP, Nesser HJ, Marwick T, Franke A, Ebner C, Freed BH, Steringer-Mascherbauer R, Pollard H, Weinert L, Niel J, Sugeng L, Lang RM. Real-time 3-dimensional echocardiographic quantification of left ventricular volumes: multicenter study for validation with magnetic resonance imaging and investigation of sources of error. *JACC Cardiovasc Imaging* 2008;1:413-23.

76. Thomson HL, Basmadjian AJ, Rainbird AJ, Razavi M, Avierinos JF, Pellikka PA, Bailey KR, Breen JF, Enriquez-Sarano M. Contrast echocardiography improves the accuracy and reproducibility of left ventricular remodeling measurements: a prospective, randomly assigned, blinded study. *J Am Coll Cardiol* 2001;38:867-75.

77. Malm S, Frigstad S, Sagberg E, Larsson H, Skjaerpe T. Accurate and reproducible measurement of left ventricular volume and ejection fraction by contrast echocardiography: a comparison with magnetic resonance imaging. *J Am Coll Cardiol* 2004;44:1030-5.

78. Krenning BJ, Kirschbaum SW, Soliman OI, Nemes A, van Geuns RJ, Vletter WB, Veltman CE, Ten Cate FJ, Roelandt JR, Geleijnse ML. Comparison of contrast agent-enhanced versus non-contrast agent-enhanced real-time three-dimensional echocardiography for analysis of left ventricular systolic function. *Am J Cardiol* 2007;100:1485-9.

79. Caiani EG, Coon P, Corsi C, Goonewardena S, Bardo D, Rafter P, Sugeng L, Mor-Avi V, Lang RM. Dual triggering improves the accuracy of left ventricular volume measurements by contrast-enhanced real-time 3-dimensional echocardiography. *J Am Soc Echocardiogr* 2005;18:1292-8.

80. Pouleur AC, le Polain de Waroux JB, Pasquet A, Gerber BL, Gerard O, Allain P, Vanoverschelde JL. Assessment of left ventricular mass and volumes by three-dimensional echocardiography in patients with or without wall motion abnormalities: comparison against cine magnetic resonance imaging. *Heart* 2008;94:1050-7.

81. Calkins H, Brugada J, Packer DL, Cappato R, Chen SA, Crijns HJ, Damiano RJ, Jr., Davies DW, Haines DE, Haissaguerre M, Iesaka Y, Jackman W, Jais P, Kottkamp H, Kuck KH, Lindsay BD, Marchlinski FE, McCarthy PM, Mont JL, Morady F, Nademanee K, Natale A, Pappone C, Prystowsky E, Raviele

A, Ruskin JN, Shemin RJ, Heart Rhythm S, European Heart Rhythm A, European Cardiac Arrhythmia S, American College of C, American Heart A, Society of Thoracic S. HRS/EHRA/ECAS expert consensus statement on catheter and surgical ablation of atrial fibrillation: recommendations for personnel, policy, procedures and follow-up. A report of the Heart Rhythm Society (HRS) Task Force on Catheter and Surgical Ablation of Atrial Fibrillation developed in partnership with the European Heart Rhythm Association (EHRA) and the European Cardiac Arrhythmia Society (ECAS); in collaboration with the American College of Cardiology (ACC), American Heart Association (AHA), and the Society of Thoracic Surgeons (STS). Endorsed and approved by the governing bodies of the American College of Cardiology, the American Heart Association, the European Cardiac Arrhythmia Society, the European Heart Rhythm Association, the Society of Thoracic Surgeons, and the Heart Rhythm Society. *Europace* 2007;9:335-79.

82. Dong J, Calkins H, Solomon SB, Lai S, Dalal D, Lardo AC, Brem E, Preiss A, Berger RD, Halperin H, Dickfeld T. Integrated electroanatomic mapping with three-dimensional computed tomographic images for real-time guided ablations. *Circulation* 2006;113:186-94.

83. Kistler PM, Rajappan K, Jahngir M, Earley MJ, Harris S, Abrams D, Gupta D, Liew R, Ellis S, Sporton SC, Schilling RJ. The impact of CT image integration into an electroanatomic mapping system on clinical outcomes of catheter ablation of atrial fibrillation. *J Cardiovasc Electrophysiol* 2006;17: 1093-101.

84. Rosenthal LS, Beck TJ, Williams J, Mahesh M, Herman MG, Dinerman JL, Calkins H, Lawrence JH. Acute radiation dermatitis following radiofrequency catheter ablation of atrioventricular nodal reentrant tachycardia. *Pacing Clin Electrophysiol* 1997;20:1834-9.

85. Kovoor P, Ricciardello M, Collins L, Uther JB, Ross DL. Risk to patients from radiation associated with radiofrequency ablation for supraventricular tachycardia. *Circulation* 1998;98:1534-40.

86. Perisinakis K, Damilakis J, Theocharopoulos N, Manios E, Vardas P, Gourtsoyiannis N. Accurate assessment of patient effective radiation dose and associated detriment risk from radiofrequency catheter ablation procedures. *Circulation* 2001;104:58-62.

87. Haissaguerre M, Jais P, Shah DC, Takahashi A, Hocini M, Quiniou G, Garrigue S, Le Mouroux A, Le Metayer P, Clementy J. Spontaneous initiation of atrial fibrillation by ectopic beats originating in the pulmonary veins. *N Engl J Med* 1998;339:659-66.

88. Chen SA, Hsieh MH, Tai CT, Tsai CF, Prakash VS, Yu WC, Hsu TL, Ding YA, Chang MS. Initiation of atrial fibrillation by ectopic beats originating from the pulmonary veins: electrophysiological characteristics, pharmacological responses, and effects of radiofrequency ablation. *Circulation* 1999;100:1879-86.

89. Lee SH, Tai CT, Hsieh MH, Tsao HM, Lin YJ, Chang SL, Huang JL, Lee KT, Chen YJ, Cheng JJ, Chen SA. Predictors of non-pulmonary vein ectopic beats initiating paroxysmal atrial fibrillation: implication for catheter ablation. *J Am Coll Cardiol* 2005;46:1054-9.

90. Heist EK, Perna F, Chalhoub F, Danik S, Barrett C, Houghtaling C, Tondo C, Mahapatra S, Ruskin J, Mansour M. Comparison of electroanatomical mapping systems: accuracy in left atrial mapping. *Pacing Clin Electrophysiol* 2013;36:626-31.

91. Faletra FF, Ho SY, Regoli F, Acena M, Auricchio A. Real-time three dimensional transoesophageal echocardiography in imaging key anatomical structures of the left atrium: potential role during atrial fibrillation ablation. *Heart* 2013;99:133-42.

Part VI

Appendix

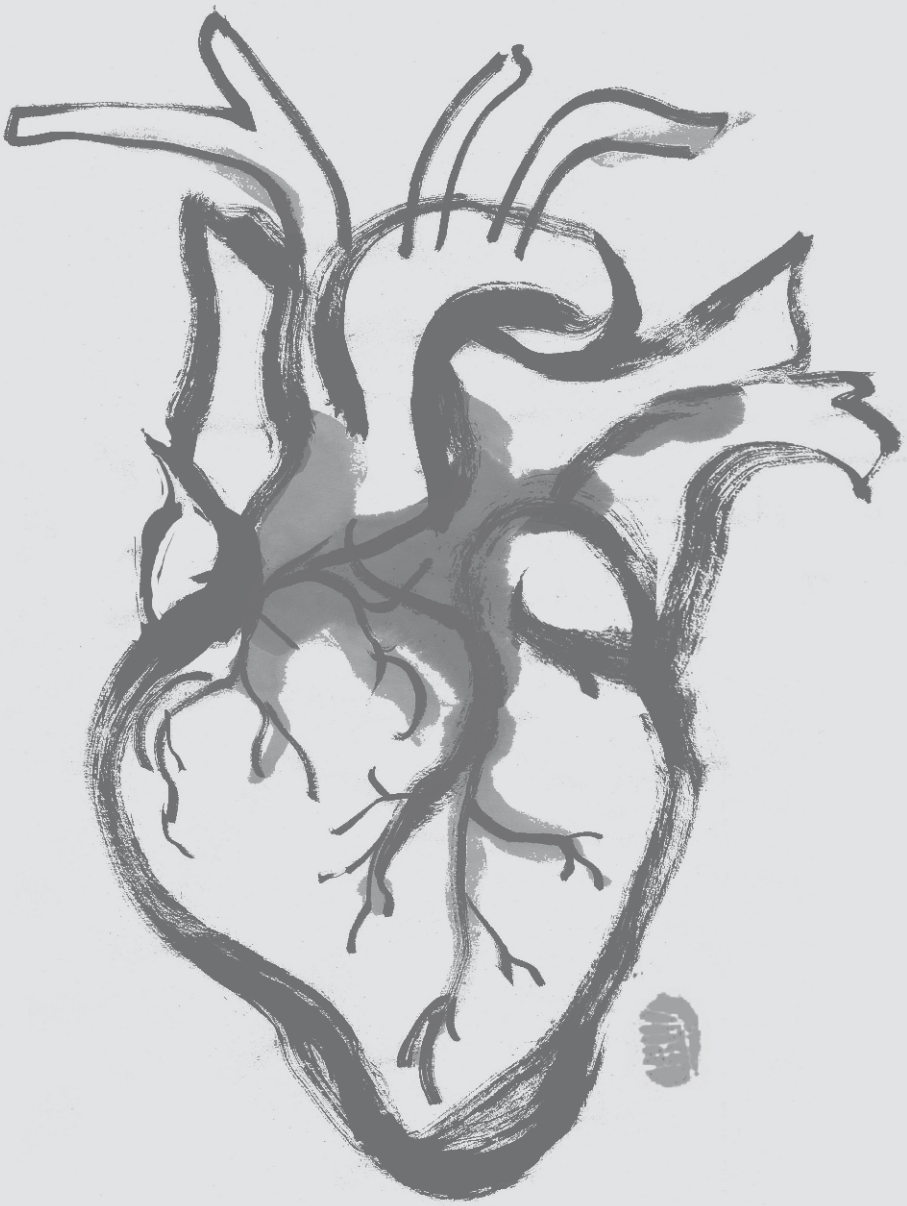

Chapter 6.1

Nederlandse samenvatting

NEDERLANDSE SAMENVATTING

Het hoofddoel van dit proefschrift is het onderzoeken van de klinische implicaties van geavanceerde driedimensionele (3D) echocardiografie voor de beoordeling van mitralisklep insufficiëntie (MI), linker atrium (LA) functie, linker ventrikel (LV) functie en LA reconstructie. **Hoofdstuk 1** is de inleiding van dit proefschrift, waarin de technieken voor kwantificatie van MI, de evaluatie van LA en LV volumes en functie, en de LA anatomie voor katheterablatie geïntroduceerd worden. Vervolgens worden de haalbaarheid en nauwkeurigheid bij toepassing van 3D echocardiografie bij de genoemde onderwerpen beschreven.

3D echocardiografie voor kwantificatie van mitralisklep insufficiëntie

Kwantificatie van MI is essentieel om de ernst van de MI te bepalen. In **Hoofdstuk 2.1** werd de fout gemaakt bij de 2D transthoracale echocardiografie (TTE) pulsed wave Doppler flow methode voor het berekenen van het insufficiëntie volume ingeschat. Met name de cirkelvormige geometrische aanname van de mitralis annulus (MA) en linker ventrikel outflow tract (LVOT) werden geanalyseerd. Dit werd gedaan door het vergelijken van deze methode met een 3D transoesofageale echocardiografie (TEE) methode waarbij de dwarsdoorsneden van de MA en LVOT in de ''en face" views direct gemeten werden. In deze studie werd aangetoond dat de MA en LVOT ovaal van vorm zijn met significant verschillend grote en kleine as diameters. Er werd ook aangetoond dat met de 2D methode het MA oppervlak met ongeveer 13% wordt overschat en het LVOT oppervlak met ongeveer 23% wordt onderschat. Belangrijk is dat de gemaakte fouten in verschillende richtingen zijn, dus de fout in de berekening van de insufficiëntie volume is nog groter, een overschatting van ongeveer 54%.

3D echocardiografie voor kwantificatie van linkeratrium functie

Chronische degeneratieve MI veroorzaakt belangrijke veranderingen van het LA. Een soepel LA kan een belangrijke rol spelen in het opvangen van stijging in de druk van het LA. In **Hoofdstuk 2.2** beoordeelden we de LA stijfheid in asymptomatische en symptomatische patiënten met degeneratieve MI met strain en strain rate imaging. Bij patiënten met gelijke insufficiëntie volumes bleken asymptomatische patiënten een minder stijf LA te hebben met hogere positieve strain en strain rate waardes gedurende het vullen van het LA; de waardes waren vergelijkbaar met die van normale controles. Het verschil in positieve strain en strain rate waarden tussen asymptomatische en symptomatische patiënten werd ook bevestigd met een 3D echocardiografische analyse van de LA volumes. Asymptomatische patiënten lieten een grotere LA volumeverandering in de LV systole zien. Ook bleken patiënten met een lagere gemiddelde pulmonale arteriële druk een soepeler LA te hebben.

In dierstudies is aangetoond dat gedurende de gecompenseerde fase van chronische MI, het LA groter en meer compliant wordt met een grotere booster pomp functie als gevolg van een optimaal gebruik van de Frank–Starling mechanisme van het LA spierweefsel. In **Hoofdstuk 2.3** werd de LA functie bij patiënten met chronische MI en een behouden LV functie ondergezocht door het berekenen van de LA volumes met 3D TTE en de LA spierfunctie met strain en strain rate imaging. In deze studie werd aangetoond dat de LA contractiele functie bij patiënten met een ernstige MI was afgenomen. De LA reservoir en conduit functies bij belangrijke MI waren verhoogd, zichtbaar door een verhoogd totale slagvolume en passieve vulvolume bij een verhoogd maximaal LA volume. Bij de strain analyse bleek ook dat de late LA negatieve strain goed correleerde met de LA actieve ejectiefractie (EF).

3D echocardiografie voor kwantificatie van linkerventrikel functie

LV volumes en EF zijn de meest gebruikte parameters in de beoordeling van LV functie en hebben belangrijke prognostische betekenis. In het 3de deel van dit proefschrift werden de nauwkeurigheid van twee automatische algoritmen voor het berekenen van LV volumes en EF onderzocht. In **Hoofdstuk 3.1** werden de metingen van de zes verschillende Siemens single-beat automatische 3D LV analyses vergeleken met Philips handmatig gecorrigeerde 3DQA QLAB analyses. In deze studie werd aangetoond dat de nauwkeurigheid van het Siemens automatische 3D algoritme sterk wordt beïnvloed door de gebruikte opname setting, veroorzaakt door belangrijke verschillen in de temporele en ruimtelijke resolutie. De beste acquisitie setting bleek de Space 1 Harmonische setting te zijn, aangevuld met de Space 1 Harmonische acquisitie setting voor vergrote LVs die niet volledig in de opname sector van de S1H mode passen. Door op deze manier beelden op te nemen konden ongeveer twee derde van de patiënten automatisch en betrouwbaar worden geanalyseerd. Om dit algoritme in de "real-world" van de dagelijkse zorg te evalueren werd in **Hoofdstuk 3.2** dit algoritme toegepast in opeenvolgende patiënten met kanker waarbij de LV functie essentieel is voor het al dan niet starten met systemische chemotherapie. De resultaten in deze studie waren consistent met de eerdere beschreven studie uitgevoerd in een meer wetenschappelijk setting. In **Hoofdstuk 3.3** werden de metingen van de TomTec automatische 3D LV analyses vergeleken met Philips handmatig gecorrigeerde 3DQA QLAB analyses en magnetische resonantie imaging (MRI). In deze studie bleek dat ook het TomTec automatische algoritme in ongeveer twee derde van de patiënten goede resultaten liet zien. De negatieve biases (onderschatting) en limits of agreement van de LV volumes en EF waren vergelijkbaar met eerder gepubliceerde getallen van handmatig gecorrigeerde 3D datasets. Vergeleken met de QLAB handmatige gecorrigeerde metingen waren de LV volumes vergelijkbaar; de "volume onderschatting" is dus niet een specifieke eigenschap van het automatische TomTec algoritme maar een inherente eigenschap van echocardiografische analyse.

3D echocardiografie in de reconstructie van het linker atrium

Beeldvorming van het LA is van cruciaal belang voor catheter ablatie van boezemfibrilleren. Voor de procedure gemaakte beelden met computed tomography (CT) worden gesegmenteerd en geregistreerd met een electro-anatomical surface mapping (EAM) systeem om real-time mapping mogelijk te maken. Echter CT heeft belangrijke nadelen zoals bijvoorbeeld het gebruik van ioniserende straling. In **Hoofdstuk 4.1** werd een 3D TEE protocol beschreven waarmee met behulp van een minimaal aantal van zes overlappende 3D TEE datasets een complete wide-view LA reconstructie gemaakt kon worden met daarin alle belangrijke anatomische structuren. In **Hoofdstuk 4.2** werd de nauwkeurigheid van de registratie en fusie van de 3D TEE datasets bepaald door het bepalen van de absolute afstanden tussen acht corresponderende herkenbare punten in de gereconstrueerde wide-view 3D echo en CT datasets. Er werd aangetoond dat de registratie en fusie van de 3D TEE datasets haalbaar is bij alle patiënten. Relatief centraal gelegen structuren zoals de mitralisklep, aortaklep, LA hartoor en fossa ovalis waren goed herkenbaar. De bovengelegen longaders waren minder goed zichtbaar en de ondergelegen longaders zelfs zeer moeilijk. De afstanden tussen de belangrijkste herkenbare cardiale structuren in de 3D TEE en CT datasets waren 5 ± 3. Deze afstanden zijn vergelijkbaar met gerapporteerde afstanden voor het routinematig gebruikt EAM systeem. In **Hoofdstuk 4.3** werd de segmentatie van multi-cavity anatomie van de gereconstrueerde wide-view 3D TEE datasets in patiënten verder onderzocht. De drietraps segmentatie werd vergeleken met een atlas gebaseerde segmentatie afgeleid van CT angiografische beelden. De nauwkeurigheid van de segmentatie van een enkele 3D TEE dataset en een gereconstrueerde 3D wide-view werd vergeleken. Er werd een even goede nauwkeurigheid van de segmentatie van het linker en rechter atrium en de aortaklep aangetoond terwijl die voor de rechterventrikel en LV gelijk was. Dit betekent dat de automatische segmentatie van de gereconstrueerde wide-view datasets haalbaar is en de nauwkeurigheid van de segmentatie meestal verbeterd.

Chapter 6.2

Curriculum vitae

CURRICULUM VITAE

Ben Ren (Claire Ren, 任奔) was born on 14th May 1985 in Chengdu, Sichuan province, China. After finishing the secondary school (No. 7 Middle School of Chengdu, China) in 2003, she was admitted to Clinical medicine (Seven-year Programme) in West China School of Medicine, Sichuan University in Chengdu. She finished the internship in West China University Hospital and West China Women's and Children's Hospital during 6th year. During her last year in medical school, under the supervision of Prof.dr. Hong Tang, she initiated the research project "3D echocardiographic evaluation of the aortic annulus" in the echolab of Cardiology department, West China University Hospital. In the meantime, she received intensive trainings in practicing transthoracic and transoesophageal echocardiographies in patients with acquired and congenital heart diseases. In 2010, she finished the master research and graduated from medical school. In the same year, she passed the national examination and obtained the Practicing Physician License of China. In October 2010, she was awarded the national grant of "Government Graduate Student Overseas Study Programme" and joined the Cardiology department, Thoraxcenter, Erasmus MC in the Netherlands as a PhD candidate. Under the supervision of Prof.dr. F. Zijlstra and Dr. M.L. Geleijnse, she performed researches in assessing valvular diseases and cardiac functions using 3D echocardiography. She also participated in the Dutch Technology Foundation STW research project "Integration of 3D ultrasound into electrophysiology for support of ablation procedures" in Biomedical Engineering department under the supervision of Dr.ir. J.G. Bosch.

Chapter 6.3

PhD portfolio

PhD PORTFOLIO

Name	B. Ren
Erasmus MC department	Cardiology
Research school	Cardiovascular Research School (COEUR), Erasmus MC
Title thesis	Advanced three-dimensional echocardiography
Promoter	Prof.dr. F. Zijlstra
Co-promoters	Dr. M.L. Geleijnse Dr.ir. J.G. Bosch
Date of defense thesis	28th October, 2014

PhD training (33,5 ECTS)

In-depth courses (11,2 ECTS)

2013	Cardiovascular Imaging and diagnostics, Rotterdam, the Netherlands
2012	Scientific English Writing Course, Rotterdam, the Netherlands
2011	Basic introduction course on SPSS, Rotterdam, the Netherlands
2011	Heart failure research, Rotterdam, the Netherlands
2011	Congenital heart disease, Rotterdam, the Netherlands
2010-2012	COEUR seminars and lectures, Erasmus MC, Rotterdam, the Netherlands
2012	EAE webinars, Rotterdam, the Netherlands

Teaching (1.8 ECTS)

06-2014	Philips teaching site: Mitral valve quantification, Rotterdam, the Netherlands
11-2013	Siemens teaching site: LV analysis in clinical practice, Rotterdam, the Netherlands
03-2013	Siemens teaching site: LV analysis in clinical practice, Rotterdam, the Netherlands

Conferences and symposiums (19,3 ECTS)

Oral presentation	
2012	ESC congress, Munich, Germany
Poster presentations	
2014	ESC congress, Barcelona, Spain
2014	ASE annual scientific session, Portland, USA
2013	EuroEcho, Istanbul, Turkey
2013	ASE annual scientific session, Minneapolis, USA
2012	EuroEcho, Athens, Greece
2012	Great wall international cardiology congress, Beijing, China
Attended	
2014	ESC congress, Barcelona, Spain
2014	ASE annual scientific session, Portland, USA

2013	EuroEcho, Istanbul, Turkey
2013	ESC congress, Amsterdam, the Netherlands
2013	ASE annual scientific session, Minneapolis, USA
2012	EuroEcho, Athens, Greece
2012	Great wall international cardiology congress, Beijing, China
2012	ESC congress, Munich, Germany
2012	Cardiology & vascular medicine, an ESC update programme, Rotterdam, the Netherlands
2011	EuroEcho, Budapest, Hungary
2011	ESC congress, Paris, France
2011	Rotterdam 3D course, Rotterdam, the Netherlands
2011	Cardiology & vascular medicine, an ESC update programme, Rotterdam, the Netherlands

Chapter 6.4

List of publications

PUBLICATIONS

Ren B, de Groot-de Laat LE, Geleijnse ML. Left Atrial function in Patients with Mitral Valve Regurgitation. AJP-Heart and Circulatory Physiology. Accepted.

Curiale AH, Haak A, Vegas-Sánchez-Ferrero G, **Ren B**, Aja-Fernández S, Bosch JG. Fully automatic detection of salient features in 3D transesophageal images. Ultrasound Med Biol. Accepted.

McGhie JS, van den Bosch AE, Haarman MG, **Ren B**, Roos-Hesselink JW, Witsenburg M, Geleijnse ML. Characterization of atrial septal defect by simultaneous multiplane two-dimensional echocardiography. Eur Heart J Cardiovasc Imaging. Epub ahead of print.

Ren B, Vletter WB, McGhie J, Soliman OII, Geleijnse ML. Single-beat real-time three-dimensional echocardiographic automated contour detection for quantification of left ventricular volumes and systolic function. Int J Cardiovasc Imaging. 2014 Feb;30(2):287-94.

McGhie JS, Vletter WB, de Groot-de Laat LE, **Ren B**, Frowijn R, van den Bosch AE, Soliman OII, Geleinse ML. Contributions of simultaneous multiplane echocardiographic imaging in daily clinical practice. Echocardiography. 2014 Feb;31(2):245-54.

Ren B, Mulder HW, Haak A, van Stralen M, Szili-Torok T, Pluim JPW, Geleinse ML, Bosch JG. A transoesophageal echocardiographic image acquisition protocol for wide-view fusion of three-dimensional datasets to support atrial fibrillation catheter ablation. J Interv Card Electrophysiol. 2013 Jun;37(1):21-6.

Ren B, de Groot-de Laat LE, McGhie J, Vletter WB, Ten Cate FJ, Geleijnse ML. Geometric errors of the pulsed-wave Doppler flow method in quantifying degenerative mitral valve regurgitation: a three-dimensional echocardiography study. J Am Soc Echocardiogr. 2013 Mar;26(3):261-9.

Mulder HW, van Stralen M, **Ren B**, Berendsen FF, Bosch JG, Pluim JPW. Simultaneous pairwise registration for image mosaicing of TEE data. ISBI 2013: 242-245

Haak A, Vegas-Sánchez-Ferrero G, Mulder HW, Kirişli H, Baka H, Metz C, Klein S, **Ren B**, van Burken G, van der Steen A, Pluim J, van Walsum T, Bosch JG. Segmentation of 3d transesophageal echocardiograms by multi-cavity active shape model and gamma mixture model. In Liao H, Linte C, Masamune K, Peters T, Zheng G, eds: Augmented Reality

Environments for Medical Imaging and Computer-Assisted Interventions. Volume 8090 of Lecture Notes in Computer Science. Springer Berlin Heidelburg (2013) 19-26

Haak A, Vegas-Sánchez-Ferrero G, Mulder HW, Kirişli H, Baka H, Metz C, Klein S, **Ren B**, van Burken G, de Jong N, van der Steen A, Pluim J, van Walsum T, Bosch JG. Simultaneous segmentation of multiple heart cavities in 3d transesophageal echocardiograms. In: Ultrasonics Symposium (IUS), 2013 IEEE International. (2013) 152-155.

Ren B, de Groot-de Laat LE, Geleijnse ML. Left Atrial Compliance in Asymptomatic versus Symptomatic Patients with Mitral Valve Regurgitation. Submitted.

Ren B, Kirschbaum SWM, Vletter WB, Houtgraaf JH, Geleijnse ML. Accuracy of Fully Automated Left Ventricular Quantification by Three-Dimensional Echocardiography. Submitted.

Ren B, Mulder HW, Haak A, McGhie J, Szili-Torok T, Nieman K, van Stralen M, Pluim JPW, Geleijnse ML, Bosch JG. Fusion of Three-Dimensional Transesophageal Echocardiographic Images of Left Atrium for Supporting Catheter Ablation Procedures: Comparison with Computed Tomography. Submitted.

Haak A, **Ren B**, Mulder HW, Vegas-Sánchez-Ferrero G, van Burken G, van der Steen AFW, van Stralen M, Pluim JPW, van Walsum T, Bosch JG. Segmentation of Multiple Cavities of the Heart in Fused Wide-View 3D Transesophageal Echocardiograms. Submitted.

Haak A, Vegas-Sánchez-Ferrero G, Mulder HW, **Ren B**, Kirişli HA, Metz G, van Burken G, van Stralen M, Pluim JPW, van der Steen AFW, van Walsum T, Bosch JG. Segmentation of multiple heart cavities in 3D transesophageal ultrasound images. Revision submitted.

Geleijnse ML, Di Martino LFM, Vletter WB, **Ren B**, Galema TW, van Mieghem NM, de Jaegere PPT, Soliman OII. Limitations of Echocardiographic short-axis assessment of paravalvular leakage after CoreValve transcatheter aortic valve implantation. Submitted.

Di Martino LFM, Vletter WB, **Ren B**, Schultz C, van Mieghem NM, Soliman OII, Di Biase M, de Jaegere PPT, Geleijnse ML. Prediction of Paravalvular Leakage After Transcatheter Aortic Valve Implantation. Submitted.

Di Martino LFM, Vletter WB, **Ren B**, van Mieghem NM, de Jaegere PPT, Soliman OII, Brunetti B, Di Biase M, Geleijnse ML. Beyond VARC-2 Criteria: Assessment of Paravalvular Regurgitation after CoreValve Implantation Using a Transthoracic Three-Dimensional Derived Short Axis Stent View. Submitted.

Di Martino LFM, Vletter WB, van Mieghem NM, **Ren B**, Galema TW, Soliman OII, Schultz C, de Jaegere PPT, Di Biase M, Geleijnse ML. Relation Between Calcium Burden, Echocardiographic Stent FrameEccentricity And Paravalvular Leakage After CoreValve Transcatheter Aortic Valve Implantation. Submitted.

Di Martino LFM, Soliman OII, Vletter WB, van Mieghem NM, **Ren B**, Galema TW, de Jaegere PPT, Di Biase M, Geleijnse ML. A New Score To Analyse Paravalvular Leakage After CoreValve Transcatheter Aortic Valve Implantation. Submitted.

van Mieghem NM, Rodriguez-Olivares R, **Ren B**, Ouhlous M, Galema TW, Geleijnse ML, Kappetein AP, de Jaegere PPT. Transcatheter BSCI Lotus valve implantation in a degenerated Carpentier-Edwards Bioprosthesis. Submitted.

Chapter 6.5

Acknowledgements

ACKNOWLEDGEMENTS

I can't believe that I'm eventually writing the final pages of my thesis in this pleasant sunny afternoon. It is not strange in the Netherlands that in sunny and warm spring you can still expect thunder and hailstones. During these four years of my PhD training, I've had many happy times together with tough moments. But still I'm grateful for the opportunity to share a life with so many great people in Erasmus MC and in this amazing country, which has made me grow so much in not only the academic but also my personal life. I would like to take this chance to express my thanks to my dear supervisors, colleagues and friends.

Firstly, I would like to thank my promoter Prof.dr. Felix Zijlstra. Thank you for being my promoter and providing advices for my thesis. And thank you so much for all your efforts in supporting me in working in the cathlab and Cardialysis. I'm grateful to be able to join the great teams. Additionally, my thanks also go to Prof.dr. Maarten Simons. Although you retired after I came to Erasmus MC, I would still like to thank you for accepting me to the PhD training programme and put me into the right team of Dr. Marcel Geleijnse.

To my co-promoter and daily supervisor, Dr. Marcel Geleijnse, dear Marcel, it would be difficult to express my thanks to you in short words. From the first day when I arrived in the Netherlands and you and Osama picked me up outside the IKEA in Delft to the very finishing point of my thesis, you were there to support and help me each step of the way. This thesis wouldn't become true without you. You always gave critical revisions and sharp comments to my articles, corrected tiny mistakes in tables and figures, helped killing tough sometimes hostile comments from reviewers and push me to speak Dutch! I always admire your criticism, discretion and logic thinking, which are the cornerstones of being a scientist. I am very lucky to have a supervisor so enthusiastic and open minded like you. I remember during the first a few months of my being here, you told me that I should try to go to as many congresses as I can, because it might be the best chance for me to see the world. Therefore, I've seen the world. In these four years, I've been to Paris, Budapest, Munich, Athens, Minneapolis, Istanbul, Portland and Barcelona. I've seen this and the other side of the world, which are beyond my imagination. I can't tell how grateful I am to have such opportunities and have my horizon broadened this way. Besides, the conversations with you are always interesting and inspiring. Although you might not agree with many religious concepts, I'd still like to share a quote from the Bible about free will – "All that your hand finds to do, do with your very power." (Ecclesiastes 9:10)

Dr. Hans Bosch, dear Hans, as my second co-promoter, thank you for having me in your project, which introduced me to the engineers' world. When Marcel first introduced me to you, I never thought that the work I would be doing with you and your team would become three chapters in my thesis. Being a graduate of medical school without the background knowledge in engineering, it would be impossible for me to conduct our

researches without your patient instructions and supervision. Thank you for your critical revisions and prudent review of my articles and thesis.

I would also like to thank the members in the reading committee, Prof.dr. Eric Boersma, Prof.dr. Ton van der Steen and Dr. Otto Kamp for reviewing my thesis. Dear Prof.dr. Boersma, special thanks to you for your patient and clarifying explanations in statistics, even for basic concepts.

My gratitude also goes to the doctors in Ba 304, Dr. Folkert ten Cate and Dr. Arend Schenkel. Dear Folkert, thank you for all your help during my PhD training. Sharing the same feeling with many other research fellows, conversations with you are always delightful and humorous, no matter it's about research, clinics or politics. It was such an experience to company you during your lecture tour in China. I've learned a lot about contrast echocardiography and bubbles, the area I had never been involved in. Dear Arend, it is always nice to talk to you. I still remember many interesting talks with you about travelling and China.

My thanks also go to Dr. Tamas Szilik-Torok and Dr. Koen Nieman for being important co-authors and providing critical revisions and comments to my articles. Dear Tamas, thank you very much for your elucidations in electrophysiology and crucial comments, which have made my articles much stronger.

Many thanks from me go to the sonographers as well. Dear Wim, thank you very much for being my co-author, 2nd observer and teacher of the research TTE. I remember in great many afternoons we sat together in front of the Siemens workplace looking at countless endocardial trackings, volume curves and measurements. Needless to say that in another a great amount of days you sat alone in front of the QLAB computer doing the analyses. The whole process would have been much more difficult without your input. Dear Jackie, it is such pleasure to learn from you and work with you. I have learned a lot about the ultrasound machine operations and analysis algorithms from you. Dear Marianne, thank you so much for inviting me and my mother to visit you in Haarlem, for we got the chance to see the real daily life of a Dutch Family. Many thanks to Jan, too! The hospitality and understanding from you and Jan made each visit such a warm and joyful experience to me. My mom and I would definitely like to visit you again! Dear Ellen, thank you for helping me with arranging the ultrasound machine. Dear Anja, thank you for demonstrating the stress echocardiography to me. And also thanks for your gifts to my mom. She likes them very much. Dear Linda, Lourus, Debbie, Beata and Kwaku and Ellen and Anja, thank you for your efforts in including patients for my Siemens article and for all your helps during these four years.

And people of Ba 302, Lotte, Pieter, Stijn, Jimmy, Marlies and René. Dear Lotte, thank you for being my 2nd observer doing all the tedious analyses, and for all the MR patients you've included, so that I could directly use the data. I also appreicate your help with all the details of my research life, such as how to use Elpado, how to find echo data in the

QLAB server, etc. Besides, when I started to do TEE in OR, you helped me a lot in surviving the OR such as the things I can do and the things I should definitely avoid!!! I wish you all the luck with your work in Maastadziekenhuis and Erasmus MC. Pieter and Stijn, it's a pleasure to share the room with you. Talks and discussions are always interesting. Thanks for being such nice and hardworking peers around me, which stopped me from being lazing when I saw your guys typing crazily on your computer. Veel success met je onderzoeken en assistante opleiding! Jimmy, it was such a pleasure to be your office mate for your seven months here. I really miss the walking and talking in the snowing winter evening in Istanbul. I wish all the best for your future career as a cardiologist. Marlies, it's really nice to become good friends with you. I really enjoyed the working time, lunch time and hangout time with you! And I appreciate very much for all your efforts of being my paranimf! And René, I am very lucky to get to sit next to you in the office. Thank you very much for helping me with all sorts of problems about computer, software, and echo machines and for answering my every little stupid question about modern techniques. With your instant help, my PhD life became much easier.

I'd also like to thank Alex and Gerard of the BME department. Alex, thanks a lot for helping me to understand ultrasound principles, and for all the MatLab scripts you wrote me and all your inputs to my articles. Working with you was definitely a pleasure. Very good luck with your researches and future career! Gerard, thank you for all your contributions during the process, too! My thanks also go to the Utrecht team, Harriet, Marijn and Josien. Dear Harriet, thank you for all the work you've done because the results of my researches highly depended on the quality of your registration and fusion work. I can understand how hard it was for you in the beginning as an engineer to understand the heart anatomy and now you're almost an expert in LA anatomy, aren't you? Marijn and Josien, thank you very much for your valuable comments and feedbacks to my articles.

Additionally, I would like to thank the TAVI team in the cathlab biplane room. Dear Prof.dr. Peter de Jaegere and Nicolas, thank you for all your trust, support and help. I was nervous when I first started with the TEE in the cathlab, but your kindness and humour made the nervousness disappear immediately. And to all the anaesthesiologists I've worked with, Dr. Hofland, Dr Orellana Ramos, Dr. Luthern, Dr. Ter Horst and Dr. de Bruijn, thank you very much for your support. And dear Annie-Marie, John, Rob, Sanders, Angelique, Gouda, Linda, and Ramon, thank you all for your help. Because of you all, every Thursday is so pleasant to me.

My thanks also go to people at Cardialysis. Peter, Hector, Ravindra and Osama, thanks for having me in Cardialysis and I'm looking forward to working with you! Osama, thank you for helping me all the way. As reminded by you, I'll stay a little bit more positive about humanity and look more at the bright side of life ;).

Bovendien, hartelijk bedankt voor alle mensen die me geholpen hebben met mijn Nederlands. De leraren van Erasmus Universiteit en Volksuniversiteit, de collega's, en de

huisgenoten, dank jullie voor alle lessen en praatjes. Hoewel ik voor het staatsexamen geslaagd ben, vind ik nog moeilijk om Nederlands te praten. Het is zeker dat ik meer Nederlands zal spreken.

Finally, I would like to thank my Chinese friends in the Netherlands and back in China. 王天时、蔡蕊，谢谢你们对我的帮助和关心，和你们的伊斯坦布尔之旅一直是我美好的回忆。栾盈，很高兴很认识、了解你，希望以后能有更多机会一起hangout，也祝你未来的生活和工作一切顺利。

由衷感谢荷兰华人基督教会鹿特丹堂的兄弟姐妹， 在教会的两年是我人生中非常重要的一段时间。申鹏传道，感谢你对我的教导、关心和理解，在你身上我看到了真正基督徒的样子。只言片语无法表达我的感恩，衷心祝愿您工作顺利，也祝您的家人平安！亲爱的Annie，虽然你不喜欢我叫你Annie姐，但是你真的犹如我的长姐一样，无论是你对我在丰盛生命中的教导、在我遇到困难时的关心，还是为我在耶路撒冷哭墙前的祷告，我都非常感动和感恩。还要感谢你和Jimmy对我多次晚餐的款待，愿神保守你们！另外还要感谢鹿特丹学生团契的各位兄弟姐妹，我很感恩我们一起的聚会和旅行，也很感谢你们的关心和帮助。

亲爱的思震和陈阿姨，谢谢你们四年来对我生活的关心和帮助。思震，还记得我到荷兰的第三天，你带着迷茫的我去超市买东西、告诉到哪里去学荷兰语，还请我去你家吃饭。每次和你见面聊天都很开心！亲爱的陈阿姨，感谢你多次邀请我去你家过圣诞、过新年，很幸运能在荷兰碰到老乡，听到乡音，吃到川菜，希望以后能多去拜访你们。

同样的感谢送给我在国内的亲人和朋友。感谢我的硕士导师唐红教授，在华西超声心动图室一年的学习和经历是我博士研究的基础。感谢在这一年所有帮助过我的老师和同窗。

感谢我高中的挚友瞿灿、吴笛，我们的友谊和关于过往所有的回忆都是我海外生活的慰藉。小时候未能意识到，长大后竟渐渐感到自己真是有点difficult的人，感谢你们这么多年对我包容和理解，对我们这十几年的友谊我非常感恩，也希望我们的友谊能永远延续下去！感谢唐璐大艺术家为我倾情设计的论文封面！感谢我的大学挚友兼室友徐梁、李晶，很怀念我们共同在医学院七年的生活，很感恩在毕业多年以后我们还能相聚在成都。

最后的最后，所有的感恩和感激送给我生命的启蒙者、我最信任的亲人、我最好的朋友——我的母亲。亲爱的妈妈，从小到大你一直是我的role model，你的聪慧、坚强和付出塑造了我的生命。我很骄傲有你这样的母亲，感谢你对我精神和物质上一切的支持，谨以此博士论文集献给你，我最亲爱的妈妈！

It is almost overwhelming for me to look back these four years. Even trivial memories become lucid. I want to thank all the people who showed up in my life and for all the time we spent together. These four years have definitely opened many windows for me and I can't wait to step up and embrace the future!

任 奔， Claire Ren
@ Rotterdam, NL

Shot on 25th July, 2013 at Azure Window, Gozo, Malta.

物格而後知至
知至而後意誠
意誠而後心正
心正而後身修
身修而後家齊
家齊而後國治
國治而後天下平

禮記・大學

吳笛甲午年書于北京